

R

TU

Rheinland-Pfälzische
Technische Universität
Kaiserslautern
Landau

P

Advancing The Applications of *In vitro* Metabolomics in Toxicology

Dem Fachbereich Chemie der Rheinland-Pfälzische Technische Universität
Kaiserslautern Landau zur Verleihung des akademischen Grades

„Doktor der Naturwissenschaften“

genehmigte Dissertation

DE-386

vorgelegt von

Sabina Ramirez Hincapie

geboren in Medellín, Kolumbien

Betreuerin: Prof. Dr. Elke Richling

Datum der wissenschaftlichen Aussprache: 14.09.2023

Kaiserslautern 2023

Promotionskommission

Vorsitzender: Prof. Dr. Stefan Kubik

Berichterstatterin 1: Prof. Dr. Elke Richling

Berichterstatter 2: Prof. Dr. Bennard van Ravenzwaay

Prüfer: Prof. Dr. Gereon Niedner-Schatteburg

Eidesstattliche Erklärung

Hiermit erkläre ich, Sabina Ramirez Hincapie, dass ich die vorliegende Dissertation mit dem Titel

„Advancing The Applications of In Vitro Metabolomics in Toxicology“

eigenständig verfasst und keine anderen als die angegebenen Quellen und Hilfsmittel verwendet habe. Kooperationen mit Mitarbeitern anderer Institutionen wurden ausdrücklich genannt. Teile dieser Arbeit wurden bereits in Vorträgen, Postern und Publikationen veröffentlicht. Diese Dissertation liegt weder im Ganzen noch in Teilen als Prüfungsarbeit bei einem anderen Fachbereich vor. Es wurde kein anderes Promotionsverfahren bei einer anderen Hochschule beantragt oder eröffnet. Die geltende Promotionsordnung des Fachbereichs Chemie der Technischen Universität Kaiserslautern vom 10.12.2019 ist mir bekannt.

Kaiserslautern, den

Sabina Ramirez Hincapie

The practical work of this dissertation was performed at the laboratories of the department of “Experimental Toxicology and Ecology” of BASF SE in Ludwigshafen, Germany and in BASF metabolome solutions GmbH in Berlin Germany.

Part of this work has already been published in peer-reviewed journals.

Ramirez-Hincapie S, Birk B, Ternes P, Giri V, Haake V, I Herold M, Zickgraf FM, Verlohner A, Huener H, Kamp H, Driemert P, Landsiedel R, Richling E, Funk-Weyer D, van Ravenzwaay B (2023) A high-throughput metabolomics in vitro platform for the characterization of hepatotoxicity. *Cell Biology and Toxicology*:1-19. <https://doi.org/10.1007/s10565-023-09809-6>.

Part of this work has been submitted to peer-reviewed journals and is under revision.

Ramirez-Hincapie S, Birk B, Ternes P, Giri V, Zickgraf FM, Haake V, I Herold M, Kamp H, Driemert P, Landsiedel R, Richling E, Funk-Weyer D, van Ravenzwaay B. Application of High Throughput In vitro Metabolomics for Hepatotoxicity Mode of Action characterization and Mechanistic-anchored Point of Departure Derivation: A Case Study with Nitrofurantoin. Submitted to *Archives of Toxicology* on May 30, 2023. Submission ID: ATOX-D-23-00403.

Ramirez-Hincapie S*, Mishra D*, Birk B, Haake V, Herold M, Pery E, Vargas-Asencio J, Razavi S, Fortuna P, Summers N, Konradi R, van Ravenzwaay B, Weiss R. Mechanistic Toxicometabolomic Studies of a Model PPAR α Agonist on Human Pluripotent Stem Cell-derived Liver Organoids. First round of revisions submitted to *Nature Scientific Reports*. Submission ID: SREP-22-01564A.

“At every moment keep a sturdy mind on the task at hand, as a Roman and a human being, doing it with strict and simple dignity, affection, freedom and justice, giving yourself a break from all other considerations. You can do this if you approach each task as if it is your last, giving up every distraction, emotional subversion of reason and all drama, vanity and complaint over your fair share.

You can see how mastery over a few things make it possible to live an abundant and devout life, for, if you keep watch over these things, the gods won't ask for more”

Marcus Aurelius, Meditations, 2.

Table of Contents

Summary	1
Zusammenfassung	3
Chapter 1: introduction.....	5
Toxicology of the 21 st century	5
Conventional <i>in vitro</i> toxicology: evaluation of single endpoints	9
Omics technologies: powerful multiparametric approaches to study toxicity.....	10
Metabolomics: a close-up view into the basic principles	15
<i>In vitro</i> metabolomics to investigate organ toxicity	23
Metabolomics technologies in Next Generation Risk Assessment	25
Liver as one of the main target organs in toxicity studies.....	28
<i>In vitro</i> models to investigate hepatotoxicity	32
Dissertation aims	37
Chapter 2.....	38
Preamble	39
Publication I: A high-throughput metabolomics <i>in vitro</i> platform for the characterization of hepatotoxicity	40
Chapter 3.....	83
Preamble	84
Publication II: application of High Throughput <i>In vitro</i> Metabolomics for Hepatotoxicity Mode of Action characterization and Mechanistic-anchored Point of Departure Derivation: A Case Study with Nitrofurantoin.....	85
Supplementary information	117
Chapter 4.....	130
Preamble	131

Publication III: Mechanistic toxicometabolomics studies of a model PPARα agonist on human pluripotent stem cell-derived liver organoids.....	133
Supplementary information	171
Chapter 5: final discussion, outlook and conclusions.....	193
Acknowledgments	208
References.....	212
Appendix.....	224
List of abbreviations.....	224
Curriculum Vitae.....	230

Summary

Toxicology, the study of the adverse effects of chemicals and physical agents on living organisms, is a critical process in chemical and drug development. The low throughput, high costs, limited predictivity and ethical concerns related to traditional animal-based toxicity studies render them impractical to assess the growing number and complexity of both existing and new compounds and their formulations. These factors together with the increasing implementation of more demanding regulations, evidence the current need to develop innovative, reliable, cost effective and high throughput toxicological methods.

The use of metabolomics *in vitro* presents the powerful combination of a human relevant system with a multiparametric approach that allows assessing multiple endpoints in a single biological sample. Applying metabolomics in a cell-based system offers an alternative to both, the ethical concerns and relevance of animal testing and the restraining nature of single endpoint evaluations characteristic of conventional toxicological *in vitro* assays. However, there are still challenges that hamper the expansion of metabolomics beyond a research tool to a feasible and implementable technology for toxicology assessment.

The aim of this dissertation is to advance the applications of *in vitro* metabolomics in toxicology by addressing three major challenges that have limited its widespread implementation in the field. In chapter 2 the restrictive high cost and low throughput of *in vitro* metabolomics was addressed through the development, standardization and proof of concept of a high throughput targeted LC-MS/MS *in vitro* metabolomics platform for the characterization of hepatotoxicity. In chapter 3, the use of the developed *in vitro* metabolomics system was expanded beyond hazard identification, to its implementation for deriving dose- and time response metrics that were shown useful for Point of departure (PoD) estimations for human risk assessment. Finally, in chapter 4 in order to increase the reliance and confidence of using *in vitro* metabolomics data for risk assessment, the human relevance of the metabolomics *in vitro* assays was attempted to be improved by the implementation and evaluation of *in vitro* metabolomics in a hiPSCs-derived 3D liver organoid system.

Summary

The work developed here demonstrates the suitability of *in vitro* metabolomics for mechanistic-based hazard identification and risk assessment. By advancing the applications of metabolomics in toxicology, this work has significantly contributed to the aim of toxicology of the 21st century for a human-relevant non-animal toxicological testing, supporting the toxicology task of protecting human health and the environment.

Zusammenfassung

Toxikologie, die Untersuchung von schädlichen Effekten von Chemikalien und physikalischen Stoffen an lebenden Organismen, ist ein kritischer Schritt in der Entwicklung von Chemikalien und Wirkstoffen. Der niedrige Durchsatz, hohe Kosten, die begrenzte Vorhersagekraft, sowie ethische Bedenken in Bezug auf traditionelle Tierstudien in der Toxikologie machen es schwierig die wachsende Anzahl und Komplexität von vorhandenen und neuen Substanzen und deren Formulierungen zu untersuchen. Dies, zusammen mit der zunehmenden Umsetzung von anspruchsvollen Vorschriften, belegen den momentanen Bedarf an innovativen, verlässlichen sowie kosteneffizienten und high-throughput toxikologischen Methoden.

Die Verwendung von Metabolomics in vitro kombiniert ein humanrelevantes System mit einem multiparametrischen Ansatz und erlaubt dadurch das Beurteilen von multiplen Endpunkten in einer einzigen biologischen Probe. Die Anwendung von Metabolomics in einem zellbasierten System ermöglicht eine Alternative, sowohl was ethische Bedenken als auch die Bedeutung von Tierversuchen und die Begrenzung auf einen einzigen Endpunkt als Beurteilungsmerkmal von konventionellen Toxikologischen in vitro-Assays, angeht. Jedoch gibt es immernoch Herausforderungen, die die Ausweitung von Metabolomics über einen Forschungsansatz hinaus zu einer realisierbaren und implementierbaren Technologie für toxikologische Bewertungen begrenzen.

Das Ziel dieser Dissertation war es die Anwendung von Metabolomics in vitro in der Toxikologie voranzubringen, indem 3 große Herausforderungen, die die Implementierung dieser Technologie behindern, angegangen wurden. In Kapitel 2 wurde die Frage der hohen Kosten und des niedrigen Durchsatzes von Metabolomics in vitro adressiert, indem eine standardisierte, high-throughput targeted LC-MS/MS Metabolomics in vitro Plattform zur Charakterisierung von Hepatoxizität entwickelt und mittels eines Proof of concepts verifiziert wurde. In Kapitel 3 wurde die Anwendung des entwickelten in vitro Metabolomics Systems über die Gefahrenidentifizierung hinaus weiterentwickelt zu einer Implementierung für die Ableitung von Dosis und Zeiteffekten, die sich auch als nützlich für die Abschätzung von Point-

of-departures (PoD) für die humane Risikobewertung erwiesen haben. Schließlich wurde in Kapitel 4 versucht die Humanrelevanz des Metabolomics in vitro Assays zu verbessern, indem von hiPSC-abgeleitete 3D Leberorganoidsysteme implementiert und evaluiert wurden, um das Vertrauen in Metabolomics in vitro hinsichtlich einer Risikobewertung zu steigern.

Die hier präsentierte Arbeit stellt eine geeignete Metabolomics in vitro Methode für die mechanismusbasierte Gefahrenidentifizierung und Risikobewertung dar. Indem die Anwendung von Metabolomics in vitro in der Toxikologie vorangetrieben wurde, hat diese Arbeit signifikant zum Ziel der Toxikologie des 21. Jahrhunderts, ein humanrelevantes und tierversuchsfreies toxikologisches Testen zu etablieren, beigetragen und unterstützt damit auch den Schutz der menschlichen Gesundheit und der Umwelt.

Chapter 1: introduction

Toxicology of the 21st century

Toxicology, a discipline that has its origins in the ancient study of poisons, has evolved over the years into an applied science that investigates the adverse effects of chemicals and physical agents on living organisms (Klaassen and Amdur 2013). Today, the field of toxicology aims to protect the human population and the environment mainly through identifying and assessing the risk posed by substances of any kind; from natural occurring compounds, pharmaceuticals, and pesticides to complex molecules such as polymers, chemical mixtures, and minuscule nanoparticles (Greim and Snyder 2018).

Classical toxicology has largely relied in the use of animal experiments coupled to evaluations of observable outcomes, such as clinical signs, histopathological lesions, and clinic-chemical data to assess the effects induced by exposures to chemical agents (OECD 1997). In the last decades, it became evident that the low throughput and high costs of animal-based toxicity studies render them impractical to assess the growing number of individual existing compounds, new substances and their formulations in the market (Hartung 2009; Wang et al. 2020). In addition, different studies demonstrating the limited predictivity of animal models to reflect human responses were increasingly reported (Basketter et al. 2004; Gottmann et al. 2001; Hartung 2008; Olson et al. 2000). In parallel to the concerns about the relevance of animal studies, societal pressure to decrease animal experimentation under the 3R principle of Reduce, Refine and Replace animal testing significantly grew stronger (Russell and Burch 1959).

In 2006, the European union announced implementation of legislation for the largest safety assessment of chemicals in history. The Registration, Evaluation, Authorisation and Restriction of Chemicals (REACH) required manufactures and companies importing chemicals into the European Union in quantities of one ton or more per year, to provide information on

the toxic properties and uses of the substances (REACH EC No. 1907/2006, European commission). At the time, it was estimated that data for about 86% of marketed chemicals were lacking (Hartung 2009). Filling the data gaps for complying with the REACH regulations requirements, would have represented massive animal testing needs (Hartung 2009). However, the legislation called for keeping the use of animals as last resort and for the integrated use of new methodologies.

In 2007, the US National Research Council (NRC) published a hallmark report on Toxicity testing in the 21st century (National Research Council 2007). This document proposed the incorporation of new technical and scientific developments and presented a new vision and roadmap for the field, officially initiating a revolution in Toxicology. Since then, the field of toxicology has sought to move away from utilizing large animal cohorts and observational sciences to the incorporation efficient and human relevant technologies that provide a better understanding of the mechanisms of toxicity at a cellular level (National Research Council 2007). The pressing need for faster, cost effective and more human relevant models, together with the ethical and political demands to reduce animal testing, evidenced a broadly perceived need for a transformation to continue to ensure the safety of human population, the field of toxicology had to change.

Since the publication of the NRC report in 2007, the vision of toxicity in the 21st century has come a long way. Numerous human cell-based methods, high throughput systems, *in silico* models and read across strategies have been incorporated as alternative approaches to *in vivo* animal testing (Krewski et al. 2020b). These New Approach Methodologies (NAMs) have majorly expanded the study of toxicity beyond the observation of apical endpoints by enabling the study of mechanisms of toxicity. Importantly, NAMs have played a key role in the development and implementation of the adverse outcome pathway model (AOP), a mechanistic-based framework, in modern toxicology (Mortensen et al. 2021; Vinken 2013). The AOP framework identifies a sequence of cellular and molecular key events that lead to an adverse effect upon chemical exposure, providing a conceptual basis and a guide for the development and implementation of non-animal testing approaches (Fig.1)(Ankley et al. 2010). This concept has been fundamental for the integration and extrapolation of *in vitro* information generated from different assays and sources (OECD 2016a; OECD 2016b; Rovida et al. 2015).

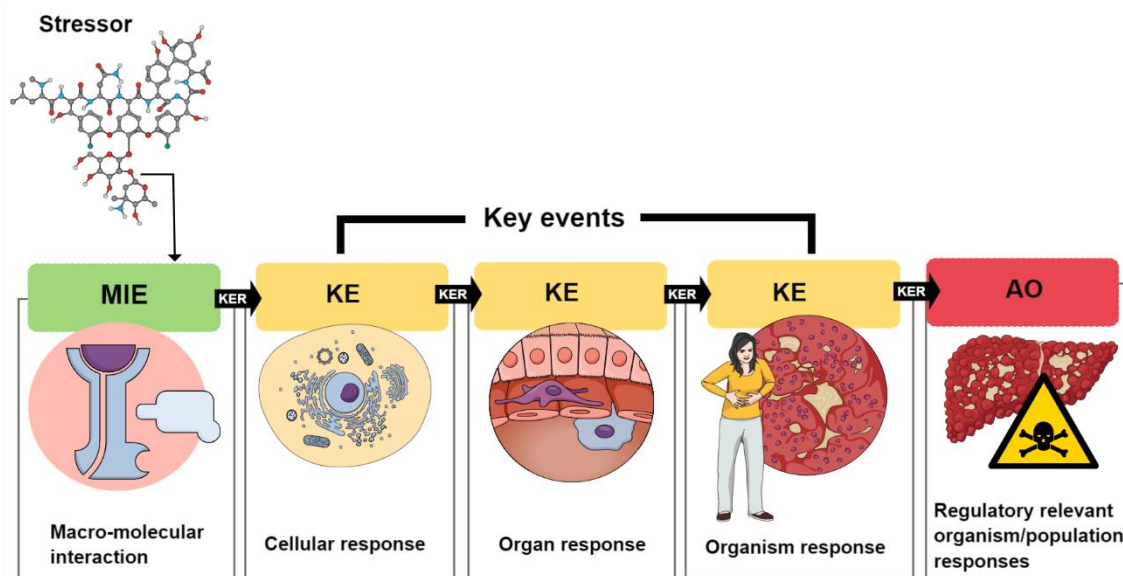


Figure 1. The adverse outcome pathway (AOP) framework. Upon contact with the stressor, a molecular initiating event (MIE) denotes an interaction between the toxic substance and an organism (e.g., binding of the substance to a receptor or protein). This interaction begins the toxicity process. Afterwards, key events (KE) are processes that characterize the progression of the toxicity. Early key events can include changes in protein production or molecular signaling that occur in individual cells. Later key events can include altered tissue or organ function. Links between key events are explained by key event relationships (KER). Adverse outcomes may occur at individual or population levels (e.g., disease, impaired development, or impaired reproduction.) Adapted from (Edwards et al. 2016). Created with Mindthegraph (<https://mindthegraph.com>).

The establishment of human health guidance values such as reference dose (RfD), derived no-effect level (DNEL) and the calculation of a safe acceptable daily intake (ADI), is the core aim of chemical risk assessment (Greim and Snyder 2018). However, results obtained from *in vitro* tests cannot be directly applied to predict the full biological responses *in vivo*. Therefore, beyond obtaining mechanistic information, that allows to classify whether a substance negatively interferes with a particular cellular process (hazard identification), one of the main challenges for the successful implementation of *in vitro* testing, is to first obtain quantitative values that reflect to which extent a pathway was perturbed and then to extrapolate these values to human relevant concentrations (Bell et al. 2018; Hartung 2018). Thus, one of the key aspects of toxicity of the 21st century relies in the use of nonlinear regression models of dose-response data as a first step for obtaining quantitative values for the determination of human and environmental risks (Andersen and Krewski 2009). The starting point for the determination of such values includes the derivation of a point of departure (POD) from dose-response modelling, which refers to the point on a toxicological dose-response curve corresponding to an estimated low effect level or no effect level (Bercu et al. 2016), followed

by an In Vitro–In Vivo Extrapolation (IVIVE) analysis to link an *in vitro* effect concentration with its *in vivo* counterpart (Wilk-Zasadna et al. 2015) (Fig. 2).

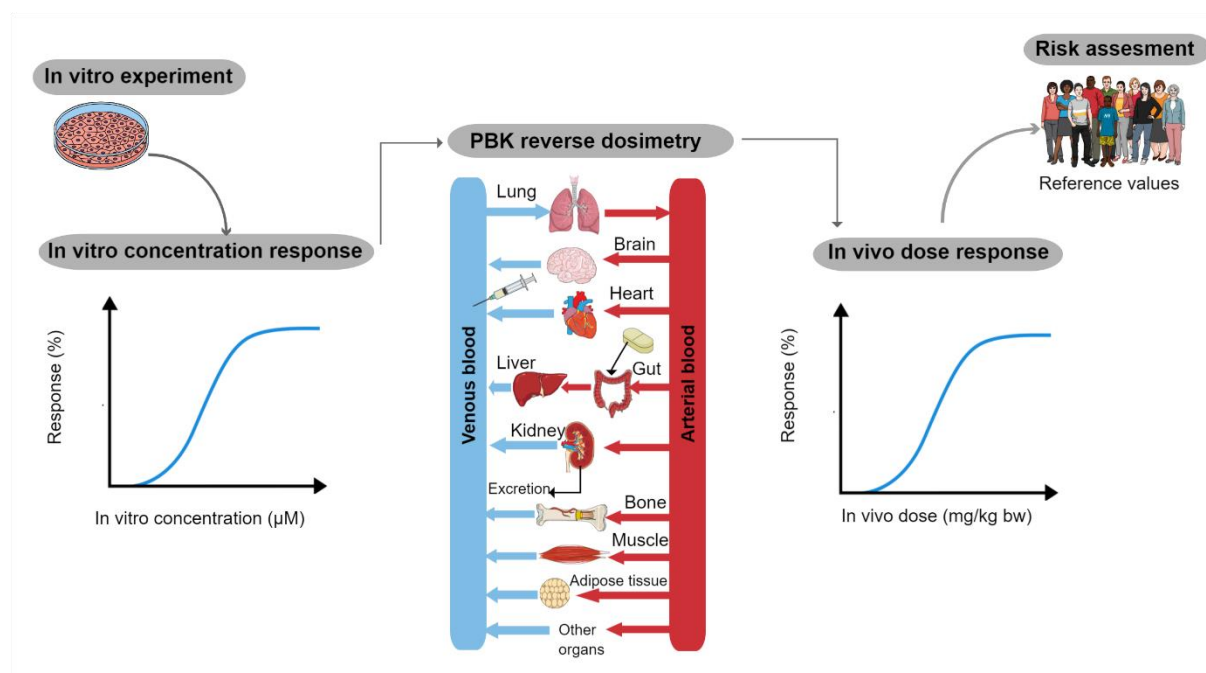


Figure 2. The use of physiologically based kinetic (PBPK) modelling to translate *in vitro* concentrations to *in vivo* doses. In PBPK model, organs important for absorption, distribution, metabolism and excretion (ADME) are included. The organs in PBPK can be defined by a differential equation. For deterministic organs for the blood concentration profile, such as the gut, liver, and kidney, details of the mechanism are considered to implement the model. Additional tissues and organs can be added according to modeling purpose and hypothesis. Modified from (Shin et al. 2017). Created with MindtheGraph (<https://mindthegraph.com>).

The successful transformation of *in vitro* concentrations into doses expressed in mg/kg body weight (bw), as derived in *in vivo* studies, represents a fundamental step in moving away from animal experimentation (Chang et al. 2022). The feasibility of IVIVE models to extrapolate *in vitro* to *in vivo* concentrations has been demonstrated in various publications (Abdullah et al. 2016; Lousse et al. 2017; Ning et al. 2019; Shi et al. 2020), yet its effective application highly depends on appropriate parameters and well characterized *in vitro* systems.

15 years have passed since the vision and strategy for toxicity testing in the 21st century was first published. To date, a lot of resources have been dedicated to this vision and significant advances have been made in the development of alternative methods (Krewski et al. 2020a). However, the consecutive implementation of stringent regulatory frameworks such as REACH EC No. 1907/2006, the European Cosmetics Act EC No. 1223/2009, and the recently put in

place chemical strategy towards sustainability COM/2022, aiming to ensure human and environmental safety of both new and already existing substances, keep challenging industries to find reliable, yet cost effective animal free methods to meet the high demand for toxicity testing (Crawford et al. 2017; van Dijk et al. 2021)

Conventional *in vitro* toxicology: evaluation of single endpoints

In the last decades, *In vitro* models have been of immense utility in the understanding of molecular mechanisms of toxicity and in the development of adverse outcome pathways (AOP) (Krewski et al. 2020a; Vinken 2013). However, toxicological *in vitro* testing has been based mainly on monoparametric strategies (one question, one answer) (Dix et al. 2007). Thus, once an AOP is defined for evaluating a certain toxicity endpoint, individual cell-based and biochemical tests that characterize each of the molecular initiating and key events of a pathway should be established. Therefore, with conventional *in vitro* methods, which are based on single endpoints, perturbations in cellular responses cannot be predicted from an individual test but instead have to be assessed in a set of several toxicity assays. Consequently, an extensive battery of tests, each performed in a different biological replicate, is needed to obtain comprehensive mechanistic information as shown in the US EPA's ToxCast and Tox21 testing battery (ToxCast website: <http://epa.gov/ncct/toxcast/>). Under these programs, data from hundreds of assays for thousands of chemicals have been produced based on individual cell-based assays that test for bioactivity upon chemical exposure at various cellular levels such as enzymatic activities, receptor activation, cytotoxicity and biomarker production (Dix et al. 2007).

In order to obtain enough information for evaluating specific adverse outcomes using conventional *in vitro* toxicological methods, data from multiple assays and technologies, covering different targets per endpoint and per pathway, have to be developed and integrated (Rovida et al. 2015). The development, integration and data interpretation processes generated from single endpoint *in vitro* tests are time consuming, tedious and rarely straightforward, which highly limits the full characterization of toxicological-related events and challenges cell-based models implementation in regulatory risk assessment (OECD 2016a).

Omics technologies: powerful multiparametric approaches to study toxicity

In the last decades, biological sciences have experienced a revolution driven by the accelerate rate of technological advances. Rapidly developing sequencing methods and analytical techniques gave rise to the development of what are known as Omics technologies. Omics technologies aim at the global characterization and quantification of pools of biological molecules that influence the structure, function, and dynamics of an organism (Micheel et al. 2012). These relatively new approaches offer the advantage of comprehensively measuring the profiles of genes (transcriptomics), proteins (proteomics), or small endogenous metabolites (metabolomics) within biological matrices like cells, tissues, blood plasma or excreta (Karczewski and Snyder 2018). The systematic screening of genes, proteins and metabolites offered by omics techniques has enabled an unprecedented large-scale analysis of biological processes in an organism (Venter et al. 2001). (Table 1)

Table 1. Comparison of advantages and limitations for different Omics technologies. Adapted from (Bouhifd et al. 2013).

	Transcriptomics/genomics	Proteomics	Metabolomics
Advantages	<ul style="list-style-type: none"> • High throughput sequencing techniques allow the cost and time efficient sequencing of complete genomes • Study of polymorphisms can give insight into the role of genetics in toxicology and explain differences in susceptibility • Gene arrays allow the simultaneous gene expression analysis of thousands of genes • Availability of gene arrays with complete genomes including the human • Sensitive endpoint of toxicity since gene expression changes often occur at an early stage 	<ul style="list-style-type: none"> • Important role of proteins in cell homeostasis • Quantitative analysis • 2D gel electrophoresis is routinely applied • MS-based approaches allow the identification of proteins • Sensitivity, specificity and low costs of protein arrays • Protein arrays allow the simultaneous analysis of thousands of proteins • Analysis of protein-protein interactions • Protein profiling can be performed in cells, tissues and non-invasively in body fluids (blood plasma, serum) 	<ul style="list-style-type: none"> • Allows the simultaneous measurement of hundreds of metabolites • The omics science considered to be the closest to the phenotype • MS analysis is sensitive, quantitative and detects a high number of metabolites • Availability of public and commercial databases with annotated metabolites • Both in vitro cell cultures and in vivo tissue and non-invasive blood, urine applications
Limitations	<ul style="list-style-type: none"> • Genome sequencing alone is not enough since polymorphisms play an important role • Alterations in gene expression do not always lead to adverse health effects • Gene array analysis can overlook modest changes in gene expression • Limited reproducibility between gene array experiments • Gene arrays are semi-quantitative and data needs confirmation by quantitative techniques • Often difficult to translate genomics results to in vivo or human toxicity or disease • Genomics often requires proteomics and metabolomics follow-up studies 	<ul style="list-style-type: none"> • Complexity and instability of the proteome • Large number of proteins and possible posttranslational modifications • Limited detection of low abundance and highly acidic or basic proteins by 2D gel electrophoresis • Limited reproducibility between 2D gel electrophoresis experiments • Not all proteins in a sample can be identified • Limited availability of antibodies for the detection of the large amounts of existing proteins 	<ul style="list-style-type: none"> • In vivo approaches influenced by variability factors, e.g. age, gender, diet, stress, housing conditions, health status • In vitro approaches are influenced by variability factors, e.g. cell culture conditions, metabolic competence, media formulations, serum additions, treatment vehicle • Quenching and metabolite extraction procedures limit the detection of metabolites • Requires costly NMR or MS technologies • Complexity of the data analysis and interpretation, e.g. metabolic pathways

In toxicology, Omics approaches have provided a valuable tool to characterize alterations in cells, tissues and organisms following exposures to chemical substances (Mortimer et al. 2022; Nguyen et al. 2022). Multiparametric Omics techniques offer the simultaneous evaluation of numerous parameters, such as multiple pathways, in a single biological sample, representing sensitive and comprehensive tools for elucidating the molecular and biochemical events underlying toxicity (García-Cañaveras, Castell, Donato, & Lahoz, 2016). The implementation of transcriptomics, proteomics and metabolomics in both *in vivo* and *in*

vitro toxicity studies has greatly contributed to diverse areas of toxicology and risk assessment such as the early prediction of toxicological effects (Van Ravenzwaay et al. 2015), analysis of compounds modes of action (Garcia-Canaveras et al. 2015; Ramirez et al. 2018a), characterization of AOPs (Brockmeier et al. 2017; Vinken 2019), identification of early biomarkers of adverse outcomes (Van Ravenzwaay et al. 2007), chemical grouping (Van Ravenzwaay et al. 2016), and more recently, in the derivation of points of departure (POD) for *in vitro* to *in vivo* data extrapolation (Crizer et al. 2021b; Malinowska et al. 2023).

Following the central concept of molecular biology, in the first step of the genetic information flow, DNA is copied into mRNA through the process of transcription. Transcriptomics is the Omics technique that deals with the global measurement of gene expression profiles based on the determination of mRNAs levels. Alterations in gene expression are the earliest quantifiable effects following a chemical exposure (Council 2007). It has been widely demonstrated that different substances induce characteristic gene expression patterns that can be associated to mechanisms of toxicity and are indicative of adverse health effect as evidenced in The Comparative Toxicogenomics Database (CTD; <http://ctdbase.org/>) which integrates the transcriptomics data of 17,100 chemicals, 54,300 genes, 6,100 phenotypes, 7,270 diseases and 202,000 exposure statements (Davis et al. 2023). From the Omics techniques, transcriptomics has been the more extensively used in toxicology. It offers the advantage of allowing high throughput and cost-effective evaluations of complete genomes. Additionally, mRNA arrays with whole genomes, including the human, are commercially available and big amount of toxicity relevant data have been produced using this technology (Mortimer et al. 2022). However, mRNA changes may or may not result in a functional implication since they are subject to complex homeostasis and feedback mechanisms such as post-translational modifications. Thus, alterations in gene expression do not always lead to adverse health effects and it is often difficult to readily translate transcriptomics results to *in vivo* toxicological endpoints (Alexander-Dann et al. 2018).

One step further in the flow of genetic information, mRNAs are translated into proteins. Proteins play an important role in cell homeostasis and therefore chemical exposure can interfere with critical biological processes through the modification of proteins. Proteomics, the large-scale measurement of proteins, has been successfully implemented to identify biomarkers of toxicity, evaluate mechanisms of action of multiple substances and detect

harmful toxicant-protein interactions such as adducts (Qiao and Wang 2019). As proteins pivot between gene transcription and phenotype, proteomics offer a closer perspective of toxic effects than transcriptomics (Madeira and Costa 2021). However, the large number and high complexity of the biological structures of proteins and their numerous isoforms, originating from post-translational modifications, make proteomics a highly technically challenging technique, which has limited its applications in toxicology (Doll and Burlingame 2015).

Finally, metabolites are the ultimate expression of gene and protein activities to meet the physiological demands for growth and survival, including adaptive responses to environmental factors such as nutrient availability, xenobiotics, and therapeutic agents (Fiehn 2002). Metabolomics is known as the systematic measurement of low molecular weight endogenous molecules (below 1.5 kDa) such as carbohydrates, amino acids, lipids, and nucleic acids. Metabolites intermediate in biochemical pathways assisting the cells to communicate messages and transmit signals (Idle and Gonzalez 2007). These molecules represent the end products of processes that occur within a cell, and thus can provide an insight into the physiological state of an organism, including its genetic makeup and current environmental influences. Therefore, while genomics and proteomics try to predict what kind of effect might occur, metabolomics offers the answer to what is actually happening (Riekeberg and Powers 2017)(Fig. 3).

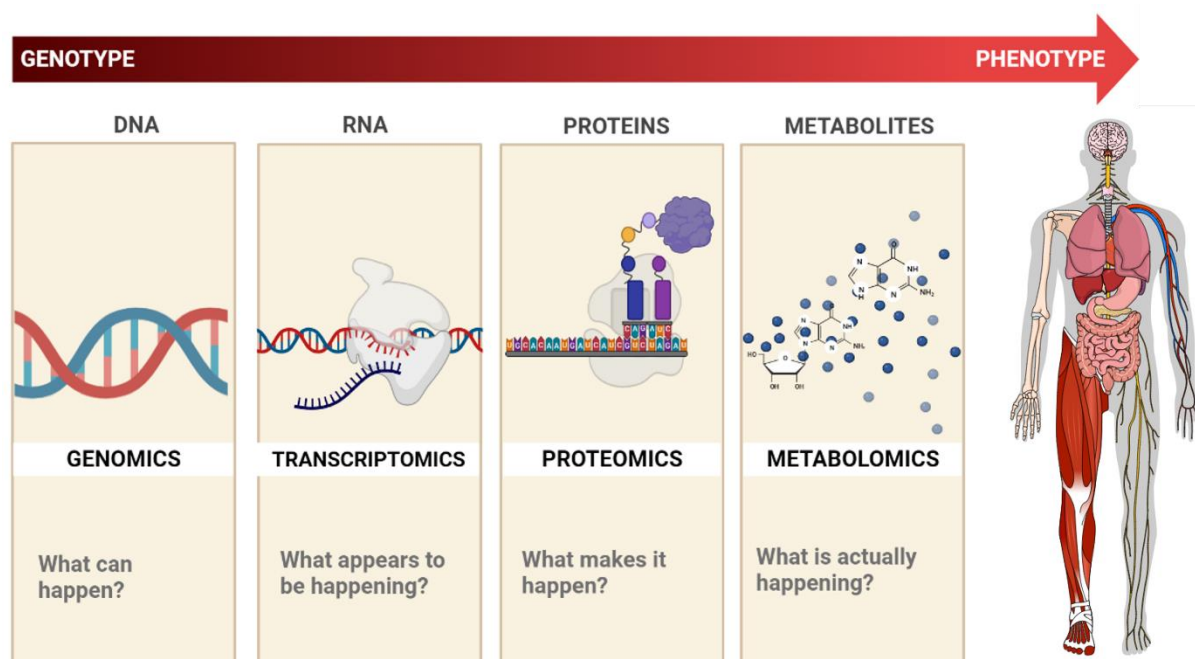


Figure 3. Genetic information flow and Omics cascade. According to the central concept of molecular biology, DNA (genomics) are transcribed to mRNA (transcriptomics) which in turn are translated to proteins (proteomics), whose activities result in the formation of metabolites (metabolomics). The metabolome is the final downstream product of the genome, and therefore metabolomics is regarded as the endpoint of the Omics cascade. Created with Biorender (<https://www.biorender.com/>).

Classical toxicology has been based on phenotypical observations from behavior to pathology and clinical chemistry evaluations. The metabolome (i.e., the collection of all small endogenous molecules in a biological system) represents the interface between the genome activity, the organism, and the environment. The combination of the genome and the environment makes up the phenotype, in that sense, the metabolome is the best indicator of the phenotype, reflecting what is occurring in terms of physiology (Fiehn 2002). Consequently, metabolomics is regarded as the omics technology which is closest to classical toxicology (Ramirez et al. 2013).

Metabolomics presents several advantages over other Omics technologies. To enable practical applications (e.g., clinical practice), an ideal biomarker should be easy to obtain and to evaluate (Van Ravenzwaay et al. 2007). mRNAs and proteins are normally not secreted into biofluids. In contrast, metabolites are detectable in biofluids such as urine and blood which make it a less invasive method and enables time course analysis (Van Ravenzwaay et al. 2007). In addition, genes and proteins can vary among organisms (species dependent), whereas

metabolites have a fixed chemical structure, regardless of the organism, simplifying the extrapolation from experimental models to humans. These factors, together with the metabolome to the phenotype and its high sensitivity to external stimuli make metabolomics technologies a powerful approach to study toxicity (Ramirez et al. 2013).

Metabolomics: a close-up view into the basic principles

Although the field of metabolomics is relatively new, the basic concept has existed throughout history in various cultures. Ancient civilizations such as the Egyptians and Chinese were able to detect metabolic conditions like diabetes from the evaluation of the urine. In the year 300 B.C., the Greeks recognized the importance of examining body fluids in order to predict diseases (Nagana Gowda and Raftery 2019). In the West, the humoral theory dominated the medical thinking for almost two millennia. In this theory, humours existed as liquids within the body; a good balance between the humours was essential to retain a healthy body, an imbalance could result in disease (Balzer and Eleftheriadis 1991).

It has been long understood that metabolites can reveal information about the physiological status of an organism. However, it was not until the beginning of the 20th century that the development of new techniques such as the mass spectrometer, nuclear magnetic resonance (NMR) and chromatographic separation, has made possible the identification and quantification of metabolites, and therefore, the evolution of metabolomics as a scientific discipline (Dunn and Hankemeier 2013).

A range of analytical technologies have been employed for the large-scale analysis of metabolites in different organisms, tissues, fluids, or cells. Today, mass spectrometry coupled to different chromatographic separation techniques, such as liquid or gas chromatography (LC-MS and GC-MS) are the main tools adopted for metabolic profiling (Alseekh et al. 2021). The general workflow for a typical mass spectrometry-based metabolomics experiment consists of several steps: (1) sample collection, (2) quenching, (3) metabolite extraction, (4) chromatography separation, (5) mass spectrometry identification and (6) data processing for analytes identification and statistical analysis (Fig 4).

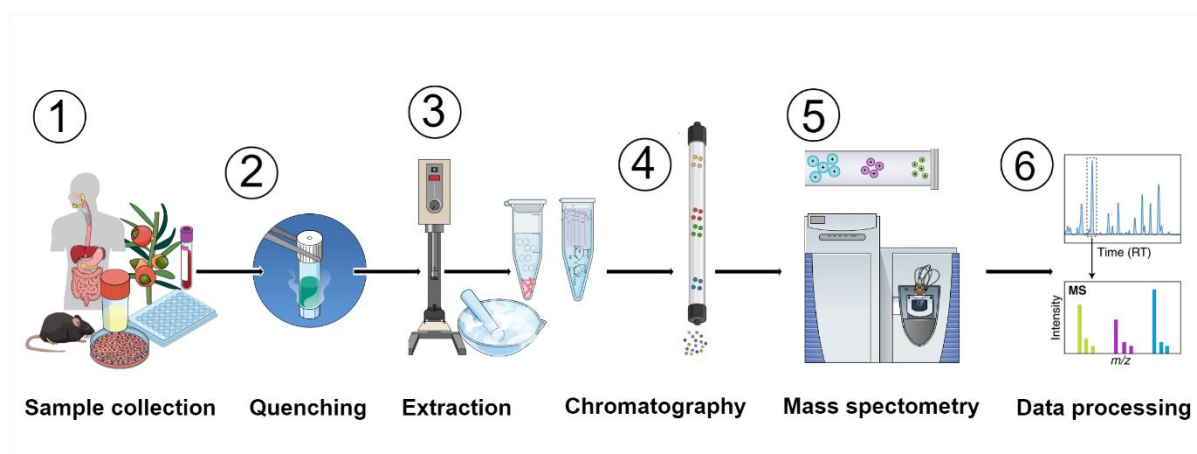


Figure 4. Metabolomics experiment workflow. Metabolomics involves several basic steps: (1) sample collection; (2) metabolism quenching (3) metabolite extraction (4) separation on a column (chromatography) such as by GC or LC (5) ionization of metabolites and separation by a mass analyzer as ions fly or oscillate based on their mass-to-charge (m/z) ratio (6) data processing for analytes identification and statistical analysis. Metabolites can be identified by a combination of retention time (RT) and MS signature. Modified from (Alosekh et al. 2021). Created with MindtheGraph (<https://mindthegraph.com>).

(1) *sample collection*: metabolites can be extracted from a wide range of biological matrices such as biofluids, tissues, and cells. Due to the high sensitivity of the metabolome, factors such as sampling time, stage of the organism development and organ specificity must be considered in order to ensure experimental reproducibility (Smith et al. 2020).

(2) *Metabolism quenching*: due to the high rate of metabolic turnover in a living organism, a critical step in metabolomics experiments is the rapid stopping of any kind of chemical or enzymatic reaction that may occur immediately after sample collection, since these can alter the original metabolite profile of the organism. This quick inactivation of all biochemical and enzymatic activity in organisms is known as quenching. Quenching is crucial to obtain a metabolic snapshot reflective of the physiological status being evaluated (León et al. 2013). Importantly, any perturbations of the existing metabolite levels during harvesting should be avoided. Usually, this step is done by snap-freezing the samples in liquid nitrogen (Viant et al. 2019b).

(3) *metabolite extraction*: to release the metabolites, the cell compartments or their protective covering need to be disrupted. Depending on the sample type, membranes

are disrupted either physically through the use of beads, homogenizers, laboratory-grade blenders and ultrasonication, or chemically by the addition of compounds such as alcohols or membrane disrupting molecules (Goldberg 2015). After metabolites are released from the matrix, organic solvents are added to separate the metabolites from other molecules such as proteins and nucleic acids. Depending on the sample type, different extraction methods using distinct combinations of organic solvents are used (Andresen et al. 2022). Different extraction methods offer various metabolite classes selectivity. Therefore, the selected protocols for the metabolite extraction play a major role in determining the reach of metabolites that could be detected (Dettmer et al. 2011). Fig 5. shows a comparison between protein precipitation, liquid-liquid extraction, and solid phase extraction, three of the most used extraction methods for metabolomics experiments.

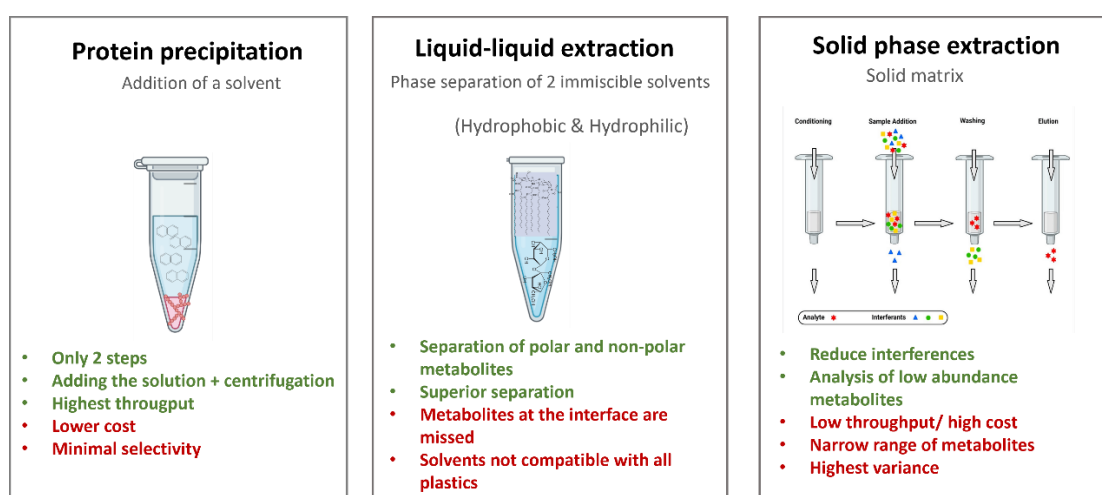


Figure 5. Sample extraction methods for metabolomics analysis. Comparison between three of the most used extraction methods for metabolomics experiments. Created with Biorender (<https://www.biorender.com/>).

(4) *chromatography separation*: once metabolites are separated from larger molecules such as proteins and organic acids, the individual components (metabolites) of the resulting mixture are separated via chromatography. Chromatography techniques work based on adsorption, a mass transfer process allowing to physically separate the different components of a mixture. In every chromatography method, there is a contact between two phases; a fixed stationary phase and a mobile phase that flows constantly during the analysis. The separation of the components from the mixture is

based on the differential partitioning between the mobile and the stationary phase and the polarity of the molecules that compose the mixture (Lundanes et al. 2013). Two types of chromatography, liquid (LC) and gas (GC) are commonly used in metabolomics studies.

In liquid chromatography, the mobile phase is a liquid mixture of organic solvents while the stationary phase is a column packed with miniature particles (e.g., silica). The sample is forced by a liquid at high pressure (the mobile phase) through the column. The components of the sample mixture are separated based on their differential interactions with the adsorbent material of the stationary phase particles which leads to the separation of the molecules as they flow through the column and finally results in different retention times for each molecule (metabolite) of the mixture (Bird 1989) (Fig 6). Liquid chromatography is divided mainly in two classes based on the polarity of the mobile and stationary phases. In normal phase liquid chromatography (NPLC), the stationary phase is more polar than the mobile phase. In reversed phase liquid chromatography (RPLC) the stationary phase is made of beads of highly hydrophobic aliphatic chains and the mobile phase is a mixture of polar organic solvents (Lough and Wainer 1995).

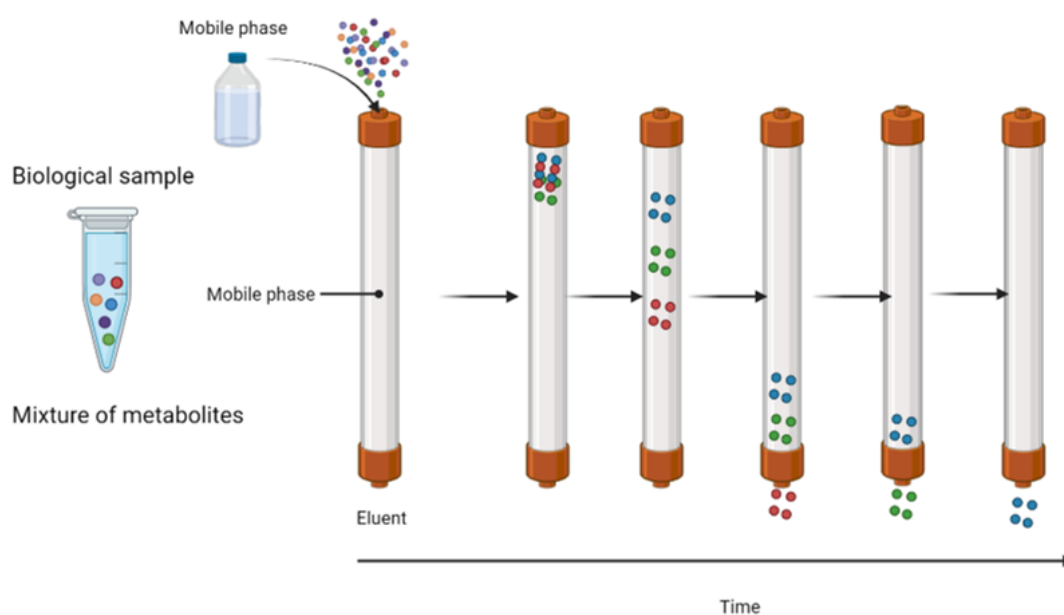


Figure 6. Liquid chromatography principle. In liquid chromatography, the mobile phase is a liquid mixture of organic solvents, and the stationary phase is a column packed with particles. The sample is

forced by a liquid through the column. The components of the sample mixture are separated based on their differential interactions with the adsorbent material of the stationary phase particles leading to the separation of the molecules as they flow through the column resulting in different retention times for each analyte of the mixture. Created with Biorender (<https://www.biorender.com/>).

In gas chromatography (GC), on the other hand, the mobile phase consists of an inert gas, usually helium, while the stationary phase is a polymer or liquid embedded in a very long thin column. In GC the sample is first vaporized and injected into a column. Molecules that have high affinity stick to the wall of the column and migrate more slowly while the ones that have lower affinity migrate more quickly (Fig 7). In order to be analyzed, the molecules in the sample must be first vaporized through a derivatization step. Chemical derivatization processes are complex and not all molecules can be volatilized, which represents the main limitation of GC chromatography (Littlewood 2013).

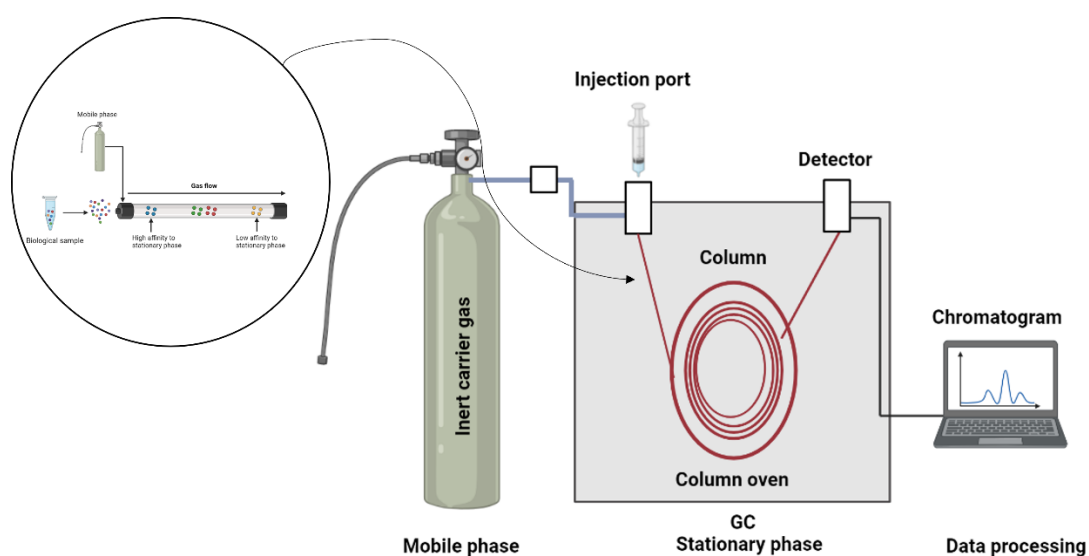


Figure 7. Gas chromatography. In gas chromatography (GC) the mobile phase consists of an inert gas while the stationary phase is a polymer or liquid embedded in a long thin column. The sample is first vaporized and injected into a column. Molecules that have high affinity stick to the wall of the column and migrate more slowly while the ones that have lower affinity migrate more quickly. A derivatization step to volatilize the sample must be done prior GC analysis. Created with Biorender (<https://www.biorender.com/>).

Both, LC and GC chromatographies separate the molecules in a mixture and measure their retention times, which is the time it takes to the analyte to pass through the

column. Molecules have specific retention times and thus this parameter can be used to identify analytes. However, in complex mixtures, different molecules elute from the column at the same time, making it necessary to implement further identification steps to fully identify individual metabolites (Thomas et al. 2022).

(5) *mass spectrometry identification*: once the metabolites in the sample are separated via chromatography techniques, the next step is to further identify them via mass spectrometry (MS). MS is an analytical method that identifies different compounds by their unique mass and fragmentation patterns. A mass spectrometer measures mass-to-charge ratios of ions (De Hoffmann and Stroobant 2007). A general MS process starts with an ionization step. Here, the sample is ionized using a beam of electrons causing it to split into charged ions. Then, these ions go through a mass analyzer where they are separated according to their mass-to-charge ratio by subjecting them to an electric or magnetic field using magnets, quadrupoles, or ion traps. The magnetic or electric field deflect ions in a different way based on their mass. Finally, there is a detector which allows to capture the signal. The final result is a spectrum of the signal intensity of the detected ions as a function of the mass-to-charge ratio (Milman 2015)(Fig 8). Different ionization methods (e.g., electron ionization, electrospray ionization, matrix-assisted laser desorption/ionization (MALDI)) and mass analyzers (Quadrupole, time of flight (TOF), Orbitrap) have been developed (Pitt 2009). They offer different resolutions, sensitivities and throughput and can be selected based on the chemical nature and size of molecules that want to be detected and the study type (targeted or untargeted) (Viant et al. 2019a).

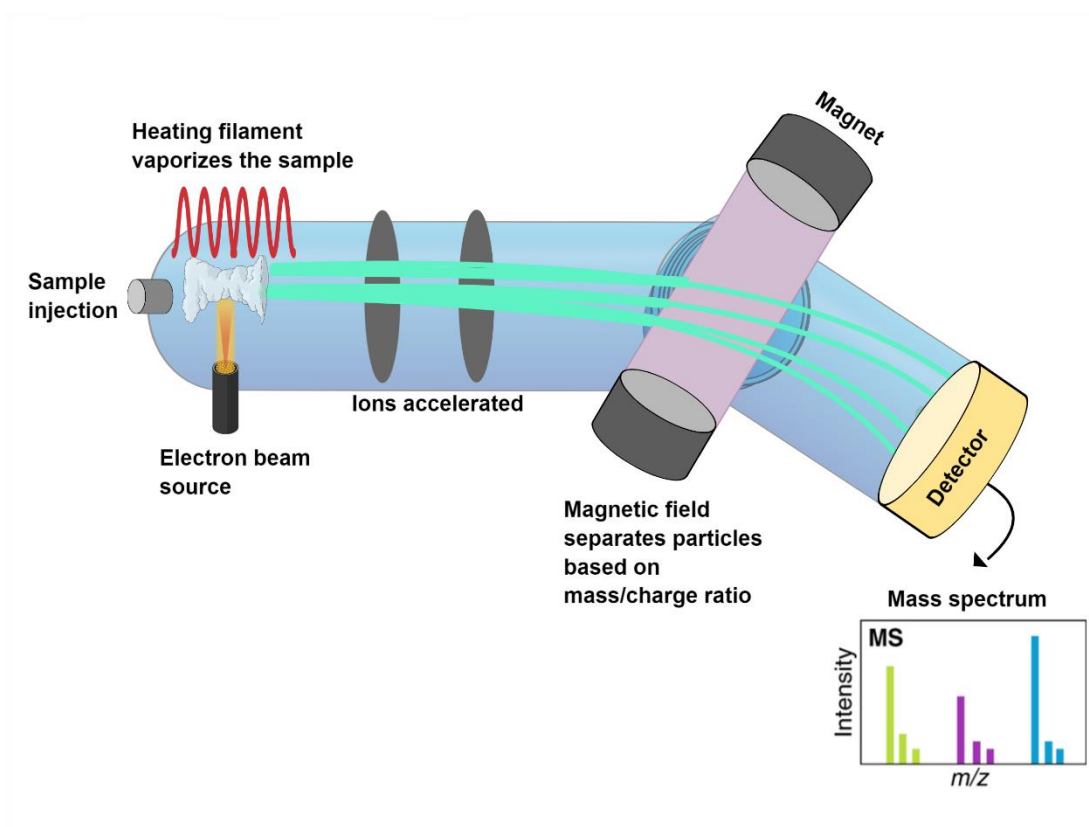


Figure 8. Mass spectrometry. A mass spectrometry process starts with an ionization step where the sample is ionized using a beam of electrons causing it to split into charged ions. These ions go through a mass analyzer where they are separated according to their mass-to-charge ratio by subjecting them to an electric or magnetic field using magnets, quadrupoles, or ion traps. The magnetic or electric field deflect ions in a different way based on their mass. A detector allows to capture the signal and a spectrum of the signal intensity of the detected ions are obtained as a function of the mass-to-charge ratio. Modified from (Chen et al. 2019). Created with Mindthegraph (<https://mindthegraph.com>).

There are two different routes to conduct metabolomics experiments: the targeted and untargeted approach. Untargeted metabolomics aims to thoroughly analyze all the measurable analytes in a sample. With this method, large quantities of data, covering a wide range of metabolites are produced, offering an unbiased exploratory approach that allows unknown molecules in a sample to be discovered. However, the analyte peak annotation is highly challenging and thus untargeted analysis often results in limited comprehensive metabolite identification (Schrimpe-Rutledge et al. 2016). On the other hand, in targeted metabolomics a pre-defined set of metabolites, with known identities, is measured with high confidence and accuracy. This type of analysis offers high precision, sensitivity, and reproducibility; however, the results are limited to a specific metabolite list impeding the identification of new metabolites (Ribbenstedt et al. 2018) (Table 2).

Table 2. Target vs untargeted metabolomics approaches.

Targeted metabolomics	Untargeted metabolomics
Hyphotesis-driven	Hyphotesis generation
Pre-defined list of metabolites	All the metabolites that are measurable
Tuned MS setting	Full scan MS
Limited analytes that can be targeted	Large quantities of data, covering a wide range of metabolites are produced
Optimal sensitivity precision and reproducibility	High resolution but lower sensitivity
Simpler data interpretation and analysis	Challenging metabolite annotation
Analytes ID are known	Many unknown analytes are identified
Correlated to reference standards	Correlated to database/libraries
No data on new analytes can be obtained	Enables discovery of unknown compounds
Semi-quantitative analysis	Offers quantitative analysis (requires purified standards)

In toxicology, untargeted metabolomics strategies have been shown to be valuable hypothesis- generating tools (Crizer et al. 2021b; Malinowska et al. 2023). Monitoring thousands of metabolites in a biological matrix after exposure to a compound can provide a general understanding of the toxic effect (Di Minno et al. 2021). Targeted metabolomics approaches present an improved sensitivity over a smaller set of analytes offering a more quantitative method that can be used to distinguish alterations in metabolite concentrations and offers a detailed characterization of pathways of interest (Griffiths et al. 2010; Olesti et al. 2021; Viant et al. 2019b).

Finally, metabolites represent a wide universe of molecules; they exhibit a broad range of chemical structures and physical properties. In addition, endogenous metabolite concentrations present a large dynamic range of abundance (Ruddigkeit et al. 2012). Therefore, a single analysis cannot provide coverage of the full range of abundance and chemical structures. LC-MS and GC-MS methods are considered complementary, covering a different range and metabolites classes. Liquid chromatography (LC), however, offers a broader coverage and does not require derivatization steps, which makes it advantageous for practical applications (Thomas et al. 2022) (Fig 9).

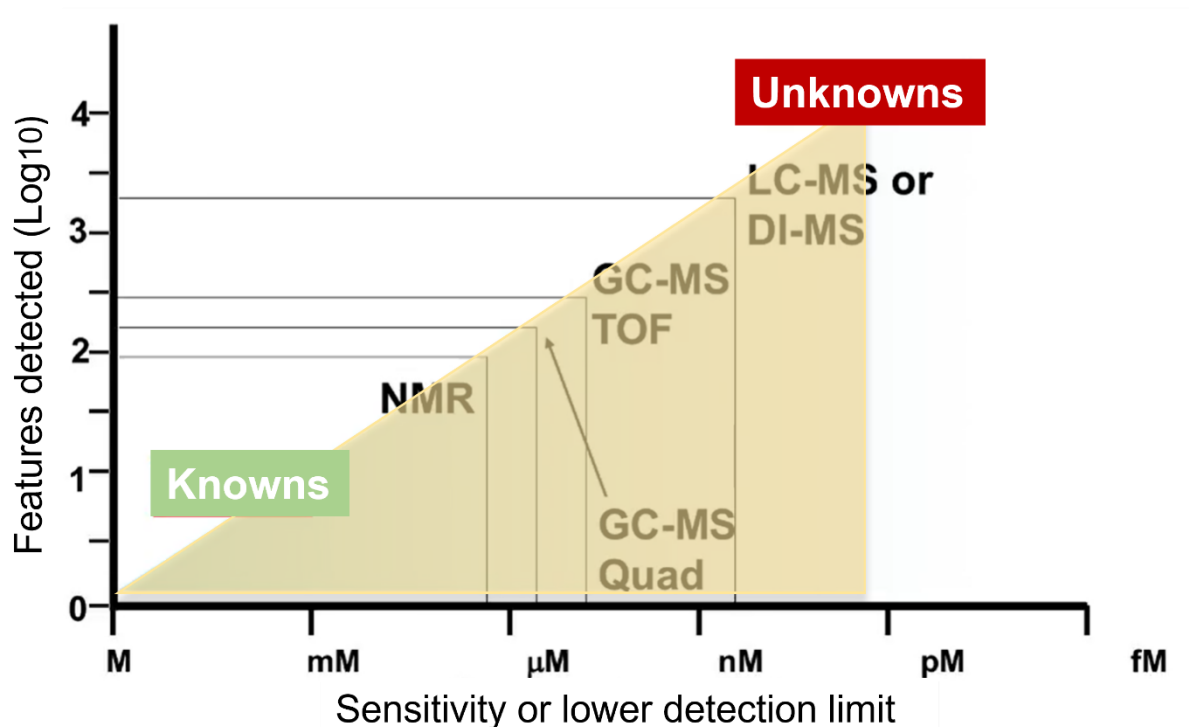


Figure 9. Range of sensitivities of metabolomic technologies. At the lower end of sensitivity or lower detection limit are NMR technologies, suitable for detection of smaller numbers of known metabolites, while at the higher end of sensitivity, LC-MS-based technologies are superior for detection of known as well as unknown metabolites. Modified from (Wishart 2011).

In vitro metabolomics to investigate organ toxicity

Metabolomics is widely established as a tool in biomedical research for disease diagnosis, biomarker detection and identification of altered metabolic pathways (Ramirez et al. 2013). Initial investigations showed that chemicals or diseases that produce a specific form of toxicity, generally through a shared mode of action (MoA), cause a subset of common specific metabolite changes (Van Ravenzwaay et al. 2007; Van Ravenzwaay et al. 2015). Such a common set of consistently regulated metabolites could be used to establish metabolic patterns specific for certain toxicities. Metabolite profiling has been successfully implemented for over a decade to identify and predict toxicological mechanisms in rodent studies (Kamp et al. 2012; Ravenzwaay et al. 2015; Van Ravenzwaay et al. 2014).

Importantly, metabolomics-based approaches have been compared side by side to classical toxicology (Van Ravenzwaay et al. 2014). After exposing rodents to different herbicides, readouts from metabolomics analysis were compared to classical apical endpoints observation in animals. This study showed that there was a good agreement between affected organs and no observed effect levels (NOAEL) determined by both approaches, demonstrating the potential of metabolomics approaches to predict adverse effects *in vivo* (Van Ravenzwaay et al. 2014).

Multiple studies have evidenced the potential of metabolomics as a promising tool for toxicology applications such as identifying and characterizing mechanisms of toxicity (Mattes et al. 2014; Van Ravenzwaay et al. 2015), performing biologically based chemical grouping and read across by showing mechanistic similarities between new and model substances (Van Ravenzwaay et al. 2016), and deriving points of departure (POD) for risk assessment (Malinowska et al. 2023). Recently, metabolomics approaches have been used in combination with *in vitro* models to expand the investigation of organ toxicity (Birk et al. 2021; Cuykx et al. 2018a; García-Cañaveras et al. 2016; Huang et al. 2021; Jeon et al. 2021; Ramirez et al. 2018a).

The use of metabolomics *in vitro* presents the powerful combination of a human relevant system with a multiparametric approach that allows assessing multiple endpoints in a single biological sample. Applying metabolomics in a cell-based system offers an alternative to both, the ethical concerns and relevance of animal testing and the restraining nature of single endpoint evaluations characteristic of conventional toxicological *in vitro* assays. Several studies with cell lines have successfully used *in vitro* metabolomics to identify and study different modes of action postulating metabolomics as a valuable tool for organ toxicity assessment (Birk et al. 2021; Cuykx et al. 2018a; García-Cañaveras et al. 2016; Gerdemann et al. 2022; Ramirez et al. 2018a).

In vitro metabolomics experiments, however, are usually costly, very labor intensive and need a large amount of cell material when compared to simple single endpoint *in vitro* assays (Cuykx et al. 2018b; Ramirez-Hincapie et al. 2023). Usually, metabolomics studies require a minimum of one million cells per sample and thus, experiments are carried out in relatively large containers such as culture flasks, 6- or 12 well-plates. Assays in these types of containers are not amenable for automatization, require large quantities of reagents and test compound

and demand extensive manual handling which represents elevated costs and highly limits the number of compounds and concentrations that can be tested (Cuykx et al. 2018a; García-Cañaveras et al. 2016; Ramirez et al. 2018b). These factors have critically limited *in vitro* metabolomics throughput and scalability and have prevented the actual implementation of this powerful technique in large scale screening analysis, compound development pipelines and chemical risk assessment.

Aim 1: the first aim of this dissertation is to increase the *in vitro* metabolomics throughput by developing a cost-effective high throughput 96-well-plate *in vitro* metabolomics platform for hepatotoxicity characterization (Chapter 2).

Metabolomics technologies in Next Generation Risk Assessment

The aim of regulatory toxicology is to prevent chemical substances and products from producing adverse effects on human health and environment. This requires the evaluation of the potential harm intrinsic to the substance (hazard assessment), together with the evaluation of the human exposure scenario. Hence, chemical risk assessment requires knowledge of both, the hazard and exposure (Eisler 2000) (Fig 10).

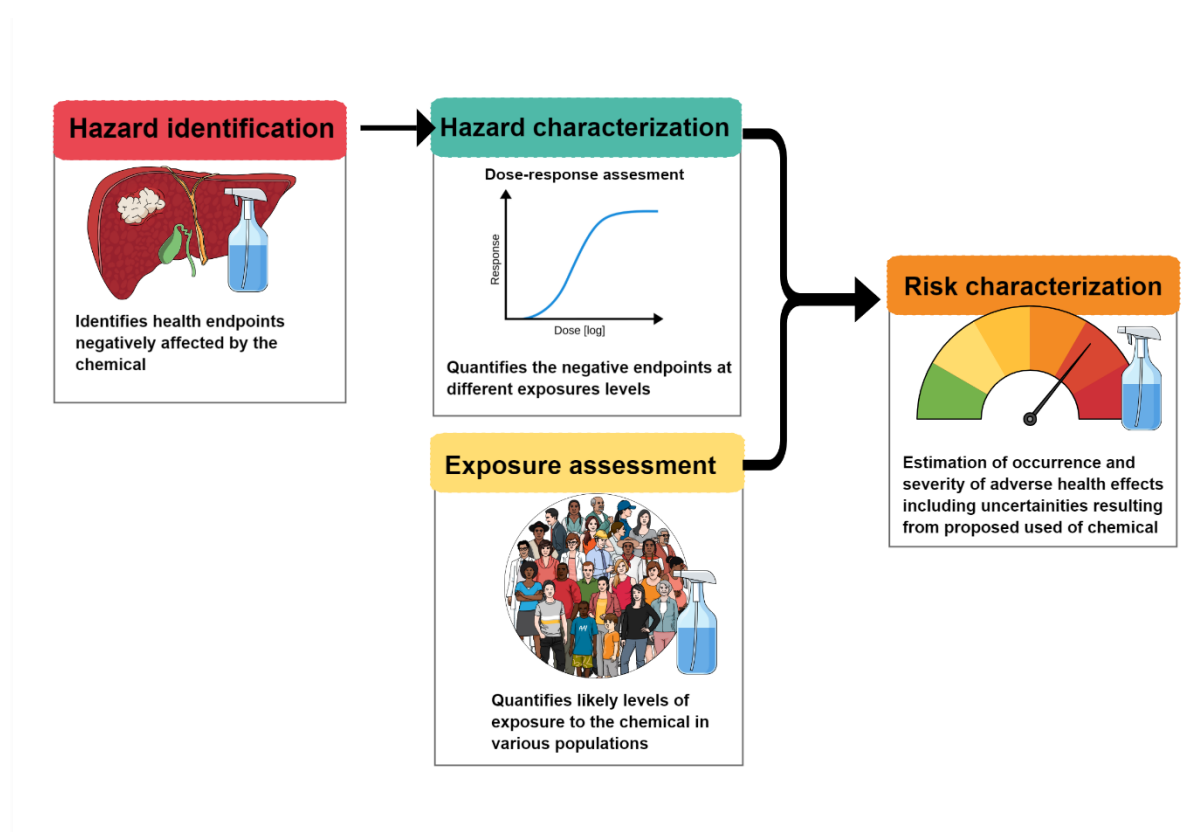


Figure 10. Risk assessment process. A chemical risk-assessment process consists of four general steps: (1) hazard identification, (2) dose-response assessment, (3) exposure assessment, and finally combining the information from the previous steps for the (4) risk characterization. Created with Mindthegraph (<https://mindthegraph.com>).

The ultimate goal of a risk assessment process is to determine reference values, expressed in mg/kg bw, which are safe for humans e.g., tolerable daily intake (TDI), acceptable daily intake (ADI), reference dose (RfD) for oral exposures and, reference concentration (RfC) for inhalation exposures (Greim and Snyder 2018). Traditionally, animal studies have been used to derive reference values by establishing the lowest dose at which an effect is observed via the no-observed-adverse-effect level (NOAEL) or lowest-adverse-effect level (LOAEL) approach together with the inclusion of several safety factors (usually 10-fold) that aim to compensate for uncertainties such as intra- and inter-species differences (Council 2007).

As previously mentioned, in the current scenario of growing number of compounds and rigorous regulations that intend to guarantee a toxic free environment, innovative methodological approaches, that do not require the use of animals, are needed to conduct a faster and more accurate health and environmental risk assessment. As part of the Toxicology

of the 21st century vision, it was anticipated that PODs for establishing human exposure guidelines in future risk assessments will increasingly be based on *in vitro* high-throughput screening (HTS) data (National Research Council 2007). Next generation risk assessment (NGRA) has been proposed as an exposure-led, hypothesis-driven alternative approach that aims at incorporating non-animal methodologies (NAM's) including the combination of different tools such as *in vitro* methods, computational analysis, systems biology and, Omics technologies for chemical safety decision-making (Pallocca et al. 2022). Yet, interpreting and extrapolating data from NAM'S into human relevant values, represents one of the major challenges for NGRA implementation (Marx-Stoelting et al. 2023).

For data generated using NAM's, the starting point for the determination of reference values includes the derivation of a point of departure (POD) from dose–response modelling (Paini et al. 2019). The point of departure refers to the point on a dose-response curve, established from experimental data, corresponding to an estimated low effect level (e.g., 1% to 10% incidence of an effect) (Bercu et al. 2016). Both NOAEL and statistical benchmark dose (BMD) can be used as point of departure (POD) to derive human reference values (Filipsson et al. 2003). A benchmark response represents a predetermined response level, generally set as a 10% increase in a specific adverse endpoint (e.g., number of tumours) for dichotomous responses or a 10% increase from controls for continuous responses (e.g., reduction in cell viability). The BMD method is statistically more powerful than the NOAEL and therefore is internationally recognized as the preferred approach for POD derivation and implemented in official Guidance Documents (Davis et al. 2011; EFSA et al. 2022; Filipsson et al. 2003; More et al. 2022).

Due to their multiparametric nature, Omics technologies allow to measure multiple endpoints and pathways simultaneously, representing a more informative alternative than traditional *in vitro* studies for PODs. The potential of Omics technologies for determining point of departures (PoD) has been highlighted. Initially, mainly data generated from transcriptomics studies were used to derive benchmark doses in order to identify concentration at which cellular processes were disrupted (Thomas et al. 2007). For *in vitro* experiments, the term “dose” is replaced by “concentration”. Several studies have shown that Benchmark concentrations (BMCs) for transcriptional changes obtained from *in vitro* studies can be concordant with BMCs for apical *in vivo* endpoints, including cancer and organ toxicity

assessment (Bourdon-Lacombe et al. 2015; Farmahin et al. 2017; Gwinn et al. 2020; Program 2018).

More recently, the implementation of metabolomics data for POD derivation has been explored. In two recently published studies, concentration-response analysis derived from untargeted *in vitro* metabolomics were used for benchmark concentration (BMC) modelling. These investigations demonstrated that metabolomics derived PODs can be used as sensitive and quantitative indicators of liver injury potential (Crizer et al. 2021b; Malinowska et al. 2023). However, these approaches were based on BMD calculation for single features and lack comprehensive metabolite annotations which hampers data interpretation. The lack of metabolite identification, characteristic of untargeted methods, challenges the biological interpretations of the results hampering the assessment of the relevance and applicability of these data in safety assessment.

Aim 2: the second aim of this dissertation is the implementation of *in vitro* metabolomics to determine dose- and time response metrics to derive a PoD suitable for human risk

Liver as one of the main target organs in toxicity studies

Each substance that gets in contact with the organism has the potential to affect different organ systems. As the primary organ connecting the intestinal track with the circulatory system, almost every substance absorbed by the body passes through the liver, rendering liver cells highly exposed to significant concentrations of external chemicals (Klaassen and Amdur 2013). Importantly, the liver is the primary site of metabolization and detoxification of exogenous compounds. Consequently, due to its particular anatomical location and its central role in detoxification, biotransformation and elimination of compounds, the liver is one of the most frequent target organs of chemical toxicity (Gu and Manautou 2012).

A comprehensive understanding of the liver's complex anatomy and physiology is essential to develop suitable alternative methods to detect liver toxicity. Located in the right upper quadrant of the abdomen, the liver is the largest internal organ in the body. It is grossly

divided in the right and left lobe, the right being about six times the size of the left and subdivided in the caudate and quadrates lobes (Kiernan 1833) (Fig. 11). Importantly, the liver has a double blood supply; through the portal vein, the liver receives all circulation coming from the small and large intestine and well as spleen and pancreas. This blood is enriched in nutrients and absorbed xenobiotics, but it is low in oxygen. On the other hand, the hepatic artery transports oxygen-rich blood from the aorta. The gallbladder, located beneath the liver, receives and stores bile produced by the liver through the common hepatic duct and releases it through the bile duct in the duodenum where it helps in the digestion of fats (Kiernan 1833).

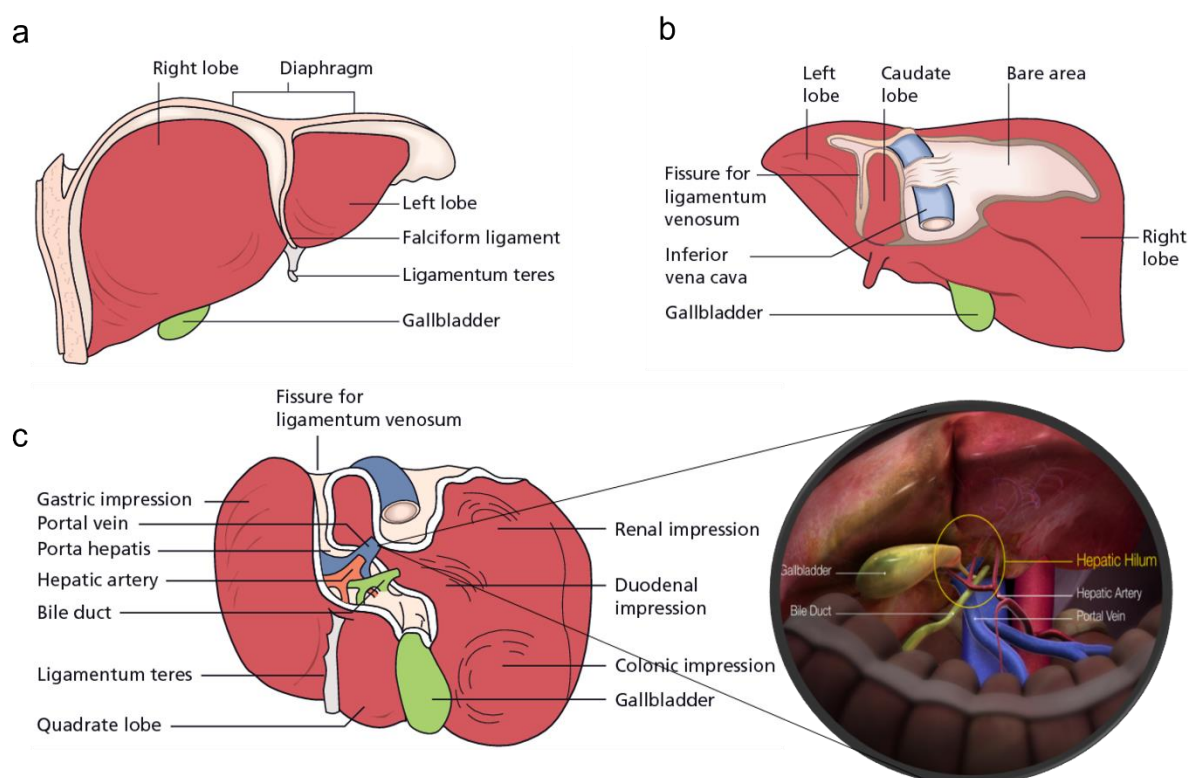


Figure 11. Gross liver anatomy. a) anterior view, b) posterior view, c) inferior view with zoom into the portal triad. Modified from (Dooley et al. 2018).

At a microscopic scale the liver is divided in hepatic lobules, presenting a characteristic hexagonal structure which consist of lines of hepatocytes radiating from the portal vein towards the portal triad (comprising the hepatic artery, bile duct and a portal vein) (Fig.12). These lines of hepatocytes are separated by vascular channels known as hepatic sinusoids (Klaassen and Amdur 2013). The acinus denotes the functional units of the liver and divides it by its metabolic zonation: the specific functions of the hepatocytes based on the differential oxygen and nutrients supply. The acinus is formed by a diamond-shape space that contains

two adjacent central veins and two adjacent portal triads (Fig. 12) and it is divided in three zones: zone 1 is closer to the portal triad. Hepatocytes in this zone are near to the entry of blood and therefore receive high oxygen supply and are specialized in oxidative functions such as gluconeogenesis, β -oxidation of fatty acids and cholesterol synthesis. Zone 3 is closer to the central vein which carries blood rich in nutrients and xenobiotics but is low in oxygen. In this zone, functions such as glycolysis, lipogenesis, and cytochrome P450 drug detoxification take place. Zone 2 is represented by the intermediate space between zone 1 and 3 (Lamers et al. 1989) (Fig. 12).

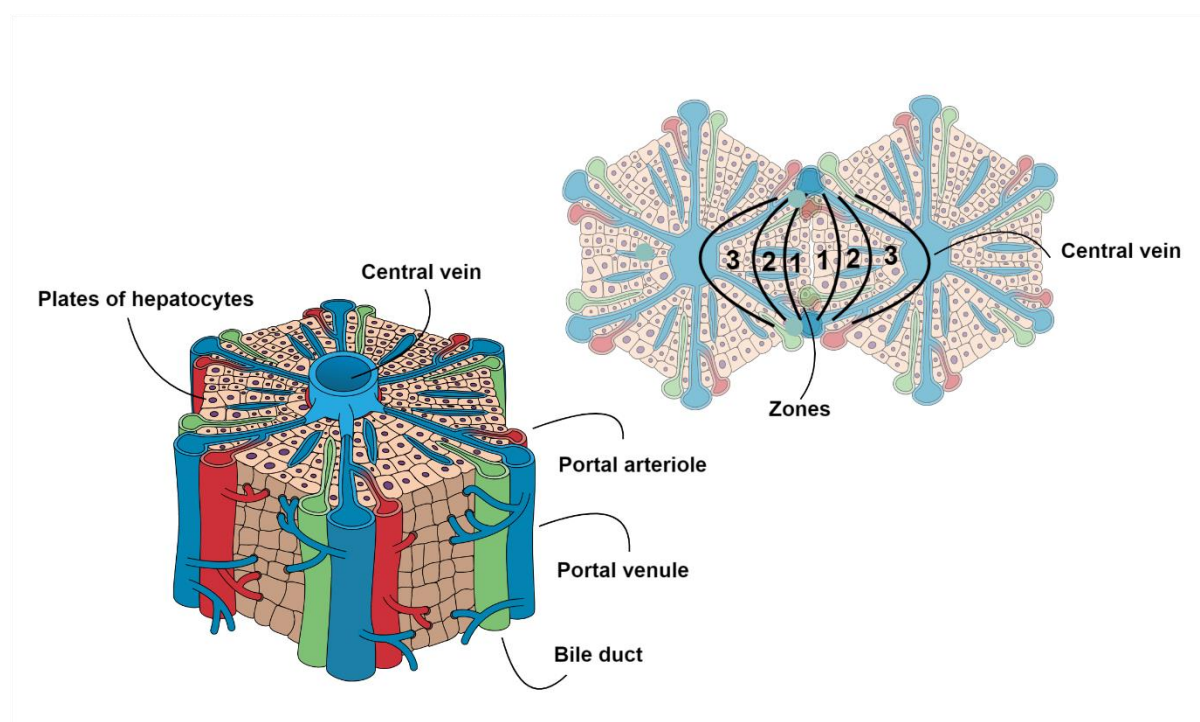


Figure 12. Microscopic liver anatomy. Liver hepatic lobule (left) and liver acinus (right) denoting metabolic zonation. Created with Mindthegraph (<https://mindthegraph.com>).

The liver is composed of a wide variety of cell types which can be differentially affected by toxicants, making it a challenging organ to study in *in vitro* systems. Hepatocytes, are the most abundant and metabolically active cells, comprising about the 80% of the total cell numbers in the liver. They are responsible for key hepatic functions such as glucogenesis, glycogenolysis, the production of cholesterol, bile salts and clotting factors. Importantly, hepatocytes contain enzymes that are essential for the xenobiotic metabolism, detoxification, and inactivation of exogenous chemicals (Mitra and Metcalf 2009). Besides hepatocytes, non-parenchymal cells also play important roles for hepatic fiction. Some of the major liver non-

parenchymal cells are cholangiocytes, stellate cells, Kupffer cells and endothelial cells (Bouwens et al. 1992). Cholangiocytes are epithelial cells from the bile duct which participate in the transport and modification of bile (Tabibian et al. 2013). Hepatic stellate cells store vitamin A and play a key role in the formation of scar tissue in response to liver damage via the activation of collagen synthesis (Senoo 2004). Kupffer cells are immune cells that act as macrophages cleaning the blood of pathogens, these cells are major sources of cytokines and can act as antigen presenting cells (Bilzer et al. 2006). Finally, endothelial cells form the wall of the blood vessels in the liver and represent a permeable barrier between the bloodstream and the parenchyma that facilitates the exchange of molecules such as albumin and lipids and play an important role in immunological functions through the secretion of different signal molecules such as cytokines (Poisson et al. 2017).

The liver plays a central role in maintaining the metabolic homeostasis of the body and it has been estimated that this organ is involved in performing numerous functions such as regulating the metabolism of carbohydrate, lipids, and proteins, the secretion and production of bile, which is essential for the absorption of fat and lipophilic nutrients, the storage of vitamins, minerals and sugar, the synthesis of important plasma proteins such as albumin and globulin and the breakdown of hormones such as insulin (Mitra and Metcalf 2009). One of the most prominent physiological functions of the liver is the metabolization of external substances. Xenobiotic metabolization consist of a biotransformation process in where exogenous compounds are converted into more polar products to facilitate their elimination from the body (Klaassen and Amdur 2013). The process of substance metabolism is divided into 3 phases. In phase I the compound is made polar by functionalization reactions such as oxidation, hydroxylation and reduction reaction so it can be excreted from the body. Importantly, the cytochrome P450 enzymes catalyze most of the reactions in the phase I and as such, any alteration of these enzymes can modify the detoxification or bioactivation of exogenous compounds. As a result of the phase I metabolism, functional groups are introduced forming a polar molecule known as primary metabolite. However, some of these intermediate products are highly reactive and harmful molecules that can finally cause liver injury. For facilitating the excretion of the chemicals compounds, the formed metabolites undergo phase II metabolism reactions where these molecules are coupled with functional groups such as acetate, glutathione, and sulfate, resulting in harmless secondary metabolites.

Finally, in phase III metabolism, compounds with high molecular weight are excreted via specific transporters in the bile while smaller and water-soluble molecules are excreted through the kidneys (Almazroo et al. 2017).

Due to its crucial roles in preserving the body homeostasis and in xenobiotic metabolization, damages and losses of liver functions as a consequence of toxicant exposure can result in serious detrimental effects in the whole organism (Bischoff et al. 2018). For this reason, the early identification of potential hepatotoxins is highly relevant for the pharmaceutical and chemical industry representing one of the main causes of safety concerns in preclinical and chemical risk assessment studies (Food and Administration 2009; Serrano 2014). In addition, liver toxicity has important public health and economic implications; adverse effects on the liver represent one of the most frequently reason for discontinuing the development of compound candidates (Babai et al. 2021; Waring et al. 2015). In the pharmaceutical industry, Drug induced liver toxicity (DILI) represents the leading cause of post approval compound withdrawals (Onakpoya et al. 2016).

In summary, hepatotoxicity represents a major health and economic issue and thus is of primary concern in compound development. In the current scenario of highly elevated toxicity testing demand, there is a requirement for test systems that reliably detect hepatotoxicity of compound candidates while reducing discovery time, cost, and the number of animal experiments. The implementation of methods that allows compound prioritization based on biological and physiological relevant information would reduce health hazards and improve cost efficacies for the industry.

***In vitro* models to investigate hepatotoxicity**

Animal testing has long been, and still is, the base for risk assessment and is required by regulatory authorities for organ toxicity studies (OECD guidelines). Yet, the liver is an organ with pronounced species differences in in xenobiotic metabolism particularly regarding the expression and enzymatic activities of pharmacokinetics factors such as absorption, distribution, metabolism, and excretion of (ADME)(Dalgaard 2015; Lin 1995). In a survey study which included input from 12 pharmaceutical companies with data collected from 150

compounds, the concordance of hepatotoxicity findings between animal studies and observed human toxicity was only 55% (Olson et al. 2000). This type of studies has demonstrated that animal models do not accurately characterize the etiology and pathogenesis of human liver injury and have evidenced a clear need for predictive models which better reflect human liver physiology and function.

In order to minimize the health risk and financial losses resulting from chemicals and pharmaceuticals hepatotoxicity, considerable efforts have been directed to the development of human cell-based assays for the early detection and evaluation of liver toxicity (Beger et al. 2010; Martínez-Sena et al. 2023; Mirahmad et al. 2022; Schadt et al. 2015; Walker et al. 2020; Yong et al. 2020). *In vitro* models offer major advantages over animal-based studies such as a highly controlled experimental conditions in which compounds' mechanisms of action can be studied, the implementation of material from human sources and the possibility of being implemented in a high throughput scale (Cuykx et al. 2018b; Pelecha et al. 2021; Villeneuve et al. 2019). Through the improved toxicological knowledge offered by *in vitro* methods during early stages of product development, increased efficiencies can be achieved; candidate compounds can be selected based on their toxicological profiles optimizing resource such as time, test compound and costs and minimizing unnecessary animal utilization (Ramirez-Hincapie et al. 2023).

Different liver models including primary human hepatocytes (PHH), liver slices, immortalized cell lines and hepatocyte-like cells have been used in hepatotoxicity assessment. Primary human hepatocytes (PHH) are considered the gold standard for *in vitro* liver studies. They exhibit hepatic functions and metabolic activities close to the *in vivo* situation (Gomez-Lechon et al. 2004). However, PHH are difficult to maintain in culture conditions, rapidly losing their functionality and viability, limiting their use. In addition, some of the major obstacles for the use of PHH are their limited availability (sourced from human liver biopsies) and their high inter-donor variability which hampers the reproducibility of the results (Ruoß et al. 2020). In contrast, liver slices offer a preserved liver architecture and the presence of different non-parenchymal cells such as Kupffer, endothelial, and hepatic stellate cells (Palma et al. 2019). However, comparable to PHH, liver slices are obtained from human liver tissue extracted from surgical procedures, limiting their availability, and exhibiting inter-donor variability. In

addition, they also undergo a rapid lost in viability and metabolic capacities (De Graaf et al. 2010).

As an alternative to PHH and liver slices, immortalized tumor cell lines have been widely used in toxicological studies. Due to its unlimited lifespan, stable phenotype, high availability, reproducibility, easy handling, and low cost, immortalized/tumor cell lines such as HepG2 and HepaRG have represented a valuable alternative for hepatotoxicity evaluations (Castell et al. 2006). The HepaRG cell line, is a human progenitor cell line capable of differentiating in biliary-like and hepatocyte-like cells. This cell line presents the advantages of physiologically relevant expression of important xenobiotic metabolizing enzymes particularly from phase II metabolism and transporters (Guo et al. 2011; Marion et al. 2010). However, the differentiation protocols can introduce variability and appropriate media is needed for maintaining a stable phenotype (Ramirez et al. 2018a).

The HepG2 cell line is the most commonly used and best characterized human hepatic cell line, showing many differentiated hepatic functions e.g., synthesis and secretion of plasma proteins, cholesterol and TG metabolism, lipoprotein metabolism and transport, bile acid synthesis, glycogen synthesis and insulin signaling (Guo et al. 2011; Jennen et al. 2010). These factors, together with their high proliferation rate and human origin make them a good option for large-scale experiments such as high throughput screenings and compound prioritization (aim 1 and 2) (Saito et al. 2016). However, the HepG2 limitations are well recognized (Gerets et al. 2012); this cell line exhibits limited drug metabolizing and transport capabilities, such as substantial low levels of phase I and phase II metabolism enzymes, failing to faithfully recapitulate liver physiology and functionality.

Aim 3: the third aim of this dissertation is the application and evaluation of *in vitro* metabolomics using iPSC-derived 3D liver organoid system as a human physiologically more relevant alternative for toxicology studies (Chapter 4).

The rapid development of protocols for the generation of induced pluripotent stem cells (iPSC), have fostered the application of stem cells in pharmacological and toxicological studies (Fritsche et al. 2021). iPSC presents several characteristics that make them highly

advantageous for the development of predictive *in vitro* systems: they can be obtained from any cell type and various donors, making them representative of phenotypic and genetic variations in population, they have unlimited availability and can be differentiated in virtually any cell type, allowing the development of models that combine hepatocytes with non-parenchymal cell such as stellate cells, endothelial cells and Kupffer cells which have been shown to play important roles in liver disease (Carberry et al. 2022; Zhang et al. 2021). Even though iPSCs are one of the most promising tools for elucidating human development and disease and have shown great potential for developing *in vitro* toxicological systems, they require complex culture conditions, present high variability, need extensive differentiation protocols and a require a detailed characterization in order to confidently identify mature and specific cell types (Suter-Dick et al. 2015).

Hepatic models were initially implemented in 2D cultures (monolayers). However, it is now broadly recognized that 2D cell cultures comprise static monolayers that lack critical architectural and biomechanical properties of the native tissue such as cell to cell interactions (Langhans, 2018). Thus, in order to overcome the limitations of 2D systems and better recapitulate the liver physiology, PHH, cell lines and iPSCs have been assembled in 3D structures and organoid models that mimic *in vivo* tissue and combine hepatocytes with various non-parenchymal cells that play important roles in liver functions and hepatotoxicity (Underhill and Khetani 2018).

In the last years, complex *in vitro* toxicity models (e.g., three-dimensional (3D) organoid models, hiPSCs derived systems, organ-on-a-chip platforms) addressing systemic toxicity endpoints have been developed (King et al. 2017; Plummer et al. 2019; Richards et al. 2020; Shinozawa et al. 2021). Despite the advantage they offer, the limited throughput, complexity, and high cost of these sophisticated *in vitro* models reduce their applicability. Therefore, there will always be a tradeoff between the complexity and completeness of an *in vitro* model and the feasibility, efficiency, and throughput (Fig.). What simple assays miss regarding physiological similarity they gain from the higher number of replicates, ease of interpretation of results, and reproducibility (Rossini and Thomas 2012). Thus, complexity does not always translate in better results.

In essence, the development and implementation of *in vitro* toxicological tests mainly rely in the scope of the question to be addressed. Different use scenarios require higher degrees of sophistication, varying from complex organotypic cultures to closely estimate human physiological reactions, to high-throughput tests that require simplicity and robustness to perform initial compound screenings (Rossini and Thomas 2012). In all cases the benefits but also the limitations of the model must be analyzed carefully and considered in the assessment of the obtained data.

Dissertation aims

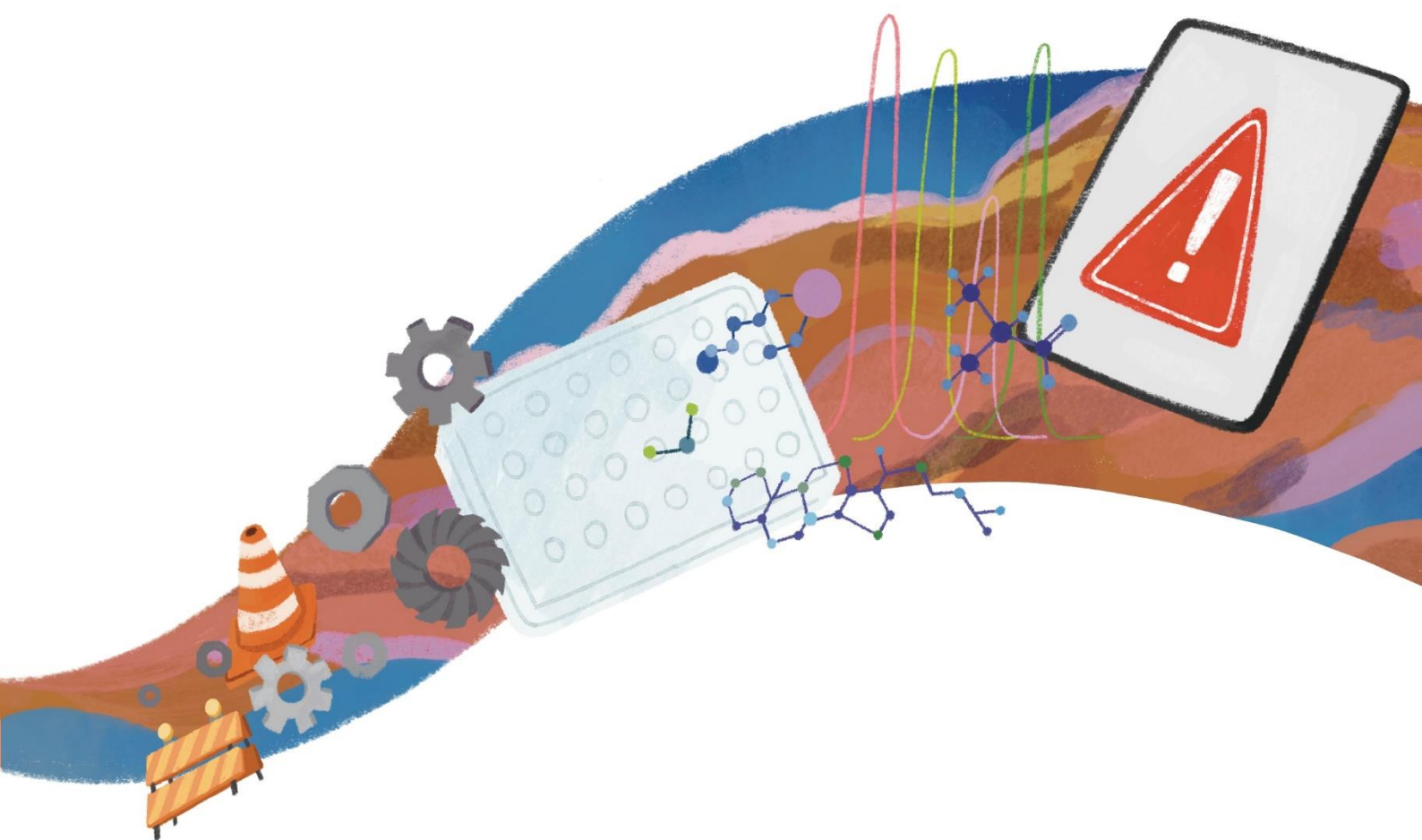
The overarching aim of the present work is to advance the applications of *in vitro* metabolomics in toxicology by addressing 3 major challenges that have limited its widespread implementation in the field. 1) Due to technical and economical limitations, *in vitro* metabolomics **throughput** and cost effectiveness has remained low, which has hampered its large-scale implementation in compound development and research 2) although *in vitro* metabolomics has been implemented as a research tool for toxicological assessment and hazard characterization, the application of metabolomics data for **risk assessment** in regulatory toxicology has been limited up to date. Lastly, 3) in order to increase the reliance and confidence of using *in vitro* metabolomics data for human risk assessment, the third challenge is to increase the **human relevance** of *in vitro* assays by implementing systems that more closely recapitulate the organ physiology and cell composition.

Therefore, this dissertation seeks to tackle each of the above-mentioned challenges by 3 corresponding specific aims.

- 1) **Aim 1:** development of a cost-effective high throughput 96-well-plate *in vitro* metabolomics platform for hepatotoxicity characterization (Chapter 2).
- 2) **Aim 2:** implementation of *in vitro* metabolomics to determine dose- and time response metrics to derive PoD for human risk assessment (Chapter 3).
- 3) **Aim 3:** application and evaluation of *in vitro* metabolomics in a 3D liver organoid system as a human physiologically relevant alternative for toxicology studies (Chapter 4).

Chapter 2

A high-throughput
metabolomics *in vitro* platform
for the characterization of
hepatotoxicity



Preamble

The early mechanistic-based identification of potential hepatotoxins and compound MoA screening is a highly relevant issue for the pharmaceutical and chemical industry and academia. Recent studies have highlighted the combination of multiparametric Omics technologies such as metabolomics and human cell-based *in vitro* systems as a powerful tool for elucidating the molecular and biochemical events underlying organ toxicity (citation). However, current *in vitro* metabolomics experiments remain expensive, time consuming and complex, which has limited its throughput scalability and application as a screening system in compound development.

The following manuscript presents the method development and proof of concept evaluation of a highly standardized, 96-well plate targeted LC-MS-based *in vitro* metabolomics screening platform for the identification and classification of liver toxicity MoAs in HepG2 cells. The assay presented here, is one of the first approaches that miniaturizes *in vitro* metabolomics methods for high throughput toxicological assessment. Following the OECD guidance documents on good *in vitro* method practices (GIVIMP) (cite) and the Metabolomics Reporting Framework (MRF)(Viant et al. 2019a), different parameters of the workflow such as cell seeding density, influence of passage number, cytotoxicity testing, sample preparation, metabolite extraction, analytical method and data processing were optimized to perform with low biomass samples. For the proof of concept, seven compounds with three different known hepatotoxicity Modes of action (MoA) were tested in five concentrations to test the applicability of the system. Overall, the results showed that, by using the developed system, a dose-dependent response of the metabolic effects and a clear differentiation between different liver toxicity MoAs can be obtained. Importantly, the metabolomics experiments carried out in this investigation led to the identification of metabolite patterns specific for each tested MoA. Key metabolites indicative of both, general and mechanistic specific hepatotoxicity were identified and discussed.

Due to the considerable resources reduction and throughput increase achieved with this assay, the developed metabolomics *in vitro* platform allows assessing a broader range of concentrations. This factor would enable a more accurate metabolome-based point of

Chapter 2: publication I

departure (PoD), *in vitro* to *in vivo* extrapolations (IVIVE) and substance kinetic analysis. This method offers a workflow that can be extended to further cell lines and iPSCs for the investigation of different organ toxicities and is suitable for a wide range of screening applications that demand rapid, cost effective and high throughput analysis.

The recently developed metabolomics *in vitro* platform is currently being used by BASF SE for the evaluation of hepatotoxicity within the frame of the European Research and Innovation project EU-TOX RISK, funded under the European Commission's Horizon 2020 programme, and the German Bundesministerium für Bildung und Forschung (BMBF) funded SysBiotopMoving project.

The following publication was prepared in collaboration with 15 co-authors. The experimental work, analysis of the data and the paper writing was done by the author of this dissertation. The co-authors were involved in the planning of the experiments, scientific discussion and guidance, the bioinformatics data analysis and significantly in the review process of the publication.

Publication I: A high-throughput metabolomics *in vitro* platform for the characterization of hepatotoxicity

Full citation:

Ramirez-Hincapie S, Birk B, Ternes P, Giri V, Haake V, Herold M, Zickgraf FM, Verlohner A, Huener H, Kamp H, Driemert P, Landsiedel R, Richling E, Funk-Weyer D, van Ravenzwaay B (2023) A high-throughput metabolomics *in vitro* platform for the characterization of hepatotoxicity. *Cell Biology and Toxicology*:1-19 doi:10.1007/s10565-023-09809-6.

This project received funds from SysBioTop Moving (BMBF, 161L0243A) and EU-Tox Risk (European Union 's Horizon 2020 research, No 681002).

<https://doi.org/10.1007/s10565-023-09809-6>

RESEARCH



A high-throughput metabolomics in vitro platform for the characterization of hepatotoxicity

Sabina Ramirez-Hincapie · Barbara Birk · Philipp Ternes · Varun Giri · Volker Haake · Michael Herold · Franziska Maria Zickgraf · Andreas Verlohner · Hans-Albrecht Huener · Hennie Kamp · Peter Driemert · Robert Landsiedel · Elke Richling · Dorothee Funk-Weyer · Bennard van Ravenzwaay

Received: 14 December 2022 / Accepted: 27 April 2023
© The Author(s) 2023

Abstract Cell-based metabolomics provides multiparametric physiologically relevant readouts that can be highly advantageous for improved, biologically based decision making in early stages of compound development. Here, we present the development of a 96-well plate *LC-MS/MS*-based targeted metabolomics screening platform for the classification of liver toxicity modes of action (MoAs) in HepG2 cells. Different parameters of the workflow (cell seeding

density, passage number, cytotoxicity testing, sample preparation, metabolite extraction, analytical method, and data processing) were optimized and standardized to increase the efficiency of the testing platform. The applicability of the system was tested with seven substances known to be representative of three different liver toxicity MoAs (peroxisome proliferation, liver enzyme induction, and liver enzyme inhibition). Five concentrations per substance, aimed at covering the complete dose-response curve, were analyzed and 221 uniquely identified metabolites were measured, annotated, and allocated in 12 different metabolite

Supplementary Information The online version contains supplementary material available at <https://doi.org/10.1007/s10565-023-09809-6>.

S. Ramirez-Hincapie (✉) · B. Birk · V. Giri · F. M. Zickgraf · A. Verlohner · H.-A. Huener · R. Landsiedel · D. Funk-Weyer
BASF SE, Experimental Toxicology and Ecology, Ludwigshafen, Germany
e-mail: sabina.ramirez-hincapie@basf.com

B. Birk
e-mail: barbara.birk@basf.com

V. Giri
e-mail: varun.giri@basf.com

F. M. Zickgraf
e-mail: franziska-maria.zickgraf@basf.com

A. Verlohner
e-mail: andreas.verlohner@basf.com

H.-A. Huener
e-mail: hans-albrecht.huener@basf.com

R. Landsiedel
e-mail: robert.landsiedel@basf.com

D. Funk-Weyer
e-mail: dorothee.funk-weyer@basf.com

P. Ternes · V. Haake · M. Herold · H. Kamp · P. Driemert
BASF Metabolome Solutions GmbH, Berlin, Germany
e-mail: philipp.ternes@basf.com

V. Haake
e-mail: volker.haake@basf.com

M. Herold
e-mail: michael.a.herold@basf.com

H. Kamp
e-mail: hennie.kamp@basf.com

P. Driemert
e-mail: peter.driemert@BASF.com

R. Landsiedel
Free University of Berlin, Pharmacy, Pharmacology and Toxicology, Berlin, Germany

Published online: 04 May 2023

Springer

classes such as amino acids, carbohydrates, energy metabolism, nucleobases, vitamins and cofactors, and diverse lipid classes. Multivariate and univariate analyses showed a dose response of the metabolic effects, a clear differentiation between liver toxicity MoAs and resulted in the identification of metabolite patterns specific for each MoA. Key metabolites indicative of both general and mechanistic specific hepatotoxicity were identified. The method presented here offers a multiparametric, mechanistic-based, and cost-effective hepatotoxicity screening that provides MoA classification and sheds light into the pathways involved in the toxicological mechanism. This assay can be implemented as a reliable compound screening platform for improved safety assessment in early compound development pipelines.

Keywords Metabolomics · Toxicology in vitro · Toxicometabolomics · Mode of action · Liver toxicity · Hepatotoxicity · High throughput

Introduction

Toxicological assessment is a critical step in chemical and drug development pipelines. The increasing number and complexity of candidate compounds keep challenging conventional toxicity evaluation procedures (Wang et al. 2020). In addition, the consecutive implementation of stringent regulatory frameworks (REACH EC No. 1907/2006, European Cosmetics Act EC No. 1223/2009, chemical strategy toward sustainability COM/2022) aiming to ensure human safety and environmental sustainability of both new and existing substances have resulted in increased testing needs (Crawford et al. 2017; van Dijk et al. 2021). Thus, to warrant the continued production and the development of new safe and sustainable chemicals, reliable, cost-effective, and high-throughput methods are needed.

E. Richling
Food Chemistry and Toxicology, Department
of Chemistry, University of Kaiserslautern-Landau,
Kaiserslautern, Germany
e-mail: richling@chemie.uni-kl.de

B. van Ravenzwaay
Environmental Sciences Consulting, Altrip, Germany
e-mail: ravenmooney@outlook.de

The low throughput and high costs of traditional animal-based toxicity studies have rendered them impractical for assessing large numbers of compounds. In 2007, a new vision and roadmap for toxicity testing in the twenty-first century was proposed, consisting of moving away from utilizing large animal cohorts and observational sciences to incorporate more efficient and human relevant technologies that provide a better understanding of the mechanisms of toxicity (National Research Council, 2007).

The development and use of in vitro human cell-based assays has been a major step in the implementation of the Toxicology of the 21st Century (Tox21 program) and have been fundamental in the understanding of molecular mechanisms of toxicity and in the development of adverse outcome pathways (AOP) (Vinken 2013; Krewski et al. 2020). More recently, complex in vitro toxicity models (e.g., three-dimensional (3D) organoid models, hiPSCs derived systems, organ-on-a-chip platforms) addressing systemic toxicity endpoints have been developed (Plummer et al. 2019; Richards et al. 2020; Shinzawa et al. 2021). Despite the advantage they offer, the limited throughput, complexity, and high cost of these sophisticated in vitro models reduce their applicability. Additionally, toxicological in vitro testing has been based mainly on mono-parametric strategies (one question, one answer) which is time consuming and limits the full characterization of toxicological-related events (Dix et al. 2007).

The use of multiparametric “omics” technologies allows the simultaneous evaluation of multiple parameters in a single biological sample and offers a more comprehensive tool for elucidating the molecular and biochemical events underlying organ toxicity (García-Cañaveras et al. 2016). In particular, metabolites represent the most downstream products and final outcome of expression of the genome, transcriptome and proteome, thus providing a snapshot of the biochemical and physiological status of a system including its response to external stressors (Guijas et al. 2018). For this reason, metabolomics is considered to be the omics technology which is closest to classical toxicology and has shown to have a similar sensitivity (Van Ravenzwaay et al. 2014). Metabolomics has been successfully implemented for more than a decade to identify toxicological mechanisms in rodent studies

(Kamp et al. 2012; Van Ravenzwaay et al. 2014; Van Ravenzwaay et al. 2015). More recently, it has been used in combination with in vitro models to expand the investigation of organ toxicity (García-Cañaveras et al. 2016; Birk et al. 2021; Huang et al. 2021; Jeon et al. 2021).

The liver is one of the most frequent target organs of chemical toxicity. Drug-induced liver injury (DILI) represents the leading cause of failure in new pharmaceutical development and post approval compound withdrawals (Onakpoya et al. 2016). Therefore, hepatotoxicity is of primary concern in compound development and considerable efforts have been directed to the development of assays to evaluate liver toxicity (Mirahmad et al. 2022). Several liver cell lines have been successfully used for in vitro metabolomics to identify modes of action of liver toxicity (Cuykx et al. 2018b). However, in contrast to popular perception, so far, in vitro experiments and, in particular, metabolomics experiments are costly and material- and labor-intensive (García-Cañaveras et al. 2016; Cuykx et al. 2018b; Ramirez et al. 2018). We have previously developed a HepG2 cell-based metabolomics in vitro platform, capable of identifying and characterizing different modes of action (MoAs) of liver toxicity. Despite its good performance as a research tool, the assay was costly, complex, and time consuming (Ramirez et al. 2018). These factors have critically limited in vitro metabolomics throughput and scalability and prevented its implementation in high-throughput screening during early stages of compound development.

Improvements in the sensitivity of analytical techniques for metabolomics have opened the possibility of scaling the throughput in metabolomics (Dubuis et al. 2018; Zampieri et al. 2018; Anglada-Girotto et al. 2022; Malinowska et al. 2022). We have used this opportunity to develop and evaluate a highly standardized, 96-well in vitro metabolomics screening platform for the identification and classification of liver toxicity MoAs in HepG2 cells. Different parameters of the workflow such as cell seeding density, influence of passage number, cytotoxicity testing, sample preparation, metabolite extraction, analytical method, and data processing were optimized to perform with low biomass samples. This new methodology was then tested with seven compounds with known hepatotoxicity modes of action (MoA) in five different concentrations.

Materials and methods

Cell culture

HepG2 cells (ECACC, UK, maximum passage number 9) were maintained and grown on Dulbecco's MEM media supplemented with 1% v/v of penicillin/streptomycin, L-glutamine (200 mM, 1% v/v), non-essential amino acids (100x, 1% v/v), and 10% FBS (PAN-Biotech, Aidenbach, Germany) in 75 cm² culture flasks (TPP, Switzerland). For cell passaging (~80% confluency) media was removed and cells were washed twice with pre-warmed calcium and magnesium free Dulbecco's PBS (PAN-Biotech, Aidenbach, Germany). Trypsin was used for cell detachment. Then, 20 mL culture medium was added, and single-cell suspensions were obtained by passing the suspension through a Combitip (Eppendorf, Germany). A fraction of the cell suspension was then transferred to a new culture vessel. For experiments, 15,000 cells per well (passage 5-9) were seeded in 96-well flat-bottom plates (TPP, Switzerland) and incubated for 24 h for cell attachment (37 °C and 5% CO₂). Afterwards, culture media were exchanged, test substances applied, and plates incubated for 48 h (37 °C and 5% CO₂).

Test substances

Test substances (Table 1) were selected based on their known in vivo liver toxicity effects and different MoAs as well as results from previous in vitro studies in our lab (Ramirez et al. 2018). Acifluorfen, bezafibrate, wy-14643, β-naphthoflavone, pendimethalin, and ketoconazole were purchased from Sigma-Aldrich (Taufkirchen, Germany) and Aroclor 1254 from Chem-Service (West Chester, PA, USA). Purity of all substances ≥ 98%.

Cytotoxicity and cell viability testing

Commercially available cytotoxicity (CellTox™ Green) and ATP content based (CellTiter-Glo®) assays (Promega GmbH, Walldorf, Germany) were multiplexed in a single 96-well plate following the manufacturer's instructions. For positive controls, lysis solution 25X was added in wells containing vehicle control treated cells (0.5% DMSO). Then, 10X CellTox Green reagent was added in all wells,

Table 1 Overview of test substances used for treatment of HepG2 cells for 48 h

Substance	CAS-Nr.	Chemical class	Category	MoA
Acifluorfen	50594-66-6	Diphenyl ether	Herbicide	Peroxisome proliferation
Bezafibrate	41859-67-0	Fibric acids	Hypolipidemic agents	Peroxisome proliferation
Wy-14643	50892-23-4	Pyrimidines	Hypolipidemic agents	Peroxisome proliferation
β -naphthoflavone	6051-87-2	Benzoflavone	Industrial chemical	Liver enzyme inducer
Aroclor 1254	11097-69-1	Polychlorinated biphenyl	Industrial chemical	Liver enzyme inducer
Pendimethalin	40487-42-1	Dinitroaniline	Herbicide	Liver enzyme inducer
Ketoconazole	65277-42-1	Imidazole derivative	Fungicide	Enzyme inhibitor

plates were shaken for 1 min, and incubated in the dark for 15 min at room temperature. Fluorescence was measured at $\lambda_{\text{ex}} = 485\text{--}500\text{ nm}/\lambda_{\text{em}} = 520\text{--}530\text{ nm}$ in the GloMax®-Multi Detection System (Promega). Afterwards, wells were washed with PBS, 100 μL of Dulbecco's MEM media were added to each well and subsequently 100 μL of 1X CellTiter-Glo were added. Plates were shaken for 2 min and incubated in the dark for 8 min at room temperature. Luminescence was measured in the GloMax®-Multi Detection System (Promega) and was normalized to the values of the vehicle control. Cytotoxicity and ATP cell viability analysis were carried out for range finder pre-tests and in parallel with metabolomics experiments in plates handled and treated exactly as the ones used for metabolite profiling.

Range finder experiments for dose setting

In order to define appropriate dose levels, range finder experiments were performed prior to metabolome experiments. Substances were administered to HepG2

cells in increasing concentrations and incubated for 48 h (6 replicates per concentration). Viability and cytotoxicity tests were performed as described previously. Luminescence values resulting from CellTiter-Glo® assays were used to build dose response curves. Curve fitting and effective concentrations (ECs) values were calculated in R using three-parameter Weibull model (W1.3). To obtain a full metabolome-based dose-response effect, five concentrations (EC1, EC5, EC15, EC50, EC85) were selected for metabolome experiments (Table 2). EC1 and EC5 were selected to evaluate mild metabolic effects, EC15 was selected to obtain a robust substance-related effect; however, within a low cytotoxicity range and EC50 and EC85 were chosen to identify cytotoxic-related metabolite patterns. Calculated ECs values were rounded to the nearest integer number for dose selection.

Live-cell imaging

To monitor cell proliferation, total well confluence was obtained by real-time cell imaging analysis using

Table 2 Concentrations selected to perform the metabolomics experiments based on range finder experiments

Substance	EC1 (μM)	EC5 (μM)	EC15 (μM)	EC50 (μM)	EC85 (μM)
Bezafibrate ^a			1000		
Acifluorfen	50	100	200	500	800
Wy-14643	25	50	150	500	1000
β -naphthoflavone	0.1	1	10	100	700
Aroclor 1254	21	38	56	94	133
Pendimethalin	24	39	56	94	157
Ketoconazole	5 ^b	0.2	1	10	50

^aBezafibrate 1000 μM was used as positive control in each experiment

^bFor Ketoconazole, the EC1 was excluded and a concentration between the EC15 and EC50 was selected instead. ECs were estimated based on the ATP dose response curves generated in the range finder experiments

IncuCyte S3 device placed in a normal incubator at 37 °C with 5% CO². Whole-well scans were taken every 6 h during the duration of the assay and evaluated using automated phase-contrast analysis (phase mask).

Metabolomics experiments

After 24 h of cell attachment, substances were administered in 0.5% DMSO to HepG2 cells in 5 concentrations (EC_{1(ATP)}, EC_{5(ATP)}, EC_{15(ATP)}, EC_{50(ATP)}, EC_{85(ATP)}) and incubated for 48 h. For each substance, one 96-well plate was set up with 6 replicates per concentration, 12 replicates for vehicle controls (yielding a final concentration of 0.5% DMSO in the well), 6 replicates for positive controls (Bezafibrate 1000 µM), and 6 replicates for blank controls (media without cells). To minimize potential evaporation, the outer rows and columns of the plate were omitted and filled with PBS instead. Reference samples prepared from lyophilized HepG2 cells were measured in parallel throughout the entire analytical process (technical replicates). Data from each metabolite in each sample were normalized against the median of the same metabolite in all reference samples on same plate to give normalized ratios. Lyophilized HepG2 cells reference samples were used to account for variability between plates and in concentration series for linearity checks. After 48 h, the assays were stopped by washing the wells once with 100 µL 0.9% NaCl followed by snap freezing the plates on liquid nitrogen for 5 s. Plates were placed immediately on dry ice and 50 µL ice-cooled isopropanol 80% (v/v) were added to quench metabolism and precipitate proteins. Plates were stored at – 80 °C until LC/MS analysis.

LC-MS/MS metabolomics

Metabolite profiling of cells was performed directly in the same 96-well plate according to a standardized protocol described below. In order to prevent any interaction with the cell material, the automatic sampler was adjusted to pick up the sample from the supernatant at a specified depth avoiding the contact with the bottom of the plate.

After the initial quenching step (50 µL isopropanol 80%), additional 70 µL of isopropanol 80%, containing internal standards (methionine-D3, tryptophan-D5, arginine-13C6-15N4, Boc-Ala-Gly-Gly-Gly-OH,

coenzyme Q1, coenzyme Q2, coenzyme Q4) were added to each well. The internal standards were used for quality control by visual inspection (signal intensity, peak shape, retention time); they were not used for normalization. Afterwards, plates were shaken for 5 min, 750 rpm at 20 °C, and placed for 30 s in the ultrasonic device. Then, the plates were centrifugated for 10 min, at 5485 g, 15 °C. Further, 2.5 µL of the extract were injected each for reversed-phase and hydrophilic interaction liquid chromatography followed by MS/MS detection (AB Sciex QTrap 6500+) using the positive and negative ionization mode. For reverse-phase high-performance liquid chromatography (RP-HPLC, Ascentis Express C18, 5 cm × 2.1 mm, 2.7 µm Supelco), gradient elution was performed with mobile phase A, water/methanol/0.1 M ammonium formate (1:1:0.02, w/w), and B, methyl-tert-butylether/2-propanol/methanol/0.1 M ammonium formate/formic acid (4:2:1:0.07:0.035, w/w) 5.9 min linear gradient: 0 min 100% A, 0.5 min 75% A, 5.9 min 10% A; followed by 0% A until 6.7 min; re-equilibration at 100% A until 7.7 min; flow rate 600 µL/min; column temperature 40 °C HILIC (ZIC-HILIC, 2.1 × 100 mm, 3.5 µm, Supelco) gradient elution was performed with mobile phase C, acetonitrile/water (99:1, v/v) with 0.2% (v) acetic acid, and D, 7 mM ammonium acetate with 0.2% (v) acetic acid (5.0 min linear gradient: 0 min 100% C, 5 min 10% C; followed by a linear gradient back to 100% C until 6.5 min; re-equilibration at 100% C until 7.5 min; flow rate 600 µL/min; column temperature 40 °C.). Two LC-MS systems with identical configuration were used for the analysis. Normalization to lyophilized reference samples (see below) was used to compensate for variation from between analytical batches. The efficiency of this normalization procedure was checked by principal component analysis (PCA), confirming that Pool samples from different analytical batches clustered together.

During the quality control process, parameters such as coverage, linearity (R²), variability (RSD), and blank contributions were evaluated for each metabolite. An analyte would pass the quality control check if the following thresholds were met.

Coverage > 80%, blank contribution < 40%, slope > 0, and any of the following conditions (a, b, c, d) regarding the linearity (R²) and variability (RSD): (a) linearity > 0.8, variability < 0.3 or (b) linearity > 0.64, variability < 0.3 or (c) linearity (R²) > 0.8,

variability (RSD) < 0.6 or (d) linearity (R^2) > 0.64, variability (RSD) < 0.6. When a metabolite failed to pass the quality control check, data for this metabolite were excluded.

In our targeted approach, a pre-defined set of metabolites are identified by their analytical parameters: polarity (lipid vs polar), MRM transition (m/z ratios), and retention time. To confirm the identity of a metabolite, samples were spiked with the pure metabolite during method development whenever possible. When metabolites were not commercially available, fragmentation patterns and library matching were used to determine the most likely identity of those metabolites. The corresponding metabolites were then marked as “plausible.” Metabolites listed as “unknown” have well-defined analytical parameters but unknown chemical identity.

The corresponding chromatography techniques, ionization modes, Q1 mass [m/z], Q3 mass [m/z], ChEBI ID, ChEBI name, and MRM parameters for the measured metabolites is provided in Suppl. Fig. 1.

Metabolomics data analysis

Reference samples derived from lyophilized untreated HepG2 cells (technical control samples) were measured in parallel throughout the entire analytical process. Data were normalized against the median of these lyophilized HepG2 cells reference samples, to give normalized ratios (performed for each sample per metabolite). This compensated for inter- and intra-instrumental variation. To correct for small differences in cell numbers within and between different treatment groups, data were also normalized to the within sample median, as described in detail by (Ramirez et al. 2018). For intracellular metabolomic analysis, the median of each sample was calculated across all the 221 measured metabolites.

To generate metabolic profiles for the different treatments, heteroscedastic *t* test (Welch test) was applied to log-transformed normalized metabolite data to compare treated groups with their respective controls.

To investigate the experimental variability, the variance of every log-transformed metabolite for both lyophilized HepG2 cells reference samples (technical replicates) and vehicle control samples was calculated (cells exposed to vehicle control during the assay

time). These variances were back-transformed to linear scale, yielding a relative standard deviation (RSD) using the following formula:

$$\text{RSD} = 1 - 10^{-\text{SDlog}}$$

Principal component analysis (PCA) and hierarchical clustering (HCA) analyses were performed using R software environment (<https://www.r-project.org/>). PCA was conducted using the *ropls* package (Thévenot et al. 2015) with log10-transformed input data and standard scaling. HCA was performed using the *pvclust* package (Suzuki et al. 2019), (<https://CRAN.R-project.org/package=pvclust>). Input: log10(Ratio), clustering method: Ward D2, distance method: Manhattan, bootstrapping: 10000 times.

Results

Method development and optimization

To develop a metabolomics in vitro assay compatible for high throughput, different parameters such as cell seeding density, influence of passage number, cytotoxicity testing, sample preparation, metabolite extraction, analytical method, and data processing known to have a significant impact on the cell metabolome were optimized in a 96-well plate format.

Optimal cell seeding density determination

To determine the optimal cell seeding density for the assay, different initial cell numbers ranging from 5000 to 25,000 cells/well were evaluated. Cells obtained from two different passage numbers (passage 5 and passage 7) were used for these experiments. Cell proliferation throughout the duration of the assay was monitored by measuring well confluence using real-time imaging analysis. After 48 h of incubation with vehicle control, the metabolic signal of vehicle control-treated cells was evaluated together with the well confluence (Fig. 1). Principal component analysis (PCA) of metabolic profiles showed that the initial cell seeding number was a strong driver for the separation along PC1, accounting for the 83.5% of the metabolic variation (see Fig. 1a). A separation of cells derived from passage 5 and passage 7 was evident in PC2, yet only accounting for a

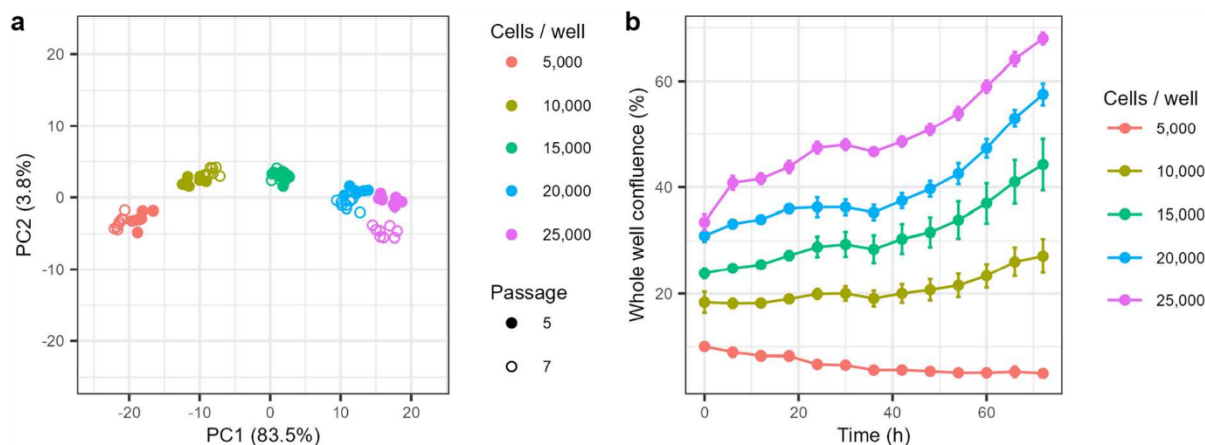


Fig. 1 15,000 cells per well was selected as the optimal seeding number for the assay. **a** PCA analysis of the metabolic profiles of different cell seeding densities and passages (passage 5,

passage 7). SAM normalization for cell number correction was not performed. **b** Cell confluence of different seeding densities during the time of the assay

very minor fraction of the overall variability (3.8%). A comparably low peak intensity was observed at the initial cell seeding density of 5000 cells/well. Metabolic profiles of 20,000 and 25,000 cells/well were found close to each other in the PCA plot, suggesting a potential saturation for some metabolites around these cell numbers. Initial seeding densities of 10,000 cells/well and 15,000 cells/well exhibited a strong metabolic signal within the linearity range of the metabolic response and presented a relatively low within samples variability. However, seeding densities up to 10,000 cells/well showed decreased proliferation rates when compared with higher seeding densities (Fig. 1b). Further, 15,000 cells/well exhibited a strong metabolic signal, low variability, and a regular HepG2 cell proliferation rate and therefore was selected as the optimal initial cell seeding density to perform metabolomics experiments. PCAs and their corresponding loading plots before and after applying a cell number normalization procedure are shown in Suppl. Fig. 2. Considering the total duration of the assay (72 h) and the HepG2 doubling time (~ 30 h), the final cell numbers obtained with 15,000 cells/well was ~ 84,000 cells per sample.

Influence of passage number on the metabolic response

To evaluate the impact of passage number on the metabolome, cells derived from three different

passages numbers (5, 7, and 9) were treated for 48 h with Bezafibrate, a substance that has served as a quality/positive control in metabolomics studies due to its pronounced and reproducible effect on the metabolome. Metabolic profiles of Bezafibrate-treated cells originating from different passage numbers were compared by PCA analysis (Fig. 2). Bezafibrate-treated samples were clearly separated from control samples. It was observed that the strongest effect was due to substance treatment, accounting for 39% of the variation in PC1. Results showed a high overlap among samples from different passage groups, indicating that cellular passage was not a major source of variation. Based on these data, different cell passages (from 5 to 9) could be used in the metabolomics in vitro assay, increasing the flexibility of the method without a major impact on the results.

Proof of concept with test substances

Once the main parameters of the assay were established, its performance as liver toxicity MoA screening test was evaluated. Seven substances known to cause liver toxicity through three different MoAs were tested (peroxisome proliferation: Acifluorfen, Wy-14643, and Bezafibrate; liver enzyme induction: Pendimethalin, Aroclor, and β -naphthoflavone; liver enzyme inhibition: Ketoconazole).

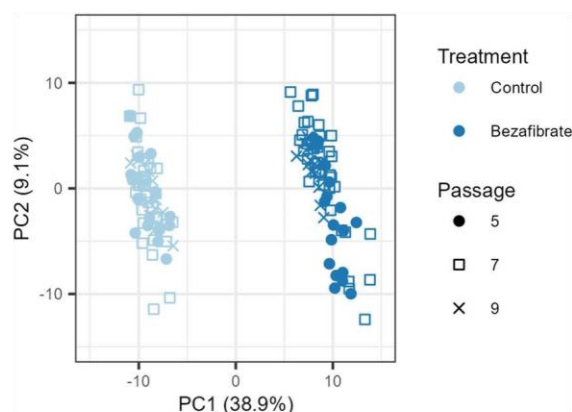


Fig. 2 Bezaifibrate-treated cells of different passages do not show a bias by experiment or cell passage. PCA analysis of the metabolic profiles of Bezaifibrate-treated cells (positive control). Bezaifibrate treatment showed a clear metabolic change compared to vehicle-treated cells. The results were obtained in 3 independent experiments using cell passages 5, 7, and 9

Cytotoxicity testing for dose selection

To select compound concentrations for the metabolome experiments, range finder experiments for each substance were carried out. After administering increasing concentrations of test compounds, cytotoxicity and cell viability were assessed (Suppl. Fig. 3). CellToxGreen assay measures cell death and therefore it was used to identify concentrations that were highly cytotoxic. ATP production, a more sensitive endpoint and likely to be a closer proxy to impairments in cellular metabolism, was used to generate dose response curves for each substance and estimate effective concentration (EC1, EC5, EC15, EC50, EC85) values. Based on ATP-estimated EC values (Table 2), five concentrations

Table 3 Cell viability in metabolomics experiments. Percentage of viability (ATP) compared to the vehicle control ($n = 6$). *Bezaifibrate 1000 μM was used as a positive control in each

Substance	C1 (%)	C2 (%)	C3 (%)	C4 (%)	C5 (%)	Bezaifibrate* (%)
Acifluorfen	104.7 \pm 4.2	105.2 \pm 4.8	99.9 \pm 1.3	58.4 \pm 1.5	27.8 \pm 1.3	84.1 \pm 2.3
Wy-14643	100.9 \pm 3.8	97.1 \pm 3.1	94.6 \pm 1.8	46.4 \pm 2.0	23.2 \pm 1.1	76.3 \pm 3.2
β -naphthoflavone	103.4 \pm 4.3	113.8 \pm 3.7	104.1 \pm 1.6	34.5 \pm 3.4	15.0 \pm 2.1	75.0 \pm 1.5
Aroclor 1254	95.5 \pm 4.1	80.5 \pm 5.7	60.6 \pm 7.5	8.7 \pm 1.6	3.9 \pm 3.2	71.8 \pm 2.8
Pendimethalin	98.3 \pm 3.9	100.3 \pm 2.9	82.4 \pm 4.9	36.1 \pm 3.2	18.5 \pm 3.2	78.0 \pm 0.7
Ketoconazole	102.4 \pm 3.1	102.0 \pm 0.9	91.2 \pm 1.5	64.7 \pm 1.5	28.2 \pm 1.9	79.3 \pm 2.2

(C1–5) covering the full dose response range were selected per substance for the metabolome experiments (see Suppl. Fig. 4). To experimentally assess cytotoxic effects of selected doses, cell viability and cytotoxicity were measured in parallel with metabolomics experiments in plates handled and treated exactly as the ones used for metabolomics (Table 3, Suppl. Fig. 5). Cells treated with C1 and C2 exhibited a percentage of viability of $\geq 97\%$ for all substances, except for Aroclor 1254 where the viability for C1 was 95.5% and for C2 was 80.5%. C3 had a stronger effect on the viability ($\geq 80\%$) for all substances except for Aroclor 1254 (60.6%) and Bezaifibrate (71–84%). As expected, C4 and C5 of all substances had a pronounced effect on the cellular viability ranging from 34 to 65% for C4 and from 3 to 28% for C5.

Metabolomics

After treatment, intracellular metabolites were extracted for semiquantitative targeted metabolomics via LC-MS/MS. 221 unique analytes were measured of which 156 were annotated and 65 remained unknown. Annotation was done during method development, using different approaches such as spiking with reference compounds or LC-Q-ToF-HRMS analysis for matching the results with library data or with results from similar compounds of the same compound class. Measured metabolites were grouped into 12 ontology classes. An enrichment analysis was carried out to evaluate the number of significantly changed metabolites per ontology class (Suppl. Fig. 6). The data revealed dose dependency in all cases, with increasing number of altered metabolites at higher concentrations.

experiment. Actual concentrations corresponding to the C1–C5 of each substance can be found in Table 2 of materials and methods

Experimental variability and reproducibility

The experimental variability of the technical (lyophilized reference samples) and biological controls (vehicle treated cells) demonstrated the robustness and reproducibility of the method. Control samples revealed RSD values of 8% to 11%. The technical replicates had an RSD of 8% to 10% (Suppl. Fig. 7). Reproducibility was also evaluated under treatment conditions using the results of Bezafibrate, which was included as positive control in all the plates. The metabolome profile of different Bezafibrate experiments clustered together in the PCA of all analyses, indicating the homogeneity of the samples and experiments. Moreover, the univariate analysis of the Bezafibrate treatment effects demonstrated consistent pattern of metabolite changes across all plates.

PCA analysis reveals dose response effect by metabolomics

Metabolite profiles were further analyzed by PCA. Concentration-dependent responses were observed for each substance (Fig. 3). For pendimethalin, aroclor, acifluorfen, and ketoconazole, low (C1 and C2) and intermediate concentrations (C3) were separated from control samples with a similar dose response trajectory: the initial separation from controls at the lowest concentrations is visible in a PC2 response followed by increasing PC1 separation at higher concentrations. For β -Naphthoflavone, all concentrations were quantitatively different but separated from control samples in the same direction (PC1). For Wy-14643, C1 and C2 clustered together with controls, the intermediate level (C3) separated along the PC2, and high concentrations clearly separated along the PC1. In summary, low and intermediate concentrations drift away from controls in the same direction in a dose response manner while high concentrations exert a strong effect on the metabolome (PC1) and separate in a different direction suggesting a different impact of middle and high concentrations levels on the metabolome. These results show that (1) a metabolome-based dose response can be obtained and (2) metabolite profiles resulting from cytotoxic effects on the metabolome are distinguishable from specific substance-related effects; (3) metabolomics is more sensitive than ATP measurement; and significant metabolite changes were already observed at concentrations that caused no reductions in ATP levels (e.g., C1, C2).

Differentiation of hepatotoxicity modes of action

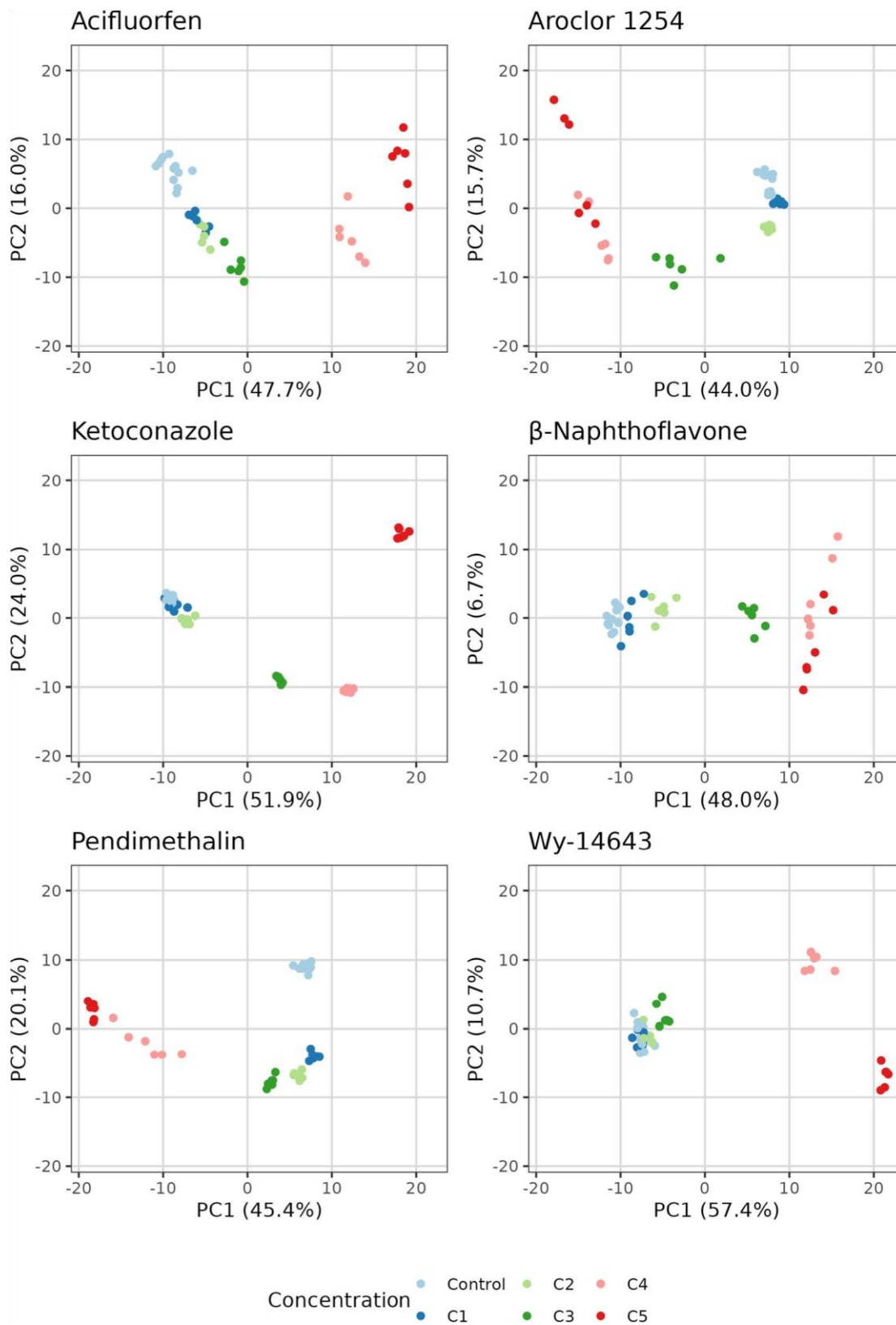
A meaningful metabolomics-based assessment of MoA requires a concentration high enough to cause biochemical alterations but not excessive to induce extensive cell damage and lethality. Intermediate concentration levels (C3 for pendimethalin, β -naphthoflavone, acifluorfen, wy-14643, and ketoconazole and C2 for aroclor) were clearly distinguishable from controls in the PCA (Fig. 3), which showed a mild reduction of cell viability (less than 10%) and presented low cytotoxicity (Suppl. Fig. 5); therefore, were selected for further analysis. Applying a PCA, a separation by mode of action was observed (Fig. 4). Treated samples were separated from vehicle controls in PC1, accounting for 21% of the total variation. Three different clusters corresponding to the evaluated MoAs were detected. The separation of the peroxisome proliferators cluster (acifluorfen, bezafibrate and wy-14643) and liver enzyme inducers cluster (aroclor, β -naphthoflavone, and pendimethalin) was visible in PC2, representing 17% of total variation. The separation of liver enzyme inhibitor (ketoconazole) was distinguishable in PC3 which accounted for 14% of the total variation. A 3D PCA plot can be found in the supplemental information (Suppl. Fig. 8).

A hierarchical clustering analysis (HCA) further confirmed the compounds clustering by MoA (Fig. 5). These results indicate that 96-well plate in vitro metabolic profiling can distinguish between different liver toxicity MoAs.

Characteristic metabolite changes for each MoA

The metabolites set of significantly altered metabolites can give a better mechanistic understanding of liver toxicity MoAs. Therefore, intracellular metabolomes of cells treated with the intermediate concentration (C3 for pendimethalin, β -naphthoflavone, acifluorfen, wy-14643, ketoconazole, and C2 for aroclor) were then evaluated at a single metabolite level and used to identify unique sets of altered metabolites for each MoA. Metabolite sets that were potentially relevant for a specific MoA were generated by comparing metabolite profiles of substances belonging to the same MoA and selecting all commonly changed significantly increased or decreased metabolites.

Peroxisome proliferators (bezafibrate, acifluorfen, wy-14643) showed a decrease in concentrations of short (propionylcarnitine) and medium



◀**Fig. 3** PCAs of metabolomics dose-response effect. PCA analysis of the metabolic profiles of **a** Acifluorfen, **b** Wy-14643, **c** β -naphthoflavone, **d** Aroclor, **e** Pendimethalin, and **f** Ketoconazole-treated cells at five different concentrations. Actual concentrations corresponding to the C1–C5 of each substance can be found in Table 2 of materials and methods. Bezafibrate was used as a positive control in all plates (data not shown)

(hexanoylcarnitine, acylcarnitines) carnitines, ketoleucine, taurine, creatine, 5-hydroxytryptophan, s-adenosylhomocysteine, deoxycytidine, glycerol-3-phosphate, and higher concentrations of *N*-acetylaspartate and some triacylglycerols. Additionally, concentrations of phospholipids, ceramides, and sphingomyelins were decreased after treatment (Suppl. Fig. 9).

Cells treated with the enzyme inducers aroclor, pendimethalin, and β -naphthoflavone showed increases of tyrosine, the redox carriers flavin adenine dinucleotide (NAD) and glutathione (GSH) and the glutathione precursor cysteinylglycine. In addition, enzyme inducers were characterized by reductions of proline, myo-inositol, *N*-acetylglucosamine, deoxycytidine, the carnitine derivative *O*-acetyl carnitine, short and medium chain carnitine derivatives, and several triacylglycerols (Suppl. Fig. 10).

The metabolite profile of ketoconazole, representative of the liver enzyme inhibitor MoA, exhibited lower concentrations of amino acids and related metabolites, the redox carriers GSH, pyroxidal and coenzyme Q10, ceramides and cholesteryl esters, and increases in levels of long chain carnitine derivatives, taurine, choline, and sphingomyelin (Suppl. Fig. 11).

In summary, our results show that different MoA were characterized by specific metabolites as common denominators for the respective MoA. Additionally, reduced levels of creatine, carnitine, and pantothenic acid and increased levels of lysophosphatidylcholine and lysophosphatidylethanolamine were found to be metabolite alterations shared by the 3 MoAs; consequently, these metabolites cannot be regarded as MoA specific but rather general for hepatotoxicity.

Discussion

Method development and optimization

Several potentially influencing factors for the development of a high-throughput in vitro metabolomics technique have been evaluated and optimized.

Cell seeding density determination

Miniaturizing an assay to a 96-well format implicates reductions in cell numbers thus limiting the available biomass for analysis. Therefore, an important issue was to select an appropriate initial cell density. Based on the assessment of cell growth and metabolomics signal strength of different cell seeding densities, 15,000 cell/well provided best results.

Our results demonstrate that seeding density has a major effect on the cellular growth rate and consequently on cell numbers at the end of the experiment. It has been shown that dose response metrics such as IC₅₀ are influenced by growth rates (Hafner et al. 2016). Therefore, optimizing seeding densities and reporting final cell numbers is critical in assay development to reduce interexperimental variability and improve the replicability and reproducibility of dose response curves (Larsson et al. 2020).

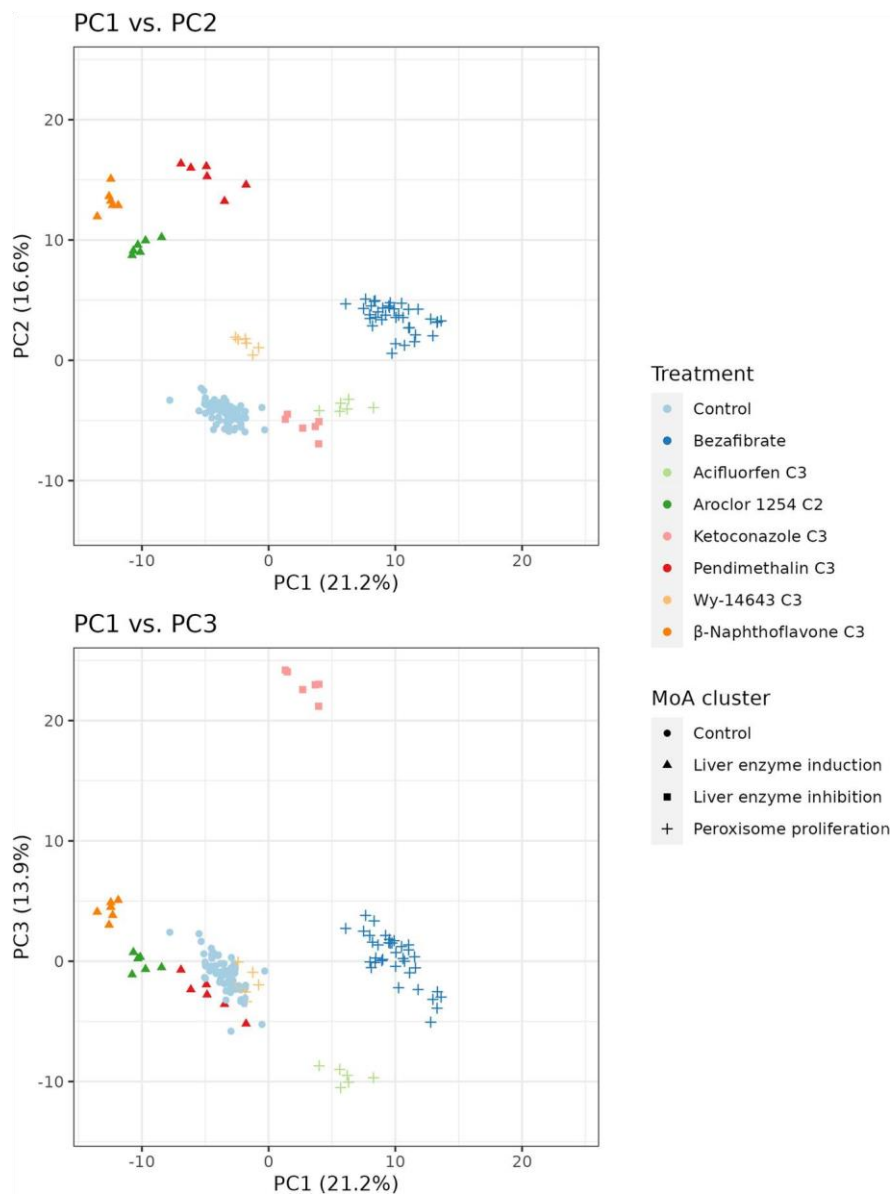
Influence of passage number on the metabolic response

Flexibility is a crucial parameter for implementing an in vitro assay. In industrial settings, studies are designed for serial running of large numbers of samples in wide ranges of experimental conditions, making the use of a single, cell passage impractical. Yet, using different passage numbers can represent a source of variability that could reduce the statistical significance of the analysis (Moreno-Torres et al. 2021). We evaluated passage number (passage 5–9) as a possible confounding factor and showed that it has no significant impact on the metabolome, increasing the flexibility of the assay without impacting the biological interpretation. A similar observation was made by (Moreno-Torres et al. 2021) who showed that cell passage has a minor contribution (6%) to the data variance in the PCA.

Sample extraction

To avoid complex sample manipulation, we have implemented a one-phase liquid extraction using isopropanol. Monophasic extractions using alcohols (mostly methanol) are usually sufficient to remove most macromolecules such as proteins and nucleic acids, avoid selection bias, cover a wide range of polar to non-polar metabolites and in contrast to

Fig. 4 PCA of metabolic profiles shows a MoA-specific clustering of liver toxicants. PCA of metabolite profiles of HepG2 cells treated for 48 h with three liver enzyme inducers (pendimethalin, aroclor, β -naphthoflavone), three peroxisome proliferators (bezafibrate, acifluorfen, wy-14643) and one liver enzyme inhibitor (ketoconazole) allows to discriminate between the different mode of actions of these substances. Intermediate concentrations (C3 for pendimethalin, β -naphthoflavone, acifluorfen, wy-14643, and ketoconazole and C2 for aroclor) were selected for the analysis. Upper panel PC1 vs. PC2; lower panel PC1 vs. PC3



other organic solvents, are compatible with polystyrene (96 well-plate material) (Andresen et al. 2022). In comparison with methanol, isopropanol allows better protein precipitation, has a higher boiling point, which reduces sample evaporation and offers a broad polarity range (Andresen et al. 2022). Metabolite extraction was done directly in 96 well-plates, avoiding cell scrapping, trypsinization or additional steps which cause cellular-perturbations or biomass loss (Bordag et al. 2016; Dubuis et al. 2018; Zampieri et al. 2018).

Optimization of the metabolome coverage by using LC-MS

In this study, we focused on using LC-MS as a single analytical technique and combined HILIC (for polar metabolites) and RP (optimized for lipid species) chromatography to expand the metabolome coverage. The results revealed that a wide range of metabolites from highly polar (amino acids, nucleobases, cofactors) to lipidic (lysoPLs, PLs, TGs) was covered. Lipid metabolites accounted for

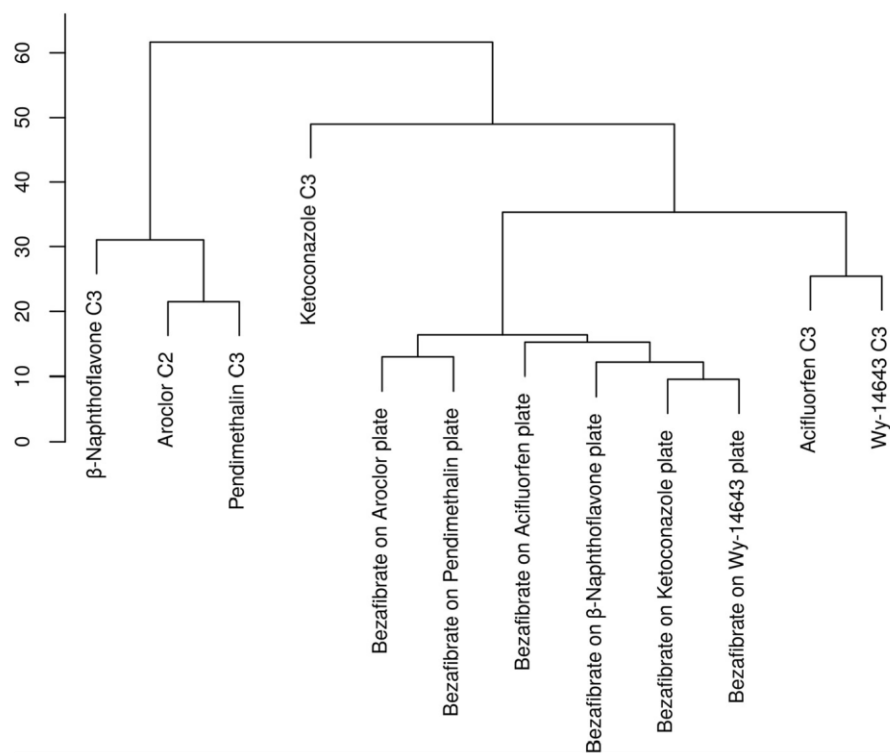


Fig. 5 Hierarchical clustering analysis of metabolic profiles shows a MoA-specific clustering of liver toxicants. HCA of metabolite profiles of HepG2 cells treated for 48 h with three liver enzyme inducers (Pendimethalin, Aroclor, β -Naphthoflavone), three peroxisome proliferators (Bezafibrate, Acifluorfen, Wy-14643), and one liver enzyme inhibitor (Ketoconazole) allows to discriminate between the dif-

ferent mode of actions of these substances. Intermediate concentrations (C3 for Pendimethalin, B-naphthoflavone, acifluorfen, Wy-14643, and Ketoconazole and C2 for Aroclor) were selected for the analysis. Input: $\log_{10}(\text{Ratio})$, clustering method: Ward D2, distance method: Manhattan, bootstrapping: 10,000 times

75% of the 221 annotated features. Therefore, even though we increased the LC spectrum significantly, the detection of polar metabolites was limited. Our current method potentially be improved by optimizing the HILIC protocol as shown by (Gerdemann et al. 2022), by adding pre-column derivatization steps (Walvekar et al. 2018) or by implementing an additional method for energy metabolism metabolites (Balcke et al. 2011). However, these additional sample preparations and the need of different aliquots would increase the experimental time and cost. Therefore, from a practical point of view, our experiments showed that performing the analysis using a single sample preparation and analytical condition represents a good tradeoff between simplifying the system and still getting sufficient information to discriminate between different MoAs.

Proof of concept: MoA differentiation

HepG2 cells have been instrumental for investigating the molecular and cellular processes involved in hepatotoxicity. Although their limited drug metabolizing and transport capabilities are well acknowledged, their low cost, high reproducibility, and human origin make them a suitable option for initial screenings and compound prioritization.

The applicability of our system to differentiate between MoAs was tested with seven substances known to be representative of three different liver toxicity MoAs (Peroxisome proliferation, liver enzyme induction, and liver enzyme inhibition). Five doses covering a wide range of concentrations from EC1 to EC85 (intracellular ATP) were used. A clear metabolomics-based dose response was observed by both multivariate and univariate analysis (Fig. 3, Suppl. Fig. 6).

Noteworthy, the dose selection was based on estimated EC values obtained from ATP-based dose response curves in the range finder experiments. The estimated EC values did not correlate exactly with the experimental ATP measured values (Table 3). This was highly dependent on the compound and might be related to the specific dose-response nature of each substance. Expanding the number of tested concentrations in the range finder experiments would enable to build improved dose-response curves that allow for more accurate EC estimations. Yet, ATP measurement represents a highly sensitive and metabolic-related endpoint and therefore represents a suitable approach for metabolomics dose setting.

Then to evaluate the specific MoA-related metabolomics response and exclude confounding cytotoxic effects, we selected a concentration that (1) did not cause any significant cell death (assessed by Cell-ToxGreen assay) and (2) induced a slight to moderate loss of ATP (ATP level decreased by less than 20% as compared to controls). In most cases, this turned out to be the C3 concentration. The results of the PCA analysis at this concentration demonstrated a good separation between peroxisome proliferators, enzyme inducers, and the enzyme-inhibiting compound.

Early identification of MoA is a powerful biologically driven classification tool essential in compound development. The next step would be to build a large database which would broaden the spectrum of covered MoAs, similar to our *in vivo* metabolomics database (MetaMap®Tox) (Van Ravenzwaay et al. 2015). Thus, following the metabolome analysis of a new compound, a PCA comparison with that of a reference compound (i.e., compounds with a known MoA) may help to quickly identify the probable MoA and offer the possibility of biological-based read across analysis.

Non-specific markers of hepatotoxicity

Following the PCA comparison, metabolic profiles of subtoxic doses were subjected to univariate statistics to identify individual metabolite changes. Concentrations of carnitine and pantothenic acid were significantly decreased and levels of lysophosphatidylcholines (LPC) and lysophosphatidylethanolamines (LPE) significantly increased in all treatments. These metabolic changes were observed irrespective of the substance MoA and therefore can be considered as nonspecific, general markers of hepatotoxicity.

Pantothenic acid is an essential nutrient required to synthesize coenzyme A (CoA) (Leonardi et al. 2007). During fatty acid degradation, CoA and carnitine are required to activate and mobilize long chain fatty acids into the mitochondria via the carnitine shuttle. Lower intracellular concentrations of carnitine and pantothenic acid suggest a higher mobilization of lipids into the mitochondria for β -oxidation. Reduced concentrations of these two metabolites have been reported consistently in *in vitro* studies after exposure to hepatotoxicants such as 2,3,7,8-tetrachlorodibenzo-*p*-dioxin (TCDD) (Ruiz-Aracama et al. 2011), peroxisome proliferators (Ramirez et al. 2018), sodium valproate (Cuykx et al. 2018a), and dichloroacetate (Dubuis et al. 2018). These metabolite changes point toward a general imbalance of the cellular energy status and could be indicative of mitochondrion malfunction, a pathway which is frequently target of hepatotoxic compounds (Mihajlovic et al. 2022).

Elevated concentrations of both LPC and LPE represent an increased turnover of phospholipids species and are as well a common finding in investigations of liver pathologies and in the nephrotoxic-related MoA—mitochondrial DNA interaction—in kidney cells (García-Canaveras et al. 2011; Beyoglu et al. 2013; Birk et al. 2021).

MoA-specific metabolite profiles

For each of the MoAs, panels of specific combinations of intracellular metabolite changes were identified which are unique for the adverse outcome pathway.

Peroxisome proliferators (PP) are pharmaceutical and chemicals that increase the number and size of peroxisomes *in vivo* via the activation of the nuclear receptor PPAR α which acts as a central regulator of hepatic lipid metabolism (Aoyama et al. 1998).

The metabolic profile of PP exhibited lower levels of short and medium acylcarnitines, ketoleucine, taurine, and creatine and higher concentrations of *N*-acetylaspartate and some triacylglycerols. Long-chain acylcarnitines are oxidized in the mitochondria and peroxisomes via β -oxidation to short- and medium-chain carnitines that can be subsequently utilized together with ketogenic amino acids for the formation of ketone bodies via the branched-chain amino acid (BCCA) metabolism. Lower levels of propionylcarnitine and hexanoylcarnitine together

with decreased levels of the ketogenic amino acid ketoleucine support the increased synthesis of ketone bodies characteristic of an energy metabolism switch from glycolysis to fatty acid β -oxidation. Taurine plays an important role in lipoprotein metabolism (Yanagita et al. 2008) and has been shown to attenuate the effects of drug induced hepatic injury by acting as an antioxidant during lipid peroxidation (Mas et al. 2004; Murakami et al. 2018). A higher utilization of taurine due to increased β -oxidation could have resulted in the lower levels of the amino acid observed in PP-treated cells.

Lower levels of creatine and *S*-adenosylhomocysteine were also observed after PP treatment. It has been shown that some PP competes for the same binding site on PPAR- α as homocysteine (Hunt et al. 2002). In addition, creatine administration is known to decrease the homocysteine production in liver, preventing fat accumulation and resulting in beneficial effects in fatty liver and non-alcoholic liver disease (Barcelos et al. 2016).

Increased levels of the acetyl-CoA precursor *N*-acetyl-aspartate (NAA) could have resulted as a consequence of the excess of acetyl-CoA produced by high rates of fatty acid oxidation in PP-treated cells (Prokesch et al. 2016).

Metabolic profiles of enzyme inducers showed decreased levels of proline. Proline can be used by cancer cells as energy source and/or as precursor of protein synthesis. Recent studies have demonstrated that proline participates in the regulation of redox balance and energy status (Zheng et al. 2021). Concentrations of the glucose derivatives myo-inositol and *N*-acetylglucosamine were as well reduced after treatment. Myo-inositol is implicated in the modulation of glucose metabolism through its role in insulin signal transduction (Bevilacqua et al. 2018). These changes together with lower concentrations of the carnitine precursor *o*-acetylcarnitine, short and medium carnitine derivatives, and several triacylglycerols suggest an alteration of the cellular energy balance.

Increased concentrations of the glutathione precursor cysteinylglycine as well as the redox carriers flavin adenine dinucleotide (FAD) and glutathione (GSH) indicate the activation of the antioxidant response. CYPs enzymes induction plays an important role in increased hepatic clearance but also contributes to the formation of chemically reactive metabolites that can lead to toxicity. However, enzyme induction by

itself is generally viewed as a compensatory and not an adverse response (Mattes et al. 2014). In line with our observations, the elevation of glutathione and its precursor cysteinylglycine suggest a stimulation of de novo synthesis of glutathione indicative of an early cellular response to counteract the ROS production generated by higher activities of CYPs enzymes.

Ketoconazole is an imidazole fungicide that acts as potent inhibitor of the human CYP 3A4 enzyme and was used in this study to assess the metabolic profile of liver enzyme inhibition. Cells exposed to Ketoconazole showed lower concentrations of amino acids (threonine, proline, and glutamate), amino acid-related metabolites, antioxidants (coenzyme Q10, pyroxydal, GSH), and ceramides, together with an increase in the levels of long-chain acylcarnitines (tetradecanoylcarnitine, hexadecanoylcarnitine, hexadecanoylcarnitine, octadecanoylcarnitine), taurine, and sphingomyelins.

The accumulation of taurine and long-chain acylcarnitines indicates an inhibition of mitochondrial fatty acid β -oxidation accompanied by an increased protein catabolism as an alternative for energy production. Reduced levels of antioxidant molecules such as GSH and its precursor glutamate indicate oxidative stress. In line with our findings, HepG2 and HepaRG cells exposed to Ketoconazole and other antimycotic azoles showed a reduction in the mitochondrial membrane potential and impaired activity of the electron transport chain. As a consequence, increased production of reactive oxygen species (ROS) was generated leading to mitochondrial oxidative stress (Haezler et al. 2017). Similar metabolic alterations were reported after exposing HepG2 cells to the hepatotoxic carcinogen TCDD. TCDD and dioxin-like chemicals have been shown to inhibit human CYP1A2 activity in vitro which could explain the similarity in their metabolic profiles (Staskal et al. 2005).

The observed reduction in ceramides and increased concentrations of sphingomyelins suggest a higher turnover of ceramides. The sphingolipid metabolism is closely linked to inflammation and the downregulation of ceramides is associated with the development and progression of different liver pathologies (Tanase et al. 2021).

As we have used only one compound representative for the MoA of CYP 3A4 enzyme inhibition, additional compounds need to be tested to verify the specific nature of the metabolome profile.

Taken together, our results are in agreement with previously described biochemical changes of the compounds tested and, although not all intracellular metabolites were measured, the combination of altered metabolites was found to be sufficient to differentiate between hepatotoxicity MoAs and shed light into the mechanisms of toxicity.

Importantly, one of the key aspects of toxicity of twenty-first century relies in dose response modeling (Andersen et al. 2009). However, current screens are usually done only in few concentrations, hampering the calculation of meaningful dose response metrics such as IC_{50} and consequently limiting the applicability of in vitro systems in risk assessment (Olesti et al. 2021). By escalating the throughput, our system allowed to cover key points of the dose response curve from very mild effects (EC_1) to overt toxicity (IC_{85}). The potential of omics technologies for determining point of departure (PoD) has been highlighted (Thomas et al. 2007; Kang et al. 2020). Recently, a concentration-response analysis derived from in vitro metabolomics was used for benchmark concentration (BMC) modeling, showing to be a sensitive and quantitative indicator of liver injury potential (Crizer et al. 2021). High-throughput metabolomics methods that allow for multiple dose testing can contribute to fast screening that directs additional studies based on PoD estimations.

Finally, strategies to induce and manipulate the gene expression of multiple CYPs enzymes in HT systems have been described (Kwon et al. 2014) and could be applied to our HepG2 platform to expand its applicability. Additionally, improved standardization and cost reduction of metabolically more competent cells (e.g., HepaRG or hiPSCs) would allow to expand their implementation in HT systems (Mirahmad et al. 2022).

Conclusion

We have designed a highly reproducible 96-well-plate targeted in vitro metabolomics platform and optimized critical experimental parameters for rapid and cost-efficient hepatotoxicity screening. The system was tested with seven model compounds representative of three different liver toxicity MoAs demonstrating the applicability of the assay to reproduce metabolomics dose response effects, distinguish

between different liver toxicity MoAs, and identify key metabolites and patterns indicative of general and MoA specific hepatotoxicity.

Identifying the MoA of a compound in the early stage of compound development can guide the selection of the most prominent leads, help to identify unwanted effects, and provide a valuable foundation for a more targeted hazard assessment. Due to resources reduction and throughput increase, this assay allows to assess a broader range of concentrations that would enable a more accurate metabolome-based PoD, in vitro to in vivo extrapolations (IVIVE), and substance kinetic analysis.

This method can be extended to further cell lines and iPSCs for the investigation of different organ toxicities and is suitable for a wide range of screening applications that demand rapid, cost effective, and high throughput analysis.

Acknowledgements We would like to thank Nadine Roth and Nicole Rocker for their skillful technical support in the lab, Dr. Saskia Sperber for the scientific advice, and the SysBioTop-Moving team for the scientific discussions.

Authors' contributions All authors contributed to the study conception and design. Methodology: [Michael Herold], [Peter Driemert], [Andreas Verlohner], [Hans-Albrecht Huener], and [Sabina Ramirez Hincapie]. Material preparation, data collection, and analysis were performed by [Barbara Birk], [Bennard van Ravenzwaay], [Franziska Maria Zickgraf], and [Sabina Ramirez-Hincapie]. Bioinformatics and statistical analysis: [Philipp Ternes], [Varun Giri], [Volker Haake]. Supervision: [Barbara Birk], [Bennard van Ravenzwaay], [Dorothee Funk-Weyer], [Elke Richling], [Hennicke Kamp], and [Robert Landsiedel]. The first draft of the manuscript was written by [Sabina Ramirez-Hincapie] and all authors commented on previous versions of the manuscript. All authors read and approved the final manuscript.

Funding This project received funds from SysBioTop Moving (BMBF, 161L0243A) and EU-Tox Risk (European Union's Horizon 2020 research, No 681002).

Data availability The datasets generated during and/or analyzed during the current study are available from the corresponding author on reasonable request.

Declarations

Ethics approval Not applicable.

Competing interests The authors have no conflicts of interest to declare. BASF may use some of the presented technologies for product development in the future.

Open Access This article is licensed under a Creative Commons Attribution 4.0 International License, which permits use, sharing, adaptation, distribution and reproduction in any medium or format, as long as you give appropriate credit to the original author(s) and the source, provide a link to the Creative Commons licence, and indicate if changes were made. The images or other third party material in this article are included in the article's Creative Commons licence, unless indicated otherwise in a credit line to the material. If material is not included in the article's Creative Commons licence and your intended use is not permitted by statutory regulation or exceeds the permitted use, you will need to obtain permission directly from the copyright holder. To view a copy of this licence, visit <http://creativecommons.org/licenses/by/4.0/>.

References

- Andersen ME, Krewski D. Toxicity testing in the 21st century: bringing the vision to life. *Toxicol Sci.* 2009;1072:324–30.
- Andresen C, Boch T, Gegner HM, Mechtel N, Narr A, Birgin E, Rasbach E, Rahbari N, Trumpp A, Poschet G. Comparison of extraction methods for intracellular metabolomics of human tissues. *Front Mol Biosci.* 2022;9:826.
- Anglada-Girotto M, Handschin G, Ortmayr K, Campos AI, Gillet L, Manfredi P, Mulholland CV, Berney M, Jenal U, Picotti P, Zampieri M. Combining CRISPRi and metabolomics for functional annotation of compound libraries. *Nat Chem Biol.* 2022;185:482–91.
- Aoyama T, Peters JM, Iritani N, Nakajima T, Furihata K, Hashimoto T, Gonzalez FJ. Altered constitutive expression of fatty acid-metabolizing enzymes in mice lacking the peroxisome proliferator-activated receptor α (PPAR α). *J Biol Chem.* 1998;27310:5678–84.
- Balcke G, Kolle S, Kamp H, Bethan B, Looser R, Wagner S, Landsiedel R, Van Ravenzwaay B. Linking energy metabolism to dysfunctions in mitochondrial respiration—a metabolomics in vitro approach. *Toxicol Lett.* 2011;2033:200–9.
- Barcelos R, Stefanello S, Mauriz J, Gonzalez-Gallego J, Soares F. Creatine and the liver: metabolism and possible interactions. *Mini Rev Med Chem.* 2016;161:12–8.
- Bevilacqua A, Bizzarri M. Inositols in insulin signaling and glucose metabolism. *Int. J. Endocrinol.* 2018;2018
- Beyoglu D, Idle JR. The metabolomic window into hepatobiliary disease. *J Hepatol.* 2013;594:842–58.
- Birk B, Haake V, Sperber S, Herold M, Wallisch SK, Huener H-A, Verlohner A, Amma MM, Walk T, Hernandez TR. Use of in vitro metabolomics in NRK cells to help predicting nephrotoxicity and differentiating the MoA of nephrotoxicants. *Toxicol Lett.* 2021;353:43–59.
- Bordag N, Rennfahrt U, Nachtigall J, Maldonado S, Reszka R, Ramirez-Hernandez T, Kamp H, Fux E, Van Ravenzwaay B. Fast sampling of adherent cell cultures for optimal metabolomics results. *Metabolomics.* 2016;6164:2153. 0769.1000164
- Crawford SE, Hartung T, Hollert H, Mathes B, van Ravenzwaay B, Steger-Hartmann T, Studer C, Krug HF. Green toxicology: a strategy for sustainable chemical and material development. *Environ Sci Eur.* 2017;291:1–16.
- Crizer DM, Ramaiahgari SC, Ferguson SS, Rice JR, Dunlap PE, Sipes NS, Auerbach SS, Merrick BA, DeVito MJ. Benchmark concentrations for untargeted metabolomics versus transcriptomics for liver injury compounds in in vitro liver models. *Toxicol Sci.* 2021;1812:175–86.
- Cuykx M, Claes L, Rodrigues RM, Vanhaecke T, Covaci A. Metabolomics profiling of steatosis progression in HepaRG® cells using sodium valproate. *Toxicol Lett.* 2018a;286:22–30.
- Cuykx M, Rodrigues RM, Laukens K, Vanhaecke T, Covaci A. In vitro assessment of hepatotoxicity by metabolomics: a review. *Arch Toxicol.* 2018b;9210:3007–29.
- Dix DJ, Houck KA, Martin MT, Richard AM, Setzer RW, Kavlock RJ. The ToxCast program for prioritizing toxicity testing of environmental chemicals. *Toxicol Sci.* 2007;951:5–12.
- Dubuis S, Ortmayr K, Zampieri M. A framework for large-scale metabolome drug profiling links coenzyme A metabolism to the toxicity of anti-cancer drug dichloroacetate. *Commun Biol.* 2018;11:1–11.
- García-Cañaveras JC, Castell JV, Donato MT, Lahoz A. A metabolomics cell-based approach for anticipating and investigating drug-induced liver injury. *Sci Rep.* 2016;61:1–12.
- García-Canaveras JC, Donato MT, Castell JV, Lahoz A. A comprehensive untargeted metabolomic analysis of human steatotic liver tissue by RP and HILIC chromatography coupled to mass spectrometry reveals important metabolic alterations. *J Proteome Res.* 2011;1010:4825–34.
- Gerdemann A, Behrens M, Esselen M, Humpf H-U. Metabolic profiling as a powerful tool for the analysis of cellular alterations caused by 20 mycotoxins in HepG2 cells. *Arch. Toxicol.* 2022;9611:2983–98.
- Guijas C, Montenegro-Burke JR, Warth B, Spilker ME, Siuzdak G. Metabolomics activity screening for identifying metabolites that modulate phenotype. *Nat Biotechnol.* 2018;364:316–20.
- Haegler P, Joerin L, Krähenbühl S, Bouitbir J. Hepatocellular toxicity of imidazole and triazole antimycotic agents. *Toxicol Sci.* 2017;1571:183–95.
- Hafner M, Niepel M, Chung M, Sorger PK. Growth rate inhibition metrics correct for confounders in measuring sensitivity to cancer drugs. *Nat Methods.* 2016;136:521–7.
- Huang J-W, Kuo C-H, Kuo H-C, Shih J-Y, Tsai T-W, Chang L-C. Cell metabolomics analyses revealed a role of altered fatty acid oxidation in neurotoxicity pattern difference between nab-paclitaxel and solvent-based paclitaxel. *PLoS One.* 2021;163:e0248942.
- Hunt MJ, Tyagi SC. Peroxisome proliferators compete and ameliorate Hcy-mediated endothelial cell activation. *Am J Phys Cell Phys.* 2002;2834:C1073–9.
- Jeon BK, Jang Y, Lee EM, Moon JH, Lee HJ, Lee DY. A systematic approach to metabolic characterization of thyroid-disrupting chemicals and their in vitro biotransformants based on prediction-assisted metabolomic analysis. *J Chromatogr A.* 2021;1649:462222.
- Kamp H, Fabian E, Groeters S, Herold M, Krennrich G, Looser R, Mattes W, Mellert W, Prokoudine A,

- Ruiz-Noppinger P. Application of in vivo metabolomics to preclinical/toxicological studies: case study on phenytoin-induced systemic toxicity. *Bioanalysis*. 2012;418:2291–301.
- Kang W, Podtelezhnikov AA, Tanis KQ, Pacchione S, Su M, Bleicher KB, Wang Z, Laws GM, Griffiths TG, Kuhls MC. Development and application of a transcriptomic signature of bioactivation in an advanced in vitro liver model to reduce drug-induced liver injury risk early in the pharmaceutical pipeline. *Toxicol Sci*. 2020;1771:121–39.
- Krewski D, Andersen ME, Tyshenko MG, Krishnan K, Hartung T, Boekelheide K, Wambaugh JF, Jones D, Whelan M, Thomas R. Toxicity testing in the 21st century: progress in the past decade and future perspectives. *Arch Toxicol*. 2020;941:1–58.
- Kwon SJ, Lee DW, Shah DA, Ku B, Jeon SY, Solanki K, Ryan JD, Clark DS, Dordick JS, Lee MY. High-throughput and combinatorial gene expression on a chip for metabolism-induced toxicology screening. *Nat Commun*. 2014;5:3739.
- Larsson P, Engqvist H, Biermann J, Werner Ronnerman E, Forssell-Aronsson E, Kovacs A, Karlsson P, Helou K, Parris TZ. Optimization of cell viability assays to improve replicability and reproducibility of cancer drug sensitivity screens. *Sci Rep*. 2020;101:5798.
- Leonardi R, Jackowski S. Biosynthesis of pantothenic acid and coenzyme A. *EcoSal Plus*. 2007;22
- Malinowska JM, Palosaari T, Sund J, Carpi D, Bouhifd M, Weber RJM, Whelan M, Viant MR. Integrating in vitro metabolomics with a 96-well high-throughput screening platform. *Metabolomics*. 2022;181:11.
- Mas MR, Comert B, Oncu K, Vural SA, Akay C, Tasci I, Ozkomur E, Serdar M, Mas N, Alcigir G. The effect of taurine treatment on oxidative stress in experimental liver fibrosis. *Hepato Res*. 2004;284:207–15.
- Mattes W, Davis K, Fabian E, Greenhaw J, Herold M, Looser R, Mellert W, Groeters S, Marxfeld H, Moeller N, Montoya-Parra G, Prokoudine A, van Ravenzwaay B, Strauss V, Walk T, Kamp H. Detection of hepatotoxicity potential with metabolite profiling (metabolomics) of rat plasma. *Toxicol Lett*. 2014;2303:467–78.
- Mihajlovic M, Vinken M. Mitochondria as the target of hepatotoxicity and drug-induced liver injury: molecular mechanisms and detection methods. *Int J Mol Sci*. 2022;236:3315.
- Mirahmad M, Sabourian R, Mahdavi M, Larijani B, Safavi M. In vitro cell-based models of drug-induced hepatotoxicity screening: progress and limitation. *Drug Metab Rev*. 2022;542:161–93.
- Moreno-Torres M, Garcia-Llorens G, Moro E, Mendez R, Quintas G, Castell JV. Factors that influence the quality of metabolomics data in in vitro cell toxicity studies: a systematic survey. *Sci Rep*. 2021;111:22119.
- Murakami S, Ono A, Kawasaki A, Takenaga T, Ito T. Taurine attenuates the development of hepatic steatosis through the inhibition of oxidative stress in a model of nonalcoholic fatty liver disease in vivo and in vitro. *Amino Acids*. 2018;509:1279–88.
- National Research Council. Toxicity testing in the 21st century: a vision and a strategy. National Academies Press; 2007.
- Olesti E, Gonzalez-Ruiz V, Wilks MF, Boccard J, Rudaz S. Approaches in metabolomics for regulatory toxicology applications. *Analyst*. 2021;1466:1820–34.
- Onakpoya IJ, Heneghan CJ, Aronson JK. Post-marketing withdrawal of 462 medicinal products because of adverse drug reactions: a systematic review of the world literature. *BMC Med*. 2016;141:1–11.
- Plummer S, Wallace S, Ball G, Lloyd R, Schiapparelli P, Quiñones-Hinojosa A, Hartung T, Pamiés D. A human iPSC-derived 3D platform using primary brain cancer cells to study drug development and personalized medicine. *Sci Rep*. 2019;91:1–11.
- Prokesch A, Pelzmann HJ, Pessentheiner A, Huber K, Madreiter-Sokolowski C, Drougard A, Schittmayer M, Kolb D, Magnes C, Trausinger G. N-acetylaspartate catabolism determines cytosolic acetyl-CoA levels and histone acetylation in brown adipocytes. *Sci Rep*. 2016;61:1–12.
- Ramirez T, Strigun A, Verlohner A, Huener HA, Peter E, Herold M, Bordag N, Mellert W, Walk T, Spitzer M, Jiang X, Sperber S, Hofmann T, Hartung T, Kamp H, van Ravenzwaay B. Prediction of liver toxicity and mode of action using metabolomics in vitro in HepG2 cells. *Arch Toxicol*. 2018;922:893–906.
- Richards DJ, Li Y, Kerr CM, Yao J, Beeson GC, Coyle RC, Chen X, Jia J, Damon B, Wilson R. Human cardiac organoids for the modelling of myocardial infarction and drug cardiotoxicity. *Nat Biomed Eng*. 2020;44:446–62.
- Ruiz-Aracama A, Peijnenburg A, Kleinjans J, Jennen D, van Delft J, Hellfrisch C, Lommen A. An untargeted multi-technique metabolomics approach to studying intracellular metabolites of HepG2 cells exposed to 2, 3, 7, 8-tetrachlorodibenzo-p-dioxin. *BMC Genom*. 2011;121:1–19.
- Shinozawa T, Kimura M, Cai Y, Saiki N, Yoneyama Y, Ouchi R, Koike H, Maezawa M, Zhang R-R, Dunn A. High-fidelity drug-induced liver injury screen using human pluripotent stem cell-derived organoids. *Gastroenterology*. 2021;1603(831-846):e810.
- Suzuki R, Terada Y, Shimodaira H. Pvcust: hierarchical clustering with P-values via multiscale bootstrap resampling. [code]. R Package Ver. 2019;2:2.
- Staskal D, Diliberto J, Devito M, Birnbaum L. Inhibition of human and rat CYP1A2 by TCDD and dioxin-like chemicals. *Toxicol Sci*. 2005;842:225–31.
- Tanase DM, Gosav EM, Petrov D, Jucan AE, Lacatusu CM, Floria M, Tarniceriu CC, Costea CF, Ciocoiu M, Rezus C. Involvement of ceramides in non-alcoholic fatty liver disease (Nafld) atherosclerosis (ats) development: Mechanisms and therapeutic targets. *Diagnostics*. 2021;1111:2053.
- Thévenot EA, Roux A, Xu Y, Ezan E, Junot C. Analysis of the human adult urinary metabolome variations with age, body mass index, and gender by implementing a comprehensive workflow for univariate and OPLS statistical analyses. *J Proteome Res*. 2015;148:3322–35.
- Thomas RS, Allen BC, Nong A, Yang L, Bermudez E, Clewell HJ III, Andersen ME. A method to integrate benchmark dose estimates with genomic data to assess the functional effects of chemical exposure. *Toxicol Sci*. 2007;981:240–8.
- van Dijk J, Leopold A, Flerlage H, van Wezel A, Seiler TB, Enrici MH, Bloor MC. The EU Green Deal's

- ambition for a toxic-free environment: Filling the gap for science-based policymaking. *Integr Environ Assess Manag.* 2021;176:1105–13.
- Van Ravenzwaay B, Montoya G, Fabian E, Herold M, Krennrich G, Looser R, Mellert W, Peter E, Strauss V, Walk T. The sensitivity of metabolomics versus classical regulatory toxicology from a NOAEL perspective. *Toxicol Lett.* 2014;2271:20–8.
- Van Ravenzwaay B, Kamp H, Montoya-Parra GA, Strauss V, Fabian E, Mellert W, Krennrich G, Walk T, Peter E, Looser R. The development of a database for metabolomics-looking back on ten years of experience. *Int J Biotechnol.* 2015;141:47–68.
- Vinken M. The adverse outcome pathway concept: a pragmatic tool in toxicology. *Toxicology.* 2013;312:158–65.
- Walvekar A, Rashida Z, Maddali H, Laxman S. A versatile LC-MS/MS approach for comprehensive, quantitative analysis of central metabolic pathways. *Wellcome Open Res.* 2018;3:122.
- Wang Z, Walker GW, Muir DC, Nagatani-Yoshida K. Toward a global understanding of chemical pollution: a first comprehensive analysis of national and regional chemical inventories. *Environ Sci Technol.* 2020;545:2575–84.
- Yanagita T, Han S-Y, Hu Y, Nagao K, Kitajima H, Murakami S. Taurine reduces the secretion of apolipoprotein B100 and lipids in HepG2 cells. *Lipids Health Dis.* 2008;71:1–6.
- Zampieri M, Szappanos B, Buchieri MV, Trauner A, Piazza I, Picotti P, Gagneux S, Borrell S, Gicquel B, Lelievre J. High-throughput metabolomic analysis predicts mode of action of uncharacterized antimicrobial compounds. *Sci Transl Med.* 2018;10429:eaa13973.
- Zheng Y, Cabassa-Hourton C, Planchais S, Lebreton S, Savouré A. The proline cycle as an eukaryotic redox valve. *J Exp Bot.* 2021;7220:6856–66.

Publisher's note Springer Nature remains neutral with regard to jurisdictional claims in published maps and institutional affiliations.

Supplementary information

High Throughput Metabolomics In vitro Platform for The Characterization of Hepatotoxicity

Cell Biology and Toxicology

Sabina Ramirez-Hincapie¹, Barbara Birk¹, Philipp Ternes², Varun Giri¹, Volker Haake², Michael

Herold², Franziska Maria Zickgraf¹, Andreas Verlohner¹, Hans-Albrecht Huener¹, Hennieke

Kamp², Peter Driemert², Robert Landsiedel^{1,3}, Elke Richling³, Dorothee Funk-Weyer¹,
Bennard van Ravenzwaay⁵

¹ BASF SE, Experimental Toxicology and Ecology, Ludwigshafen, Germany

² BASF Metabolome Solutions GmbH, Berlin, Germany

³ Free University of Berlin, Pharmacy, Pharmacology and Toxicology, Berlin, Germany.

⁴ Food Chemistry and Toxicology, Department of Chemistry, University of Kaiserslautern
Landau, Kaiserslautern, Germany

⁵ Environmental Sciences Consulting, Altrip, Germany

E-mail corresponding author: sabina.ramirez-hincapie@basf.com

Supplementary information

Suppl Fig. 1. Mass spectrometry parameters. corresponding chromatography techniques, ionization modes, Q1 mass [m/z], Q3 Mass [m/z], ChEBI ID, ChEBI name, and MRM parameters for the measured metabolites

Metabolite Name	Metabolite Class	Chromatography	Ionization	Q1 Mass [m/z]	Q3 Mass [m/z]	ChEBI ID	ChEBI Name
Glutamate	Amino acids	HILIC	ESI negative	145.9	101.7	CHEBI:18237	glutamic acid
Proline	Amino acids	HILIC	ESI negative	114	67.9	CHEBI:17203	L-proline
Taurine	Amino acids	HILIC	ESI negative	124	80	CHEBI:15891	taurine
Threonine	Amino acids	HILIC	ESI negative	117.9	73.9	CHEBI:16857	L-threonine
Tyrosine	Amino acids	HILIC	ESI negative	180	118.9	CHEBI:17895	L-tyrosine
5-Hydroxytryptophan	Amino acids related	HILIC	ESI positive	220.9	91	CHEBI:28171	5-hydroxytryptophan
Creatine	Amino acids related	HILIC	ESI negative	129.9	88.1	CHEBI:16919	creatine
Cysteinylglycine	Amino acids related	HILIC	ESI positive	178.8	76.1	CHEBI:4047	L-cysteinylglycine
Glycylleucine	Amino acids related	HILIC	ESI positive	189.1	86.1	CHEBI:73514	Gly-Leu
Ketoleucine	Amino acids related	RP-HPLC	ESI negative	129.2	129.2	CHEBI:48430	4-methyl-2-oxopentanoic acid
N-Acetylaspartate	Amino acids related	HILIC	ESI positive	175.9	134.1	CHEBI:21547	N-acetyl-L-aspartic acid
N-Acetylleucine	Amino acids related	HILIC	ESI positive	174.2	86.1	CHEBI:17786	N-acetyl-L-leucine
N-Acetylserine	Amino acids related	HILIC	ESI positive	148.1	106.2	CHEBI:45441	N-acetyl-L-serine
Pipecolic acid	Amino acids related	HILIC	ESI positive	129.9	84.1	CHEBI:17964	pipecolic acid
S-Adenosylhomocysteine	Amino acids related	HILIC	ESI positive	385.1	136	CHEBI:16680	S-adenosyl-L-homocysteine
myo-Inositol-2-phosphate	Carbohydrates and related	RP-HPLC	ESI negative	259.2	79.2	CHEBI:62383	1D-myo-inositol 2-phosphate
N-Acetylglucosamine	Carbohydrates and related	HILIC	ESI positive	222	203.8	CHEBI:506227	N-acetyl-D-glucosamine
Adenosine monophosphate, cyclic (cAMP)	Energy metabolism and related	HILIC	ESI positive	330.1	136.1	CHEBI:27844	2',3'-cyclic AMP
Carnitine	Energy metabolism and related	HILIC	ESI positive	162.1	103	CHEBI:3424	carnitinium
Glycerol-3-phosphate	Energy metabolism and related	RP-HPLC	ESI negative	170.9	78.8	CHEBI:15978	sn-glycerol 3-phosphate
Hexadecanoylcarnitine	Energy metabolism and related	RP-HPLC	ESI positive	400.2	85	CHEBI:73067	O-palmitoylcarnitine
Hexadecenoylcarnitine	Energy metabolism and related	RP-HPLC	ESI positive	398.2	85	CHEBI:88544	9-Hexadecenoylcarnitine
Hexanoylcarnitine	Energy metabolism and related	HILIC	ESI positive	260.1	85	CHEBI:70749	O-hexanoylcarnitine
O-Acetylcarnitine	Energy metabolism and related	HILIC	ESI positive	204.1	85.2	CHEBI:57589	O-acetyl-L-carnitine
Octadecenoylcarnitine	Energy metabolism and related	RP-HPLC	ESI positive	426.2	85	CHEBI:85460	O-octadecenoyl-L-carnitine
Propionylcarnitine	Energy metabolism and related	HILIC	ESI positive	218.1	85.2	CHEBI:53210	O-propanoyl-L-carnitine
Tetradecanoylcarnitine	Energy metabolism and related	RP-HPLC	ESI positive	372.2	85	CHEBI:73061	O-tetradecanoylcarnitine
2'-Deoxycytidine	Nucleobases and related	HILIC	ESI positive	228.1	112.1	CHEBI:15698	2'-deoxycytidine
Guanine	Nucleobases and related	HILIC	ESI positive	151.9	135.1	CHEBI:16235	guanine

Uridine	Nucleobases and related	HILIC	ESI positive	245.1	113.1	CHEBI:16704	uridine
Uridine	Nucleobases and related	HILIC	ESI negative	243	109.9	CHEBI:16704	uridine
Coenzyme Q10	Vitamins, cofactors and related	RP-HPLC	ESI positive	863.7	197	CHEBI:46245	coenzyme Q10
Coenzyme Q9	Vitamins, cofactors and related	RP-HPLC	ESI positive	795.7	197	CHEBI:18160	ubiquinone-9
Flavin adenine dinucleotide (FAD)	Vitamins, cofactors and related	HILIC	ESI negative	784.4	437.1	CHEBI:16238	FAD
Glutathione (GSH)	Vitamins, cofactors and related	HILIC	ESI negative	306	143	CHEBI:16856	glutathione
Nicotinamide adenine dinucleotide (NAD)	Vitamins, cofactors and related	RP-HPLC	ESI negative	662	540.1	CHEBI:57540	NAD(1-)
Pantothenic acid	Vitamins, cofactors and related	HILIC	ESI negative	218.2	88.1	CHEBI:46905	(R)-pantothenic acid
Pyridoxal	Vitamins, cofactors and related	HILIC	ESI positive	167.9	150	CHEBI:17310	pyridoxal
Thiamine	Vitamins, cofactors and related	HILIC	ESI positive	265.3	122	CHEBI:18385	thiamine(1+)
Triacylglycerol (C30:0,C18:1)	Acylglycerols	RP-HPLC	ESI positive	822.8	523.5	CHEBI:85726	triacylglycerol 48:1
Triacylglycerol (C30:0,C18:2)	Acylglycerols	RP-HPLC	ESI positive	820.8	523.5	CHEBI:85725	triacylglycerol 48:2
Triacylglycerol (C32:0,C16:0)	Acylglycerols	RP-HPLC	ESI positive	824.8	551.5	CHEBI:85870	triacylglycerol 48:0
Triacylglycerol (C32:0,C16:1)	Acylglycerols	RP-HPLC	ESI positive	822.8	551.5	CHEBI:85726	triacylglycerol 48:1
Triacylglycerol (C32:1,C16:1)	Acylglycerols	RP-HPLC	ESI positive	820.8	549.5	CHEBI:85725	triacylglycerol 48:2
Triacylglycerol (C34:0,C16:0)	Acylglycerols	RP-HPLC	ESI positive	852.9	579.6	CHEBI:85874	triacylglycerol 50:0
Triacylglycerol (C34:0,C17:0)	Acylglycerols	RP-HPLC	ESI positive	866.8	579.6	CHEBI:140862	triacylglycerol 51:0
Triacylglycerol (C34:0,C18:0)	Acylglycerols	RP-HPLC	ESI positive	880.9	579.6	CHEBI:167005	triacylglycerol 52:0
Triacylglycerol (C34:0,C18:1)	Acylglycerols	RP-HPLC	ESI positive	878.9	579.6	CHEBI:90302	triacylglycerol 52:1
Triacylglycerol (C34:1,C16:0)	Acylglycerols	RP-HPLC	ESI positive	850.8	577.5	CHEBI:84665	triacylglycerol 50:1
Triacylglycerol (C34:1,C18:1)	Acylglycerols	RP-HPLC	ESI positive	876.9	577.5	CHEBI:85736	triacylglycerol 52:2
Triacylglycerol (C34:1,C18:3)	Acylglycerols	RP-HPLC	ESI positive	872.8	577.5	CHEBI:84660	triacylglycerol 52:4
Triacylglycerol (C34:2,C18:0)	Acylglycerols	RP-HPLC	ESI positive	876.9	575.6	CHEBI:85736	triacylglycerol 52:2
Triacylglycerol (C34:2,C18:1)	Acylglycerols	RP-HPLC	ESI positive	874.9	575.6	CHEBI:84661	triacylglycerol 52:3
Triacylglycerol (C36:1,C18:0)	Acylglycerols	RP-HPLC	ESI positive	906.9	605.4	CHEBI:90305	triacylglycerol 54:1
Triacylglycerol (C36:1,C18:1)	Acylglycerols	RP-HPLC	ESI positive	904.8	605.4	CHEBI:85743	triacylglycerol 54:2
Triacylglycerol (C36:1,C18:2)	Acylglycerols	RP-HPLC	ESI positive	902.9	605.6	CHEBI:84659	triacylglycerol 54:3
Triacylglycerol (C36:2,C18:1)	Acylglycerols	RP-HPLC	ESI positive	902.9	603.6	CHEBI:84659	triacylglycerol 54:3
Triacylglycerol (C36:3,C18:1)	Acylglycerols	RP-HPLC	ESI positive	900.8	601.5	CHEBI:85742	triacylglycerol 54:4
Triacylglycerol (C36:3,C18:2)	Acylglycerols	RP-HPLC	ESI positive	898.8	601.5	CHEBI:85741	triacylglycerol 54:5
Triacylglycerol (C36:4,C16:0)	Acylglycerols	RP-HPLC	ESI positive	872.8	599.5	CHEBI:84660	triacylglycerol 52:4
Triacylglycerol (C36:4,C18:0)	Acylglycerols	RP-HPLC	ESI positive	900.8	599.5	CHEBI:85742	triacylglycerol 54:4
Choline plasmalogen (C36:4)	Glycerophospholipids	RP-HPLC	ESI positive	768.8	184.1	new	phosphatidylcholine P-36:3
Choline plasmalogen (C36:5)	Glycerophospholipids	RP-HPLC	ESI positive	766.8	184.1	CHEBI:132586	phosphatidylcholine P-36:4
Phosphatidylcholine (C32:0)	Glycerophospholipids	RP-HPLC	ESI positive	734.6	184.1	CHEBI:66850	phosphatidylcholine 32:0

Phosphatidylcholine (C34:0)	Glycerophospholipids	RP-HPLC	ESI positive	762.6	184.1	CHEBI:66855	phosphatidylcholine 34:0
Phosphatidylcholine (C34:1)	Glycerophospholipids	RP-HPLC	ESI positive	760.6	184.1	CHEBI:64517	phosphatidylcholine 34:1
Phosphatidylcholine (C34:2)	Glycerophospholipids	RP-HPLC	ESI positive	758.6	184.1	CHEBI:64516	phosphatidylcholine 34:2
Phosphatidylcholine (C34:3)	Glycerophospholipids	RP-HPLC	ESI positive	756.6	184.1	CHEBI:64424	phosphatidylcholine 34:3
Phosphatidylcholine (C36:0)	Glycerophospholipids	RP-HPLC	ESI positive	790.6	184.1	CHEBI:66858	phosphatidylcholine 36:0
Phosphatidylcholine (C36:1)	Glycerophospholipids	RP-HPLC	ESI positive	788.6	184.1	CHEBI:66857	phosphatidylcholine 36:1
Phosphatidylcholine (C36:2)	Glycerophospholipids	RP-HPLC	ESI positive	786.6	184.1	CHEBI:64433	phosphatidylcholine 36:2
Phosphatidylcholine (C36:3)	Glycerophospholipids	RP-HPLC	ESI positive	784.6	184.1	CHEBI:64523	phosphatidylcholine 36:3
Phosphatidylcholine (C36:4)	Glycerophospholipids	RP-HPLC	ESI positive	782.6	184.1	CHEBI:64520	phosphatidylcholine 36:4
Phosphatidylcholine (C36:5)	Glycerophospholipids	RP-HPLC	ESI positive	780.6	184.1	CHEBI:64504	phosphatidylcholine 36:5
Phosphatidylcholine (C38:4)	Glycerophospholipids	RP-HPLC	ESI positive	810.6	184.1	CHEBI:64526	phosphatidylcholine 38:4
Phosphatidylcholine (C38:5)	Glycerophospholipids	RP-HPLC	ESI positive	808.6	184.1	CHEBI:64525	phosphatidylcholine 38:5
Phosphatidylcholine (C38:6)	Glycerophospholipids	RP-HPLC	ESI positive	806.6	184.1	CHEBI:64519	phosphatidylcholine 38:6
Phosphatidylcholine (C40:6)	Glycerophospholipids	RP-HPLC	ESI positive	834.6	184.1	CHEBI:64431	phosphatidylcholine 40:6
Phosphatidylcholine (C40:7)	Glycerophospholipids	RP-HPLC	ESI positive	832.6	184.1	CHEBI:64521	phosphatidylcholine 40:7
Phosphatidylcholine (C40:8)	Glycerophospholipids	RP-HPLC	ESI positive	830.6	184.1	CHEBI:85851	phosphatidylcholine 40:8
Phosphatidylethanolamine (C32:0)	Glycerophospholipids	RP-HPLC	ESI positive	692.6	551.6	CHEBI:71711	phosphatidylethanolamine 32:0
Phosphatidylethanolamine (C34:0)	Glycerophospholipids	RP-HPLC	ESI positive	720.6	579.6	CHEBI:71718	phosphatidylethanolamine 34:0 zwitterion
Phosphatidylethanolamine (C34:1)	Glycerophospholipids	RP-HPLC	ESI positive	718.6	577.6	CHEBI:71720	phosphatidylethanolamine 34:1 zwitterion
Phosphatidylethanolamine (C34:2)	Glycerophospholipids	RP-HPLC	ESI positive	716.5	575.6	CHEBI:71721	phosphatidylethanolamine 34:2 zwitterion
Phosphatidylethanolamine (C36:0)	Glycerophospholipids	RP-HPLC	ESI positive	748.6	607.6	CHEBI:134435	phosphatidylethanolamine 36:0
Phosphatidylethanolamine (C36:1)	Glycerophospholipids	RP-HPLC	ESI positive	746.6	605.6	CHEBI:134451	phosphatidylethanolamine 36:1
Phosphatidylethanolamine (C36:2)	Glycerophospholipids	RP-HPLC	ESI positive	744.6	603.6	CHEBI:141588	phosphatidylethanolamine 36:2
Phosphatidylethanolamine (C36:3)	Glycerophospholipids	RP-HPLC	ESI positive	742.6	601.6	CHEBI:141589	phosphatidylethanolamine 36:3
Phosphatidylethanolamine (C36:4)	Glycerophospholipids	RP-HPLC	ESI positive	740.5	599.6	CHEBI:71730	phosphatidylethanolamine 36:4 zwitterion
Phosphatidylethanolamine (C38:3)	Glycerophospholipids	RP-HPLC	ESI positive	770.6	629.6	CHEBI:141590	phosphatidylethanolamine 38:3
Phosphatidylethanolamine (C38:4)	Glycerophospholipids	RP-HPLC	ESI positive	768.6	627.6	CHEBI:134270	phosphatidylethanolamine 38:4
Phosphatidylethanolamine (C38:5)	Glycerophospholipids	RP-HPLC	ESI positive	766.5	625.6	CHEBI:134239	phosphatidylethanolamine 38:5
Phosphatidylethanolamine (C38:6)	Glycerophospholipids	RP-HPLC	ESI positive	764.5	623.6	CHEBI:134428	phosphatidylethanolamine 38:6
Phosphatidylethanolamine (C40:6)	Glycerophospholipids	RP-HPLC	ESI positive	792.6	651.6	CHEBI:134241	phosphatidylethanolamine 40:6
Phosphatidylethanolamine (C40:7)	Glycerophospholipids	RP-HPLC	ESI positive	790.6	649.6	CHEBI:134429	phosphatidylethanolamine 40:7

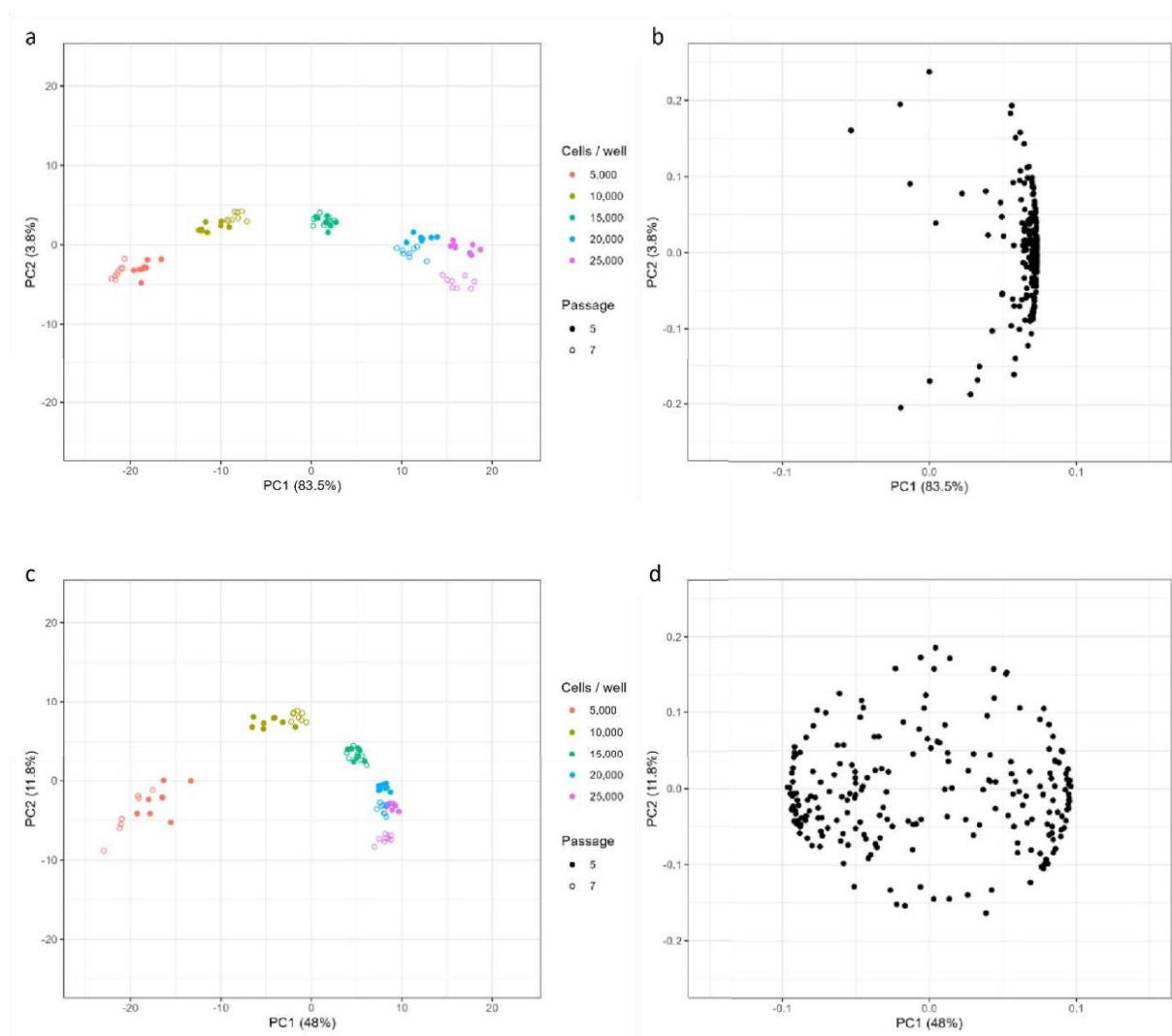
Lysophosphatidylcholine (C14:0)	Lysoglycerophospholipids	RP-HPLC	ESI positive	468.3	184.1	CHEBI:64483	lysophosphatidylcholine 14:0
Lysophosphatidylcholine (C16:0)	Lysoglycerophospholipids	RP-HPLC	ESI positive	496.3	184.1	CHEBI:64563	lysophosphatidylcholine 16:0
Lysophosphatidylcholine (C16:1)	Lysoglycerophospholipids	RP-HPLC	ESI positive	494.4	184.1	CHEBI:64560	lysophosphatidylcholine 16:1
Lysophosphatidylcholine (C20:0)	Lysoglycerophospholipids	RP-HPLC	ESI positive	552.4	184.1	CHEBI:67058	lysophosphatidylcholine 20:0
Lysophosphatidylcholine (C20:1)	Lysoglycerophospholipids	RP-HPLC	ESI positive	550.4	184.1	CHEBI:67057	lysophosphatidylcholine 20:1
Lysophosphatidylcholine (C20:4)	Lysoglycerophospholipids	RP-HPLC	ESI positive	544.4	184.1	CHEBI:64568	lysophosphatidylcholine 20:4
Lysophosphatidylcholine (C22:0)	Lysoglycerophospholipids	RP-HPLC	ESI positive	580.4	184.1	CHEBI:67061	lysophosphatidylcholine 22:0
Lysophosphatidylcholine (C24:0)	Lysoglycerophospholipids	RP-HPLC	ESI positive	608.5	184.1	CHEBI:74470	lysophosphatidylcholine 24:0
Lysophosphatidylcholine (C24:1)	Lysoglycerophospholipids	RP-HPLC	ESI positive	606.5	184.1	CHEBI:74471	lysophosphatidylcholine 24:1
Lysophosphatidylethanolamine (C16:0)	Lysoglycerophospholipids	RP-HPLC	ESI positive	454.3	313.2	CHEBI:90452	lysophosphatidylethanolamine 16:0
Lysophosphatidylethanolamine (C18:0)	Lysoglycerophospholipids	RP-HPLC	ESI positive	482.3	341.2	CHEBI:64576	lysophosphatidylethanolamine 18:0
Lysophosphatidylethanolamine (C18:1)	Lysoglycerophospholipids	RP-HPLC	ESI positive	480.3	339.2	CHEBI:64575	lysophosphatidylethanolamine 18:1
Lysophosphatidylethanolamine (C20:4)	Lysoglycerophospholipids	RP-HPLC	ESI positive	502.3	361.2	CHEBI:64569	lysophosphatidylethanolamine 20:4
Lysophosphatidylethanolamine (C22:6)	Lysoglycerophospholipids	RP-HPLC	ESI positive	526.3	385.2	CHEBI:72734	lysophosphatidylethanolamine 22:6
Ceramide (d16:1,C24:0)	Sphingolipids	RP-HPLC	ESI positive	604.2	236.2	new	ceramide d16:1,24:0
Ceramide (d17:1,C24:0)	Sphingolipids	RP-HPLC	ESI positive	618.6	250.2	new	ceramide d17:1,24:0
Ceramide (d18:1,C16:0)	Sphingolipids	RP-HPLC	ESI positive	520.5	264.2	CHEBI:184082	N-palmitoyl-d-sphingosine
Ceramide (d18:1,C18:0)	Sphingolipids	RP-HPLC	ESI positive	548.5	264.2	new	ceramide d18:1,18:0
Ceramide (d18:1,C20:0)	Sphingolipids	RP-HPLC	ESI positive	576.6	264.2	new	ceramide d18:1,20:0
Ceramide (d18:1,C21:0)	Sphingolipids	RP-HPLC	ESI positive	590.5	264.2	new	ceramide d18:1,21:0
Ceramide (d18:1,C22:0)	Sphingolipids	RP-HPLC	ESI positive	604.6	264.2	new	ceramide d18:1,22:0
Ceramide (d18:1,C22:1)	Sphingolipids	RP-HPLC	ESI positive	602.6	264.2	new	ceramide d18:1,22:1
Ceramide (d18:1,C23:0)	Sphingolipids	RP-HPLC	ESI positive	618.6	264.2	new	ceramide d18:1,23:0
Ceramide (d18:1,C24:0)	Sphingolipids	RP-HPLC	ESI positive	632.6	264.2	new	ceramide d18:1,24:0
Ceramide (d18:1,C24:1)	Sphingolipids	RP-HPLC	ESI positive	630.6	264.2	new	ceramide d18:1,24:1
Ceramide (d18:1,C24:2)	Sphingolipids	RP-HPLC	ESI positive	628.6	264.2	new	ceramide d18:1,24:2
Ceramide (d18:2,C16:0)	Sphingolipids	RP-HPLC	ESI positive	518.5	262.2	new	ceramide d18:2,16:0
Ceramide (d18:2,C18:0)	Sphingolipids	RP-HPLC	ESI positive	546.5	262.2	new	ceramide d18:2,18:0
Ceramide (d18:2,C22:0)	Sphingolipids	RP-HPLC	ESI positive	602.6	262.2	new	ceramide d18:2,22:0
Ceramide (d18:2,C23:0)	Sphingolipids	RP-HPLC	ESI positive	616.5	262.2	new	ceramide d18:2,23:0
Ceramide (d18:2,C24:0)	Sphingolipids	RP-HPLC	ESI positive	630.6	262.2	new	ceramide d18:2,24:0
Ceramide (d18:2,C24:1)	Sphingolipids	RP-HPLC	ESI positive	628.6	262.2	new	ceramide d18:2,24:1

Ceramide (d18:2,C24:2)							262.2	new	ceramide d18:2,24:2
Sphingomyelin (d32:1)	Sphingolipids	RP-HPLC	ESI positive	626.6			184.1	CHEBI:64586	sphingomyelin 32:1
Sphingomyelin (d32:2)	Sphingolipids	RP-HPLC	ESI positive	675.5			184.1	CHEBI:72510	sphingomyelin 32:2
Sphingomyelin (d33:1)	Sphingolipids	RP-HPLC	ESI positive	689.6			184.1	CHEBI:64585	sphingomyelin 33:1
Sphingomyelin (d34:0)	Sphingolipids	RP-HPLC	ESI positive	705.5			184.1	CHEBI:72513	sphingomyelin 34:0
Sphingomyelin (d34:1)	Sphingolipids	RP-HPLC	ESI positive	703.6			184.1	CHEBI:72514	sphingomyelin 34:1
Sphingomyelin (d34:2)	Sphingolipids	RP-HPLC	ESI positive	725.6			542.5	CHEBI:72514	sphingomyelin 34:1
Sphingomyelin (d34:2)	Sphingolipids	RP-HPLC	ESI positive	701.5			184.1	CHEBI:64587	sphingomyelin 34:2
Sphingomyelin (d35:1)	Sphingolipids	RP-HPLC	ESI positive	723.6			540.6	CHEBI:64587	sphingomyelin 34:2
Sphingomyelin (d35:2)	Sphingolipids	RP-HPLC	ESI positive	717.5			184.1	CHEBI:133629	sphingomyelin 35:1
Sphingomyelin (d36:1)	Sphingolipids	RP-HPLC	ESI positive	715.5			184.1	new	sphingomyelin 35:2
Sphingomyelin (d36:2)	Sphingolipids	RP-HPLC	ESI positive	731.5			184.1	CHEBI:72518	sphingomyelin 36:1
Sphingomyelin (d36:3)	Sphingolipids	RP-HPLC	ESI positive	729.5			184.1	CHEBI:72519	sphingomyelin 36:2
Sphingomyelin (d37:1)	Sphingolipids	RP-HPLC	ESI positive	727.5			184.1	CHEBI:72520	sphingomyelin 36:3
Sphingomyelin (d38:1)	Sphingolipids	RP-HPLC	ESI positive	745.5			184.1	CHEBI:85759	sphingomyelin 37:1
Sphingomyelin (d38:2)	Sphingolipids	RP-HPLC	ESI positive	759.5			184.1	CHEBI:72523	sphingomyelin 38:1
Sphingomyelin (d39:1)	Sphingolipids	RP-HPLC	ESI positive	757.5			184.1	CHEBI:72524	sphingomyelin 38:2
Sphingomyelin (d40:1)	Sphingolipids	RP-HPLC	ESI positive	773.5			184.1	CHEBI:85761	sphingomyelin 39:1
Sphingomyelin (d40:2)	Sphingolipids	RP-HPLC	ESI positive	787.5			184.1	CHEBI:72528	sphingomyelin 40:1
Sphingomyelin (d41:1)	Sphingolipids	RP-HPLC	ESI positive	785.5			184.1	CHEBI:72529	sphingomyelin 40:2
Sphingomyelin (d41:2)	Sphingolipids	RP-HPLC	ESI positive	801.5			184.1	CHEBI:83893	sphingomyelin 41:1
Sphingomyelin (d42:1)	Sphingolipids	RP-HPLC	ESI positive	799.7			184.1	CHEBI:85762	sphingomyelin 41:2
Sphingomyelin (d42:2)	Sphingolipids	RP-HPLC	ESI positive	815.7			184.1	CHEBI:72533	sphingomyelin 42:1
Sphingomyelin (d42:2)	Sphingolipids	RP-HPLC	ESI positive	813.7			184.1	CHEBI:72534	sphingomyelin 42:2
Cholesteryl ester (C20:2)	Cholesterol and related	RP-HPLC	ESI positive	694.7			369.3	CHEBI:183804	CE(20:2)
Cholesteryl ester (C20:3)	Cholesterol and related	RP-HPLC	ESI positive	692.7			369.3	CHEBI:138331	cholesteryl icosatrienoate
Isopentenyl pyrophosphate (IPP)	Cholesterol and related	RP-HPLC	ESI negative	245			78.8	CHEBI:16584	isopentenyl diphosphate
Phosphocholine	Miscellaneous lipids	HILIC	ESI positive	183.8			86.2	CHEBI:18132	phosphocholine
Biliverdin	Miscellaneous	HILIC	ESI positive	583.3			297.2	CHEBI:17033	biliverdin
Unknown lipid (849590045)	Unknown	RP-HPLC	ESI positive	794.6			184.1	n/a	n/a
Unknown lipid (849590046)	Unknown	RP-HPLC	ESI positive	811.6			183.9	n/a	n/a
Unknown lipid (849590126)	Unknown	RP-HPLC	ESI positive	772.6			184.1	n/a	n/a
Unknown lipid (849590204)	Unknown	RP-HPLC	ESI positive	870.8			597.5	n/a	n/a
Unknown lipid (849590225)	Unknown	RP-HPLC	ESI positive	904			904	n/a	n/a
Unknown lipid (849590328)	Unknown	RP-HPLC	ESI positive	428.1			136.2	n/a	n/a
Unknown lipid (849590410)	Unknown	RP-HPLC	ESI positive	523.5			211.2	n/a	n/a
Unknown lipid (849590418)	Unknown	RP-HPLC	ESI positive	575.5			237.2	n/a	n/a
Unknown lipid (849590419)	Unknown	RP-HPLC	ESI positive	575.5			265.3	n/a	n/a
Unknown lipid (849590423)	Unknown	RP-HPLC	ESI positive	577.5			239.2	n/a	n/a

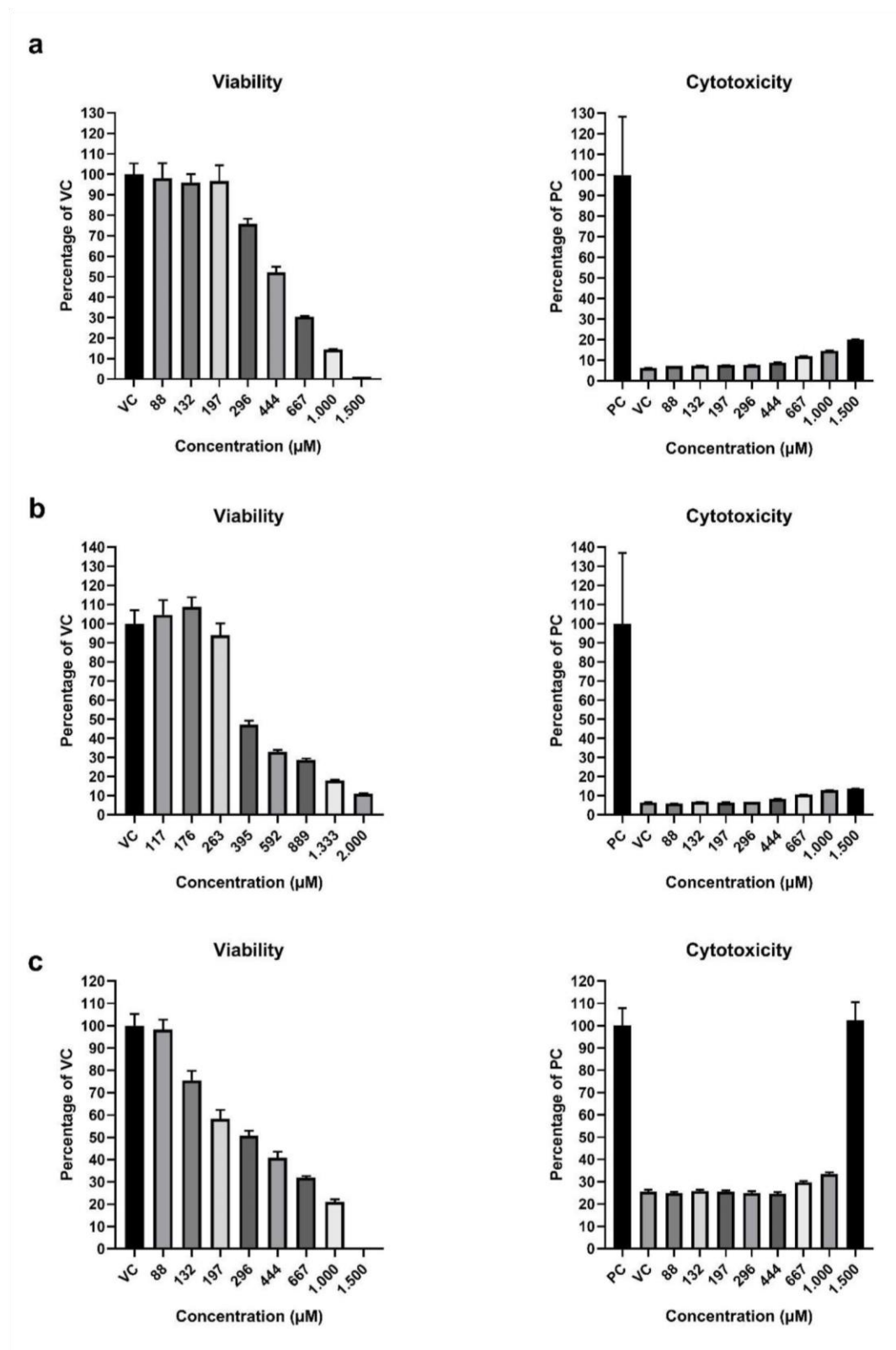
Unknown lipid (849590430)	Unknown	RP-HPLC	ESI positive	603.5	135.1	n/a	n/a
Unknown lipid (849590434)	Unknown	RP-HPLC	ESI positive	620.6	236.2	n/a	n/a
Unknown lipid (849590435)	Unknown	RP-HPLC	ESI positive	620.6	262.2	n/a	n/a
Unknown lipid (849590436)	Unknown	RP-HPLC	ESI positive	620.6	264.2	n/a	n/a
Unknown lipid (849590437)	Unknown	RP-HPLC	ESI positive	622.6	236.2	n/a	n/a
Unknown lipid (849590438)	Unknown	RP-HPLC	ESI positive	622.6	264.2	n/a	n/a
Unknown lipid (849590439)	Unknown	RP-HPLC	ESI positive	631.6	265.3	n/a	n/a
Unknown lipid (849590442)	Unknown	RP-HPLC	ESI positive	634.6	262.2	n/a	n/a
Unknown lipid (849590443)	Unknown	RP-HPLC	ESI positive	634.6	264.2	n/a	n/a
Unknown lipid (849590444)	Unknown	RP-HPLC	ESI positive	636.6	250.2	n/a	n/a
Unknown lipid (849590445)	Unknown	RP-HPLC	ESI positive	636.6	264.2	n/a	n/a
Unknown lipid (849590446)	Unknown	RP-HPLC	ESI positive	646.6	264.2	n/a	n/a
Unknown lipid (849590448)	Unknown	RP-HPLC	ESI positive	648.6	262.2	n/a	n/a
Unknown lipid (849590449)	Unknown	RP-HPLC	ESI positive	648.6	264.2	n/a	n/a
Unknown lipid (849590450)	Unknown	RP-HPLC	ESI positive	650.6	264.2	n/a	n/a
Unknown lipid (849590451)	Unknown	RP-HPLC	ESI positive	662.6	264.2	n/a	n/a
Unknown lipid (849590452)	Unknown	RP-HPLC	ESI positive	662.6	278.2	n/a	n/a
Unknown lipid (849590454)	Unknown	RP-HPLC	ESI positive	704.5	184.1	n/a	n/a
Unknown lipid (849590455)	Unknown	RP-HPLC	ESI positive	716.5	184.1	n/a	n/a
Unknown lipid (849590456)	Unknown	RP-HPLC	ESI positive	728.5	184.1	n/a	n/a
Unknown lipid (849590457)	Unknown	RP-HPLC	ESI positive	730.5	184.1	n/a	n/a
Unknown lipid (849590458)	Unknown	RP-HPLC	ESI positive	732.5	184.1	n/a	n/a
Unknown lipid (849590459)	Unknown	RP-HPLC	ESI positive	732.6	184.1	n/a	n/a
Unknown lipid (849590460)	Unknown	RP-HPLC	ESI positive	738.5	184.1	n/a	n/a
Unknown lipid (849590462)	Unknown	RP-HPLC	ESI positive	744.6	184.1	n/a	n/a
Unknown lipid (849590463)	Unknown	RP-HPLC	ESI positive	764.5	184.1	n/a	n/a
Unknown lipid (849590464)	Unknown	RP-HPLC	ESI positive	774.6	184.1	n/a	n/a
Unknown lipid (849590465)	Unknown	RP-HPLC	ESI positive	778.5	184.1	n/a	n/a
Unknown lipid (849590466)	Unknown	RP-HPLC	ESI positive	792.6	184.1	n/a	n/a
Unknown lipid (849590467)	Unknown	RP-HPLC	ESI positive	794.6	653.6	n/a	n/a
Unknown lipid (849590468)	Unknown	RP-HPLC	ESI positive	796.6	184.1	n/a	n/a
Unknown lipid (849590469)	Unknown	RP-HPLC	ESI positive	796.6	655.6	n/a	n/a
Unknown lipid (849590472)	Unknown	RP-HPLC	ESI positive	824.6	184.1	n/a	n/a
Unknown lipid (849590473)	Unknown	RP-HPLC	ESI positive	824.6	683.6	n/a	n/a
Unknown lipid (849590480)	Unknown	RP-HPLC	ESI positive	838.6	184.1	n/a	n/a
Unknown lipid (849590481)	Unknown	RP-HPLC	ESI positive	842.6	184.1	n/a	n/a
Unknown lipid (849590482)	Unknown	RP-HPLC	ESI positive	848.8	549.5	n/a	n/a
Unknown lipid (849590483)	Unknown	RP-HPLC	ESI positive	848.8	575.5	n/a	n/a
Unknown lipid (849590484)	Unknown	RP-HPLC	ESI positive	848.8	577.5	n/a	n/a
Unknown lipid (849590485)	Unknown	RP-HPLC	ESI positive	850.8	551.5	n/a	n/a

Unknown lipid (849590486)	Unknown	RP-HPLC	ESI positive	850.8	605.5	n/a	n/a
Unknown polar (869590388)	Unknown	HILIC	ESI positive	102.1	56.1	n/a	n/a
Unknown polar (869590390)	Unknown	HILIC	ESI positive	116.1	70.1	n/a	n/a
Unknown polar (869590398)	Unknown	HILIC	ESI positive	132.1	90.1	n/a	n/a
Unknown polar (869590402)	Unknown	HILIC	ESI positive	148.1	56	n/a	n/a
Unknown polar (869590442)	Unknown	HILIC	ESI positive	230.2	100.1	n/a	n/a
Unknown polar (869590444)	Unknown	HILIC	ESI positive	232.2	85	n/a	n/a
Unknown polar (869590448)	Unknown	HILIC	ESI positive	246.2	85	n/a	n/a
Unknown polar (869590452)	Unknown	HILIC	ESI positive	268.1	136.1	n/a	n/a
Unknown polar (869590453)	Unknown	HILIC	ESI positive	296.1	104.1	n/a	n/a
Unknown polar (869590456)	Unknown	HILIC	ESI positive	298.1	136.1	n/a	n/a
Unknown polar (869590459)	Unknown	HILIC	ESI positive	330.1	285.1	n/a	n/a
Unknown polar (879590076)	Unknown	HILIC	ESI negative	245.1	245.1	n/a	n/a
Unknown polar (879590422)	Unknown	HILIC	ESI negative	308.1	146.1	n/a	n/a
Unknown polar (879590425)	Unknown	HILIC	ESI negative	540.1	273	n/a	n/a

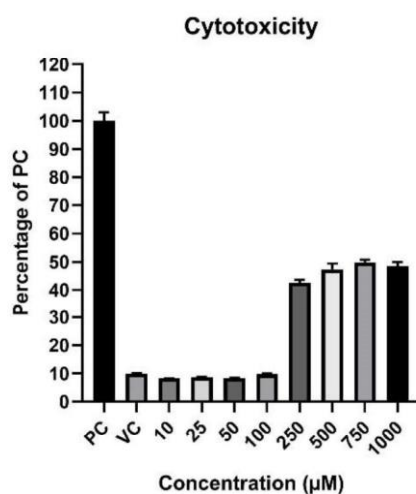
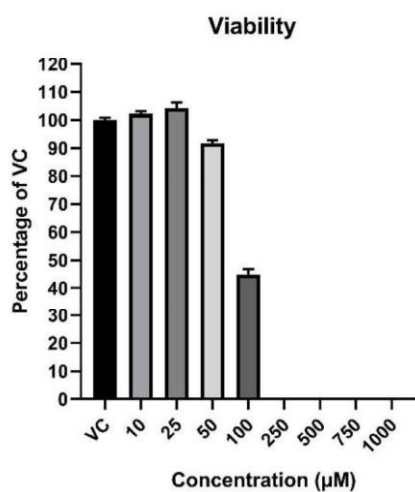
Suppl Fig 2. PCA and loading plots the metabolic profiles of different cell seeding densities and passages before and after biomass normalization. a) PCA and b) loading plots of unnormalized metabolic profiles of different cell seeding densities and passages (5 and 7). Normalization for cell number correction was not performed. c) PCA and c) loading plots of Sample Analyte Median (SAM) normalized metabolic profiles of different cell seeding densities and passages and passages (5 and 7).



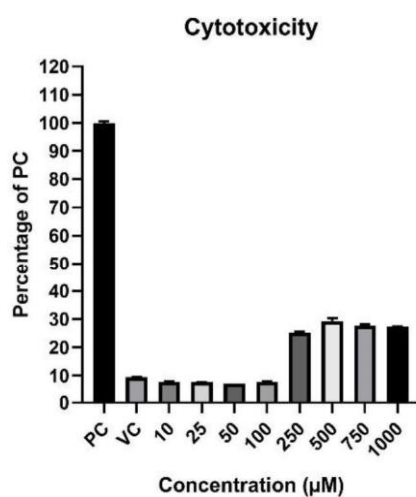
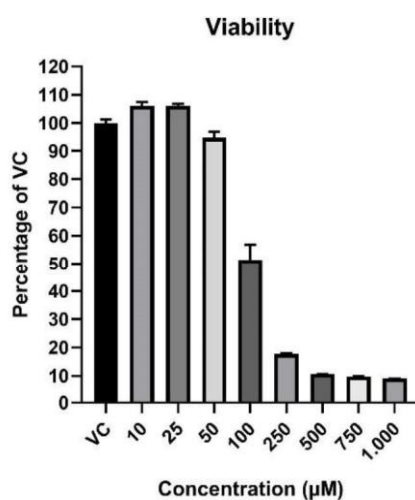
Suppl Fig. 3 Cytotoxicity and cell viability range finder for dose selection. Cell viability assay (CellTiter-Glo®) and Cytotoxicity assay (CellTox™ Green) n=6. a) Acifluorfen, b) Wy-14643, c) β Naphthoflavone, d) Aroclor 1254, e) Pendimethalin, f) Ketoconazole. Values are presented as percentage of vehicle controls for CellTiter-Glo® and as percentage of positive control (lysis buffer) for CellTox™ Green.



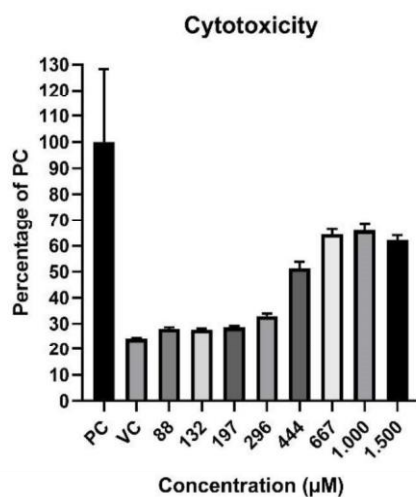
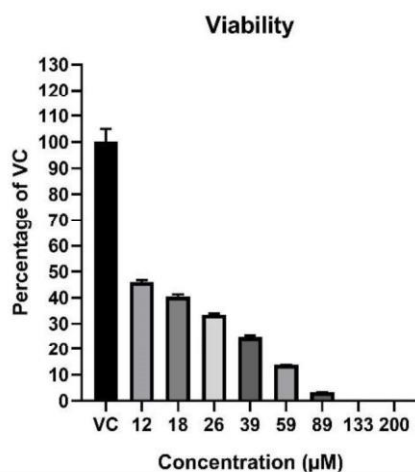
d



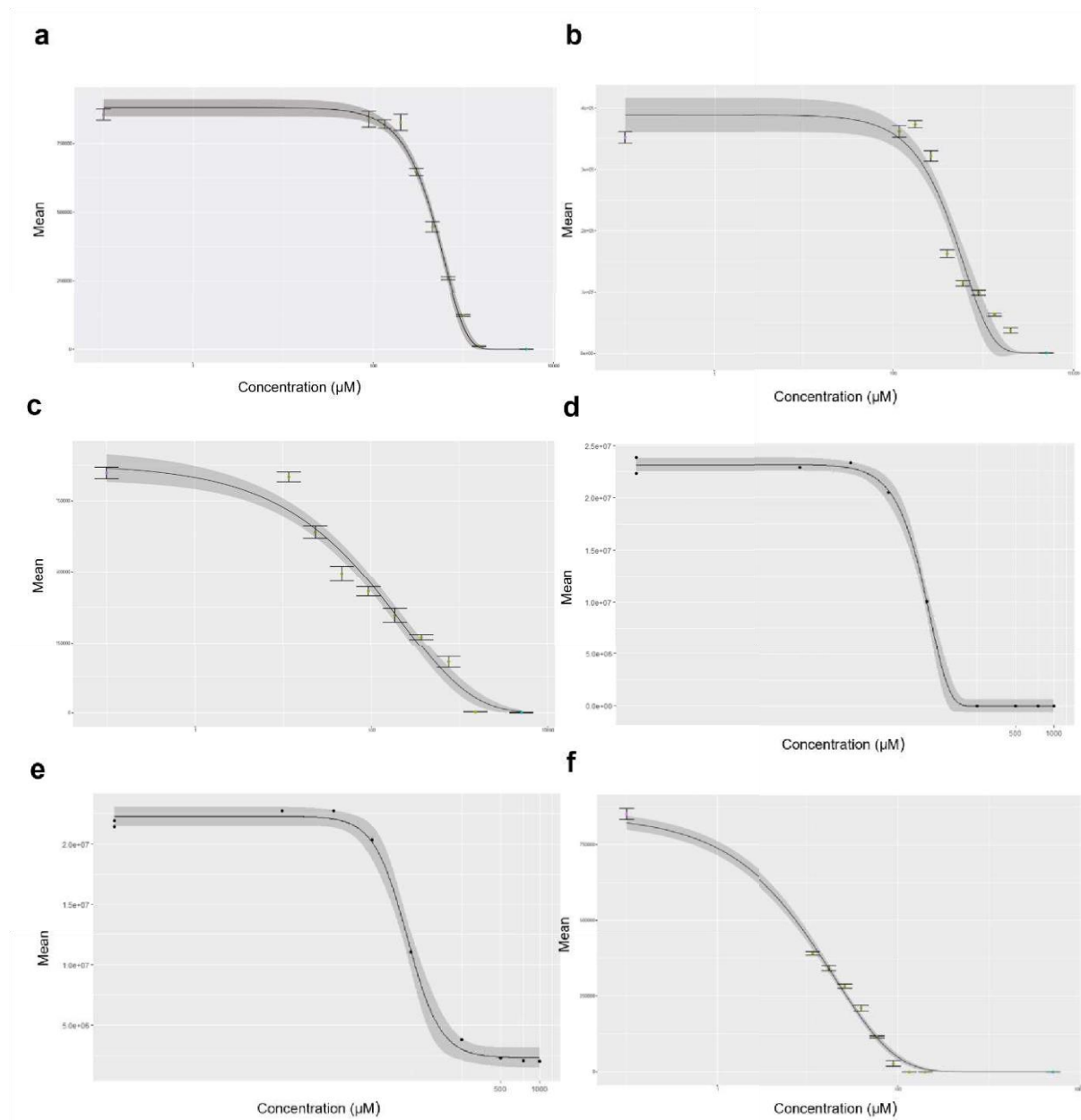
e



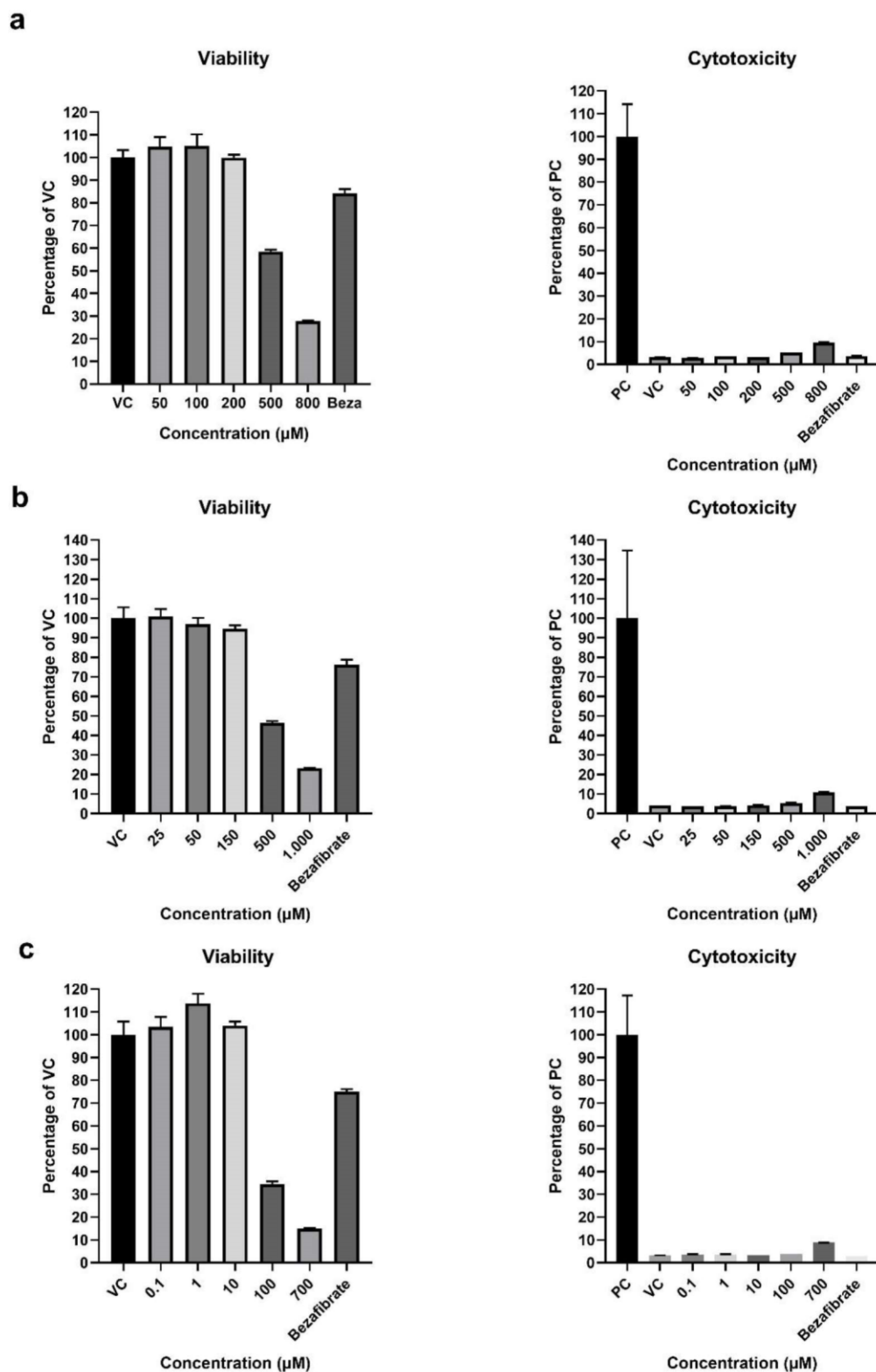
f



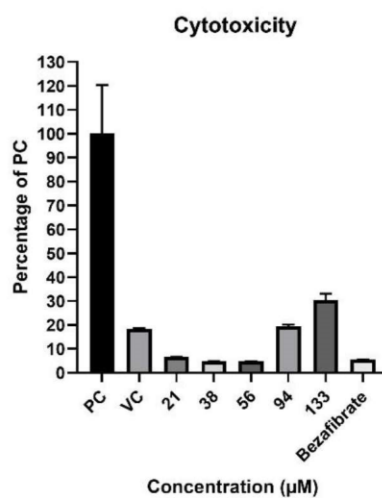
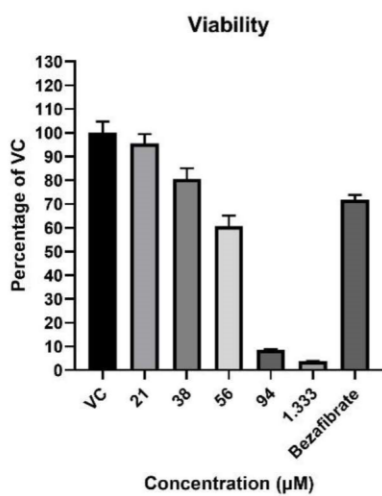
Suppl Fig. 4 Dose response curves for dose selection. Dose response curves were built with the ATP measurement (CellTiter-Glo®) in the range finder experiments (see Suppl. Figure 2) and used to derive effective concentration (EC) for the metabolomics dose setting. Acifluorfen, b) Wy-14643, c) β -Naphthoflavone, d) Aroclor 1254, e) Pendimethalin, f) Ketoconazole.



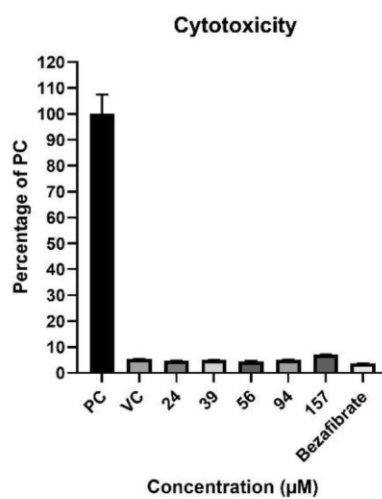
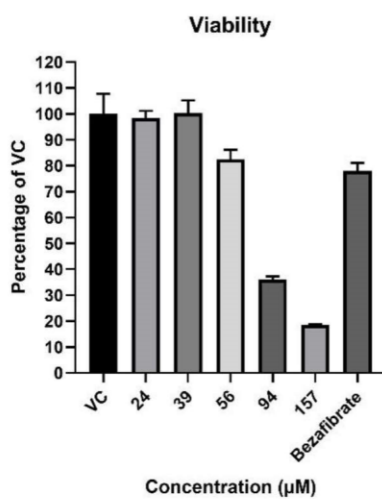
Suppl Fig. 5 Metabolomics experiment cell viability and cytotoxicity testing. Cell viability assays (CellTiter-Glo®) and Cytotoxicity assays (CellTox™ Green) n=6 were carried out in parallel with metabolomics experiments in plates handled and treated exactly as the ones used for metabolite profiling. a) Acicfluorfen, b) Wy-14643, c) β -Naphthoflavone, d) Aroclor 1254, e) Pendimethalin, f) Ketoconazole.



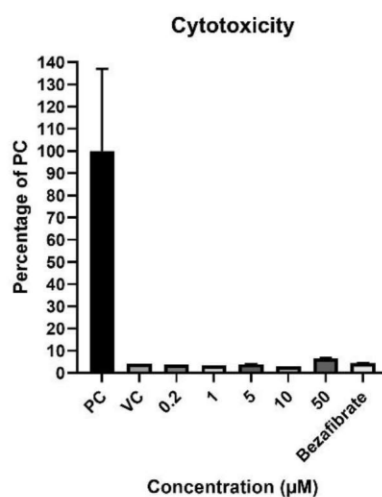
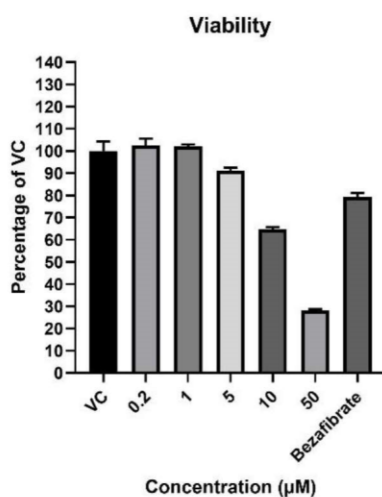
d



e



f



Suppl Fig 6. Enrichment analysis of significantly altered metabolites by ontology class after substance treatment. The distribution of the 241 measured metabolites across the ontology classes is provided in the column “measured metabolites”. The number of metabolite changes are shown for each metabolite ontology class. Numbers yellow represent that a treatment caused a significant (p -value<0.05) enrichment in an ontology class. C1 to C5: substance concentrations. Acifluorfen, b) Wy-14643, c) β -Naphthoflavone, d) Aroclor 1254, e) Pendimethalin, f) Ketoconazole.

	Substance	Acifluorfen				
		Concentration	C1	C2	C3	C4
Metabolite Class	Measured metabolites	UP	UP	UP	UP	UP
Acylglycerols	17	14	16	17	16	15
Amino acids	13	1	1	1	5	8
Amino acids related	9	1	1	1	3	3
Cholesterol and related	3	0	0	0	1	2
Energy metabolism and related	9	1	1	0	2	3
Glycerophospholipids	32	2	4	3	7	10
Hormones, signal substances and related	2	0	0	0	0	0
Lysoglycerophospholipids	29	4	8	10	23	24
Miscellaneous	1	0	0	1	1	0
Nucleobases and related	4	0	0	0	0	0
Sphingolipids	37	4	3	3	4	7
Unknown	76	17	18	22	29	31
Vitamins, cofactors and related	9	1	0	0	1	1
Total # Metabolites	241	45	52	58	92	104

	Substance	Wyth				
		Concentration	C1	C2	C3	C4
Metabolite Class	Measured metabolites					
Acylglycerols	17	0	4	4	10	10
Amino acids	13	0	0	2	1	1
Amino acids related	9	0	0	1	3	3
Cholesterol and related	3	0	0	0	0	1
Energy metabolism and related	9	0	0	1	4	3
Glycerophospholipids	32	1	1	9	8	17
Hormones, signal substances and related	2	0	0	0	2	2
Lysoglycerophospholipids	29	0	1	1	6	6
Miscellaneous	1	0	0	0	0	0
Nucleobases and related	4	0	0	1	1	0
Sphingolipids	37	2	3	12	17	17
Unknown	76	1	4	19	35	40
Vitamins, cofactors and related	9	0	1	3	2	4
Total # Metabolites	241	4	14	53	89	104

	Substance	Aroclor				
		Concentration	C1	C2	C3	C4
Metabolite Class	Measured metabolites					
Acylglycerols	17	1	0	6	10	8
Amino acids	13	0	0	7	11	11
Amino acids related	9	0	2	3	5	4
Cholesterol and related	3	0	0	0	2	2
Energy metabolism and related	9	0	0	4	5	5
Glycerophospholipids	32	10	13	11	9	8
Hormones, signal substances and related	2	0	0	0	0	0
Lysoglycerophospholipids	29	13	15	20	17	18
Miscellaneous	1	0	0	0	0	0
Nucleobases and related	4	0	0	1	3	4
Sphingolipids	37	6	16	11	8	13
Unknown	76	5	14	17	24	26
Vitamins, cofactors and related	9	1	4	1	3	3
Total # Metabolites	241	36	64	81	97	102

	Substance	Pendimethalin				
		Concentration	C1	C2	C3	C4
Metabolite Class	Measured metabolites					
Acylglycerols	17	3	4	4	7	8
Amino acids	13	0	0	1	10	11
Amino acids related	9	1	1	1	2	3
Cholesterol and related	3	0	0	0	0	2
Energy metabolism and related	9	0	0	0	2	5
Glycerophospholipids	32	7	7	8	13	10
Hormones, signal substances and related	2	0	0	0	0	0
Lysoglycerophospholipids	29	21	22	25	24	21
Miscellaneous	1	0	0	0	0	0
Nucleobases and related	4	0	0	1	1	0
Sphingolipids	37	4	5	9	15	18
Unknown	76	5	7	12	18	17
Vitamins, cofactors and related	9	0	1	1	2	2
Total # Metabolites	241	41	47	62	94	97

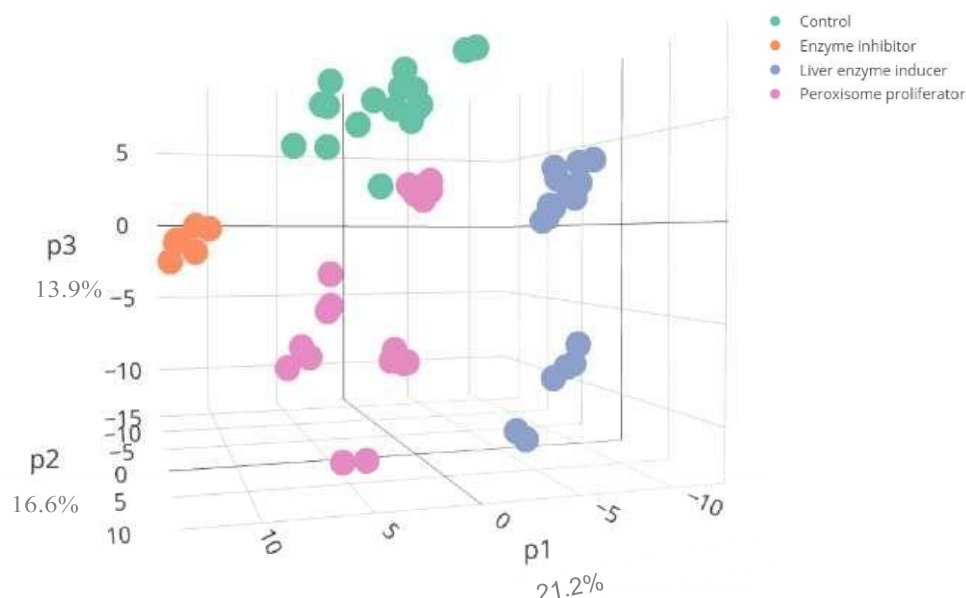
	Substance	β -Naphthoflavon plate				
	Concentration	C1	C2	C3	C4	C5
Metabolite Class	Measured metabolites					
Acylglycerols	17	0	0	0	0	0
Amino acids	13	0	0	0	4	0
Amino acids related	9	0	0	0	0	0
Cholesterol and related	3	0	0	0	0	1
Energy metabolism and related	9	0	0	3	2	2
Glycerophospholipids	32	4	11	16	15	13
Hormones, signal substances and related	2	0	0	0	0	0
Lysoglycerophospholipids	29	15	19	25	27	26
Miscellaneous	1	0	0	1	1	1
Nucleobases and related	4	0	0	0	1	1
Sphingolipids	37	4	4	6	7	6
Unknown	76	4	9	14	13	13
Vitamins, cofactors and related	9	1	2	4	4	2
Total # Metabolites	241	28	45	69	74	65

	Substance	Ketoconazole				
	Concentration	C1	C2	C3	C4	C5
Metabolite Class	Measured metabolites					
Acylglycerols	17	0	8	9	9	11
Amino acids	13	4	3	6	7	2
Amino acids related	9	3	1	5	8	5
Cholesterol and related	3	0	0	2	1	0
Energy metabolism and related	9	0	0	1	4	4
Glycerophospholipids	32	2	10	19	22	25
Hormones, signal substances and related	2	0	0	0	2	2
Lysoglycerophospholipids	29	1	2	1	2	0
Miscellaneous	1	0	0	0	0	1
Nucleobases and related	4	0	0	0	1	1
Sphingolipids	37	1	6	13	14	6
Unknown	76	10	17	44	51	51
Vitamins, cofactors and related	9	2	0	2	5	5
Total # Metabolites	241	23	47	102	126	113

Suppl Fig 7. Experimental variability and reproducibility. The variance of every log-transformed metabolite for both pooled samples (technical replicates) and control samples was calculated. These variances were back transformed to linear scale, yielding a relative standard deviation (RSD).

Plate	RSD-Pool	RSD Controls
Acifluorfen	0.10	0.11
Aroclor 1254	0.10	0.11
Ketoconazole	0.09	0.09
Naphthoflavone	0.10	0.09
Pendimethalin	0.08	0.11
Wy-14643	0.10	0.10

Suppl Fig. 8 3D-PCA of metabolic profiles shows a MoA-specific clustering of liver toxicants. PCA of metabolite profiles of HepG2 cells treated for 48h with three liver enzyme inducers (pendimethalin, aroclor, β -Naphthoflavone), three peroxisome proliferators (bezafibrate, acifluorfen, Wy-14643) and one liver enzyme inhibitor (ketoconazole) allows to discriminate between the different mode of actions of these substances.



Suppl Fig.9 Metabolome changes induced by peroxisome proliferators. Heatmap of common statistically significantly ($p < 0.05$) altered metabolites after bezafibrate, acifluorfen and Wy-14643 treatment. Red represents significantly upregulated metabolites and blue represents significantly downregulated metabolites as compared to controls. C3 equivalent to EC15ATP was used for the analysis. Bezafibrate was used as a positive control in each of the 6 plates of the experiment ($n=6$ per condition).

Metabolite	Bezafibrate Plate 1	Bezafibrate Plate 2	Bezafibrate Plate 3	Bezafibrate Plate 4	Bezafibrate Plate 5	Bezafibrate Plate 6	Wy-14643	Acifluorfen	Metabolite class
Taurine	0.93	0.92	0.68	0.93	0.90	0.88	0.97	0.61	Amino acids
5-Hydroxytryptophan	0.85	0.74	0.65	0.84	0.77	0.76	0.85	0.74	Amino acids related
Creatine	0.80	0.82	0.73	0.78	0.67	0.66	0.85	0.87	
Ketoleucine	0.73	0.72	0.74	0.73	0.77	1.10	0.86	0.80	
N-Acetylaspartate	1.54	1.49	1.66	1.48	1.41	1.25	1.22	1.50	
S-Adenosylhomocysteine	0.92	0.98	0.70	0.93	0.78	0.79	1.03	0.84	
Carnitine	0.72	0.74	0.84	0.72	0.77	0.80	0.99	0.98	Energy metabolism and related
Glycerol-3-phosphate	0.68	0.43	0.45	0.54	0.44	0.39	0.72	0.90	
Hexanoylcarnitine	0.65	0.54	0.50	0.59	0.59	0.62	0.93	0.70	
Propionylcarnitine	0.66	0.78	0.40	0.58	0.54	0.57	0.97	0.79	
2'-Deoxycytidine	0.37	0.42	0.16	0.27	0.22	0.21	0.75	0.56	Nucleobases and related
Pantothenic acid	0.68	0.77	0.59	0.72	0.70	0.76	0.74	0.68	Vitamins, cofactors and related
Triacylglycerol (C34:1.C18:3)	1.57	2.06	2.37	1.58	1.93	2.00	1.01	1.73	Acylglycerols
Triacylglycerol (C34:2.C18:0)	1.63	1.54	1.78	1.17	1.31	1.39	1.14	2.66	
Triacylglycerol (C34:2.C18:1)	1.40	1.62	1.81	1.26	1.79	1.43	1.01	2.04	
Triacylglycerol (C36:4.C16:0)	1.74	2.34	2.73	1.73	1.97	2.11	1.09	1.86	
Triacylglycerol (C36:4.C18:0)	2.15	2.38	2.26	1.72	1.82	2.28	1.18	2.14	
Choline plasmalogen (C36:4)	0.65	0.80	0.68	0.69	0.73	0.72	1.00	0.75	Glycerophospholipids
Choline plasmalogen (C36:5)	0.78	0.90	0.80	0.83	0.82	0.79	1.03	0.70	
Phosphatidylcholine (C32:0)	0.82	0.70	0.79	0.88	0.83	0.76	0.81	0.82	
Phosphatidylcholine (C34:1)	0.83	0.75	0.78	0.82	0.82	0.74	0.91	0.81	
Phosphatidylcholine (C34:3)	1.02	1.18	1.17	1.09	1.15	1.04	1.04	1.23	
Phosphatidylcholine (C36:1)	0.86	0.88	0.73	0.84	0.79	0.90	0.96	0.76	
Phosphatidylcholine (C36:2)	0.66	0.71	0.62	0.69	0.71	0.65	0.86	0.78	
Phosphatidylcholine (C36:3)	0.90	1.03	0.84	0.96	0.97	0.89	0.93	0.82	
Phosphatidylcholine (C36:4)	1.00	0.93	0.81	0.98	0.95	0.94	0.98	0.66	
Phosphatidylcholine (C36:5)	0.78	0.81	0.63	0.76	0.72	0.75	0.92	0.71	
Phosphatidylethanolamine (C36:3)	0.90	0.87	0.87	0.90	0.87	0.84	0.82	0.86	
Phosphatidylethanolamine (C38:3)	0.72	0.70	0.64	0.75	0.68	0.66	0.92	1.05	
Phosphatidylethanolamine (C38:5)	0.90	1.00	0.86	0.98	0.87	0.90	0.89	0.82	

Phosphatidylethanolamine (C38:6)	0.92	0.91	0.95	1.01	0.98	0.92	0.96	0.91	
Phosphatidylethanolamine (C40:7)	0.79	0.81	0.75	0.88	0.82	0.88	0.92	0.68	
Lysophosphatidylcholine (C14:0)	2.27	1.82	2.09	1.97	1.85	1.87	1.51	1.75	Lysoglycerophospholipids
Lysophosphatidylcholine (C16:0)	1.86	1.92	1.98	2.08	1.93	2.14	1.26	1.17	
Lysophosphatidylcholine (C16:1)	1.95	2.13	2.01	2.17	1.86	1.72	1.06	1.22	
Lysophosphatidylcholine (C20:4)	1.22	1.67	1.47	1.90	1.86	1.44	1.28	0.94	
Lysophosphatidylcholine (C24:0)	1.01	1.18	1.11	1.20	1.21	1.29	1.50	1.25	
Lysophosphatidylcholine (C24:1)	1.10	1.03	1.13	1.26	1.10	1.12	1.20	1.00	
Lysophosphatidylethanolamine (C16:0)	2.47	2.37	2.23	2.12	2.10	2.19	1.18	1.67	
Lysophosphatidylethanolamine (C18:0)	2.21	2.07	1.76	2.07	1.77	2.04	1.26	1.69	
Lysophosphatidylethanolamine (C18:1)	2.45	2.31	1.97	2.19	2.11	2.16	1.12	1.09	
Ceramide (d18:1.C20:0)	0.63	0.66	0.56	0.62	0.64	0.59	0.66	0.74	Sphingolipids
Ceramide (d18:1.C24:1)	0.80	0.85	0.68	0.66	0.91	0.98	0.92	0.72	
Ceramide (d18:1.C24:2)	0.83	1.08	1.11	0.89	0.90	0.91	0.71	0.68	
Ceramide (d18:2.C24:1)	0.56	0.62	0.68	0.68	0.89	0.63	0.97	0.64	
Sphingomyelin (d32:2)	0.49	0.71	0.69	0.75	0.59	0.78	0.79	0.65	
Sphingomyelin (d33:1)	1.19	1.34	1.15	1.32	1.18	1.20	1.13	0.93	
Sphingomyelin (d34:0)	0.96	1.09	1.25	1.15	1.11	1.11	1.04	1.12	
Sphingomyelin (d35:1)	0.86	0.95	0.86	0.88	0.85	0.92	0.99	0.85	
Sphingomyelin (d36:1)	0.86	0.96	0.86	0.90	0.82	0.84	0.90	0.84	
Sphingomyelin (d36:2)	0.73	0.90	0.90	0.85	0.87	0.88	0.97	0.76	
Sphingomyelin (d37:1)	0.70	0.80	0.79	0.80	0.76	0.80	0.81	0.89	
Sphingomyelin (d38:1)	0.88	0.84	0.85	0.87	0.87	0.91	0.84	0.89	
Sphingomyelin (d38:2)	0.61	0.66	0.64	0.67	0.71	0.66	0.74	0.83	
Sphingomyelin (d39:1)	0.77	0.77	0.83	0.87	0.81	0.86	0.94	1.01	
Sphingomyelin (d40:2)	0.73	0.83	0.81	0.87	0.78	0.84	0.81	0.87	
Sphingomyelin (d41:2)	0.78	0.79	0.82	0.88	0.77	0.80	0.79	0.90	
Sphingomyelin (d42:2)	0.86	0.95	0.81	0.98	0.89	0.91	0.79	0.85	
Phosphocholine	0.78	0.69	0.56	0.69	0.63	0.63	0.91	0.79	Miscellaneous lipids

Suppl Fig. 10 Metabolome changes induced by liver enzyme inducers. Heatmap of common statistically significantly ($p < 0.05$) altered metabolites after pendimethalin, aroclor and β -naphthoflavone treatment. Red represents significantly upregulated metabolites and blue represents significantly downregulated metabolites as compared to controls. C3 for β -naphthoflavone and pendimethalin and C2 for aroclor (equivalent to EC15ATP) was used for the analysis ($n=6$ per condition).

Metabolite	Aroclor 1254	β -Naphthoflavone	Pendimethalin	Metabolite class
Proline	0.54	0.64	0.89	Amino acids
Tyrosine	1.13	1.14	1.14	
N-Acetyserine	1.07	1.03	1.47	Amino acids related
Cysteinylglycine	1.52	3.16	1.14	
myo-Inositol-2-phosphate	0.83	0.65	0.76	Carbohydrates and related
N-Acetylglucosamine	0.92	0.79	0.93	
Carnitine	0.68	0.88	0.76	Energy metabolism and related
O-Acetylcarnitine	0.81	0.87	1.02	
Propionylcarnitine	0.75	1.03	0.65	
Hexanoylcarnitine	0.68	1.02	0.69	
Pantothenic acid	0.76	0.96	0.78	Vitamins, cofactors and related
Flavin adenine dinucleotide (FAD)	1.11	1.63	1.14	
Glutathione (GSH)	1.16	2.59	1.12	
Triacylglycerol (C32:1.C16:1)	0.46	0.26	0.58	Acylglycerols
Triacylglycerol (C30:0.C18:1)	0.72	0.36	0.81	
Triacylglycerol (C32:0.C16:1)	0.58	0.41	0.66	

Triacylglycerol (C34:1.C16:0)	0.70	0.39	0.79	
Triacylglycerol (C34:2.C18:1)	0.49	0.24	0.44	
Triacylglycerol (C34:2.C18:0)	0.67	0.40	0.87	
Triacylglycerol (C34:1.C18:1)	0.82	0.47	0.71	
Triacylglycerol (C34:0.C18:1)	0.91	0.47	0.96	
Triacylglycerol (C36:3.C18:1)	0.65	0.38	0.78	
Triacylglycerol (C36:2.C18:1)	0.67	0.41	0.49	
Triacylglycerol (C36:1.C18:2)	0.82	0.46	0.83	
Triacylglycerol (C36:1.C18:1)	0.70	0.35	0.65	
Triacylglycerol (C36:1.C18:0)	0.78	0.46	0.86	
Phosphatidylethanolamine (C32:0)	2.54	1.63	3.04	Glycerophospholipids
Phosphatidylethanolamine (C34:2)	0.76	0.93	0.68	
Phosphatidylethanolamine (C34:1)	1.36	1.38	1.48	
Phosphatidylethanolamine (C34:0)	2.09	1.79	2.78	
Phosphatidylethanolamine (C36:3)	0.83	0.84	0.82	
Phosphatidylethanolamine (C36:1)	1.65	1.81	1.46	
Phosphatidylethanolamine (C36:0)	2.75	2.10	3.98	
Phosphatidylethanolamine (C38:5)	0.84	0.93	0.79	
Phosphatidylethanolamine (C40:7)	0.84	0.79	0.57	
Phosphatidylcholine (C32:0)	2.06	1.16	1.93	
Phosphatidylcholine (C34:3)	0.71	0.60	0.79	
Phosphatidylcholine (C34:2)	0.74	0.77	0.64	
Phosphatidylcholine (C34:0)	1.79	1.39	1.83	
Phosphatidylcholine (C36:4)	1.27	1.08	1.10	
Phosphatidylcholine (C36:3)	0.81	0.87	0.73	
Phosphatidylcholine (C36:2)	0.66	0.80	0.52	
Phosphatidylcholine (C36:1)	1.20	1.21	0.93	
Phosphatidylcholine (C36:0)	2.17	1.62	2.49	
Phosphatidylcholine (C38:6)	1.31	1.09	1.15	
Choline plasmalogen (C36:5)	0.86	0.84	0.68	
Choline plasmalogen (C36:4)	0.78	0.82	0.63	
Lysophosphatidylethanolamine (C16:0)	1.12	1.77	1.81	Lysoglycerophospholipids
Lysophosphatidylethanolamine (C18:0)	1.26	2.25	2.07	
Lysophosphatidylcholine (C14:0)	1.20	1.48	2.28	
Lysophosphatidylcholine (C16:0)	1.50	2.15	2.37	
Lysophosphatidylcholine (C20:4)	1.34	1.68	2.32	
Lysophosphatidylcholine (C20:1)	1.05	2.23	1.47	
Lysophosphatidylcholine (C20:0)	1.67	2.34	2.37	
Lysophosphatidylcholine (C22:0)	1.76	1.99	3.44	
Lysophosphatidylcholine (C24:1)	2.03	2.34	3.59	
Lysophosphatidylcholine (C24:0)	1.92	2.67	4.49	
Sphingomyelin (d32:1)	0.94	0.84	0.92	Sphingolipids

Sphingomyelin (d34:2)	1.22	1.05	1.11	
Sphingomyelin (d35:1)	1.17	1.06	1.07	
Sphingomyelin (d38:2)	0.85	0.94	0.76	
Sphingomyelin (d40:2)	0.98	0.77	0.93	
Sphingomyelin (d41:2)	0.88	0.85	0.79	
Sphingomyelin (d42:2)	0.84	0.74	0.73	
Sphingomyelin (d34:2)	1.35	1.07	1.27	
Ceramide (d18:2.C16:0)	2.15	1.48	2.06	
Ceramide (d18:1.C20:0)	0.97	0.73	0.81	
Ceramide (d18:1.C22:1)	0.75	0.65	0.43	
Ceramide (d16:1.C24:0)	1.58	1.20	1.35	
Ceramide (d18:2.C23:0)	1.29	1.56	1.14	
Ceramide (d17:1.C24:0)	1.42	1.24	1.40	
Ceramide (d18:2.C24:1)	1.18	1.23	1.17	
Ceramide (d18:2.C24:0)	1.91	1.41	1.87	
Ceramide (d18:1.C24:1)	0.75	0.64	0.54	
Isopentenyl pyrophosphate (IPP)	1.37	2.43	2.79	Cholesterol and related

Suppl Fig. 11 Metabolome changes induced by a liver enzyme inhibitor. Heatmap of statistically significantly ($p < 0.05$) altered metabolites after ketoconazole treatment. Red represents significantly upregulated metabolites and blue represents significantly downregulated metabolites as compared to controls. C3 (equivalent to EC15ATP) was used for the analysis ($n=6$ per condition).

Metabolite	Ketoconazole	Metabolite class
Threonine	0.85	Amino acids
Proline	0.79	
Glutamate	0.92	
Taurine	1.32	
Pipecolic acid	0.86	Amino acids related
N-Acetylserine	0.84	
N-Acetylaspartate	0.69	
S-Adenosylhomocysteine	0.69	
5-Hydroxytryptophan	0.87	
myo-Inositol-2-phosphate	0.50	Carbohydrates and related
Tetradecanoylcarnitine	2.20	Energy metabolism and related
Hexadecanoylcarnitine	3.61	
Hexadecanoylcarnitine	1.97	
Octadecanoylcarnitine	3.35	
Carnitine	0.77	
2'-Deoxycytidine	0.76	Nucleobases and related
Coenzyme Q10	0.65	Vitamins, cofactors and related
Pyridoxal	0.82	
Pantothenic acid	0.85	

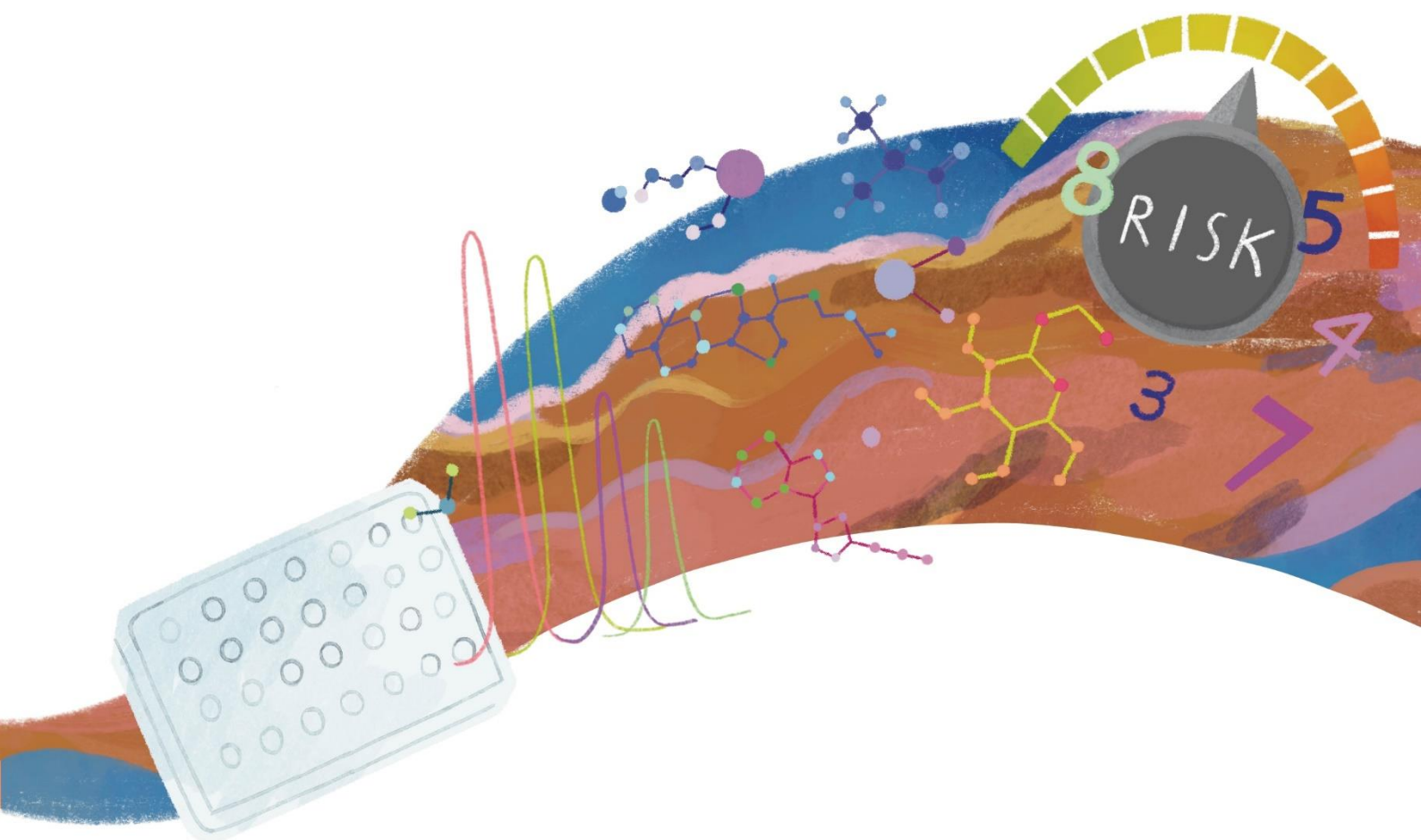
Glutathione (GSH)	0.90	
Triacylglycerol (C30:0.C18:1)	0.61	Acylglycerols
Triacylglycerol (C32:0.C16:1)	0.51	
Triacylglycerol (C32:0.C16:0)	0.23	
Triacylglycerol (C34:1.C16:0)	0.44	
Triacylglycerol (C34:0.C16:0)	0.16	
Triacylglycerol (C34:0.C17:0)	0.34	
Triacylglycerol (C34:1.C18:3)	1.33	
Triacylglycerol (C36:4.C16:0)	1.15	
Triacylglycerol (C34:2.C18:1)	1.31	
Triacylglycerol (C34:2.C18:0)	0.68	
Triacylglycerol (C34:1.C18:1)	0.83	
Triacylglycerol (C34:0.C18:1)	0.31	
Triacylglycerol (C34:0.C18:0)	0.14	
Triacylglycerol (C36:3.C18:2)	2.03	
Triacylglycerol (C36:4.C18:0)	1.19	
Triacylglycerol (C36:3.C18:1)	1.57	
Triacylglycerol (C36:2.C18:1)	1.14	
Triacylglycerol (C36:1.C18:1)	0.61	
Triacylglycerol (C36:1.C18:0)	0.27	
Phosphatidylethanolamine (C32:0)	0.86	
Phosphatidylethanolamine (C34:1)	0.82	
Phosphatidylethanolamine (C34:0)	0.73	
Phosphatidylethanolamine (C36:4)	0.96	
Phosphatidylethanolamine (C36:2)	0.93	
Phosphatidylethanolamine (C36:1)	0.78	
Phosphatidylethanolamine (C36:0)	0.70	
Phosphatidylethanolamine (C38:6)	0.86	
Phosphatidylethanolamine (C38:5)	1.10	
Phosphatidylethanolamine (C38:4)	1.10	
Phosphatidylethanolamine (C38:3)	0.90	
Phosphatidylethanolamine (C40:7)	1.09	
Phosphatidylcholine (C32:0)	0.81	
Phosphatidylcholine (C34:3)	1.19	
Phosphatidylcholine (C34:2)	0.89	
Phosphatidylcholine (C34:1)	0.79	
Phosphatidylcholine (C34:0)	0.81	
Phosphatidylcholine (C36:5)	0.66	
Phosphatidylcholine (C36:4)	0.67	
Phosphatidylcholine (C36:3)	0.89	
Phosphatidylcholine (C36:2)	0.64	
Phosphatidylcholine (C36:1)	0.77	
Phosphatidylcholine (C38:6)	0.74	
Phosphatidylcholine (C38:4)	1.06	
Phosphatidylcholine (C40:8)	1.11	
Phosphatidylcholine (C40:7)	1.16	

Phosphatidylcholine (C40:6)	1.10	
Choline plasmalogen (C36:5)	1.44	
Choline plasmalogen (C36:4)	1.23	
Lysophosphatidylethanolamine (C16:0)	0.82	Lysoglycerophospholipids
Lysophosphatidylethanolamine (C18:0)	1.22	
Lysophosphatidylethanolamine (C20:4)	4.71	
Lysophosphatidylethanolamine (C22:6)	4.79	
Lysophosphatidylcholine (C14:0)	1.21	
Lysophosphatidylcholine (C16:1)	2.67	
Lysophosphatidylcholine (C16:0)	1.96	
Lysophosphatidylcholine (C20:4)	6.43	
Lysophosphatidylcholine (C20:1)	1.07	
Lysophosphatidylcholine (C20:0)	1.34	
Lysophosphatidylcholine (C22:0)	1.53	
Lysophosphatidylcholine (C24:1)	2.21	
Sphingomyelin (d32:2)	1.28	
Sphingomyelin (d32:1)	1.49	
Sphingomyelin (d33:1)	1.18	
Sphingomyelin (d34:2)	1.31	
Sphingomyelin (d34:1)	1.40	
Sphingomyelin (d34:0)	2.87	
Sphingomyelin (d35:2)	1.71	
Sphingomyelin (d35:1)	1.86	
Sphingomyelin (d36:3)	1.48	
Sphingomyelin (d36:2)	1.45	
Sphingomyelin (d36:1)	1.62	
Sphingomyelin (d37:1)	1.49	
Sphingomyelin (d38:2)	1.21	
Sphingomyelin (d38:1)	1.42	
Sphingomyelin (d39:1)	1.79	
Sphingomyelin (d40:2)	1.67	
Sphingomyelin (d40:1)	1.85	
Sphingomyelin (d41:2)	1.88	
Sphingomyelin (d41:1)	1.75	
Sphingomyelin (d42:2)	1.83	
Sphingomyelin (d42:1)	1.54	
Sphingomyelin (d34:1)	1.16	
Ceramide (d18:2.C16:0)	0.55	
Ceramide (d18:1.C16:0)	0.74	
Ceramide (d18:2.C18:0)	0.38	
Ceramide (d18:1.C18:0)	0.58	
Ceramide (d18:1.C20:0)	0.38	
Ceramide (d18:1.C21:0)	0.64	
Ceramide (d18:2.C22:0)	0.39	
Ceramide (d16:1.C24:0)	0.48	
Ceramide (d18:1.C22:0)	0.54	

Ceramide (d18:2.C23:0)	0.49	
Ceramide (d18:1.C23:0)	0.50	
Ceramide (d17:1.C24:0)	0.40	
Ceramide (d18:2.C24:2)	0.36	
Ceramide (d18:2.C24:1)	0.66	
Ceramide (d18:2.C24:0)	0.48	
Ceramide (d18:1.C24:1)	0.70	
Ceramide (d18:1.C24:0)	0.60	
Cholesterylester (C20:2)	0.58	Cholesterol and related
Isopentenyl pyrophosphate (IPP)	0.50	
Phosphocholine	0.82	Miscellaneous lipids

Chapter 3

Application of High Throughput In vitro Metabolomics for Hepatotoxicity Mode of Action characterization and Mechanistic-anchored Point of Departure Derivation: A Case Study with Nitrofurantoin.



Preamble

The combination of Omics technologies such as metabolomics and *in vitro* systems offer a powerful tool for elucidating the molecular and biochemical events underlying organ toxicity. In contrast to traditional *in vitro* methods, the use of Omics techniques offers the advantage of enabling the simultaneous measurement of multiple cellular endpoints and thus, they have been proposed as key tools in Next Generation Risk assessment (NGRA). Several studies have successfully employed transcriptomics methods for the derivation of points of departure (PoD) as the first step to extrapolate *in vitro* generated data to *in vivo*, human relevant, reference values. The use of metabolomics technologies for PoD derivation has been, however, less explored.

Given the advantages of metabolomics technologies as the closest Omics characterization of the phenotype, untargeted metabolomics data have been recently used for PoD estimations via benchmark concentration (BMC) modeling, showing the potential of metabolomics as sensitive and quantitative tool to investigate liver injury potential. However, the lack of comprehensive metabolite identification, characteristic of untargeted metabolomics methods, challenged the biological interpretations of the results which might hamper the evaluation of the relevance and applicability of these data in safety assessment.

Targeted metabolomics offers the advantage of providing readily interpretable mechanistic information about perturbed biological pathways. In the following manuscript, the previously presented high throughput targeted *in vitro* metabolomics platform (chapter 2) was leveraged in order to **advance the utility and application of metabolomics data for use in human health risk assessment**. By exposing HepG2 cells to the antibiotic nitrofurantoin as a DILI model compound, data on time-series and dose–response experiments were generated to study compound dynamics. The suitability of the system to elucidate metabolic dynamics over time and concentration was shown and a mechanistic-anchored approach to derive and interpret dose and time response metrics from metabolomics data was provided. A total of 256 uniquely identified metabolites were measured, annotated, and allocated in 13 different metabolite classes. Both PCA and univariate analysis showed clear metabolome-based time and concentration response effects. In addition, mechanistic information matched the

previously described compounds' Mode of Action (MoA) and allowed to track the differential activation of cellular pathways as potential indicators of early adaptive and hepatotoxic responses.

Importantly, in the following manuscript, metabolomics-based PoD was derived by multivariate PCA using the whole set of measured metabolites. In contrast to previously proposed BMD method, the new PCA approach proposed here allows using the entire dataset to derive PoD that can be mechanistically anchored to established key events.

The generated results show the suitability of high throughput targeted metabolomics systems to investigate mechanisms of hepatotoxicity and the feasibility of deriving PoDs that can be linked to existing adverse outcome pathways and contribute to the development of new ones.

The following work was developed within the frame of the SysBiotopMoving project, funded by the German Bundesministerium für Bildung und Forschung (BMBF). The publication was prepared in collaboration with 12 co-authors. The experimental work, analysis of the data and the paper writing was done by the author of this dissertation. The co-authors were involved in the planning of the experiments, scientific discussion and guidance, the bioinformatics data analysis and significantly in the review process of the publication.

The generated results show the suitability of high throughput targeted metabolomics system to investigate mechanisms of hepatotoxicity and the feasibility of deriving PoDs that can be linked to existing adverse outcome pathways and contribute to the development of new ones.

Publication II: application of High Throughput In vitro Metabolomics for Hepatotoxicity Mode of Action characterization and Mechanistic-anchored Point of Departure Derivation: A Case Study with Nitrofurantoin

Status of the publication:

Submitted to Archives of Toxicology on May 30, 2023. Submission ID: ATOX-D-23-00403.

This project received funds from SysBioTop Moving (BMBF, 161L0243A) and EU-Tox Risk (European Union 's Horizon 2020 research, No 681002).

Application of High Throughput In vitro Metabolomics for Hepatotoxicity Mode of Action characterization and Mechanistic-anchored Point of Departure Derivation: A Case Study with Nitrofurantoin.

Sabina Ramirez-Hincapie¹, Barbara Birk¹, Philipp Ternes², Varun Giri¹, Franziska Maria Zickgraf¹, Volker Haake², Michael Herold², Hennicke Kamp², Peter Driemert², Robert Landsiedel^{1,3}, Elke Richling⁴, Dorothee Funk-Weyer¹, Bennard van Ravenzwaay⁵

¹ BASF SE, Experimental Toxicology and Ecology, Ludwigshafen, Germany

² BASF Metabolome Solution GmbH, Berlin, Germany

³ Free University of Berlin, Pharmacy, Pharmacology and Toxicology, Berlin, Germany.

⁴ Food Chemistry and Toxicology, Department of Chemistry, RPTU Kaiserslautern-Landau, Kaiserslautern, Germany

⁵ Environmental Sciences Consulting, Altrip, Germany

E-mail corresponding author:

E-mail corresponding author: sabina.ramirez-hincapie@basf.com (<https://orcid.org/0000-0002-8795-7061>)

sabina.ramirez-hincapie@basf.com (<https://orcid.org/0000-0002-8795-7061>),
barbara.birk@basf.com (<https://orcid.org/0000-0002-1208-8527>), philipp.ternes@basf.com
(<https://orcid.org/0000-0003-0886-5474>), varun.giri@basf.com (<https://orcid.org/0000-0002-8795-7061>),
franziska-maria.zickgraf@basf.com (<https://orcid.org/0000-0003-4269-1316>),
volker.haake@basf.com (<https://orcid.org/0000-0001-7124-6727>),
michael.a.herold@basf.com (<https://orcid.org/0000-0001-7733-0196>),
hennicke.kamp@basf.com (<https://orcid.org/0000-0002-1316-8756>),
peter.driemert@BASF.com (<https://orcid.org/0000-0001-5650-5380>),
robert.landsiedel@basf.com (<https://orcid.org/0000-0003-3756-1904>),
richling@chemie.uni-kl.de (<https://orcid.org/0000-0001-5746-8032>), dorothee.funk-weyer@basf.com,
ravenmooney@outlook.de (<https://orcid.org/0000-0002-4264-9217>).

Journal: Archives of toxicology

Acknowledgments

We would like to thank the SysBioTopMoving team (BMBF funded project) and in particular, Prof. Dr. Joost Beltman, Prof. Dr. Bob van de Water, Prof. Dr. Stefan Schildknecht for the

scientific advice and valuable discussions. We would also like to thank Hans-Albrecht Huener, Andreas Verlohner and Nadine Roth for their skillful technical support in the lab.

Funding

This project received funds from SysBioTop Moving (BMBF, 161L0243A) and EU-Tox Risk (European Union 's Horizon 2020 research, No 681002).

Abstract

Omics techniques have been increasingly recognized as promising tools for Next Generation Risk Assessment (NGRA). Targeted metabolomics offer the advantage of providing readily interpretable mechanistic information about perturbed biological pathways. In this study, a high-throughput LC-MS/MS-based broad targeted metabolomics system was applied to study nitrofurantoin metabolic dynamics over time and concentration and to provide a mechanistic-anchored approach for point of departure (PoD) derivation. Upon nitrofurantoin exposure at five concentrations (7.5 μ M, 15 μ M, 20 μ M, 30 μ M and 120 μ M) and four time points (3, 6, 24 and 48 hours), the intracellular metabolome of HepG2 cells was evaluated. In total, 256 uniquely identified metabolites were measured, annotated, and allocated in 13 different metabolite classes. Principal component analysis (PCA) and univariate statistical analysis showed clear metabolome-based time and concentration effects. Mechanistic information evidenced the differential activation of cellular pathways indicative of early adaptive and hepatotoxic response. At low concentrations, effects were seen mainly in the energy and lipid metabolism, in the mid concentration range, the activation of the antioxidant cellular response was evidenced by increased levels of glutathione (GSH) and metabolites from the de novo GSH synthesis pathway. At the highest concentrations, the depletion of GSH, together with alternations reflective of mitochondrial impairments, were indicative of a hepatotoxic response. Finally, a metabolomics-based PoD was derived by multivariate PCA using the whole set of measured metabolites. This approach allows using the entire dataset and derive PoD that can be mechanistically anchored to established key events. Our results show the suitability of high throughput targeted metabolomics to investigate mechanisms of hepatotoxicity and derive point of departures that can be linked to existing adverse outcome pathways and contribute to the development of new ones.

Keywords

metabolomics in vitro, high throughput, nitrofurantoin, hepatotoxicity, New Approach Methodologies, Next Generation risk assessment, Point of Departure.

Introduction

The realization of the vision of “toxicity in the 21st century” has significantly progressed since the publication of the NRC report in 2007 (National Research Council 2007). Scientific and technical advances of the last decades have fostered the development of numerous cell-based methods, high throughput systems and *in silico* models as alternative approaches to *in vivo* animal testing. These New Approach Methodologies (NAMs) have contributed to the understanding of mechanisms of toxicity and have played an important role in the development of adverse outcome pathways (AOP) (Krewski et al. 2020a; Vinken 2013). While the development of these new methods has been instrumental for the evolution of toxicology, the number of chemicals in the market for which there are insufficient toxicological data are evidencing the pressing need to increase the implementation of NAMs in human and environmental risk assessment (Stucki et al. 2022).

Conventional toxicological *in vitro* testing relies largely on the evaluation of single endpoints, which in most cases is not sufficient for a comprehensive risk assessment and not always translates well to the *in vivo* situation (Ball et al. 2022; Dix et al. 2007). The implementation of Omics technologies enable the simultaneous measurement of multiple cellular endpoints, providing a multiparametric and comprehensive assessment of different biochemical pathways in a single sample (García-Cañaveras et al. 2016). In particular metabolomics, described as the systematic study of small endogenous molecules known as metabolites, represents the last step in the Omics cascade and as such provides an insight into the current physiological state of an organism including biological responses to external factors such as xenobiotics and therapeutic agents (Guijas et al. 2018). Thus, metabolomics is the “omics” technology that closest represents the phenotype and for this reason has been considered to be closer to classical toxicology than other omics techniques (Ramirez et al. 2013). Metabolomics approaches have been successfully employed in toxicity assessment for identifying mechanisms of toxicity and characterizing key molecular events (Birk et al. 2021; Cuykx et al. 2018a; Kamp et al. 2012; Mattes et al. 2014; Van Ravenzwaay et al. 2007; Van

Ravenzwaay et al. 2015). For cell-based metabolomics, however, requirements for large biomass quantities have previously restricted the throughput scalability, limiting the testing to few concentrations and single (static) time points (Cuykx et al. 2018a; García-Cañaveras et al. 2016; Ramirez et al. 2018b). These factors reduce the potential of dose and time-based calculation of dose-response metrics, hampering the applicability of *in vitro* metabolomics systems in risk assessment (Olesti et al. 2021). In addition, such information may also contribute to discriminate between adaptive and adverse changes.

Given that the liver is one of the main target organs, early mechanistic-based identification of potential hepatotoxins is a highly relevant issue for the pharmaceutical and chemical industry. Recently, *in vitro* liver models have been employed to derive metabolomics-based points of departure (PoDs) via benchmark concentration modeling (Crizer et al. 2021b; Malinowska et al. 2023).

We have previously developed and standardized a high throughput, targeted LC-MS-based *in vitro* metabolomics platform for the identification and differentiation of liver toxicity Modes of Action (MoAs) in HepG2 cells (Ramirez-Hincapie et al. 2023). Importantly, this assay measures a set of pre-identified metabolites representative of main cellular pathways. Due to its high throughput nature, a broad range of concentrations, covering key points of the dose response curve can be assessed, offering the possibility of studying substance effect dynamics and allowing accurate and mechanistic anchored metabolome-based PoD estimations.

The aim of this study was to generate metabolome-based dose-response and time series analysis which can be useful to derive dose response metrics from metabolomics data. For this aim, we have selected nitrofurantoin as a model compound. Nitrofurantoin is an antibiotic employed in clinical practice to treat urinary infections. For humans, nitrofurantoin presents a significant drug induced liver injury (DILI) concern, classified as a well-known cause of liver injury (Serrano 2014). The activation of cellular oxidative stress response pathways by nitrofurantoin has been previously demonstrated (Wijaya et al. 2021). At low doses, nitrofurantoin has been shown to activate the endogenous antioxidant machinery by being a potent stimulator of intracellular glutathione synthesis (Wijaya et al. 2022), at high concentrations however, it has been linked to oxidative stress-related hepatotoxicity (Wang

et al. 2008). Because of its characteristic dose-related biological responses nitrofurantoin was considered as a suitable compound to assess the applicability of the high throughput targeted metabolomics to provide a basis for a mechanistic-grounded PoD determination.

Materials and Methods

Cell culture

HepG2 cells (ECACC, UK, maximum passage number 9) were maintained and grown on Dulbecco's MEM media supplemented with 1 v/v% of penicillin/streptomycin, L-glutamine (200 mM, 1% v/v), non-essential amino acids (1% v/v) and 10% FBS (PAN-Biotech, Aidenbach, Germany) in 75 cm² culture flasks (TPP, Switzerland). For cell passaging (~80% confluency) media was removed and cells were washed twice with pre-warmed calcium and magnesium free Dulbecco's PBS (PAN-Biotech, Aidenbach, Germany). Trypsin was used for cell detachment. A fraction of the cell suspension was then transferred to a new culture vessel. For experiments, 15.000 cells per well (passage 5-9) were seeded in 96-well flat-bottom plates (TPP, Switzerland) and incubated for 24 h for cell attachment (37 °C and 5% CO₂). After 24h, culture media were exchanged, and the test substance was added in five concentrations (0.5% DMSO) and incubated in a corresponding 96-well-plate per time point for 3, 6, 24 and 48h at 37 °C and 5% CO₂. 72h post seeding, the assay was stopped by quenching all plates with isopropanol 80% and freezing at -80°C. See "*metabolomics experiments*" for more details.

Test substances

Nitrofurantoin ($\geq 98\%$) and bezafibrate ($\geq 98\%$), used as a positive/quality control *in each experiment*, were purchased from Sigma Aldrich (Buchs, Switzerland). DMSO (+99.8%,) was used as a solvent and vehicle control at a final concentration of 0.5% Thermo Fisher (Geel, Belgium).

Cytotoxicity and cell viability testing

Commercially available cytotoxicity (CellTox™ Green) and ATP content based (CellTiter-Glo®) assays (Promega GmbH, Walldorf, Germany) were multiplexed in a single 96 well-plate following the manufacturer's instructions. For positive controls, lysis solution 25X was added in wells containing vehicle control treated cells (0.5% DMSO). Fluorescence was measured at λ_{ex} = 485–500 nm/ λ_{em} = 520–530 nm in the GloMax®-Multi Detection System (Promega).

Luminescence was measured in the GloMax®-Multi Detection System (Promega) and was normalized to the values of the vehicle control. Cytotoxicity and ATP cell viability analysis were carried out for range finder pre-tests and in parallel with metabolomics experiments in plates handled and treated exactly as the ones used for metabolite profiling.

Range finder experiments for concentrations selection

Concentration levels for the metabolomics experiments were based on range finder experiments. Nitrofurantoin was administered to HepG2 cells in 14 concentrations ranging from 0.234 μM to 1.920 μM to following two-fold serial dilutions and incubated for 48h (6 replicates per concentration). Viability and cytotoxicity tests were performed as described previously. Luminescence values resulting from ATP measurement (CellTiter-Glo® assay) were used to build dose response curves. Curve fitting and effective concentrations (ECs) values were calculated in R using four-parameter Weibull model (W2.4). Calculated EC values were rounded to the nearest integer number for dose selection.

Live-cell imaging

To monitor cell proliferation, total well confluence was obtained by real time cell imaging analysis using IncuCyte S3 device placed in a normal incubator at 37 °C with 5% CO₂. Whole-well scans were taken every 1.5 hours during the duration of the assay and evaluated using automated phase-contrast analysis (phase mask).

Metabolomics experiments

After 24h of cell attachment, substances were administered in 0.5% DMSO (final concentration) to HepG2 cells in 5 concentrations (EC_{1(ATP)}, EC_{15(ATP)}, EC_{25(ATP)}, EC_{50(ATP)}, EC_{85(ATP)}) in a corresponding 96-well-plate per time point. In order to harvest all plates simultaneously, aiming to achieve same final cell number, treatment was applied by reverse application. 1) 24 h post seeding (48h substance exposure), 2) 48 h post seeding (24h substance exposure), 3) 66 h post seeding (6h substance exposure) and 4) 69 h post seeding (3 h substance exposure) Fig 1.

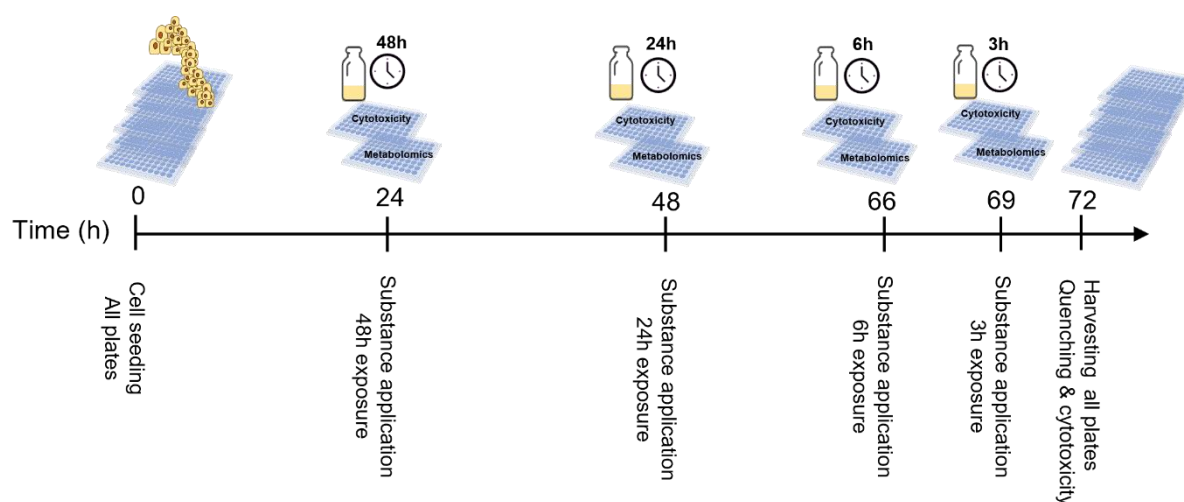


Fig.1 Nitrofurantoin administration for metabolomics experiment. 15000 HepG2 cells were seeded per well in 96-well plates and incubated for 24h for initial cell attachment. 24h post seeding, nitrofurantoin was administered in 5 concentrations ($EC_{1(ATP)}$: 7.5 μ M, $EC_{15(ATP)}$: 15 μ M, $EC_{25(ATP)}$: 30 μ M, $EC_{50(ATP)}$: 60 μ M, $EC_{85(ATP)}$: 120 μ M) in a corresponding 96-well-plate per time point by reverse application. After 72h post seeding, the assays were stopped simultaneously by washing the wells once with 100 μ L of 0.9% NaCl followed by snap freezing the plates on liquid nitrogen for 5 secs. Metabolomics plates were placed immediately on dry ice and stored at -80 $^{\circ}$ C until LC-MS/ MS analysis while cytotoxicity plates were used for ATP content and membrane integrity multiplexed assays.

After 72h post seeding, the assays were stopped simultaneously by washing the wells once with 100 μ L of 0.9% NaCl followed by snap freezing the plates on liquid nitrogen for 5 secs. Plates were placed immediately on dry ice and stored at -80 $^{\circ}$ C until LC-MS/ MS analysis.

For each time point, one 96 well-plate was set up with 6 replicates per concentration, 12 replicates for vehicle controls (0.5% DMSO), 6 replicates for positive controls (Bezafibrate 1000 μ M) and 6 replicates for blank controls (media without cells). Bezafibrate has been shown to provide a clear and consistent metabolic response (BASF, unpublished results) that is used to confirm the quality of the cell batch used in the analysis. To minimize potential evaporation, the outer rows and columns of the plate were omitted and filled with PBS instead. Reference samples prepared from lyophilized untreated HepG2 cells were measured in parallel throughout the entire analytical process (QC technical replicates). Data from each metabolite in each sample were normalized against the median of the same metabolite in all reference samples on the same plate to give normalized ratios. Lyophilized HepG2 cells reference samples were used to account for variability between plates (inter- and intra-

instrumental variation) and in concentration series (0%, 25%, 50%, 75%, 100%, 125%, 150%, 200%) for linearity checks.

LC-MS/MS metabolomics

Metabolite profiling of cells was performed directly in the 96-well plate according to a standardized protocol described below.

For quenching and extraction 120 μ l of isopropanol 80%, containing internal standards (quality control only, not used for normalization) were added to each well of the frozen samples plate. Afterwards, plates were shaken for 5 min, 750 rpm at 20°C and placed for 30 sec in the ultrasonic device. Then, the plates were centrifugated for 10 min, at 5485 g, 15°C. 2.5 μ l of the extract were injected each for reversed-phase and hydrophilic interaction liquid chromatography followed by MS/MS detection (AB Sciex QTrap 6500+) using the positive and negative ionization mode. For reverse-phase high performance liquid chromatography (RP-HPLC, Ascentis Express C18, 5cm x 2.1mm, 2.7 μ m, Supelco), gradient elution was performed with mobile phase A, water/methanol/0.1 M ammonium formate (1:1:0.02, w/w), and B, methyl-tert-butylether/2-propanol/methanol/0.1M ammonium formate/formic acid (4:2:1:0.07:0.035, w/w) (linear gradients, 0 min 100% A, 0.5 min 75% A, 5.9 min 10% A, 600 μ l/min). HILIC (ZIC-HILIC, 10 cm x 2.1mm, 3.5 μ m, Merck) gradient elution was performed with mobile phase C, acetonitrile/water (99:1, v/v) with 0.2% (v) acetic acid, and D, 7 mM ammonium acetate with 0.2% (v) acetic acid (linear gradients, 0 min 100% C, 5 min 10% C, 600 μ l/min).

Due to the high sample number, the analysis was performed in batches with each batch comprising one 96-well plate. To ensure that the analytical system was suitable for measurement, for each analysis batch a solvent (80% isopropanol) and two external standard calibration samples (covering 213 lipid and polar metabolites) followed by another solvent sample were run at the start of the analysis. The border wells of the 96-well plate were used for linearity samples (resulting in 4 replicates per concentration (except 100% with 5 replicates – the latter samples are used for normalization as described below). This setup ensured that data can be compared across analysis batches. Each 96-well plate was analyzed row-wise starting from well A1. This way one replicate from each treatment was run followed by two linearity samples (in column A and H) before moving to the next treatment replicate.

For bioanalytical quality control, the linearity samples were evaluated regarding coverage (signal in >80% of linearity samples), linearity ($R^2 > 0.64$), variability ($RSD < 0.6$ for the 100% linearity samples) and blank contribution (blank signal <40% of the 100% linearity samples). When a metabolite failed the quality control check, data for this metabolite were excluded (Ramirez-Hincapie et al. 2023).

Metabolomics data analysis

To correct for small differences in cell numbers within and between different treatment groups, data were also normalized to the within sample median, as described in detail by (Ramirez et al. 2018). For intracellular metabolomic analysis, the median of each sample was calculated across all the 256 measured metabolites.

To generate metabolic profiles for the different concentrations and time points, heteroscedastic t-test (Welch test) was applied to log-transformed normalized metabolite data to compare treated groups with their respective controls.

To investigate the experimental variability, the variance of every log-transformed metabolite for both pooled samples (technical replicates) and control samples was calculated. These variances were back-transformed to linear scale, yielding a relative standard deviation (RSD) using the following formula:

$$RSD = 1 - 10^{-SD \log}$$

Principal Component Analysis (PCA) analyses were performed using R software environment (<https://www.r-project.org/>) using the `ropls` package (Thévenot et al. 2015) with \log_{10} -transformed input data and standard scaling. The input data were normalized to the median of each metabolite in the control samples on each 96-well plate to compensate for differences between plates.

The binomial distribution enrichment analysis was performed using Excel. For this purpose, the number of significant changes (s) at p -value < 0.05 were counted per treatment and ontology class. The binomial distribution test is used to indicate the probability of a specific number of successes (the number of significant changes) occurring from a specific number of independent evaluations (total metabolites number in the given ontology class). The resulting

p-value for this enrichment is indicated (as category) by color in the tables (grey, light yellow or intense yellow).

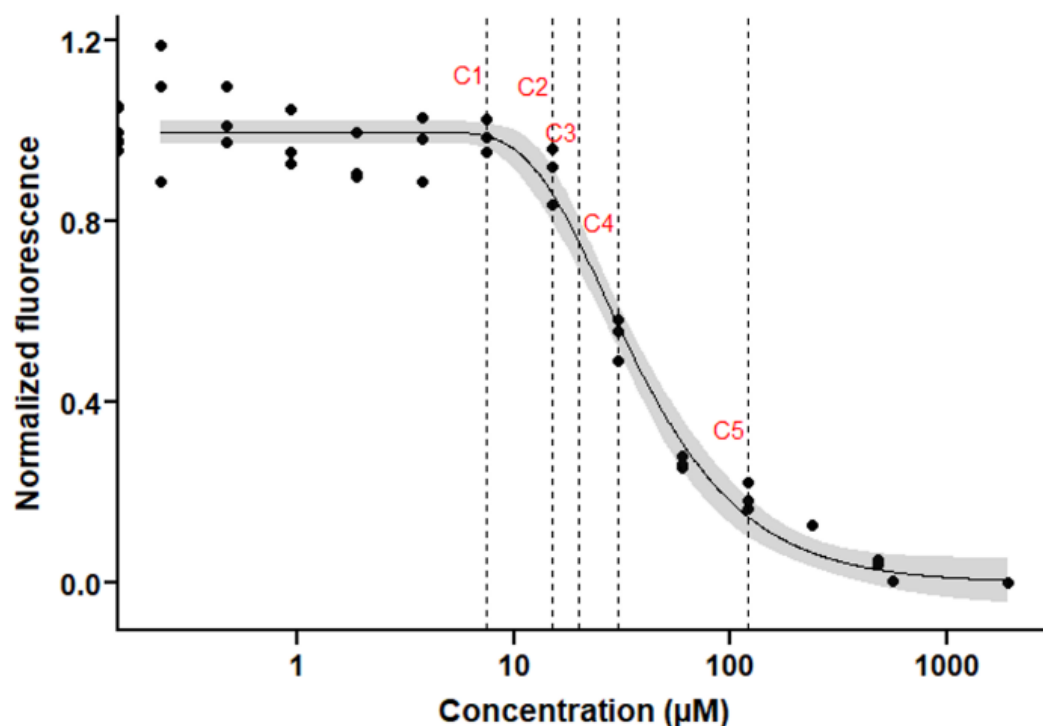
Point of departure derivation

A concentration-dependent response was modeled based on PC1 values obtained from the PCAs. PC1 values for each sample were plotted against the test concentration and a 3-parameter log-logistic model was fitted through the data, using 'drc' package (Ritz and Streibig 2005). A confidence interval of 95 % was used for the dose-response curve and the control variability was described by the 2.5 % and 97.5 % quantiles, which correspond to 95% spread of the controls. The PoD marks the concentration at which the confidence interval of the curve surpasses the corresponding quantile of the controls, i.e., the curve with its 95% confidence interval has crossed the 95% spread of the controls.

Results and discussion

Range finder pre-test for concentration selection

Initial range-finding experiments were conducted to guide the concentration selection for the metabolomics experiments. After administering increasing concentrations of nitrofurantoin following two-fold serial dilutions (from 0.234 μ M to 1.920 μ M), cytotoxicity and cell viability were assessed in parallel upon 48 h of exposure (Suppl Fig. 1). CellToxGreen, a cell impermeable DNA-binding dye which measures membrane integrity was used to identify concentrations that caused overt cell death. ATP production, a more sensitive endpoint expected to reflect earlier alterations in cellular metabolism, was used to generate a dose response curve and derive effective concentration values (EC). Based on ATP content viability pretest, five nitrofurantoin concentrations (C1:EC_{1(ATP)}, C2; EC_{15(ATP)}, C3:EC_{25(ATP)}, C4:EC_{50(ATP)}, C5:EC_{85(ATP)}) were selected for the following metabolome experiment (Fig. 2). The concentration selection aimed to cover important aspects of the concentration response dynamics from no and mild effects to hepatotoxic-related effects. EC_{1(ATP)} was selected to evaluate non-toxic but potentially mild metabolic effects, EC_{15(ATP)} and EC_{25(ATP)} was selected to obtain a moderate substance effect, however, within a low cytotoxicity range and EC_{50(ATP)} and EC_{85(ATP)} were chosen to identify hepatotoxic related metabolite patterns.



	Selected concentration (µM)	Corresponding ECx level
C1	7.5	EC _{1(ATP)}
C2	15	EC _{15(ATP)}
C3	20	EC _{25(ATP)}
C4	30	EC _{50(ATP)}
C5	120	EC _{85(ATP)}

Fig. 2 Nitrofurantoin concentration selection for metabolomics experiments. ATP values obtained from the viability pre-test were used to build a dose-response curve. Five concentrations (indicated by the red arrows) were selected. Upper panel; dose-response curve. Lower panel; corresponding estimated EC concentrations. ECs were estimated based on the computationally fitted ATP dose response curves generated in the range finder experiments upon 48h of exposure. Five test concentration levels (indicated by the arrows) were set based on the dose-response curve generated from ATP measurement (CellTiterGlo[®]) pre-test (Suppl Fig 1). Values were approximated to the nearest integer number.

Experimental cytotoxicity and cell viability of selected test concentrations

A critical factor of metabolomics experiments is to distinguish substance-specific effects from unspecific effects produced by overt cytotoxicity. To experimentally assess the effect of the selected test concentrations on both cell viability and cytotoxicity, ATP content (CellTiterGlo)

and cell death (CellToxGreen) assays were multiplexed and measured in parallel with the metabolomics experiment in plates handled and treated exactly as the ones used for metabolomics (Suppl. Fig. 2).

The estimated ECs calculated in the pre-test from ATP values after 48 hours of exposure corresponded closely to the experimentally obtained values in the low ($EC_{1(ATP)}$) and high effect area ($EC_{50(ATP)}$, $EC_{85(ATP)}$) of the dose response curve. In comparison to the vehicle treated cells, the estimated EC_{15ATP} resulted in a mild experimental reduction of ATP (down to 94%) while the EC_{25ATP} caused a higher-than-anticipated reduction in ATP levels (down 63%), suggesting a steep slope in the dose response curve.

At the three highest concentrations ($EC_{25(ATP)}$, $EC_{50(ATP)}$ and $EC_{85(ATP)}$) and the last time point (48 hours), ATP levels were markedly affected when compared to untreated controls, suggesting significant impairments in the cellular energy generation. However, this apparent drastic “loss” in viability failed to induce significant cell death measured by means of membrane integrity, suggesting a cytostatic rather than a cytotoxic effect of the highest nitrofurantoin concentrations. Cell growth was monitored by real time imaging during the duration of the assay. After 48h of exposure, the concentrations corresponding to $EC_{25(ATP)}$, $EC_{50(ATP)}$ and $EC_{85(ATP)}$ had a clear impact on the cellular growth rate (Suppl. Fig 3), confirming the cytostatic effect that resulted in lower cell numbers and consequently produced an apparent reduction in viability when compared to untreated cells. These findings point out that experimental concentration selection based only on viability markers such as ATP, could potentially overestimate the substance cytotoxic effect missing important markers of potential adversity and resulting in an incomplete coverage of the substance response effect. Our results indicate that including additional parameters such as the parallel assessment of two different endpoints in cytotoxicity readouts is important for proper concentration selection and data interpretation.

Metabolomics experiments

The HepG2 cell line was selected due to its unlimited lifespan, stable phenotype, availability, reproducibility, easy handling, and low cost. Although the limited drug metabolizing and transport capabilities of HepG2 cells are well acknowledged, a comparable stimulation of de novo synthesis of glutathione and gene expression profiles were found in primary human

hepatocytes (PHH) and HepG2 when exposed to different nitrofurantoin concentrations (Wijaya et al. 2022) indicating the suitability of the HepG2 cells to investigate nitrofurantoin dynamics.

To study the metabolite dynamics upon nitrofurantoin exposure, HepG2 cells were treated with five different concentrations (C1:7.5 μ M, C2:15 μ M, C3:30 μ M, C4:60 μ M, C5:120 μ M) at four time points (3, 6, 24, 48h). A total of 256 unique metabolites was measured of which 181 were annotated and 75 remained unknown. Annotated metabolites were allocated in 13 different metabolite classes such as amino acids, carbohydrates, energy metabolism, nucleobases, vitamins and cofactors and diverse lipid classes (Suppl. Fig 4).

Relative standard deviation (RSD) values of the individual metabolites in the control samples ranged from 19% (1st quartile) to 39% (3rd quartile) with a median of 28% after control normalization (to compensate for differences between plates). The median RSD values of the individual metabolites in the control samples on individual plates ranged from 23% to 28%. The median RSD values of the individual metabolites in the technical replicates on the individual plates were between 9% and 10% (Suppl Fig. 5) The experimental variability of the technical (QC samples) and biological (vehicle) controls in our study was thus below the recommended threshold of 30% (Viant et al. 2019b).

Metabolome analysis of Nitrofurantoin-treated cells shows concentration and time response effects

Metabolite profiles of nitrofurantoin-treated cells were first analyzed by PCA. Both concentration- and time-dependent responses were observed (Fig.3). After 3h, none of the tested concentrations induced a visible effect. At this time point, the levels of intracellular nitrofurantoin were below the limit of quantification (data not shown). At the lowest tested concentration (C1), significant treatment effects were observed only at the 48h time point (Fig. 4A). From the C2 onwards, clear treatment effects were evident after 24h of exposure (Fig. 4B, C, D). The strongest effect and highest resolution of concentration and time effects was observed at the highest concentration (C5) and latest time point (48h) (Fig. 4E, F). Our findings suggest that at low concentrations, nitrofurantoin exposures time below 6h are not sufficient to produce an identifiable effect on the metabolome. While at higher concentrations effects can be identified at earlier time points. In line with our observations,

Malinowska and coworkers evaluated the variability of the HepaRG cellular baseline metabolome at different time points, suggesting that a reliable detection of metabolic changes upon a toxicant exposure is achieved minimum after 6 h of exposure (Malinowska et al. 2022a).

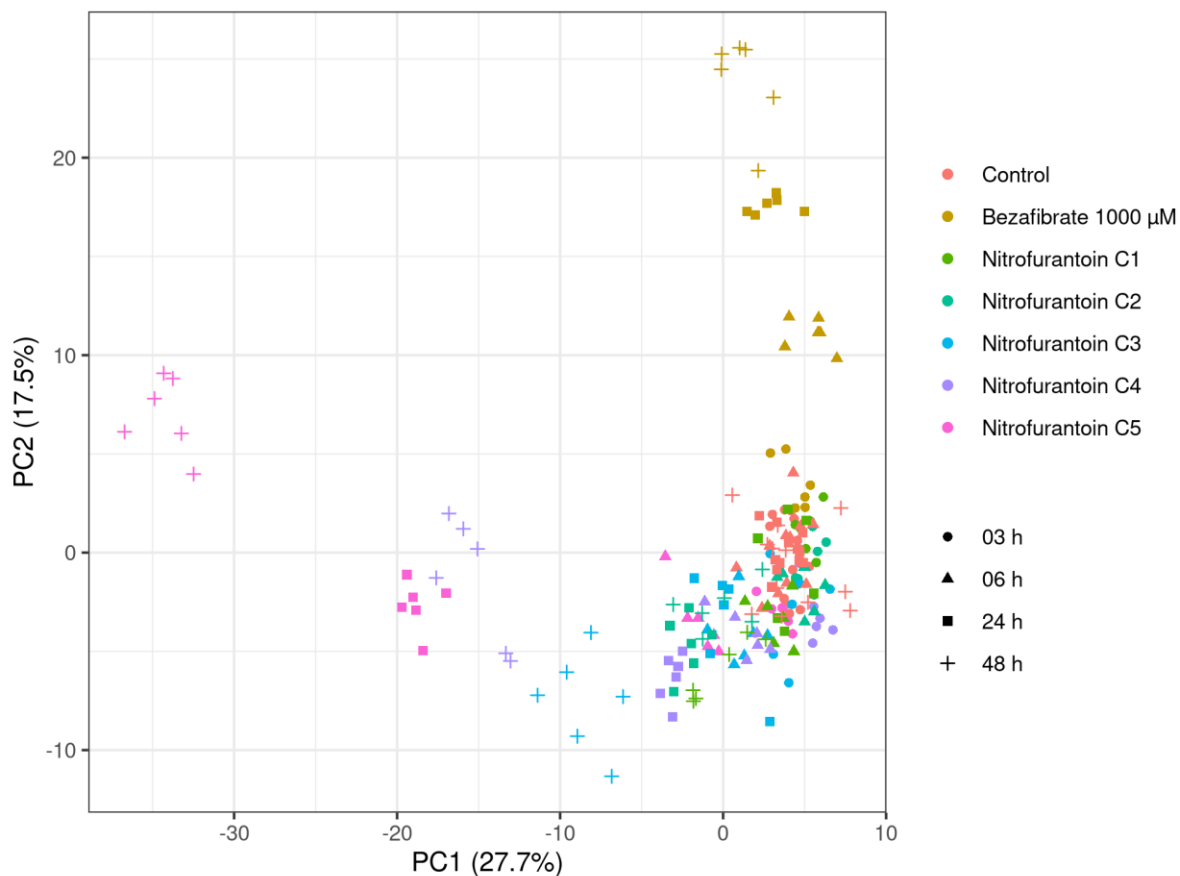


Fig 3. PCA of nitrofurantoin metabolic profiles show time and concentration response effects. PCA analysis of the metabolic profiles of HepG2 cells upon nitrofurantoin treatment. Bezafibrate was used as a positive control. C1:7.5 μM , C2:15 μM , C3:30 μM , C4:60 μM , C5:120 μM .

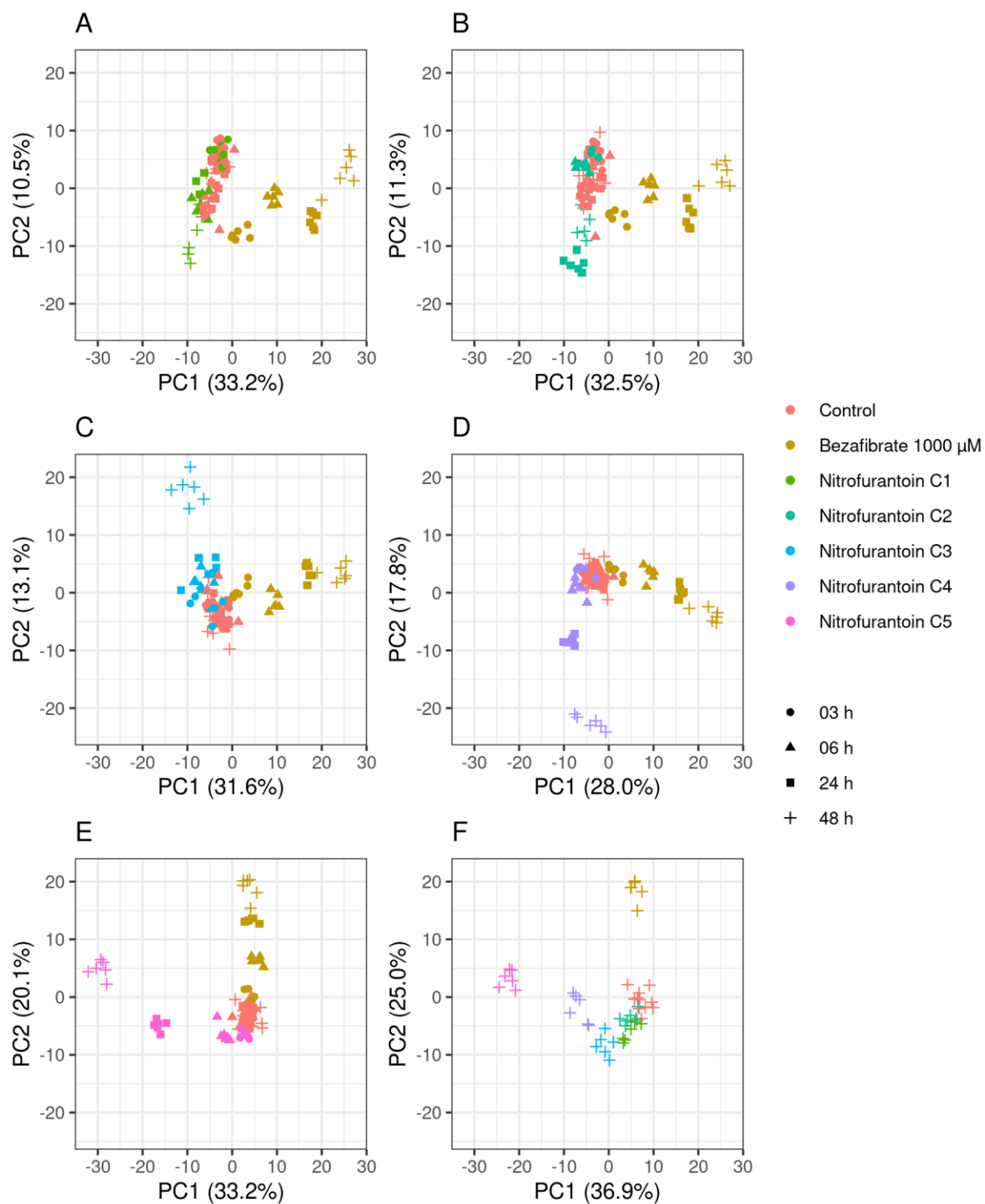


Fig. 4. PCAs of metabolomics time-response effect for each tested concentration. a) C1: 7.5 μ M, b) C2: 15 μ M, c) C3: 30 μ M d) C4: 60 μ M) C5: 120 μ M and f) metabolic profiles of the five tested concentrations: C1-C2, upon 48 hours of exposure.

Following the PCA evaluation, metabolic profiles of nitrofurantoin-treated cells were subjected to univariate statistics to identify changes in individual metabolites. A univariate enrichment analysis was carried out to evaluate the number of significantly changed

metabolites per ontology class (Suppl. Fig 6). The data revealed dose and time dependency, with increasing number of altered metabolites at higher concentrations and later time points. These results demonstrate that the high throughput *in vitro* metabolomics assay presented here is able to distinguish the effects at different concentrations and time points and therefore is suitable to perform metabolome-based time and dose responses analysis.

The implementation of tools such the one presented here allows to integrate a temporal dimension in the assessment of compound metabolic dynamics. This type of information not only provides mechanistic temporal insights but is also valuable for the selection of relevant *in vitro* sampling time points for risk assessment.

Metabolite dynamics over time and concentrations show differential profiles as potential indicators of initial, adaptive, and toxic responses

Heatmaps of metabolite changes per class were generated in order to assess the metabolic dynamics over concentration and time (Suppl Fig. 7). This type of analysis allows the identification of key metabolites or metabolite class dynamics useful to follow up on the development and progression of a hepatotoxic phenotype. Suppl Fig. 7A shows metabolite changes by class over the different exposure times while Suppl Fig. 7B depicts the metabolite changes per class as a function of the applied compound concentration.

Predicting adversity from omics data remains an important limitation for the use of these technologies in risk assessment (Olesti et al. 2021). Therefore, the investigation of multiple endpoints at various time-points is fundamental to understand the progression of different key events along an adverse outcome pathway (AOP). By evaluating consistent metabolite changes in low, medium, and high concentrations at different time points, we generated a dataset which closely captured the previously reported nitrofurantoin effect evolution and allowed to identify differential pathway activation and metabolic markers potentially indicative of a transition from adaptive to adverse effects (Table. 1).

Response		Low		Middle	High	
Pathway	Metabolite	C1	C2	C3	C4	C5
Glycolysis	Glucose-6-phosphate	↓	↓	↓	↓	↓
TCA cycle	Fumarate	↓	↓	↓	↓	↓
	Malate	↓	↓	↓	↓	↓
	N-Acetylaspartate	↓	↓	↓	↓	↓
	Glycerol-3-phosphate	↓	↓	↓	↑	↑
Fatty acid oxidation	O-acetylcarnitine	↓	↓	↓	↓	↓
	Carnitine	↑		↓	↓	↓
	Propionylcarnitine (C3)	↑	↑	↑	↑	↓
	Hexanoylcarnitine (C6)	↑				↓
	Hexanodecanoylcarnitine (C16)		↑	↑	↑	↑
	Tetradecanoylcarnitine (C14)			↓		↑
	Octadecenoylcarnitine (C18)			↑	↑	↑
	3-Hydroxybutyrate	↑	↑	↑		↑
Nucleobases	Deoxycytidine	↑			↓	↓
	Guanine	↓				↑
Antioxidants/coenzymes	Nicotinamide adenine dinucleotide (NAD)	↓	↓	↓		↓
	Pantothenic acid	↑	↑		↓	↓
	Taurine		↓	↓	↓	↓
	Ophthalmic acid		↓	↓	↓	↓
	Coenzyme Q10			↓	↓	↓
	Coenzyme Q9					↓
De novo GSH synthesis	S-Adenosylhomocysteine	↓	↓	↓	↓	↓
	2-Methylserine	↑	↑	↑		↑
	Cysteinylglycine	↑	↑	↑		↓
	Glutamine	↑	↑	↑		↑
	Glutamate	↑	↑	↑		↓
	Glutathione (GSH)			↑	↑	↓
Lipid metabolism	TAG's	↓	↓	↓	↓	↑
	Phosphatidylcholine	↓	↓	↓	↓↑	↓↑
	Phosphatidylethanolamine	↓	↓	↓	↓	↓
	Lysophosphatidylcholine	↑	↑	↑	↑	↑
	Cholesteryl ester		↑	↑	↑	↑
	Sphingomyelins				↓↑	↓↑
	Ceramides				↓↑	↓↑
Essential amino acids	Arginine	↑	↑	↑		↑
	Tryptophan		↓		↑	↑
	Phenylalanine			↑	↑	↑
	Isoleucine			↑	↑	↑
	Leucine			↑	↑	↑
	Tyrosine			↑		↑
	Threonine			↑		↑
	Proline			↓	↓	↓
	Valine			↑	↑	↑
	Asparagine					↑
Amino acids related	Creatine	↓	↓	↓	↓	↓
	Proline		↑	↓	↓	↓
	Hydroxytryptophan			↓	↓	↓
	Pipecolic acid			↓		↑

Table. 1 characteristic metabolite changes of early, adaptive and hepatotoxic nitrofurantoin response. Consistent metabolite changes in metabolic profiles of HepG2 cells treated with low (C1: 7.5 μ M, C2: 15 μ M) middle (C3: 30 μ M) and high (C4: 60 μ M, C5: 120 μ M) nitrofurantoin concentrations. Red arrows represent elevated levels and blue arrows represent reduced levels. Changes are calculated relative to the controls. Consistent time response changes are depicted; the majority of consistent changes were evident upon 24 hours of exposure. In the the highest concentrations, some consistent changes were evident already upon 6h of exposure.

Metabolic profile of cells exposed to low concentrations

Low concentrations (C1 and C2), corresponding to 7.5 μ M and 15 μ M, showed no significant reduction in viability, as well as no cell death or detrimental effects on the cell growth. Metabolic profiles of cells treated with these concentrations exhibited alterations mainly in the energy and lipid metabolism as well as in antioxidant molecules as an early response to nitrofurantoin exposure. Concentrations of TCA cycle metabolites (fumarate and malate), glycolysis intermediates (glucose-6-phosphate) and acetyl-CoA donors (N-acetyl aspartate), decreased consistently from the lowest concentrations onwards in a time and dose response manner. Pantothenic acid, a precursor to CoA and a part of the anchoring system of the fatty acid synthase complex, increased in the lowest concentrations and shifted to an increase in the highest (C4-C5). Levels of glycerol-3-phosphate decreased in the lower and middle concentrations (C1-C3) but increased in the highest concentration. Changes in metabolites from the fatty acid oxidation pathway were as well observed in the low concentrations.

O-Acetylcarnitine, the acetylated derivative of carnitine, which facilitates the movement of acetyl-CoA into the mitochondrial matrix during fatty acid oxidation was reduced from the C1 onwards while levels of short and long chain acylcarnitines (propionylcarnitine and hexanodecanoylcarnitine), increased consistently from C1-C2 to C4. The observed decreased levels of glycolysis and TCA intermediates together with increased concentrations of acylcarnitines and the ketone 3-hydroxybutyrate, suggest a shift towards β -oxidation for energy production.

Decreased concentrations of the cofactor nicotinamide adenine dinucleotide (NAD), the amino acid taurine and the glutathione analogue ophthalmic acid, indicated the presence of reactive oxygen species (ROS). Through its action as an antioxidant, taurine has been shown

to play a role in counterbalancing oxidative stress attenuating the development of liver steatosis *in vitro* and *in vivo* (Murakami et al. 2018). In line with our observations of decreased antioxidant molecules, it has been demonstrated that the redox cycling during nitrofurantoin metabolization generates different ROS such as superoxide anion, hydrogen peroxide, and hydroxyl radicals (Wang et al. 2008). In addition, metabolic profiles of cells treated with the lowest nitrofurantoin concentrations, showed that precursors of glutathione such as glutamine, glutamate, cysteinylglycine and 2-methylserine started to increase while S-adenosylhomocysteine decreased possibly as an early indicator of the stimulation of *de novo* glutathione synthesis as it became evident in the middle concentration (C3).

Some of the earliest metabolic changes with respect to both concentration and time were observed in the lipid metabolism. Decreased levels of triacylglycerols (TAGs) were evident already in the lowest concentration (C1) and from an early time point (6 hours onwards). Phosphatidylcholine levels were found reduced across the low and mid doses (C1-C3) while lysophosphatidylcholine concentrations increased in all C1-C5 concentrations. Phosphatidylethanolamine levels decreased in all five tested concentrations while cholesterylesters showed increased levels from the D2 onwards. Our data evidence that nitrofurantoin exerts significant effects on different lipids species even at low concentrations. These types of alterations in the lipid metabolism have, so far, not been reported in the literature as a direct consequence of nitrofurantoin exposure. These findings add to the current knowledge of nitrofurantoin mechanisms and represent an avenue for future research.

Metabolic profile of cells exposed to the middle concentrations:

The mid concentration (C3), corresponding to 20 μ M, caused a moderate effect on ATP production and cell growth but failed to induce significant cell death. At this concentration, differential changes mainly in metabolites involved in the cellular antioxidant response, the *de novo* glutathione synthesis and amino acids were observed. Levels of coenzyme Q10 decreased in a concentration and time response manner starting from the middle concentration while glutathione (GSH) increased consistently after 24h of exposure to the C3. Following the observed GSH dynamics, levels of proline (amino acid synthesized from glutamate) started to decrease from the C3 consistently. Metabolite changes in the middle

nitrofurantoin concentration are reflective of a higher utilization of antioxidant molecules and are in line with the reported stimulation of intracellular GSH synthesis by nitrofurantoin (Wijaya et al. 2022).

Levels of essential amino acids (phenylalanine, isoleucine, leucine, tyrosine, threonine, and valine) were significantly increased starting at the C3 concentration onwards resulting in high levels in the highest concentrations. High intracellular levels of amino acids suggest a reduced amino acid utilization. Reduction of protein synthesis has been reported as a common consequence of stress response pathway activation, resulting in increased intracellular amino acids concentrations and reduced cell growth to conserve amino acids and energy and decrease the cellular protein load as one adaptive measure to overcome stresses (Santiago-Díaz et al. 2023). Attenuation of protein translation is characteristic of the unfolded protein response (UPR) pathway activation. UPR-activating compounds are mostly classified as the severe DILI compounds. Nitrofurantoin has been shown to significantly activate the UPR pathway in HepG2 cells (Wijaya et al. 2021). Importantly, it has been proposed that UPR response could represent a key predictor for adverse cellular outcomes for DILI compounds (Wijaya et al. 2021).

Through the activation of adaptive cellular stress response pathways, oxidative stress, and endoplasmic reticulum stress (resulting in unfolded proteins) are typically counteracted. Reactive metabolites generated from nitrofurantoin metabolism can be inactivated by the cellular antioxidant defense system (e.g., GSH). The UPR pathway responds to an accumulation of misfolded proteins in the endoplasmic reticulum by restoring the normal function via decreasing protein translation, degrading misfolded proteins, and activating the signaling pathways that lead to increasing the synthesis of molecular chaperones involved in protein folding (Hetz and Papa 2018). Thus, the metabolic profiles at this concentration are potentially reflective of an adaptive phenotype.

Metabolic profile of cells exposed to high concentrations

The highest tested concentrations, particularly C5 corresponding to 120 μ M, showed significant impairments on cell growth and ATP production which correlated with the strong effect observed in the metabolome. Therefore, metabolites that were differentially altered in the profiles of cells treated with the two highest nitrofurantoin concentrations (C4, C5) were

used to identify hepatotoxic responses. GSH concentrations were significantly reduced upon 48h of exposure to the highest concentration (C5). Alongside GSH reduction, levels of its precursors glutamate cysteinylglycine and S-adenosylhomocysteine decreased. An excess of reactive metabolites, beyond homeostasis, can modify cellular macromolecules leading to cellular dysfunction. Intracellular levels of antioxidants have been suggested as important regulators of nitrofurantoin-induced cytotoxicity which has been correlated to hepatitis and tissue necrosis observations in vivo (Wang et al. 2008). Particularly, GSH plays an important role in nitrofurantoin detoxification; nitrofurantoin metabolites have been shown to produce a dose-dependent depletion of total cellular glutathione content, likely due to conjugation of drug metabolites with GSH (Spielberg and Gordon 1981). Our results indicate that at the highest concentration, the capacity of cells to synthesize GSH was compromised, leading to the final depletion of GSH rendering the cells vulnerable for ROS damage.

Glycerol-3-phosphate levels increased in the two highest concentrations. This metabolite is involved in transporting reducing equivalents across the mitochondrial membrane via the glycerol phosphate shuttle for oxidative phosphorylation (Liu et al. 2021). Metabolites from the fatty acid oxidation pathway were also changed in the highest concentrations.

Long chain acylcarnitines (tetradecanoylcarnitine) switched from reduced levels in the low and mid concentrations, to an upregulation at C5. Propionylcarnitine switched from a consistent increase in the lower concentrations to an increase in the highest concentration while tetradecanoylcarnitine changed from decreased levels in the C3 to increased levels at the C5. Alterations in octadecenoylcarnitine (increase) and hexanoylcarnitine (decrease) were uniquely observed at the highest concentrations. Noteworthy, concentrations of TAGs switched from consistently lower levels in C1-C4 to highly increased concentrations in C5.

The high concentrations of glycerol-3-phosphate, long chain acylcarnitines and TAG's together with lower levels of short chain acylcarnitines are reflective of an impairment of the mitochondrial activity and fatty acid β -oxidation pathway. In agreement with our findings, it has been shown that cell viability decreases significantly at nitrofurantoin concentrations higher than 100 μ M, accompanied by impaired mitochondrial respiration (Wijaya et al. 2022). In our study, an inhibition of β -oxidation in the highest nitrofurantoin concentrations is evidenced by reduced free carnitine, and an increase in the fatty acid pool. Free fatty acids

can incorporate in lipid species such as TGA and ceramides. In our study, the concentrations of both lipid species were highly elevated. Higher levels of TAGs and ceramides are typical findings in liver toxicity studies (Beyoglu and Idle 2013). Accumulation of TAGs is the hallmark of steatosis while high ceramides levels have been implicated in the impairment of different metabolic processes, being considered as lipotoxic species (Kawano and Cohen 2013; Kurz et al. 2019).

Finally, levels of pipecolic acid were increased only at the highest concentration and latest time point (48h). Significantly elevated levels of pipecolic acid have been found in plasma of patients with chronic liver disease (Fujita et al. 1999).

In summary, the observed metabolomics alterations matched thoroughly with the nitrofurantoin toxicological mechanisms described in literature such as the de novo stimulation of GSH synthesis and the activation of oxidative stress and unfolded protein response pathways in low and middle concentrations, and the mitochondrial impairment and GSH depletion in the high concentrations. Metabolic profiles of cells exposed to low concentrations (C1, C2) revealed initial responses in metabolite changes upon nitrofurantoin exposure. The middle concentration (C3) reflected changes potentially indicative of an adaptive phenotype which progressed into a more severe hepatotoxic metabolic phenotype in the highest concentrations (C4, C5).

Point of departure determination based on metabolomics data

The establishment of human health reference values is a key outcome of chemical risk assessment. For in vitro data, the starting point for the determination of such values includes the derivation of a point of departure (POD) from dose–response modelling followed by an In Vitro–In Vivo Extrapolation (IVIVE) analysis to link an in vitro effect concentration with its in vivo counterpart. The successful application of IVIVE to transform in vitro concentrations into doses expressed in mg/kg bw, as derived in in vivo studies has been demonstrated in various publications (Abdullah et al. 2016; Lousse et al. 2017; Ning et al. 2019; Shi et al. 2020). This approach was also proposed recently by Ball et al, in which a more generalised framework for the transition from in vivo to NAM-based approaches was presented (Ball et al. 2022). Due to their multiparametric nature, Omics technologies allow to measure multiple endpoints and pathways simultaneously, representing a more informative alternative than traditional in

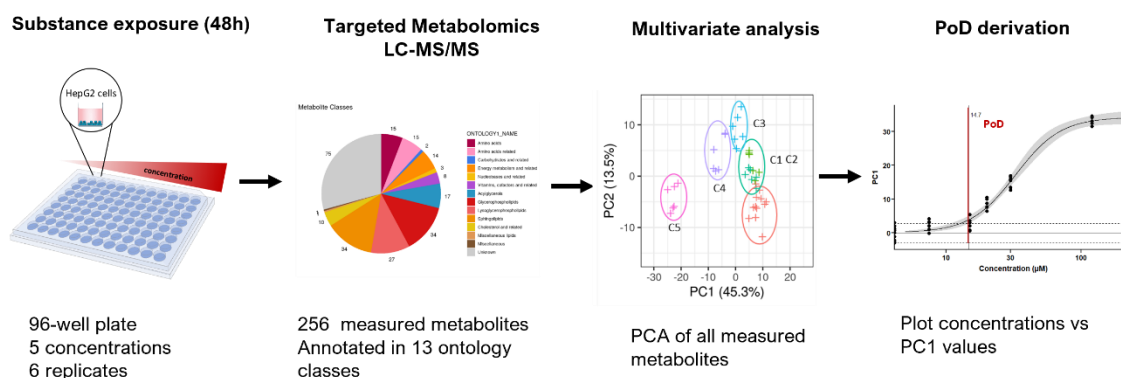
vitro studies. Here we explore a PCA-based approach using the complete set of previously annotated metabolites to derive a PoD. We selected the 48 hours' time point since it showed the most pronounced concentration response resolution, and such is most conservative. As the PC1 accounts for the strongest response in metabolome changes for the different test concentrations, PC1 values for each replicate were plotted against the concentration tested. Then, a concentration response curve was fitted and the 95 % confidence interval for the curve was determined represented by the grey ribbon (Fig.5). To account for the variability of the controls, the 2.5 % and 97.5% quantiles were used, covering 95% of the data (dotted line in Fig. 5). The PoD was defined as the point where the 95% confidence interval of the curve diverges from the corresponding quantile of the controls for the first time. The PoD represented the onset of a global change in the metabolome. Above this concentration, early changes in the novo GSH synthesis pathway, energy and lipid metabolism become evident which increased at higher concentrations. Recent studies have used untargeted metabolomics data to derive PoD via benchmark dose (BMD) (Crizer et al. 2021b; Malinowska et al. 2023). These approaches have been based on BMD calculation for single features and lack comprehensive metabolite annotations which could hamper data interpretation. Here we propose an alternative way on how to derive mechanistic-anchored PoD based on the complete set of biological data obtained from metabolomics experiments. Both methods provide a biologically based starting point that can be used to transform the PoD concentration by means of IVIVE into a reference value in expressed in mg/kg bw for human health risk assessment. The advantage of using a broad targeted approach with annotated metabolites is that only with this knowledge adverse outcome pathways can be identified and that an attempt can be made to discriminate between non adverse (adaptive) responses and adverse effects. Differentiation between adverse effects and adaptive responses are a critical consideration for the broad implementation of NAM's and in particular for multiparametric Omics data. Recently, ECETOC has published a paper on their workshop about Omics threshold on non-adversity with particular emphasis on the determination of PoD (Gant et al. 2023).

Adverse responses are considered changes that likely result in impairments of functional capacity, impairments of the capacity to compensate for additional stress or increase the susceptibility to other influences (Keller et al. 2012). Although it is not the purpose of this

paper to derive such a value for nitrofurantoin, we believe that using a PC1 approach, takes into account the multiparameter nature of Omics data and is considered more robust than single parameter data. However, further research is needed to identify (groups of) metabolites that are representative of an adverse effect, so that these can be used to derive a PoD for adverse effects and to extrapolate this value into relevant *in vivo* concentrations for risk assessment.

Recovery studies, for example, can be introduced to further characterize adversity in *in vitro* studies. It is acknowledged that approaches solely based on biological responses will be conservative, and as such will not underestimate the characterization of hazard and can be used in a tiered approach.

a



b

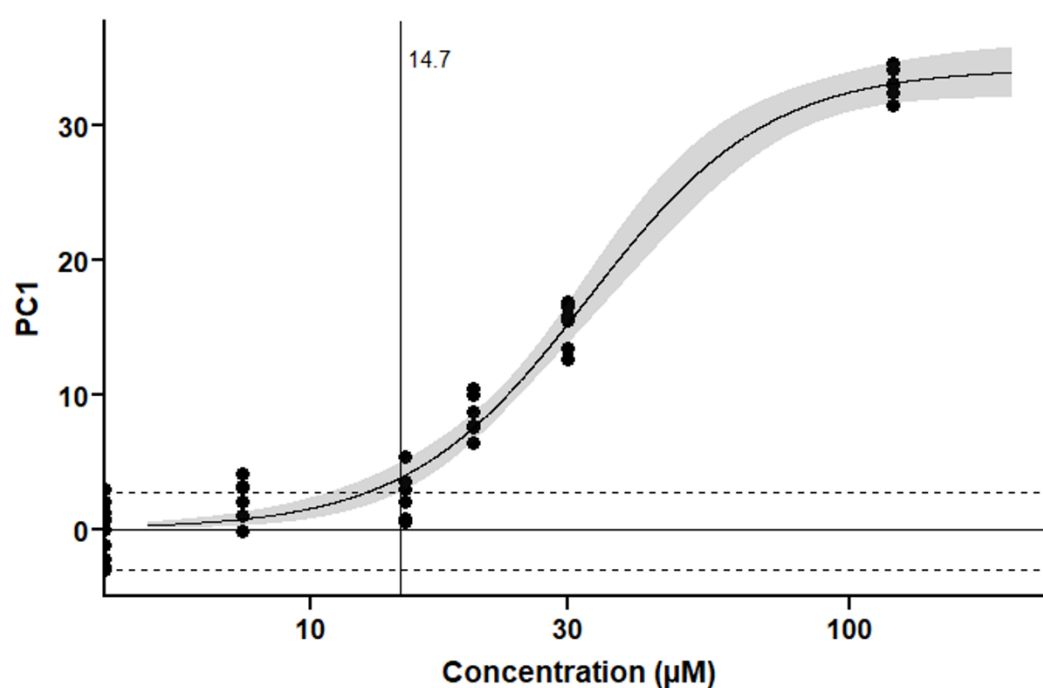


Fig 5. Point of departure (PoD) derivation from metabolomics data. *a)* PoD derivation workflow, *b)* Nitrofurantoin PoD. Global metabolite changes as estimated by principal component analysis (PCA) exhibit exposure concentration dependency. For the PoD derivation, a concentration-dependent response was fitted based on PC1 values obtained from the PCAs of 48 hours nitrofurantoin treated cells at five concentrations. PC1 values for each sample were plotted against the test concentration and a 3-parameter log-logistic model was fitted through the data. A confidence interval of 95 % was used for the dose-response curve (denoted by the grey ribbon). The spread of controls is marked by the horizontal dashed lines, which represent the 2.5 % and 97.5 % quantiles; the mean is represented as horizontal solid line. The point of departure (PoD), marked by a vertical solid line, marks the concentration at which the confidence interval of the curve surpasses the corresponding quantile of the controls for the first time.

Conclusion

Recent investigations have shown the potential of applying high throughput untargeted metabolomics approaches to derive hepatotoxicity-related PoD. However, lack of metabolite identification, a characteristic of untargeted methods, challenges the biological interpretations of the results hampering the assessment of the relevance and applicability of these data in safety assessment. In the present study, we have implemented a high-throughput targeted metabolomics platform (covering metabolites from relevant biological pathways) and showed the suitability of the system to elucidate metabolic dynamics over time and concentration to provide a mechanistic-anchored approach to derive and interpret dose and time response metrics from metabolomics data. Both PCA and univariate analysis evidenced clear metabolome-based time and concentration response effects. Mechanistic information allowed to track the differential activation of cellular pathways indicative of early adaptive and hepatotoxic response. At low concentrations, effects were seen mainly in the energy and lipid metabolism, in the mid concentration the activation of the antioxidant cellular response was evidenced by increased levels of GSH and metabolites from the de novo GSH synthesis pathway. At the highest concentrations, the depletion of GSH, accumulation of essential amino acids, ceramides and pipecolic acid together with alternations reflective of mitochondrial impairments, were indicative of a hepatotoxic response. Our results were in line with the broad range of reported concentration-dependent effects of nitrofurantoin. In addition, effects of nitrofurantoin exposure on the lipid metabolism, which to our knowledge have not yet been documented in the literature, were observed. After confirming the mechanistic relevance of the data, we proposed an alternative way to derive metabolomics-based PoD by PCA using the whole set of measured metabolite profiles at each concentration. This approach allows to obtain values from the entire dataset and to derive PoDs that can be mechanistically anchored to established key events. This study demonstrates a very good sensitivity of the high throughput in vitro metabolomics method to explore mechanisms of hepatotoxicity, and dynamics progression to potential adversity. However, further studies are needed in order to define solid parameters for adversity in vitro. Importantly, our work proposes a workflow for PoD derivation that offers the possibility of obtaining mechanistic information and therefore serves to build trust in implementing metabolomics data in risk assessment. Follow up investigations on the integration of these data into in vitro to in vivo

extrapolations models (IVIVE) and on the characterization of adaptive vs adverse responses are granted. In the absence of clear guidance to discriminate between adaptive/non-adverse changes and adverse effects, using initial biological responses is a conservative approach which can be used in a tiered system.

This method can be extended to further cell lines and iPSCs for the investigation of different organ toxicities and is suitable for a wide range of next generation risk assessment applications such as MoA investigation, read across and PoD derivation that demand rapid, cost effective and multiparametric high throughput analysis.

Statements and Declarations

Competing interests

The authors have no conflicts of interest to declare. BASF may use some of the presented technologies for product development in the future.

Ethical standards

The manuscript does not contain clinical studies or patient data.

References

- Abdullah R, Alhusainy W, Woutersen J, Rietjens IM, Punt A (2016) Predicting points of departure for risk assessment based on in vitro cytotoxicity data and physiologically based kinetic (PBK) modeling: the case of kidney toxicity induced by aristolochic acid I. *Food and chemical toxicology* 92:104-116
- Ball N, Bars R, Botham PA, et al. (2022) A framework for chemical safety assessment incorporating new approach methodologies within REACH. *Archives of Toxicology* 96(3):743-766
- Beyoglu D, Idle JR (2013) The metabolomic window into hepatobiliary disease. *J Hepatol* 59(4):842-58 doi:10.1016/j.jhep.2013.05.030
- Birk B, Haake V, Sperber S, et al. (2021) Use of in vitro metabolomics in NRK cells to help predicting nephrotoxicity and differentiating the MoA of nephrotoxicants. *Toxicology Letters* 353:43-59
- Crizer DM, Ramaiahgari SC, Ferguson SS, et al. (2021) Benchmark Concentrations for Untargeted Metabolomics Versus Transcriptomics for Liver Injury Compounds in In Vitro Liver Models. *Toxicol Sci* 181(2):175-186 doi:10.1093/toxsci/kfab036
- Cuykx M, Claes L, Rodrigues RM, Vanhaecke T, Covaci A (2018) Metabolomics profiling of steatosis progression in HepaRG® cells using sodium valproate. *Toxicology letters* 286:22-30
- Dix DJ, Houck KA, Martin MT, Richard AM, Setzer RW, Kavlock RJ (2007) The ToxCast program for prioritizing toxicity testing of environmental chemicals. *Toxicological sciences* 95(1):5-12

- Fujita T, Amuro Y, Hada T, Higashino K (1999) Plasma levels of pipercolic acid, both L- and D-enantiomers, in patients with chronic liver diseases, especially hepatic encephalopathy. *Clinica chimica acta* 287(1-2):99-109
- Gant T, Auerbach S, Von Bergen M, et al. (2023) Applying genomics in regulatory toxicology: a report of the ECETOC workshop on omics threshold on non-adversity. *Archives of Toxicology* doi:10.1007/s00204-023-03522-3
- García-Cañaveras JC, Castell JV, Donato MT, Lahoz A (2016) A metabolomics cell-based approach for anticipating and investigating drug-induced liver injury. *Scientific reports* 6(1):1-12
- Guijas C, Montenegro-Burke JR, Warth B, Spilker ME, Siuzdak G (2018) Metabolomics activity screening for identifying metabolites that modulate phenotype. *Nature biotechnology* 36(4):316-320
- Hetz C, Papa FR (2018) The unfolded protein response and cell fate control. *Molecular cell* 69(2):169-181
- Kamp H, Fabian E, Groeters S, et al. (2012) Application of in vivo metabolomics to preclinical/toxicological studies: case study on phenytoin-induced systemic toxicity. *Bioanalysis* 4(18):2291-2301
- Kawano Y, Cohen DE (2013) Mechanisms of hepatic triglyceride accumulation in non-alcoholic fatty liver disease. *Journal of gastroenterology* 48:434-441
- Keller DA, Juberg DR, Catlin N, et al. (2012) Identification and characterization of adverse effects in 21st century toxicology. *Toxicological Sciences* 126(2):291-297
- Krewski D, Andersen ME, Tyshenko MG, et al. (2020) Toxicity testing in the 21st century: progress in the past decade and future perspectives. *Archives of toxicology* 94(1):1-58
- Kurz J, Parnham MJ, Geisslinger G, Schiffmann S (2019) Ceramides as novel disease biomarkers. *Trends in molecular medicine* 25(1):20-32
- Liu S, Fu S, Wang G, et al. (2021) Glycerol-3-phosphate biosynthesis regenerates cytosolic NAD⁺ to alleviate mitochondrial disease. *Cell metabolism* 33(10):1974-1987. e9
- Louisse J, Beekmann K, Rietjens IM (2017) Use of physiologically based kinetic modeling-based reverse dosimetry to predict in vivo toxicity from in vitro data. *Chemical Research in Toxicology* 30(1):114-125
- Malinowska JM, Palosaari T, Sund J, et al. (2022) Integrating in vitro metabolomics with a 96-well high-throughput screening platform. *Metabolomics* 18(1):11 doi:10.1007/s11306-021-01867-3
- Malinowska JM, Palosaari T, Sund J, et al. (2023) Derivation of metabolic point of departure using high-throughput in vitro metabolomics: investigating the importance of sampling time points on benchmark concentration values in the HepaRG cell line. *Archives of toxicology*:1-15
- Mattes W, Davis K, Fabian E, et al. (2014) Detection of hepatotoxicity potential with metabolite profiling (metabolomics) of rat plasma. *Toxicol Lett* 230(3):467-78 doi:10.1016/j.toxlet.2014.07.021
- Murakami S, Ono A, Kawasaki A, Takenaga T, Ito T (2018) Taurine attenuates the development of hepatic steatosis through the inhibition of oxidative stress in a model of nonalcoholic fatty liver disease in vivo and in vitro. *Amino Acids* 50(9):1279-1288

- National Research Council (2007) Toxicity testing in the 21st century: a vision and a strategy. National Academies Press
- Ning J, Chen L, Strikwold M, Louisse J, Wesseling S, Rietjens IM (2019) Use of an in vitro–in silico testing strategy to predict inter-species and inter-ethnic human differences in liver toxicity of the pyrrolizidine alkaloids lasiocarpine and riddelliine. *Archives of toxicology* 93:801-818
- Olesti E, Gonzalez-Ruiz V, Wilks MF, Boccard J, Rudaz S (2021) Approaches in metabolomics for regulatory toxicology applications. *Analyst* 146(6):1820-1834 doi:10.1039/d0an02212h
- Ramirez-Hincapie S, Birk B, Ternes P, et al. (2023) A high-throughput metabolomics in vitro platform for the characterization of hepatotoxicity. *Cell Biology and Toxicology*:1-19 doi:10.1007/s10565-023-09809-6
- Ramirez T, Daneshian M, Kamp H, et al. (2013) Metabolomics in toxicology and preclinical research. *Altex* 30(2):209
- Ramirez T, Strigun A, Verlohner A, et al. (2018) Prediction of liver toxicity and mode of action using metabolomics in vitro in HepG2 cells. *Arch Toxicol* 92(2):893-906 doi:10.1007/s00204-017-2079-6
- Ritz C, Streibig JC (2005) Bioassay analysis using R. *Journal of statistical software* 12:1-22
- Santiago-Díaz P, Rivero A, Rico M, González González A, González-Dávila M, Santana-Casiano M (2023) Copper toxicity leads to accumulation of free amino acids and polyphenols in *Phaeodactylum tricornutum* diatoms. *Environmental Science and Pollution Research*:1-10
- Serrano J (2014) LiverTox: An online information resource and a site for case report submission on drug-induced liver injury. *Clinical Liver Disease* 4(1):22
- Shi M, Bouwmeester H, Rietjens IM, Strikwold M (2020) Integrating in vitro data and physiologically based kinetic modeling-facilitated reverse dosimetry to predict human cardiotoxicity of methadone. *Archives of toxicology* 94:2809-2827
- Spielberg S, Gordon G (1981) Nitrofurantoin cytotoxicity. In vitro assessment of risk based on glutathione metabolism. *The Journal of Clinical Investigation* 67(1):37-41
- Stucki AO, Barton-Maclaren TS, Bhuller Y, et al. (2022) Use of new approach methodologies (NAMs) to meet regulatory requirements for the assessment of industrial chemicals and pesticides for effects on human health. *Frontiers in Toxicology*:98
- Van Ravenzwaay B, Cunha GC-P, Leibold E, et al. (2007) The use of metabolomics for the discovery of new biomarkers of effect. *Toxicology letters* 172(1-2):21-28
- Van Ravenzwaay B, Kamp H, Montoya-Parra GA, et al. (2015) The development of a database for metabolomics-Looking back on ten years of experience. *International Journal of Biotechnology* 14(1):47-68
- Viant MR, Ebbels TMD, Beger RD, et al. (2019) Use cases, best practice and reporting standards for metabolomics in regulatory toxicology. *Nat Commun* 10(1):3041 doi:10.1038/s41467-019-10900-y
- Vinken M (2013) The adverse outcome pathway concept: a pragmatic tool in toxicology. *Toxicology* 312:158-165
- Wang Y, Gray JP, Mishin V, Heck DE, Laskin DL, Laskin JD (2008) Role of cytochrome P450 reductase in nitrofurantoin-induced redox cycling and cytotoxicity. *Free Radical Biology and Medicine* 44(6):1169-1179

Wijaya LS, Rau C, Braun TS, et al. (2022) Stimulation of de novo glutathione synthesis by nitrofurantoin for enhanced resilience of hepatocytes. *Cell biology and toxicology*:1-18

Wijaya LS, Trairatphisan P, Gabor A, et al. (2021) Integration of temporal single cell cellular stress response activity with logic-ODE modeling reveals activation of ATF4-CHOP axis as a critical predictor of drug-induced liver injury. *Biochemical Pharmacology* 190:114591

Supplementary information

Application of High Throughput *In vitro* Metabolomics for Hepatotoxicity Mode of Action characterization and Mechanistic-anchored Point of Departure Derivation: A Case Study with Nitrofurantoin.

Sabina Ramirez-Hincapie¹, Barbara Birk¹, Philipp Ternes², Varun Giri¹, Franziska Maria Zickgraf¹, Volker Haake², Michael Herold², Hennicke Kamp², Peter Driemert², Robert Landsiedel^{1,3}, Elke Richling⁴, Dorothee Funk-Weyer¹, Bennard van Ravenzwaay⁵

¹ BASF SE, Experimental Toxicology and Ecology, Ludwigshafen, Germany

² BASF Metabolome Solution GmbH, Berlin, Germany

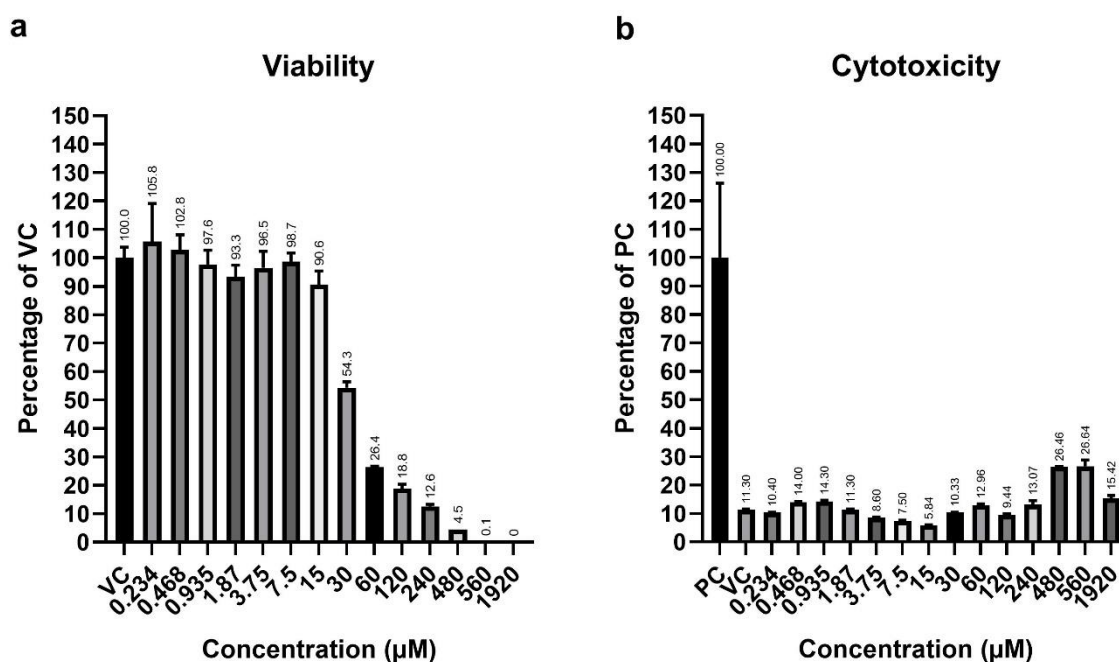
³ Free University of Berlin, Pharmacy, Pharmacology and Toxicology, Berlin, Germany.

⁴ Food Chemistry and Toxicology, Department of Chemistry, RPTU Kaiserslautern-Landau, Kaiserslautern, Germany

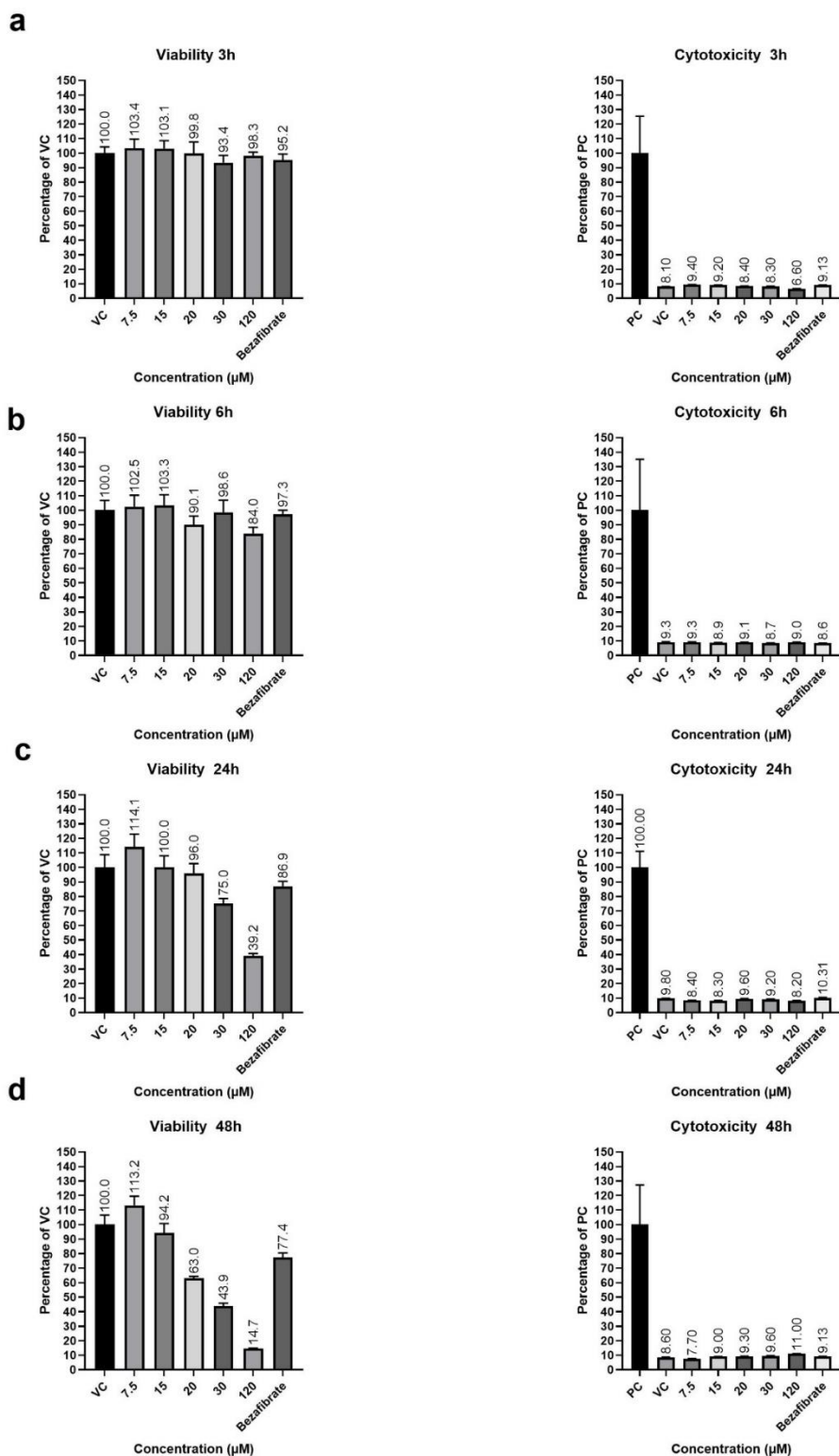
⁵ Environmental Sciences Consulting, Altrip, Germany

Supplementary information

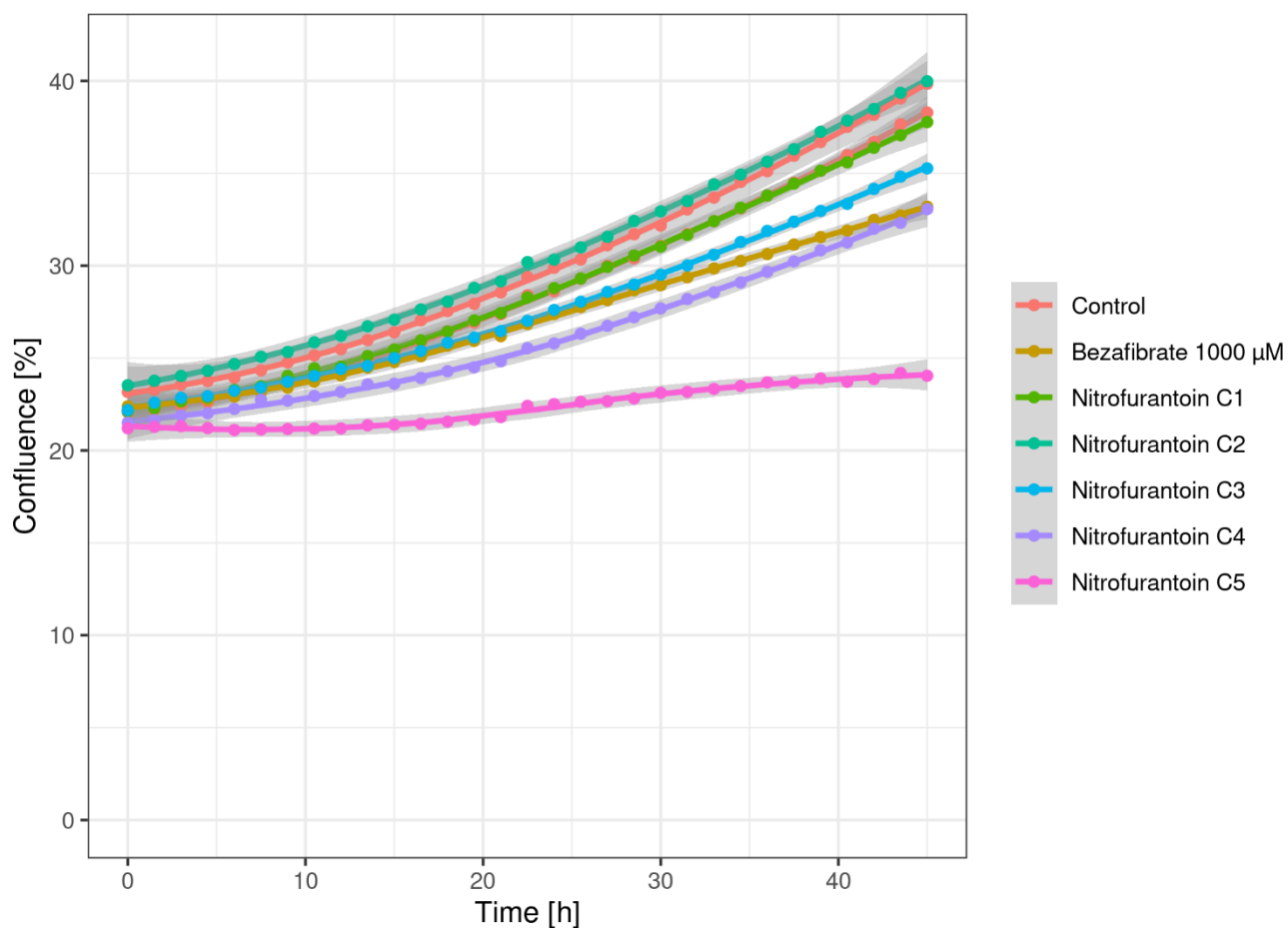
Suppl Fig. 1 Cytotoxicity and cell viability range finder for dose selection. (a) Cell viability ATP content-based assay (CellTiter-Glo®) and (b) membrane impermeable DNA-binding dye-based cytotoxicity assay (CellTox™ Green) n=6. Values are presented as percentage of vehicle controls (VC) for CellTiter-Glo® and as percentage of positive control (PC) (lysis buffer) for CellTox™ Green.



Suppl. Fig.2 Cell viability and cytotoxicity testing in metabolomics experiments. Cell viability ATP content-based assay (CellTiter-Glo®) and membrane impermeable DNA-binding dye-based cytotoxicity assay (CellTox™ Green) were carried out in parallel with metabolomics experiments in plates handled and treated exactly as the ones used for metabolite profiling. n=6. a) 3h, b) 6h, c) 24h, d) 48h. Values are presented as percentage of vehicle controls (VC) for CellTiter-Glo® and as percentage of positive control (PC) (lysis buffer) for CellTox™ Green. Bezafibrate 1000µM was used as a positive control in each experiment.

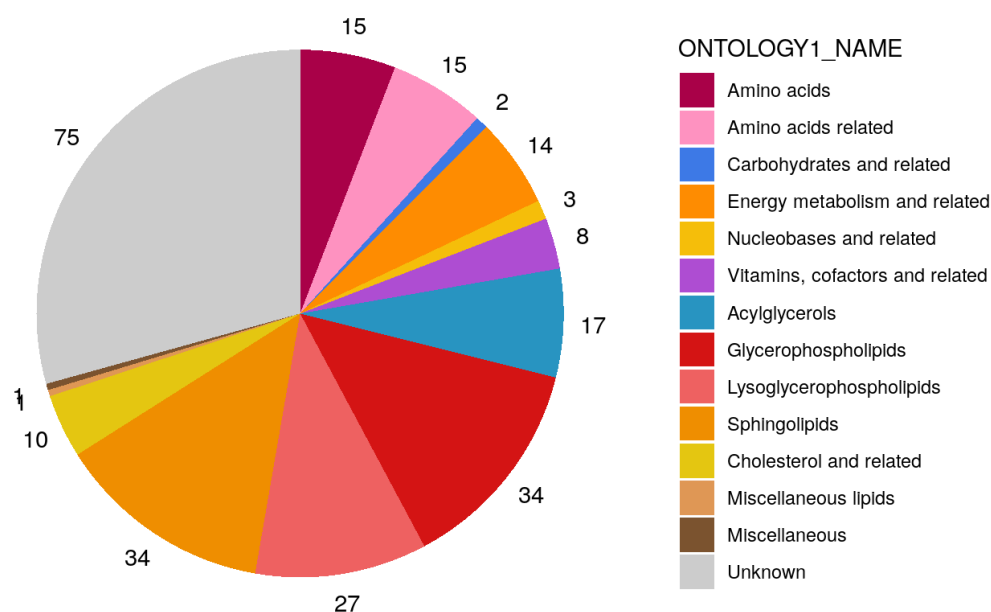


Suppl. Fig .3 Cell confluence during 48h of nitrofurantoin exposure at different concentrations. HepG2 were exposed for 48h to five different cocentrations of nitrofurantoin (C1:7.5µM, C2:15µM, C3:30µM, C4:60µM, C5:120µM) Cell confluence was minitored in realtime during the time of the assay. VC: vehivle control (0.5% DMSO), bezafibrate 100µM was used as a possitive control. n=6. Grey ribbon represents the confidence interval for each curve.



Suppl. Fig 4 Measured metabolite classes. Pie chart of the number of metabolites measured per ontology class. A total of 256 unique analytes were measured in this study.

Metabolite Classes



Suppl. Fig.5 Experimental variability and reproducibility. the variance of every log-transformed metabolite for both pooled samples (technical replicates) and control samples was calculated. These variances were back transformed to linear scale, yielding a relative standard deviation (RSD).

Time point	Pools	Controls
03 h	9.2%	26.3%
06 h	10.0%	23.5%
24 h	9.7%	24.6%
48 h	10.3%	27.8%

Suppl Fig. 6 Enrichment analysis of significantly altered metabolites by ontology class after nitrofurantoin treatment. The distribution of the 256 measured metabolites across the ontology classes is provided in the column “# metabolites”. The number of metabolite changes are shown for each metabolite ontology class. Numbers yellow represent that a treatment caused a significant (p -value<0.05) enrichment in an ontology class. C1 to C5: nitrofurantoin concentrations. a) changes over time, b) over concentration.

a)

Metabolite Class	# Metabolites	Bezafibrate				3h					6h					24h					48h					
		3h	6h	24h	48h	C1	C2	C3	C4	C5	C1	C2	C3	C4	C5	C1	C2	C3	C4	C5	C1	C2	C3	C4	C5	
		Amino acids	15	9	5	4	10	9	6	0	2	4	5	1	7	7	9	0	11	4	9	15	4	2	11	8
Amino acids related	15	8	7	5	13	4	2	2	1	4	6	0	6	6	7	1	10	5	3	7	8	7	11	6	14	
Carbohydrates and related	2	1	1	0	2	2	1	0	1	0	1	0	1	2	2	1	2	0	0	0	1	1	2	0	2	
Energy metabolism and related	13	10	9	7	8	4	4	4	3	6	9	4	8	8	10	2	5	8	7	12	7	7	10	10	12	
Nucleobases and related	4	0	1	3	2	0	0	0	1	0	1	0	1	0	1	0	0	1	1	1	1	3	0	0	1	3
Vitamins, cofactors and related	8	4	5	2	3	2	1	1	0	1	4	0	4	4	4	0	6	1	2	5	4	3	5	1	6	
Acylglycerols	17	3	10	14	13	1	1	8	10	11	7	5	9	8	12	4	15	11	12	16	11	4	12	12	11	
Glycerophospholipids	34	19	22	26	28	1	2	1	3	11	1	1	2	5	13	1	11	2	21	29	8	12	24	29	29	
Lysoglycerophospholipids	27	15	21	19	24	9	4	1	3	8	0	5	5	4	7	1	14	4	10	13	6	10	13	20	21	
Sphingolipids	34	8	16	23	25	2	1	2	2	16	0	1	1	3	17	0	8	5	17	28	2	3	8	20	24	
Cholesterol and related	10	7	8	9	2	1	0	0	7	7	0	0	5	1	6	2	10	8	5	10	0	4	7	8	9	
Miscellaneous lipids	1	0	0	1	1	0	1	1	1	0	0	0	1	1	0	0	0	0	0	0	1	0	1	1	1	
Miscellaneous	1	0	1	1	1	0	0	0	0	0	0	0	1	0	0	0	1	0	0	1	1	1	1	0	1	
Unknown	75	26	36	41	59	10	10	7	15	25	15	9	21	23	40	9	28	22	49	60	28	27	49	50	59	
Total # Metabolites	256	110	142	155	191	45	33	27	49	93	49	26	72	72	128	21	121	71	136	198	83	82	154	166	207	

b)

Metabolite Class	# Metabolites	Bezafibrate				Nitrofurantoin C1				Nitrofurantoin C2				Nitrofurantoin C3				Nitrofurantoin C4				Nitrofurantoin C5			
		3h	6h	24h	48h	3h	6h	24h	48h	3h	6h	24h	48h	3h	6h	24h	48h	3h	6h	24h	48h	3h	6h	24h	48h
		Amino acids	15	9	5	4	10	9	5	0	4	6	1	11	2	0	7	4	11	2	7	9	8	4	9
Amino acids related	15	8	7	5	13	4	6	1	8	2	0	10	7	2	6	5	11	1	6	3	6	4	7	7	14
Carbohydrates and related	2	1	1	0	2	2	1	1	1	1	0	2	1	0	1	0	2	1	2	0	0	0	2	0	2
Energy metabolism and related	13	10	9	7	8	4	9	2	7	4	4	5	7	4	8	8	10	3	8	7	10	6	10	12	12
Nucleobases and related	4	0	1	3	2	0	1	0	3	0	0	0	0	0	1	1	0	1	0	1	1	0	1	1	3
Vitamins, cofactors and related	8	4	5	2	3	2	4	0	4	1	0	6	3	1	4	1	5	0	4	2	1	1	4	5	6
Acylglycerols	17	3	10	14	13	1	7	4	11	1	5	15	4	8	9	11	12	10	8	12	12	11	12	16	11
Glycerophospholipids	34	19	22	26	28	1	1	1	8	2	1	11	12	1	2	2	24	3	5	21	29	11	13	29	29
Lysoglycerophospholipids	27	15	21	19	24	9	0	1	6	4	5	14	10	1	5	4	13	3	4	10	20	8	7	13	21
Sphingolipids	34	8	16	23	25	2	0	0	2	1	1	8	3	2	1	5	8	2	3	17	20	16	17	28	24
Cholesterol and related	10	7	8	9	2	1	0	2	0	0	0	10	4	0	5	8	7	7	1	5	8	7	6	10	9
Miscellaneous lipids	1	0	0	1	1	0	0	0	0	1	0	0	1	1	1	0	1	1	1	0	1	0	0	1	1
Miscellaneous	1	0	1	1	1	0	0	0	1	0	0	1	1	0	1	0	1	0	0	0	0	0	0	1	1
Unknown	75	26	36	41	59	10	15	9	28	10	9	28	27	7	21	22	49	15	23	49	50	25	40	60	59
Total # Metabolites	256	110	142	155	191	45	49	21	83	33	26	121	82	27	72	71	154	49	72	136	166	93	128	198	207

Suppl Fig. 7 Metabolome changes induced by nitrofurantoin treatment. Heatmap of statistically significantly ($p < 0.05$) altered metabolites after nitrofurantoin treatment. Red represents significantly upregulated metabolites and blue represents significantly downregulated metabolites as compared to controls. (n=6 per condition). a) individual metabolite changes over time, b) individual metabolite changes over concentration.

a)

Unknown	Unknown lipid (849590482)	1,01	1,03	0,86	0,83	0,77	0,99	1,02	0,97	0,9	0,94	0,94	0,66	0,75	0,59	0,52	0,75	0,84	0,59	0,59	0,78
Unknown	Unknown lipid (849590483)	1,01	1,02	0,95	0,81	0,79	1	0,89	0,9	0,91	0,91	0,66	0,66	0,56	0,61	0,65	0,81	0,54	0,58	1,18	
Unknown	Unknown lipid (849590484)	1,01	1	0,9	0,77	0,71	0,97	1	0,85	0,85	0,85	0,83	0,62	0,63	0,52	0,53	0,73	0,8	0,55	0,59	1,11
Unknown	Unknown lipid (849590485)	0,95	0,95	0,89	0,85	0,75	0,87	0,82	0,8	0,72	0,83	0,64	0,56	0,48	0,52	0,71	0,82	0,58	0,53	0,93	
Unknown	Unknown lipid (849590486)	1,06	1,02	0,93	0,91	0,87	0,91	0,99	0,85	0,89	0,84	0,9	0,66	0,66	0,54	0,58	0,72	0,78	0,62	0,72	1,33
Unknown	Unknown lipid (849590487)	0,99	1,08	0,94	1,02	0,98	0,96	0,98	0,92	0,95	0,85	1,1	1,11	0,96	0,48	0,41	0,45	0,39	0,51	0,75	0,79
Unknown	Unknown lipid (849590488)	1,04	0,96	1,05	1,11	1,12	1	1,09	1,12	1,09	0,95	1,59	1,91	1,53	0,59	0,57	0,44	0,43	0,31	0,64	0,81
Unknown	Unknown lipid (849590489)	0,88	0,81	0,91	0,96	1	0,93	0,87	0,89	0,96	0,85	1,21	1,38	0,86	0,41	0,58	0,43	0,57	0,41	0,74	1,13
Unknown	Unknown lipid (849590500)	0,92	1,03	1,02	1,02	0,95	1,11	0,88	1,14	0,95	0,85	0,82	0,95	0,84	0,98	0,98	1,31	0,98	1,38	1,45	2,31
Unknown	Unknown lipid (859590013)	0,9	0,97	1,14	0,95	1,02	0,98	0,9	1,13	1,17	1,09	0,86	0,98	0,99	1,26	1,75	1,02	1	1,17	1,31	2,3
Unknown	Unknown lipid (859590071)	0,95	0,94	1,01	0,93	0,95	0,91	0,92	1,13	0,99	0,81	0,91	0,9	0,86	1,17	1,11	1,21	1,25	1,7		
Unknown	Unknown polar (869590388)	0,95	0,94	1	1,02	1,21	1,03	1,01	1,14	1,2	1,26	1,02	1,09	1,12	1,13	0,93	1,19	1,31	1,07	1,3	
Unknown	Unknown polar (869590390)	0,95	0,99	0,99	0,96	0,71	1,14	1	1,09	1,01	0,87	0,99	1,13	0,89	0,81	0,8	1,08	1,11	1,02	0,77	0,84
Unknown	Unknown polar (869590395)	0,88	0,87	0,96	0,93	1	1,04	0,96	1,11	1,09	1,16	0,98	1,27	1,02	1,17	1,25	1,28	1,13	1,43	1,47	
Unknown	Unknown polar (869590398)	0,75	1,04	1,04	1,08	1,2	1,07	1,06	1,06	1,06	0,96	0,91	0,76	0,64	0,49	1	0,92	0,66	0,78		
Unknown	Unknown polar (869590400)	0,71	0,85	1,14	0,87	0,91	1,5	0,96	1,81	1,63	1,53	0,86	1,67	1,04	1,02	1,25	2,43	1,82	2,36	0,96	1,33
Unknown	Unknown polar (869590402)	0,91	0,96	1,04	1,05	1,4	0,96	1,03	1,16	1,27	1,28	1,01	1,04	1,22	1,13	0,74	1,18	1,13	1,24	1,06	0,63
Unknown	Unknown polar (869590406)	0,78	0,86	1,22	1	0,98	1,38	0,98	1,73	1,65	1,63	0,93	1,53	1,12	1,25	1,69	2,02	1,53	2,12	1,12	1,57
Unknown	Unknown polar (869590410)	0,87	0,94	1,21	0,98	0,94	1,39	1,08	1,46	1,57	1,6	0,96	1,8	1,62	1,47	1,87	1,39	0,88	1,26	1,11	1,43
Unknown	Unknown polar (869590417)	0,99	1,09	1,1	1,09	1,1	0,7	1,17	0,91	0,69	0,73	0,95	2,06	1,34	1,28	1,67	1,68	1,32	2,29	0,96	1,57
Unknown	Unknown polar (869590424)	0,71	0,86	1,25	0,94	0,96	1,45	0,94	1,75	1,59	1,52	0,87	1,63	1,12	0,98	1,34	2,28	1,81	2,27	0,97	1,39
Unknown	Unknown polar (869590431)	0,67	0,86	1,31	0,89	1,12	1,85	1,17	2,34	2,28	2,05	0,84	2,44	1,21	0,89	1,14	2,16	1,54	2,1	0,96	1,42
Unknown	Unknown polar (869590432)	0,68	0,8	1,06	0,83	0,84	1,31	0,98	1,64	1,46	1,45	1,05	0,93	1,44	1,48	1,93	1,16	1,22	2,01	1,46	1,91
Unknown	Unknown polar (869590436)	1	1,1	1,2	1,15	1,12	1,21	1,21	1,19	1,19	1,03	1,01	1,01	0,91	0,71	0,42	1,08	0,97	0,76	0,59	0,39
Unknown	Unknown polar (869590442)	1,02	1,07	1,15	1,14	1,11	1,16	1,1	1,19	1,19	1,05	1,04	1,26	1,51	2,18	1,1	1,08	1,55	2,03	4,22	
Unknown	Unknown polar (869590444)	1,16	1,31	1,35	1,41	1	1,19	1,19	1,16	1,16	0,7	1,21	0,8	1,05	0,72	0,22	1,23	1,16	0,83	0,34	0,1
Unknown	Unknown polar (869590448)	1,02	1,26	1,12	1,08	0,81	1,21	1,16	1,24	1,03	0,73	1,12	1,25	0,97	0,74	0,22	1,21	1,06	1,01	0,55	0,48
Unknown	Unknown polar (869590452)	0,87	0,94	0,86	0,86	0,8	1,51	1,14	1,07	1,32	1,57	0,84	1,08	1	1,04	0,83	1,01	1,07	1,57	0,84	0,66
Unknown	Unknown polar (869590456)	1,01	1,06	1,02	1,12	1,2	1,01	1,05	1,05	1,09	1,37	1,06	0,88	1,05	1,06	0,77	0,76	0,81	0,83	0,97	0,52
Unknown	Unknown polar (879590076)	1,04	1,09	1	1,15	0,94	1,01	1	1,02	0,93	0,72	1,02	0,46	0,7	0,82	0,56	0,82	0,93	0,73	0,74	0,63
Unknown	Unknown polar (879590422)	1,04	1,78	1,66	1,82	1,1	1,07	1,24	1,13	1,39	1,5	1,5	1,12	1,61	1,66	1,72	0,68	0,76	1,07	1,05	0,7
Unknown	Unknown polar (879590425)	1	0,96	0,96	1,02	0,92	1,37	1,04	1,2	1,22	1,01	1,42	0,97	0,91	1,11	0,87	1,01	0,96	0,96	0,82	0,72

b) over concentration

Unknown	Unknown lipid (849590482)	1,1	0,99	0,94	0,75	1,03	1,02	0,66	0,84	0,86	0,97	0,75	0,59	0,83	0,9	0,59	0,59	0,77	0,94	0,52	0,78
Unknown	Unknown lipid (849590483)				0,65	1,02	1	0,66	0,81	0,95	0,69	0,66	0,54	0,81	0,9	0,56	0,58	0,79	0,92	0,61	1,18
Unknown	Unknown lipid (849590484)	1,01	0,97	0,83	0,73	1	1	0,62	0,8	0,9	0,57	0,63	0,55	0,77	0,5	0,52	0,59	0,71	0,57	0,53	1,11
Unknown	Unknown lipid (849590485)	0,95	0,87	0,83	0,71	0,95		0,64	0,62	0,89	0,62	0,56	0,58	0,85	0,8	0,48	0,53	0,75	0,72	0,52	0,93
Unknown	Unknown lipid (849590486)	1,06	0,91	0,9	0,72	1,02	0,99	0,66	0,78	0,93	0,57	0,66	0,62	0,91	0,89	0,54	0,72	0,87	0,84	0,58	1,33
Unknown	Unknown lipid (849590487)	0,99	0,96	1,1	0,45	1,08	0,98	1,11	0,39	0,94	0,92	0,96	0,51	1,02	0,95	0,48	0,75	0,98	0,85	0,41	0,79
Unknown	Unknown lipid (849590488)	1,04	1	1,59	0,44	0,96	1,09	1,91	0,43	1,05	1,12	1,53	0,31	1,11	1,09	0,59	0,64	1,12	0,95	0,57	0,81
Unknown	Unknown lipid (849590489)	0,88	0,93	1,21	0,43	0,81	0,87	1,38	0,57	0,91	0,89	0,86	0,41	0,96	0,96	0,41	0,74	1	0,85	0,58	1,13
Unknown	Unknown lipid (849590500)	0,92	1,11	0,82	1,31	1,03	0,88	0,95	0,98	1,02	1,14	0,84	1,38	1,02	0,95	0,98	1,45	0,95	0,85	0,98	2,31
Unknown	Unknown lipid (859590013)	0,9	0,98	0,86	1,02	0,97	0,9	0,98	1	1,14	1,13	0,99	1,17	0,95	1,17	1,26	1,31	1,02	1,09	1,75	2,3
Unknown	Unknown lipid (859590071)	0,95	0,91	0,91	1,17	0,94	0,92	1,11	1,01	1,13	0,57	1,21	0,93	0,99	0,9	1,25	0,95	0,81	0,86	1,7	
Unknown	Unknown polar (869590388)	0,95	1,03	1,02	1,19	0,94	1,01	1,09	1	1,14	1,12	1,34	1,02	1,2	1,13	1,07	1,21	1,26	0,93		
Unknown	Unknown polar (869590390)	0,95	1,14	0,99	1,08	0,99	1	1,13	1,11	0,99	1,09	0,89	1,02	0,96	1,01	0,81	0,77	0,71	0,87	0,8	0,84
Unknown	Unknown polar (869590395)	0,88	1,04	0,98	1,28	0,87	0,96	1,27	1,13	0,96	1,14	1,02	1,43	1,09	1,17	1	1,16	1,25	1,47		
Unknown	Unknown polar (869590398)	1,05	1,07	0,96	1	1,04	1,06	0,91	0,57	1,04	1,06	0,76	0,92	1,08	1,06	0,64	0,66	1,2	0,57	0,49	0,79
Unknown	Unknown polar (869590400)	0,71	1,5	0,86	2,43	0,85	0,96	1,67	1,82	1,14	1,84	1,04	2,36	0,87	1,63	1,02	0,96	0,91	1,53	1,25	1,33
Unknown	Unknown polar (869590402)	0,91	0,96	1,01	1,18	0,96	1,03	1,04	1,13	1,04	1,16	1,22	1,24	1,05	1,27	1,13	1,06	1,4	1,28	0,74	0,63
Unknown	Unknown polar (869590406)	0,78	1,38	0,93	2,02	0,86	0,98	1,59	1,53	1,22	1,73	1,12	2,12	1	1,65	1,25	1,12	0,98	1,63	1,69	1,57
Unknown	Unknown polar (869590410)	0,87	1,39	0,96	1,39	0,94	1,08	1,8	0,88	1,21	1,46	1,62	1,26	0,98	1,57	1,47	1,11	0,94	1,6	1,87	1,43
Unknown	Unknown polar (869590417)	0,99	0,7	0,95	1,68	1,09	1,17	2,06	1,32	1,1	0,91	1,34	2,29	1,09	0,69	1,28	0,96	1,1	0,73	1,67	1,57
Unknown	Unknown polar (869590424)	0,71	1,45	0,87	2,28	0,86	0,94	1,63	1,81	1,25	1,75	1,12	2,27	0,94	1,59	0,98	0,97	0,96	1,52	1,34	1,39
Unknown	Unknown polar (869590431)	0,67	1,85	0,84	2,16	0,86	1,17	2,44	1,54	1,31	2,34	1,21	2,1	0,89	2,28	0,89	0,96	1,12	2,05	1,14	1,42
Unknown	Unknown polar (869590432)	0,68	1,31	1,05	1,16	0,8	0,98	0,93	1,22	1,06	1,64	1,44	2,01	0,83	1,46	1,48	1,46	0,84	1,45	1,93	1,91
Unknown	Unknown polar (869590436)	1	1,21	1,01	1,08	1,1	1,21	1,01	0,97	1,2	1,19	0,91	0,76	1,15	1,19	0,71	0,59	1,12	1,03	0,42	0,39
Unknown	Unknown polar (869590442)	1,02	1,11	1,05	1,1	1,07	1,16	1,04	1,08	1,1	1,26	1,55	1,15	1,51	2,03	1,14	1,19	2,18	4,22		
Unknown	Unknown polar (869590444)	1,16	1,19	1,21	1,23	1,31	1,19	0,8	1,16	1,35	1,16	1,05	0,83	1,41	1,16	0,72	0,34	1	0,7	0,22	0,1
Unknown	Unknown polar (869590448)	1,02	1,21	1,12	1,21	1,26	1,16	1,25	1,06	1,12	1,24	0,97	1,01	1,08	1,03	0,74	0,55	0,81	0,72	0,22	0,48
Unknown	Unknown polar (869590452)	0,87	1,51	0,84	1,01	0,94	1,14	1,08	1,07	0,86	1,07	1	1,57	0,86	1,32	1,04	0,84	0,8	1,57	0,83	0,66
Unknown	Unknown polar (869590456)	1,01	1,01	1,06	0,76	1,06	1,05	0,88	0,81	1,02	1,05	1,05	0,83	1,12	1,09	1,06	0,97	1,2	1,37	0,77	0,52
Unknown	Unknown polar (879590076)	1,04	1,01	1,02	0,82	1	0,46	0,93	1	1,02	0,57	1,15	0,93	0,82	0,74	0,94	0,71	0,56	0,63		
Unknown	Unknown polar (879590422)	1,04	1,07	1,5	0,68	1,78	1,24	1,12	0,76	1,66	1,13	1,61	1,07	1,82	1,39	1,66	1,05	1,1	1,5	1,72	0,7
Unknown	Unknown polar (879590425)	1	1,37	1,42	1,01	0,96	1,04	0,97	0,96	0,96	1,2	0,91	0,96	1,02	1,22	1,11	0,82	0,92	1,01	0,87	0,72

Increase	Decrease
p < 0.01	p < 0.01
0.01 ≤ p < 0.05	0.01 ≤ p < 0.05
0.05 ≤ p < 0.10	0.05 ≤ p < 0.10

Chapter 4

Toxicometabolomics studies of a model PPAR α agonist on human pluripotent stem cell-derived liver organoids



Preamble

In the last years, there has been a continued interest in the use of human induced pluripotent stem cells (hiPSC)-derived organoids for fundamental research, elucidation of disease progression, and utility for translational research development. In particular, human *in vitro* derived liver organoids and liver microphysiological systems (MPS) have the potential to guide in a paradigm shift in all aspects of chemical and drug development. Due to the unique role the liver plays in metabolic elimination of xenobiotics, evaluating hepatotoxicity of potential chemicals and drugs is of particular importance. Current toxicology and screening studies often utilize human cell culture models such as HepG2s and/or pre-clinical animal studies but they frequently do not faithfully recapitulate human *in vivo* liver metabolism. The 'gold standard' model utilizing primary human hepatocytes recapitulates human metabolism more accurately but suffers from scarce availability of samples, limited supply from a consistent donor, and a very limited lifespan alongside a high cost. Thus, there is a need for leveraging modern biological multiplexed measurements on improved human derived liver models that better recapitulate human physiology and sensitivity to hepatotoxicants for elucidating drug and chemical toxicology.

In this manuscript, a combined team of academic (Massachusetts institute of technology, MIT) and industry (BASF) scientists developed genetically engineered human induced pluripotent stem cells (hiPSCs) to form 3-dimensional, self-organized liver organoids, characterized them, and utilized them for toxicometabolomic studies.

In order to increase the physiological relevance of metabolomics data, the aim of this work was to test the applicability of the developed hiPSCs liver organoid for studying toxicological Mechanisms of Action (MoA). Specifically, by utilizing the tools and design principles of synthetic biology, scientists from the MIT genetically engineered hiPSC cells by delivering a small synthetic gene network (containing the transcription factor GATA6) into the cells that enabled controlled ectopic expression of a master cell fate regulator, Gata6, in a heterogenous distribution within a 3-D initial spheroid. The initial single population of hiPSCs proliferated and underwent a symmetry breaking operation that resulted in bifurcation into

mesoderm and endoderm lineages that were characterized in this paper via single cell RNA sequencing. This population enabled co-development and 3-D emergence of hepatocytes and non-parenchymal cells including stellate, cholangiocytes, Kupffer and additional haematopoietic cells. The resulting liver organoid after 30 days of maturation produced urea and albumin at physiological equivalent levels when normalized for hepatocyte composition (Ballmer et al. 1990; Rudman et al. 1973). To illustrate the utility of the *in vitro* liver MPS in toxicological studies, the model compound bezafibrate, a well-known PPAR α agonist, was administered, and metabolic and transcriptomic shifts within the organoid model were measured. Analysis of the bezafibrate effects for 48-hours on the organoids produced a metabolome profile of 314 measured metabolites, of which 80% were altered due to treatment. Guided by the metabolome profile analysis, 30 genes that were relevant to the altered metabolite profile were identified and found 21 of these to be changed. The observed metabolic and gene expression changes due to bezafibrate included alterations in the metabolism of lipids, cholesterol, energy, and amino acids. The class of effects are also similar to beta oxidation of fatty acids, in agreement with reported *in vivo* bezafibrate pharmacological effects. These metabolic results are in concordance with those observed in human patient-derived serum. Multi-Omics approaches provide useful insights into the flow of biological information at multiple levels and thus can assist in a more comprehensive understanding of mechanisms underlying toxicological effects (Subramanian et al. 2020). In particular, by leveraging transcriptomics together with metabolomics results, the organoid model elucidates potential mechanism of actions for drug development immediately relevant to human models.

In sum, the development of the 3D hiPSC liver organoid represents a more physiologically relevant system for the administration and elucidation of mechanisms of action for potential hepatotoxicity of chemical entities. Importantly, the utility but also diverse challenges (e.g., reproducibility) of 3-D liver MPS to be incorporated into drug and chemical developmental pipelines were shown. The further development and standardization of liver organoids such as the one presented in this manuscript and more generally 3D *in vitro* MPS will help address the observed differences between pre-clinical and clinical models and human responses. Combining metabolomics and transcriptomics on standardized and well characterized

microphysiological systems will potentially enable studies that establish human toxicity via mechanism of action with improved relevance and higher throughput than animal studies.

The following publication was prepared in cooperation with 12 co-authors. Under a BASF funded collaboration with the Massachusetts institute of technology, MIT, in Boston. Scientist from the MIT conducted the experimental work concerning the development and characterization of the organoids and exposure to the test substance. Frozen substance-treated organoids were delivered to Germany for the metabolomics analysis at BASF Metabolome solutions, Berlin. The author of this dissertation took part in the project management, definition of the study protocols and the overall project planning. In addition, the author analyzed the metabolomics data and wrote the paper (together with MIT). The co-authors were involved in the bioinformatics data analysis, planning of the experiments, scientific discussions, and guidance, and significantly in the review process of the publication.

Publication III: Mechanistic toxicometabolomics studies of a model PPAR α agonist on human pluripotent stem cell-derived liver organoids

Status of the manuscript: first round of revisions submitted to Nature Scientific reports.
Submission ID. SREP-22-01564A.

Authors:

Sabina Ramirez-Hincapie^{1, #}, Deepak Mishra^{2, #}, Barbara Birk¹, Volker Haake³, Michael Herold³, Erez Pery², Jose Vargas-Asencio², Shiva Razavi², Patrick Fortuna², Nevin M. Summers², Rupert Konradi⁴, Bennard van Ravenzwaay^{1, *}, Ron Weiss^{2*}

¹: BASF SE, Experimental Toxicology and Ecology, Ludwigshafen, Germany

²: Synthetic Biology Center, Department of Biological Engineering, Massachusetts Institute of Technology, Cambridge, MA, USA

³: BASF Metabolome Solutions GmbH

⁴: BASF Corporation, Northeast Research Alliance (NORA), Cambridge, USA

#: *These authors contributed equally*

*: *Corresponding authors*

Abstract

Toxicology assessment of drug and chemical developmental pipeline candidates in cell culture models and preclinical animal studies do not faithfully recapitulate human *in vivo* liver metabolism. Human-derived *in vitro* 3-dimensional liver microphysiological systems (MPS) that enable emergent tissue formation of multiple cell types and structural elements may constitute a more physiologically relevant model system. Here, we employ genetically engineered human induced pluripotent stem cells (hiPSCs) to form 3-dimensional, self-organized human liver organoids for conducting toxicometabolomics studies. We characterized the bifurcation of a single population of hiPSCs into mesoderm and endoderm lineages, imaged underlying cell types and structures, and measured urea and albumin production at physiological levels in a day 30 organoid. Next, we administered bezafibrate, a model peroxisome proliferator-activated receptor-alpha (PPAR α) agonist. We analyzed the intracellular concentrations of bezafibrate and a metabolome spectrum of 314 metabolites, of which 80% were altered by treatment. We also measured gene expression changes for 30 genes possibly relevant to the altered metabolites and found 21 of these to be changed. The observed metabolic and gene expression changes within our organoids due to bezafibrate treatment were concentration dependent and included metabolism of lipids, cholesterol, energy, and amino acids as well as beta oxidation of fatty acids, in agreement with reported *in vivo* bezafibrate pharmacological effects. We demonstrated that liver MPS such as ours may serve as a physiologically relevant tool to understand mechanisms of action and evaluate hepatotoxicity of chemical entities. We anticipate that chemical treatment and metabolome analysis of 3D liver MPS will become a valuable tool in assessing toxicology within chemical and pharmaceutical development pipelines.

Introduction

Toxicology, the study of the adverse effects of chemicals or physical agents on living organisms, is a critical process in chemical and drug development. Conventionally, toxicity testing has relied on proxies including immortalized cell lines from humans or animals and successively larger animal models coupled with experimental observational measurements. However, there remains open questions in the concordance between pre-clinical toxicity findings and predictive human toxicity¹⁻⁵. Moreover, intrapopulation variation within humans further confounds pre-clinical toxicity findings⁶. Concurrently, the role of toxicology in maintaining human health and safety in the production of materials for consumers has led to a complex world-wide set of regulatory requirements¹⁻³. A systematic analysis of toxicology integrating current limitations, consumer safety, and regulatory requirements proposed a radical overhaul^{1,2}. This new toxicology system for testing adverse effects of chemicals on humans and the environment relies on technical advances in *in vitro* models and 'omics' technologies^{4,7}.

In *in vivo* toxicology, plasma metabolite profiling has been successfully used for over a decade to identify toxicological mechanisms in rodent studies^{8,9}. At BASF, a large *in vivo* metabolomics database has been established for the identification and prediction of the mode of action of chemicals and pharmaceuticals¹⁰. The advent of omics technologies (genomics, transcriptomics, proteomics and metabolomics) has enabled comprehensive analysis of biological processes in an organism, allowing detailed characterization of pathways of toxicity (PoT) and identification of potential biomarkers for elucidating molecular mechanisms underlying toxicity¹¹⁻¹³. However, *in vivo* animal models have limitations due to the fact that observed metabolic byproducts and identified modes of action are not always predictive for humans⁴. The use of *in vitro* models that augment and eventually replace *in vivo* studies is the next crucial step in toxicometabolomics research.

In vitro models are typically based on human-derived cells and offer the possibility of gaining improved understanding of human-specific mechanisms underlying toxicity and pathways that lead to adverse outcomes¹⁴. As the liver is the major organ for endogenous and xenobiotics metabolism, it has the largest influence on compound induced changes in the metabolome and thus is the main target for toxicity in preclinical and chemical safety studies. Liver toxicity is a major cause of failure in new pharmaceutical development and post-market withdrawal^{6,15}. Failure of drugs during their clinical development due to hepatotoxicity arises

as a result of poor translation of pre-clinical *in vitro* 2-dimensional cell cultures to phased trials¹⁶. Primary human hepatocytes (PHH) in culture are considered the best available model for xenobiotic metabolism and cytotoxicity studies¹⁷. However, scarce availability of fresh human liver samples, lack of consistent supply from the same donor, the limited lifespan, and cost limit their use¹⁸. Thus, the use of immortalized cell lines, such as HepG2, has been of immense utility, offering the advantages of unlimited number of cell divisions, robustness, high reproducibility, simple handling and rapidly availability. Metabolomics approaches have been increasingly used in the assessment of hepatotoxicity *in vitro* with such cell lines^{8,13,19}. For example, we have previously described the development of a LC-MS, GC-MS metabolomics *in vitro* method (MIV) for identifying mode of action of liver toxicants in HepG2 cells²⁰. However, HepG2 is a hepatoma cell line with reduced expression of drug metabolizing enzymes and transporters, lower production of important hepatic markers such as urea and albumin, and limited human metabolic capacity compared to PHH^{21,22}. Moreover, *in vitro* 2-dimensional cultures of PHH or HepG2 comprise static monolayers that lack critical architectural and biomechanical properties of the native tissue and other cell to cell interactions²³. Development of *in vitro* models that can better recapitulate human physiology and sensitivity to hepatotoxicants in combination with -omics technologies offer a powerful system to expand the investigation of organ toxicity^{24,25}.

To overcome the limitations of 2D systems, there has been considerable advancement in human microphysiological systems (MPS). These systems expand beyond traditional 2D sandwich cultures and usually include multi-cellular environments incorporated within a biopolymer or tissue-derived matrix, 3D structure, media flow, and/or use of primary or stem cell derived cells^{6,26}. Organoids, 3D multicellular *in vitro* stem-cell-derived constructs that mimic *in vivo* tissue are one type of MPS. Development of organoids across many organ types including heart, kidney, gut, brain, and liver has fostered a paradigm shift in elucidating human development and disease²⁷⁻³¹. Typically, organoids rely on sequential administration and orchestration of external factors and cues to human-induced pluripotent stem cells (hiPSC) cultures and may include multi-culture growth and assembly. However, these batch approaches suffer from challenges in spatial-temporal guidance of multilineage differentiation as well as optimal media formulations that support diverse cell types^{32,33}. Utilizing tools of synthetic biology, cellular differentiation and organoid production has been

significantly improved by introduction of synthetic gene networks into engineered hiPSCs^{34,35}. These engineered iPSC lines enable controllable but non-uniform cell-type specific expression of cell fate regulators to achieve symmetry breaking that guides development of diverse cell types, to create emergent architectural features, and increase cellular maturation^{34–38}. Previously, we engineered 2D hiPSC-derived self-organized liver tissues via heterogeneous overexpression of transcription factor GATA6³⁷. These emergent liver tissues comprise a variety of co-developed cell types including hepatocytes, endothelial, cholangiocytes, Kupffer, hepatic stellate, and additional haematopoietic cells arranged in liver bud-like and vascular structures.

In this paper, we extended our 2D hiPSC-derived liver tissues into 3D organoids and assessed if they could serve as an *in vitro* model system for metabolomics-based assessment and mechanistic investigation of hepatotoxicity. Optimization and investigation of hiPSC-Gata6 differentiation in 3D revealed formation of vascularized liver organoids comprising ~70% hepatocytes as well as endothelial, stellate, Kupffer, cholangiocytes, and additional cell types within 30-days. These organoids are capable of urea and albumin production comparable to adult human physiological levels. To test our 3D liver organoid as a suitable *in vitro* model system for metabolomics-based toxicological studies, we introduce the hypolipidemic agent bezafibrate, a United States Federal Drug Administration (FDA) approved compound. An important reason for choosing to study bezafibrate is the difference between observed effects in animal models and those observed in patients. In particular, bezafibrate administration to rodents results in a marked proliferation of hepatic peroxisomes via the activation of the peroxisome proliferator-activated receptor alpha (PPAR α)³⁹ and if exposed chronically, leads to PPAR α -induced liver hyperplasia and hepatocarcinoma^{40,41}. In patients following bezafibrate dosing, PPAR α activation is observed but peroxisome proliferation is marginal and liver diseases have not been observed^{42,43}. The extensively characterized mode of action, the interspecies differences in the toxicological profiles and the high expression levels of PPAR α in the human liver made bezafibrate a good candidate to test our system.

In the work presented in this paper, we identified multiple metabolic pathways sensitive to bezafibrate treatment and recapitulated bezafibrate's expected mode of action within the Gata6 liver organoid using a combination of transcriptomics and metabolomics. Within our metabolome spectrum of 314 metabolites, 80% were altered by treatment, particularly

within pathways involved in lipid metabolism, energy, and amino acid synthesis. A qPCR screen of 30 genes relevant to the altered metabolites revealed that 21 of these were either up- or down- regulated within our organoids. Our studies set forth the utility of engineered hiPSC-derived liver organoids as an *in vitro* model for further toxicological studies.

Results

Formation and characterization of 3D self-organized liver organoids from engineered hiPSC-Gata6 cell populations

The hiPSC-Gata6 line was engineered by integration of a small gene network delivered by lentivirus³⁷. The network enables administration of doxycycline (Dox) to control ectopic expression of Gata6-encoding transgenes. Due to the heterogeneity of lentiviral transduction, cells receive different copy numbers of the gene network and exhibit a wide range of GATA6 protein expression levels in response to the same level of Dox. It has been shown that heterogeneity of GATA6 expression enables co-development of multiple liver-associated cell types^{37,38}. The polyclonal population of hiPSC-Gata6 cells is induced with Dox for 5 days in pluripotency supporting medium before removal of Dox and subsequent culturing in basal medium (Fig. 1A).

To generate 3D organoids, we utilized Corning ultra-low attachment U-bottom 96-well plates with a single organoid seeded per well. To determine the optimal seeding density of hiPSC-Gata6 cells at day zero required to form and proliferate as spheroids initially, we varied the number of starting cells across two orders of magnitude ranging from 468 to 30,000 cells and monitored organoid growth via brightfield microscopy until day 33 (Supplemental Fig. 1). We concurrently assayed urea and albumin production at day 25 and day 26 respectively to evaluate differentiation and development of hepatocytes within our organoids (Supplemental Fig. 2). We found that seeding 15,000 iPSC-Gata6 cells per well at day zero produced spherical organoids that were viable at day 30, not physically constrained within a well, and produced urea and albumin at physiologically relevant levels. For organoids seeded with fewer cells, organoid growth was slower or in some cases stalled yielding lower production of urea and albumin. For all subsequent iPSC-Gata6 organoid experiments, 15,000 cells were seeded at day zero.

To elucidate differentiation trajectories and establishment of cell lineages necessary for co-development of hepatocytes, endothelial cells, and other liver associated cell types within 3D organoids, we performed single cell RNA sequencing (scRNAseq) (Fig. 1B). Organoids were grown for nine days, and single-cell suspensions of developing organoids were generated at days 0, 3, 5, and 8 days for scRNAseq. Processing of scRNA-seq data is described in full within the methods and follows standard analysis techniques⁴⁴⁻⁴⁷. Briefly, the entire data set was filtered and normalized with highly-variable genes extracted before downstream dimension reduction (UMAP) and Leiden clustering. Examination of enriched genes within each cluster enabled identification of intermediate differentiated cell lineages. Further identification of intermediate populations and cell-types were enabled by comparing gene expression in observed clusters to a hepatic cell atlas⁴⁸. Analysis of our scRNAseq results revealed cellular clusters corresponding to two primary lineage trajectories, the first from iPSCs to endoderm and downstream cell types and the second from iPSCs to mesoderm and downstream cell types (Supplemental Fig. 3). In the former case, we observed developmental states for fetal hepatocytes that differentiated from hiPSC (NANOG+) to primitive endoderm (GATA6+ SOX17+) to hepatic lineages (HNF4a+). In the latter case, we observed development of endothelial and non-parenchymal liver cells that differentiated from hiPSC (NANOG+) to mesoendoderm (TBXT+) to endoderm (HAND+) to hemangioblasts (COL3A1).

To understand emergence of structural elements arising from co-development and co-differentiation of hepatic-progenitor cells, endothelial-progenitor cells, and other non-parenchymal cell populations, we seeded iPSC-Gata6 wells and performed immunostaining of endothelial-progenitor cells (CD34+) and hepatic-progenitor cells (HNF4+) within organoids at days 5, 8, and 30 followed by analysis via confocal microscopy. Development of initial endothelial-progenitor and hepatic-progenitor populations in days 5-8 were observed in concurrence with the scRNAseq datasets. Moreover, by day 30, formation of CD34+ emergent tube-like structures were observed throughout the hepatocyte clusters and organoid (Fig. 1C, Supplemental Fig. 4, Supplemental Movies 1-2).

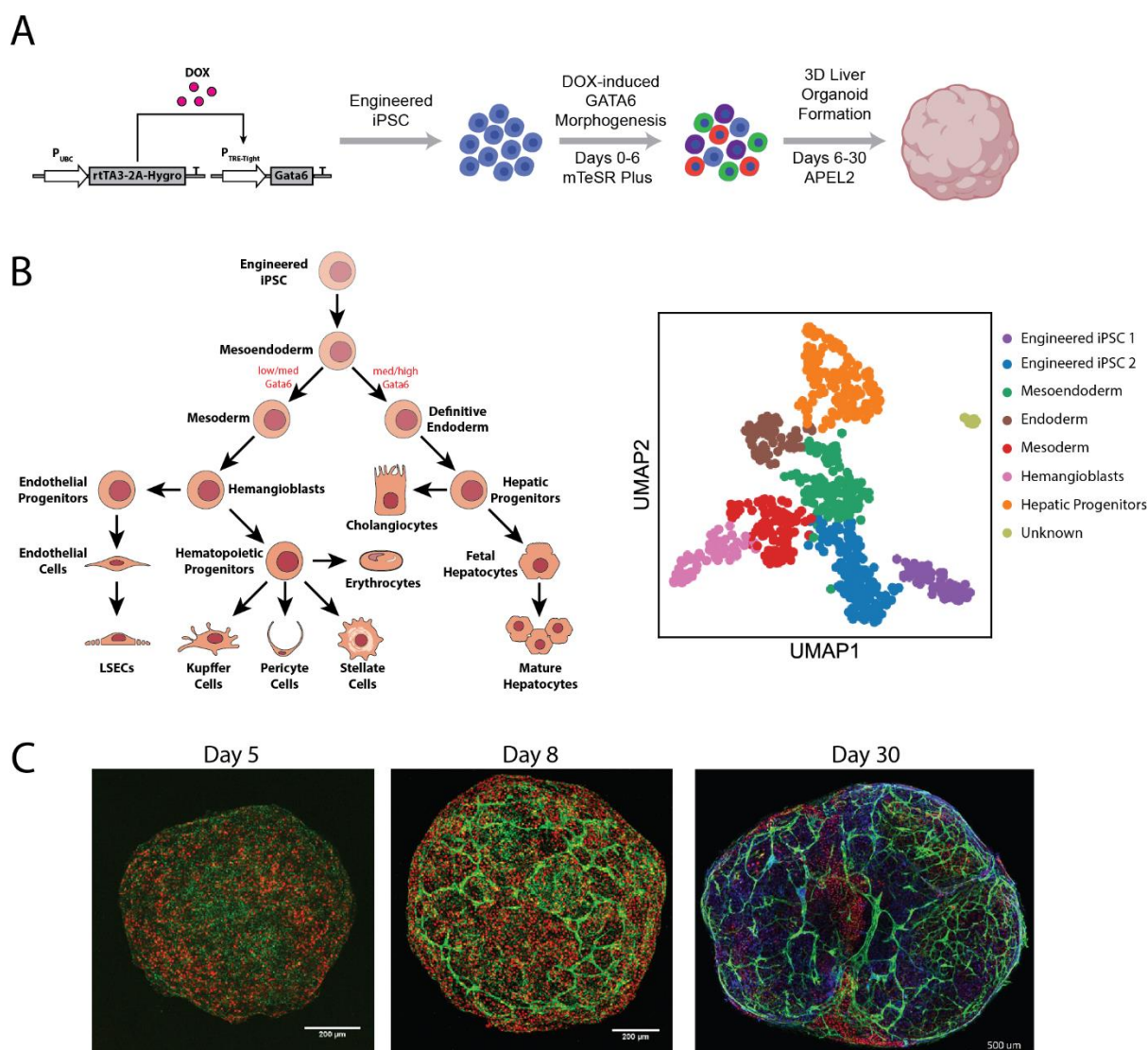


Figure 13. hiPSC-Gata6 liver organoid development. A) Genetic network encoding doxycycline (DOX) inducible Gata6 delivered into iPSC via lentivirus infection to form hiPSC-Gata6 cell line. hiPSC-Gata6 are seeded at 15,000 cells/well and grown in pluripotent media with DOX for 5 days prior to transfer to APEL2 media. B) Schematic of cell fates generated via ectopic Gata6 expression (left) and corresponding populations identified with scRNAseq of dissociated organoids (right). C) Immunostaining micrographs of hiPSC-Gata6 liver organoids. At Day 5 and 8, endothelial cells stained for CD34 (green) and hepatic cells for HNF4a (red) from a single confocal slice. Day 30 is a 3D projection of several confocal slices and also includes staining for cell nuclei using DAPI (blue).

To further probe cellular composition of organoids, we performed immunostaining of intact organoids (Supplemental Fig. 5) as well as dissociated representative organoids into single-cell suspensions, performed immunostaining, and analyzed the cells via flow cytometry. Within our 3D day 30 organoids, approximately 80% of all cells identified within our liver organoids were reflective of the three most common cell types found in healthy adult human livers: hepatocytes (HNF4+), Stellate cells (Desmin+), and endothelial cells (CD34+) (Fig. 2A)⁴⁹.

These population ratios developed temporally as individual cells underwent differentiation and proliferation (Supplemental Fig. 6). Our prior studies within 2-dimensional liver organoids identified additional cell-types present (e.g., Kupffer cells, cholangiocytes)³⁷ and comprehensive follow-up studies are underway on these 3D organoids.

As a proxy for hepatocyte activity, we non-destructively measured urea production at days 14, 19, 21, 25, and 30 and albumin production at days 15 and 30 for intact organoids (Figs. 2B, 2C). These measurements revealed that at day 30, organoids comprised on average 73,000 total cells of which 68% were hepatocytes capable of producing urea and albumin levels of 65 and 50 micrograms/day/ 10^6 hepatocytes respectively, levels comparable to those found in healthy adult livers (56-159 μg urea/ 10^6 hepatocytes/day and 37-105 μg albumin/ 10^6 hepatocytes/day)^{50,51}. Furthermore, we further characterized intact day 30 liver organoids with respect to alpha-1-fetoprotein expression, bulk RNA qPCR, and cytochrome P450 activity to gauge hepatocyte maturation (Supplemental Figs. 7-9). The 3D liver organoids do have a pulse of AFP expression comparable to that seen in human development and microsomes generated from intact liver organoids have cytochrome P450 enzymatic turnovers comparable to commercially sourced microsomes. Examining differences in gene expression and elucidating subtle differences in compound bioavailability for intact organoids and microsomes as well as a comparison of adult liver development mapping (20 years) to 3D organoid developmental time (30 days) represent avenues for additional follow-up studies.

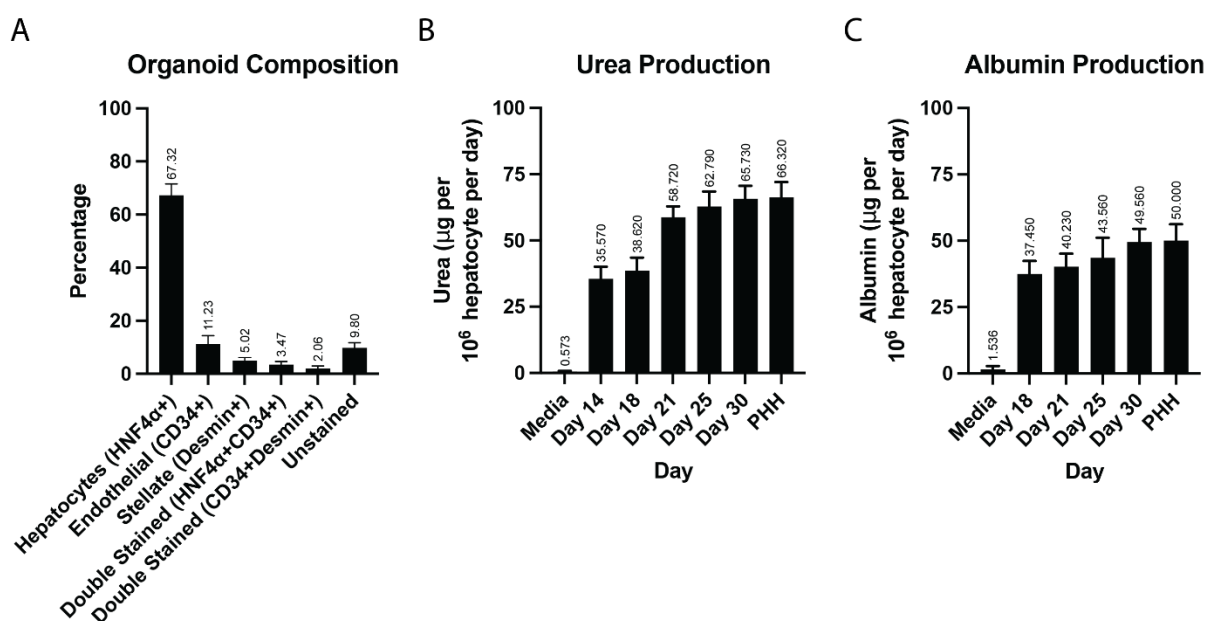


Figure 2. Composition and hepatocyte function of Day 30 organoids. a) Immunostaining of dissociated organoids for cellular composition. b-c) Hepatocyte function measured within whole organoids by proxy of urea and albumin production. b) Urea production measured via BioAssay Systems QuantiChrom Urea Assay Kit. c) Albumin production measured via Bethyl Albumin ELISA Kit. For a, n=6 biological replicates and error bars represent standard deviation. For b and c, n=8 biological replicates and error bars represent standard deviation.

Determination of appropriate bezafibrate dosage on hiPSC-Gata6 organoids

Following characterization of the 3D hiPSC-Gata6 organoids, we sought to employ our organoids in toxicometabolomic studies utilizing bezafibrate, a model agonist of PPAR α . Bezafibrate was administered from 0 to 2.0 millimolar final concentration in dimethyl sulfoxide (DMSO) to day 28 organoids for 48 hours before measuring cytotoxicity and viability of the bulk organoid. In particular, we sought to select a bezafibrate dosage that has a strong effect, but also has both minimal cytotoxicity and less than a 10% reduction of viability due to treatment (Fig. 3). We observed a viability of 93.5% and cytotoxicity of 2.6% for 0.5 mM bezafibrate dosing and utilized this concentration for all subsequent experiments.

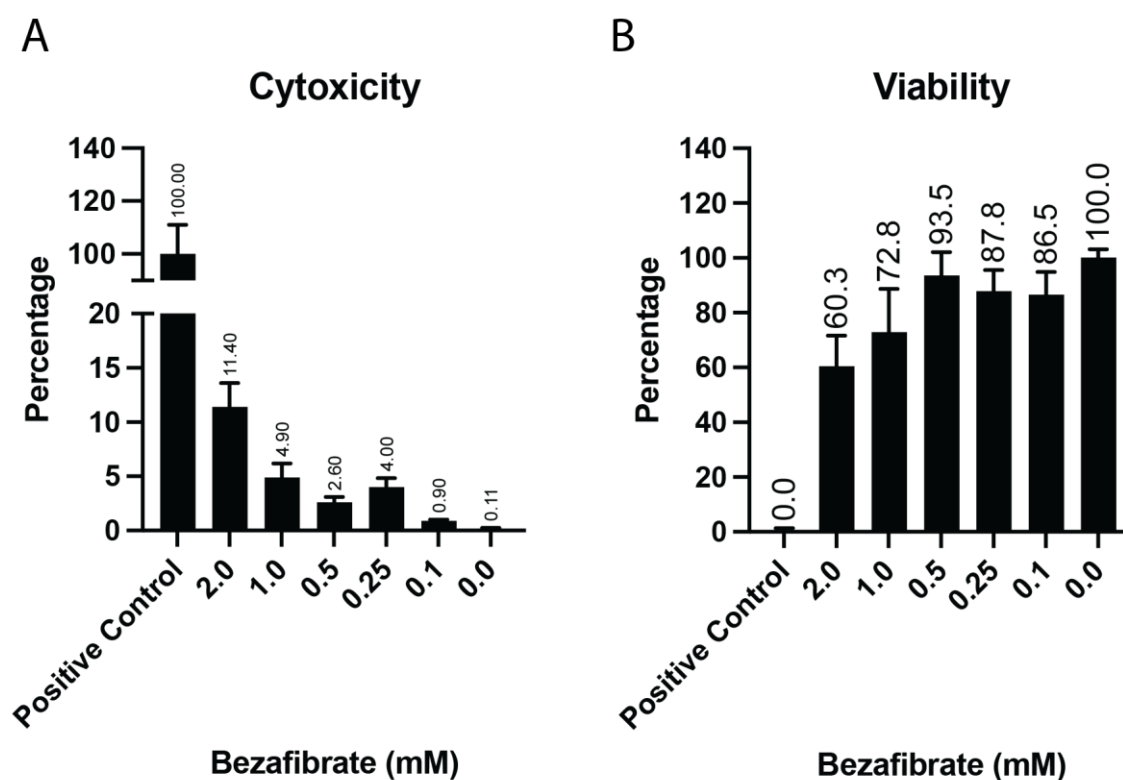


Figure 3. Cytotoxicity testing for dose selection. a) Cytotoxicity assay (CellTox Green) measured on whole organoids. b) Cell viability assay (CellTiter-Glo) measured on whole organoids. For a and b, n=6 biological replicates and error bars represent standard deviation.

Metabolomic measurement and analysis for bezafibrate treatment of 3D hiPSC-Gata6 organoids

To perform toxicometabolomics studies on our liver organoids, day 28 organoids were treated with 0.5mM bezafibrate in 0.5% DMSO in APEL2 media or with 0.5% DMSO in APEL2 media as a negative control for 48 hours with a media refresh at 24 hours. Organoids were subsequently harvested. An organoid subset was dissociated and immunostained for composition as previously described, a second subset of organoids were processed for bulk RNA extraction, and the remainder weighed and flash frozen as described in detail within the methods. For bezafibrate treated versus untreated organoids, total number and composition of cells within a single organoid did not change and flow cytometry characteristics related to size including forward, and side-scatter also did not change (data not shown). A slight increase in weights for treated versus untreated groups was observed (Supplemental Table. 5). Further investigation is needed to deduce the exact mechanism of this weight increase (e.g.,

hypertrophy, hyperplasia, increase of extracellular space). Hepatomegaly reflects a classical response to fibrates treatment in rodents, however, this effect appears not to occur upon bezafibrate administration in humans^{52,53}.

Following shipment of frozen organoids, intracellular metabolites were extracted for semiquantitative targeted metabolite profiling via LC-MS/MS. The entire analysis covered 2 separate mass spectrometry batched runs with a total of 192 organoids. Each batch comprised 60 untreated (controls) and 36 treated organoids. Organoids were pooled into groups of 6 to satisfy the minimum biomass needed for metabolomics analysis resulting in 10 control pools and 6 treated pool per batch. One treated pool from the first batch and 3 treated pools of the second batch did not pass the instrument-level data quality control process and were excluded from the analysis.

To confirm and quantify substance uptake by the organoids, the intracellular concentrations of bezafibrate were determined via mass-spectrometry. The results indicated the presence of bezafibrate in the organoids with concentrations of $2.20 \mu\text{g} \pm 0.13$ in batch 1 and $12.88 \mu\text{g} \pm 1.88$ in batch 2. These values indicate that although the same nominal concentration was applied, there was approximately a 6-fold difference in the intracellular bezafibrate concentrations between the two batches. Based on intracellular compound concentrations, experimental treatment pools are referred hereafter as low (LC) and high (HC) concentration.

The principal component analysis (PCA) of the metabolic profiles showed a clear treatment effect. This was evidenced by separation of the untreated and bezafibrate-treated organoids correlating with the first principal component, accounting for 63% of the variability. Noteworthy, the strength of the treatment effect on the metabolome correlated with the intracellular concentrations of bezafibrate. The magnitude of the distance between the controls and each data point along PC1 reflects increased bezafibrate levels. Metabolic profiles corresponding to the LC group were closer to the controls than metabolic profiles of the HC group, evidencing a concentration response effect based on intracellular compound levels. A minor inter-experiment variability was observed in the second principal component (explaining 11% of the total variance) (Fig. 4). In addition to the treatment compound, a total of 314 unique analytes were measured of which 217 were annotated and 97 remained

unknown. The full metabolite profile can be found in the supplementary section (Supplementary Table 12).

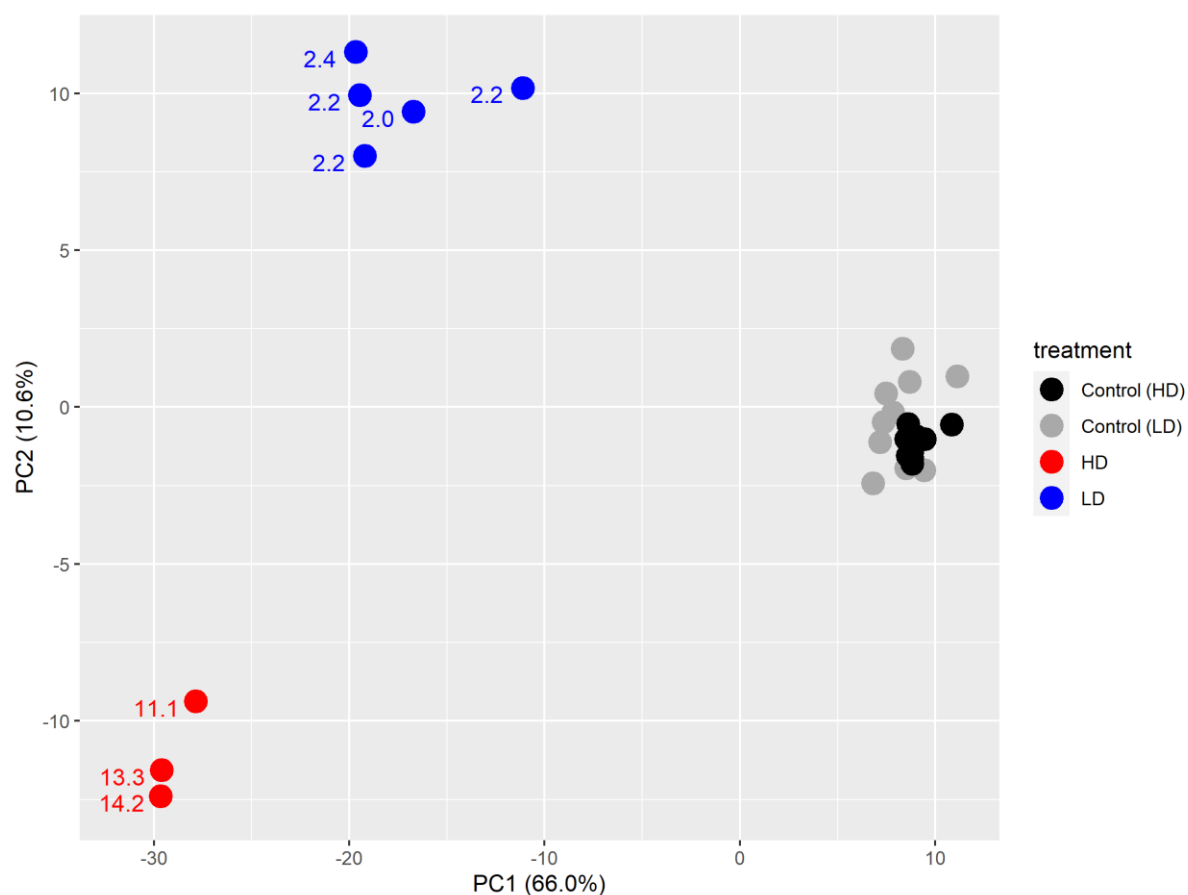


Figure 4. PCA analysis of the metabolic profiles of bezafibrate treated 3D hiPSC-Gata6 organoids. The organoids were treated for 48h with bezafibrate at 500 μ M. The analysis is based on log₁₀-transformed metabolite ratios. Each point represents a sample of 6 pooled organoids. Two independent batches were analyzed. The numbers in the squares represent the measured intracellular bezafibrate concentration per sample. LC; low intracellular bezafibrate concentrations HC; high bezafibrate concentrations.

Transcriptomics and metabolomics analysis of bezafibrate treated organoids reveal PPAR α -associated pathway activation

Bezafibrate is a well-known PPAR α agonist widely used as a hypolipidemic agent to lower serum triglycerides and cholesterol levels⁵⁴. PPAR α acts as a central regulator of hepatic lipid metabolism, modulating the transcription of fatty acid transporters and fatty acid β -oxidation enzymes^{55,56}. More recently, it has been demonstrated that PPAR α also influences glucose, lipoprotein, cholesterol and amino acid metabolism and plays a role in inflammation and cellular redox state⁵⁷. Bezafibrate treatment for 48 hours on day 28 hiPSC-Gata6 organoids

showed transcriptome (Fig. 5) and metabolome (Table 1, Supplementary Tables 4-12) effects on both PPAR α and the main known PPAR α associated signalling pathways (Fig. 6). Importantly, these effects exhibited a concentration response behaviour correlated with the detected intracellular bezafibrate levels; both, transcriptome and metabolome changes were more pronounced in the HC group.

Table 3. Enrichment analysis of significantly altered metabolites by ontology class after bezafibrate treatment. The distribution of the 314 metabolites across the ontology classes is provided in the column “measured metabolites”. The number of metabolite changes are shown for each metabolite ontology class). All metabolite classes except for “miscellaneous” exhibited a significant enrichment in the ontology class (p -value<0.05). LC; low intracellular bezafibrate concentrations HC; high bezafibrate concentrations.

Ontology name	Measured metabolites	LC		HC	
		Altered metabolites	% Altered metabolites	Altered metabolites	% Altered metabolites
Vitamins, cofactors and related	18	14	77.8	12	66.7
Acylglycerols	24	19	79.2	20	83.3
Amino acids	14	12	85.7	14	100.0
Amino acids related	15	11	73.3	15	100.0
Carbohydrates and related	3	3	100.0	3	100.0
Cholesterol and related	14	13	92.9	11	78.6
Energy metabolism and related	13	7	53.9	7	53.85
Glycerophospholipids	34	33	97.1	31	91.2
Lysoglycerophospholipids	29	23	79.3	19	65.5
Miscellaneous	2	2	100.0	2	100.0
Nucleobases and related	7	7	100.0	7	100.0
Signal substances and related	4	2	50.0	3	75.0
Sphingolipids	40	37	92.5	37	92.5
Unknown	97	70	72.2	77	79.38
Total	314	253	80.6	258	82.17

Following treatment with bezafibrate, we observed increased expression of the PPAR α gene (Fig. 5). In the LC group the PPAR α gene was 1.25-fold upregulated and in the HC group it was 2.35-fold upregulated (**). Next, we investigated downstream signalling pathways implicated

in PPAR α activation starting with lipid metabolism. Briefly, after treatment, a general decrease of triglycerides (TGs) together with an increase in the expression of Lipoprotein lipase (LPL) gene, which encodes for the enzyme that Hydrolyzes TGs was observed. Bezafibrate treated organoids also exhibited increased concentrations and increase gene expression of metabolites and enzymes belonging to fatty acid shuttling, β -oxidation and Acetyl-CoA synthesis pathways. Different sphingolipids were also affected after treatment; a general increase in sphingomyelins was observed while the levels of ceramides decreased significantly. At the transcriptome level, an upregulation of gene expression of different enzymes involved in sphingolipid synthesis was detected. Additionally, glycerophospholipids such as various phosphatidylcholines and phosphatidylethanolamines were generally downregulated in comparison to controls.

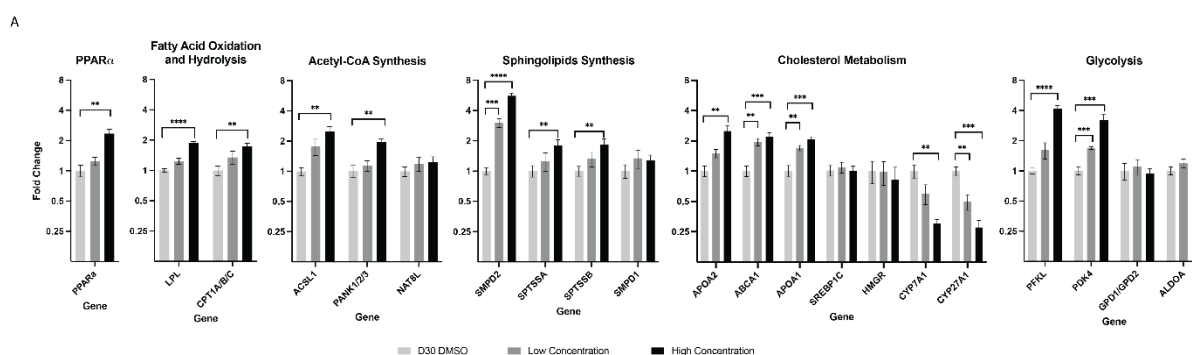


Figure 5. qPCR Transcriptomics of hiPSC-Gata6 organoids following dosage. a) Relative gene expression was calculated via modified Pfaffl equation using mean of 7 housekeeping genes for denominator and using efficiency as 2 for all samples. Fold-change calculated for treated organoids versus untreated organoids. For DMSO treatment, n = 6 biological replicates and for bezafibrate treatments, n = 3 biological replicates. Error bars represent standard deviation. Running an unpaired t-tests between untreated organoids and each treatment independently for genes yielded p-values. Low concentration: SMPD2:0.000335 ***, ABCA1:0.001232 **, APOA1:0.001979 **, CYP27A1:0.002412 **, PDK4:0.000319 ***. High concentration: PPAR α :0.001106 **, LPL:0.000030 ****, CPT1A/B/C:0.001292 **, ACSL1:0.001145 **, PANK1/2/3:0.001065 **, SMPD2:0.000032 ****, SPTSSA:0.009239 **, SPTSSB:0.00781 **, APOA2:0.001492 **, ABCA1:0.000717 ***, APOA1:0.000521 ***, CYP7A1:0.001152 **, CYP27A1:0.000288 ****, PFKL:0.000069 ****, PDK4:0.000971 ***.

Metabolites associated with cholesterol metabolism were also highly affected after exposure to bezafibrate with a profound increase in the levels of cholesteryl esters. qPCR analysis showed an upregulation of the expression of apolipoproteins (APO1, APO2) and Cholesterol Efflux Regulatory protein (ABCA1) and a downregulation of 3-hydroxy-3-methylglutaryl-

coenzyme (HMGCR) gene. No significant changes were observed in the expression of the sterol regulatory element binding proteins (SREBPs) gene. Increased concentrations of metabolites of the bile acid metabolism were detected together with decrease expression of CYP7A1 and CYP27 which are two key enzymes of bile acid synthesis. Energy metabolism was also altered by bezafibrate treatment, resulting in elevated levels of glucose and carbohydrates in treated organoids as well as glycolysis intermediates. At transcriptome level, gene expression of glycolytic enzymes such as phosphofructokinase (PFK), aldolase (ALDO) and pyruvate dehydrogenase kinase isoform 4 (PDK4) was upregulated. Furthermore, our results indicated a general increase in the levels of amino acids and a decrease in the concentration of antioxidants molecules.

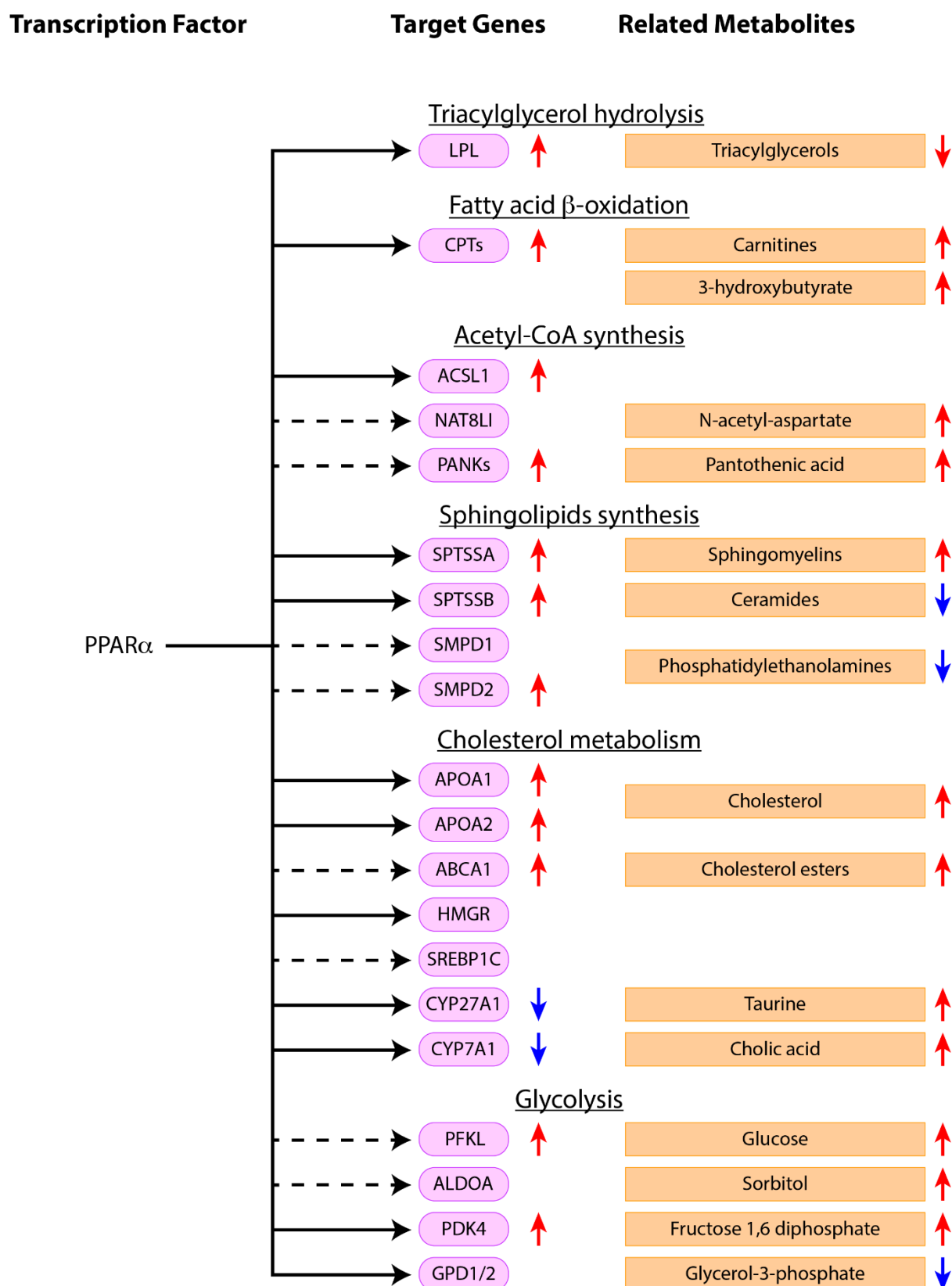


Figure 6. Overview of altered PPAR α target genes and related metabolites upon bezafibrate exposure of hiPSC-Gata6 organoids. qPCR and metabolomics analysis were performed after 48h Bezafibrate treatment. Solid black lines indicate direct PPAR α target genes and dashed black lines indicate indirect PPAR α targets. Red arrows indicate upregulation and blue arrows indicate downregulation following bezafibrate treatment.

Discussion

PPAR α acts as a central regulator of lipid metabolism, modulating transcription of fatty acid transporters and fatty acid β -oxidation enzymes⁵⁵. After bezafibrate exposure, our transcriptomic and metabolomic analysis revealed clear intracellular concentration-response changes in pathways spanning lipid metabolism, beta oxidation of fatty acids, cholesterol metabolism, energy metabolism, amino acids and antioxidants. Critically, the present work demonstrates the importance of determining intracellular concentration of the test substance as a good *in vitro* practice⁵⁸. Although we applied the same nominal concentrations of bezafibrate in the experimental batches, the intracellular compound concentrations were markedly different, deviating by approximately 6-fold (Fig. 4). The differences in intracellular organoid compound concentration correlated extraordinarily well, in a dose-response manner, with the observed biological response reflected in the magnitude of the metabolite's changes. This highlights a major and unique advantage of metabolomics, specifically the ability to measure both the biological response and the intracellular concentration of the test substance in the same sample at the same time.

Our findings demonstrate that bezafibrate activates the PPAR α pathways within our liver organoids (Fig. 6) particularly for the HC group. Moreover, the biochemical consequences of this activation correlate very well with the findings of our metabolome investigation (Fig. 5, Table 1). Overall, our results provide clear evidence that the 3D liver organoid system, in combination with transcriptomics and metabolomics, is capable of detecting human relevant changes associated with the mode of action of the reference compound. In this respect, our metabolome is in concordance with metabolic datasets collected from HepG2 cells, rat plasma, and human plasma following bezafibrate administration in some classes of metabolites^{10,20,43}. Additional studies are needed to elucidate differences and similarities in exact chemical species among HepG2, rat, and human plasma compared to our hiPSC liver MPS alongside a suitable method for comparing disparate sources of data. Moreover, inclusion of transcriptomics of the genes tested here in HepG2, rat, and human specimens will bolster effective comparisons. In the discussion that follows the altered pathways are analyzed in the context of PPAR α activation.

The expression of genes involved in mitochondrial and extramitochondrial **fatty acid oxidation** is largely regulated by PPAR α activity⁵⁵. PPAR α is one of the key transcription factors taking part in regulation of ketone body metabolism⁶¹. PPAR α knockout mice fail to activate hepatic fatty acid oxidation and ketogenesis during fasting, indicating that PPAR α activation is necessary for initiating the ketogenic transcriptional program⁶². Analysis of the metabolome revealed higher levels of carnitines and derivatives (O-acetylcarnitine and propionylcarnitine) in both low (LC) and high bezafibrate concentrations groups (HC) (Supplemental Table 4), indicating higher mobilization of fatty acids. Carnitine helps mobilize long-chain fatty acids into the mitochondria via the carnitine shuttle. Fatty acids are first conjugated to carnitine by carnitine-palmitoyl transferase I (CPT1), a direct target of PPAR α , that catalyzes the first and rate-limiting step of the carnitine shuttle pathway^{56,59,60}. After treatment, increased levels of the ketone body 3-hydroxybutyrate were observed as well in both groups (Supplemental Table 4). After bezafibrate treatment, transcriptomics analysis showed 1.35 and 1.74-fold (***) upregulation of carnitine-palmitoyl transferase 1 (CPT1A/B/C) genes in the LC and HC groups respectively, a finding corroborating metabolic measurements.

PPAR α activation enhances hepatic fatty acid transport and catabolism inducing **triacylglycerol hydrolysis** by upregulation of lipoprotein lipase (LPL), leading to reduction of serum and liver triglyceride levels⁵³. In this study we observed LPL expression in the LC/HC batches to be 1.24 and 1.88-fold (****) upregulated respectively. Consistent with our data and the *in vivo* pharmacological effect of bezafibrate, the metabolome experiments revealed a significant decrease in triglycerides concentrations in both LC and HC groups (Supplemental Table 4).

At the metabolome level, treated organoids showed tremendously high concentrations of the Acetyl-CoA derivatives N-Acetyl-Aspartate (NAA) and pantothenic acid (Supplemental Table. 4) implicating an **Acetyl-CoA metabolism** response. In agreement with metabolic analysis, several genes that code for **Acetyl-CoA metabolism**-related enzymes were upregulated: Acyl-CoA synthetase (ACSL1) (1.76 and 2.48-fold (**)) respectively for LC and HC), N-acetyl aspartate synthetase (NAT8L) (1.18 and 1.24-fold respectively for LC and HC) and Pantothenate Kinases (PANK1/2/3) (1.13 and 1.96-fold (**)) respectively for LC and HC). NAA has been shown to participate as an acetyl-CoA donor for lipid biosynthesis in the liver⁶³. Pantothenic acid is an essential nutrient required to synthesize Coenzyme A (CoA). Of note,

an increase of pantothenic acid is a classical observation in metabolic patterns of rodents treated with PPAR α agonists⁶⁴. Together, these results suggest that excess acetyl-CoA caused directly by upregulation of ACS and indirectly by high rates of fatty acid oxidation in the organoids resulted in increased synthesis of acetyl-coA precursors.

PPAR α activation is involved in regulation of the first and rate limiting step in **sphingolipid biosynthesis** within the liver by directly increasing gene expression of palmitoyltransferase (SPT) as well as regulating palmitoyl-CoA levels^{55,65}. At the transcriptional level, we observed up-regulation of both SPT gene subunits A and B (SPTSSA and SPTSSB). For SPTSSA, 1.25 and 1.79-fold (***) respectively for LC and HC and for SPTSSB, 1.32 and 1.82-fold (**) respectively for LC and HC. In addition to de novo synthesis, ceramides are also generated by hydrolysis of sphingomyelin by the action of two sphingomyelinase (SMase) enzymes, SMPD1 and SMPD2. For the LC group we detected a 1.34-fold upregulation of SMPD1 and a 3.01-fold (***) upregulation of SMPD2. In the HC group, the upregulation for SMPD1 was 1.28-fold and for SMPD2 was 5.60-fold (****). These transcriptional measurements contrast with the decreased metabolic measurements of ceramides found after bezafibrate treatment (Supplemental Table 5) suggesting that there are different mechanisms/enzymes involved in ceramides generation which are negatively affected by PPAR α activation. Two different types of sphingomyelinases (neutral and lipid) have been described⁶⁶. The precise cellular function of each of these SMases in sphingomyelin turnover is not yet well understood. Previous studies have indicated that PPAR α activation interferes negatively with the neutral SMase pathway in primary Human Macrophages⁶⁷. Interestingly, PPAR activation inhibited the activity of neutral sphingomyelinase and increased the activity of acid sphingomyelinase in the myocardium of mice treated with a PPAR alpha agonist⁶⁸. This results points towards a differential regulation of the SMases by PPAR α which might be a possible explanation to our observations.

Additionally, phosphatidylcholine (PC) and phosphatidylethanolamine (PE) levels were also significantly altered after bezafibrate treatment (Supplemental Tables 6, 7). PC and PE are the most abundant phospholipids in mammalian cell membranes. The role of phospholipids in regulating lipid and energy metabolism has been widely demonstrated⁶⁹. It has been reported that PPAR α is required to maintain phospholipid homeostasis during energy deprivation⁷⁰.

However, the exact mechanism of PPAR α regulation in different classes of phospholipids is not well understood and informs future studies.

The liver is the principal site for maintenance of **cholesterol** homeostasis. Growing evidence indicates a key role of PPAR α in the regulation of cholesterol synthesis and bile acid metabolism⁷¹⁻⁷³. Highly increased concentrations of intracellular cholesteryl esters together with higher levels of free cholesterol were found in the bezafibrate treated organoids (Supplemental Table 8). To determine the cause, we examined genes within pathways for cholesterol synthesis, incorporation, and export. We measured 3-hydroxy-3-methylglutaryl-coenzyme (HMGR), the rate limiting enzyme in de novo cholesterol synthesis as well as sterol regulatory element binding proteins (SREBPs), genes involved in regulating cholesterol metabolism. Treatment resulted in no significant changes in expression in LC and HC groups. The cholesterol pool obtained from de novo synthesis in hepatocytes can be esterified to cholesteryl esters and incorporated into lipoproteins, which are then secreted into the bloodstream for transport⁷⁴. The two most abundant proteins of the high-density lipoprotein particles (HDL) are apolipoprotein A-1 (APOA1) and apolipoprotein A-II (APOA2) and they attach to cell membranes and promote excretion of cholesterol. Once outside the cell, cholesterol binds to apolipoproteins to form HDL. We observed a 1.70 and 2.07-fold upregulation respectively for LC and HC groups in apolipoprotein A-I (APOA1) and a 1.50 and 2.50-fold upregulation respectively for LC and HC groups in apolipoprotein A-II (APOA2). Subsequently, we measured expression of the gene that codes for Cholesterol Efflux Regulatory protein (ABCA1), a primary exporter within the cellular lipid removal pathway. Bezafibrate treatment yielded a 1.95 and 2.22-fold upregulation of ABCA1 in LC and HC groups respectively.

Together, the analysis shows that neither expression of genes involved in cholesterol synthesis increased nor did expression of apolipoproteins and cholesterol transport protein decline. Therefore, it is possible that activation of PPAR α by bezafibrate treatment led to an accumulation of cholesterol and cholesteryl esters in our organoids. Then, due to a lack of a fully mature bile duct and vascular system, these metabolites could not be excreted and consequently accumulated in the organoids as cholesteryl esters, resulting in highly increased concentrations of these metabolites detected after bezafibrate treatment. Another avenue congruent with our liver organoids being excrement limited is that bezafibrate and fibrates

have been reported to reduce bile acid synthesis, a major pathway of cholesterol elimination. In agreement with previous studies⁷³, PPAR α activation in our organoids resulted in downregulation of the mRNA levels of two important enzymes of bile acid synthesis: cholesterol 7 α hydroxylase (CYP7A1) (1.7-fold in low concentration, 3.33-fold (**)) in high concentration), the rate limiting step, and Sterol 27-Hydroxylase (CYP27) (2.0-fold (**)) in low concentration, 3.62-fold (***) in high concentration). Higher levels of taurine were observed after treatment, potentially reflecting an accumulation of this amino acid caused by reduced synthesis of primary bile acids in the bezafibrate treated organoids (Supplemental Table. 8).

PPAR α activation has been shown to directly alter **glycolysis** and glucose utilization in the liver through production of pyruvate dehydrogenase kinase isoform 4 (PDK4)⁷⁵. Pdk4 inactivates pyruvate dehydrogenase, limiting carbon flux through glycolysis⁷⁶. At the metabolome level, higher concentrations of glucose and sorbitol suggest lower carbohydrate utilization. Increased metabolic levels of fructose 1,6 diphosphate were also observed. Following bezafibrate treatment, gene expression levels of phosphofructokinase (PFK) and PDK4, enzymes that participate in **glycolysis**, were upregulated by 3.83-fold and 2.94-fold respectively. While expression of Glycerol-3-Phosphate Dehydrogenase (GPD1/2) was minimally downregulated in treated organoids, concentrations of glycerol-3-phosphate appeared lower (Supplemental Table. 9). GPD1/2 serves as a major link between carbohydrate metabolism and lipid metabolism by participating in the conversion of glycerol to glucose.

Besides its role in lipid metabolism, PPAR α influences expression of different genes implicated in **amino acid metabolism**^{77,78}. In our study, concentrations of 86% (LC group) and 100% (HC group) of all measured amino acids (AA) were significantly increased after bezafibrate treatment (Supplemental Table 10). These results are in line with previous evidence of higher plasma and hepatic AA levels in rodents treated with PPAR α agonists⁷⁹. It has been shown that PPAR α activation suppresses expression of numerous genes participating in AA catabolism, leading to an overall decrease in amino acid degradation. These observations are supported by evidence of enhanced AA catabolism in PPAR α -null mice. Impaired β -oxidation leads to a compensatory increase in amino acid catabolism and urea synthesis in liver of PPAR α -null mice, but not in their wild-type counterparts⁸⁰. In order to preserve body proteins and maintain nitrogen balance, PPAR α regulates protein metabolic homeostasis by down

regulating liver amino acid catabolism and utilizing fatty acids as the main energy source⁷⁸. After PPAR α induction through bezafibrate, the overall elevated AA levels in our 3D hiPSC-Gata6 organoids suggest an AA accumulation possibly resulting from a reduction of their breakdown rates. Quantifying expression levels of proteins responsible for AA breakdown represent future studies to test this hypothesis.

The metabolomics analysis revealed lower levels of alpha- and gamma-Tocopherol (vitamin E isoforms), beta-carotene, glutathione (GSH) and Coenzymes Q7, Q9 and Q10 (Supplemental Table 11). Since redox activity is a fundamental part of **oxidative metabolism**, changes in PPAR α signaling lead to alterations of the cellular redox state⁸¹. These changes suggest a higher utilization of antioxidant molecules in bezafibrate treated organoids. These observations might not be transcriptionally directly connected to PPAR α activation but rather reflect the physiological response to increased lipid oxidation in order to counteract oxidative stress and maintain redox balance.

Conclusion

Nearly a quarter of the 21st century has passed and still society relies largely on animal studies for regulatory decision making. This indicates that new approaches to the “toxicology in the 21st century” goal set out by the US national academy of sciences is needed. We believe that this requires an approach which includes the incorporation of new biological techniques and more predictive models that bridge animal to human pre-clinical information alongside an overhaul of regulatory requirements 1.2⁷. One emerging technology in evaluating chemical toxicity is the incorporation of *in vitro* MPS models combined with biological -omic measurements to establish mechanism of action. Here, we presented a method for building 3-dimensional multicellular liver organoids from engineered human induced pluripotent stem cells. Our organoids support emergence of a diversity of cell types found in the liver, structural self-assembly of vasculature and other elements, and functionally produce physiologically relevant levels of albumin and urea. Following administration to our organoids of bezafibrate, a model FDA-approved compound that acts as a PPAR α agonist, we were able to measure altered metabolomic and transcriptomic profiles. The altered metabolites fell broadly into classes that are consistent with bezafibrate acting as a PPAR α agonist. Analysis via qPCR of pathways that were considered responsible for the change in metabolic profile enabled more

comprehensive understanding of bezafibrate treatment within the 3D organoid and elucidated areas where results within rodent, cellular, and patient samples could be reconciled.

Importantly, although the same nominal concentrations of bezafibrate were applied in the two experimental batches, the intracellular compound concentrations were markedly different, a phenomenon similar to those seen in patient-to-patient variability. The observed biological responses directly correlated to the magnitude of the metabolites fold changes. The metabolic response to bezafibrate was qualitative comparable in the two batches with common altered metabolites in the same direction (up- or down- regulated). However, the magnitude of the fold changes in the high concentration group (HC), which exhibited about a 6-fold higher intracellular bezafibrate concentration in comparison with the low concentration group, were notably higher. The reasons of this differences in concentrations are not clear and require further examination. It evidences, however, the importance of measuring the intracellular concentrations of the test compounds in *in vitro* assays and highlights a major advantage of integrating metabolomics technologies in *in vitro* studies.

Integrated systems and methods such as ours and more generally 3D *in vitro* MPS will help address the observed differences between pre-clinical and clinical models and human deployment. Incorporation of metabolomics and transcriptomics on MPS will enable studies that establish human toxicity via mechanism of action at a lower cost and higher throughput than animal studies. The *in vitro* model presented here provides an in depth understanding of human relevant pathways in toxicology and is a potential game changes to achieve the goals of toxicology in the 21st century, i.e. reducing animal use, while providing human relevant data for risk assessment.

Alongside the progress we have demonstrated here utilizing liver MPS for toxicology, there are additional opportunities for liver MPS in chemical and pharmaceutical development. Further studies may map extracellular to intracellular concentration profiles in vitro to clinically relevant in vivo concentrations needed for drug effects. Moreover, development of varying 3D MPS by utilizing iPSCs differing in age, sex, race, disease-state, and other factors may enable study of variation in chemical toxicology across a range of organs within the human population. Advanced 3D MPS systems may include burgeoning technologies such as

gene editing, trans-gene expression, or even viral infection to reflect disease aspects of a target patient population that may change the liver – for example, drug susceptibility interaction that impacts safety and toxicity profiles. The usage of liver MPS as well as other organ MPS will become invaluable tools in assessing toxicology, mode of action, and dosing for candidates in chemical and pharmaceutical development pipelines.

Materials and Methods:

Cell culture

The PGP1 hiPSCs were a kind gift from George Church (Harvard University, USA) and can be obtained from Coriell (NJ, USA). The hiPSC-GATA6 model was generated as previously described in Guye et al, 2016. hiPSC-GATA6 cells were cultivated under sterile conditions in mTeSR Plus (Stem Cell Technologies, Vancouver) changed daily in a humidified incubator at 37C and 5% CO₂. Tissue culture plates were coated for 1 hour at room temperature with BD ES-qualified Matrigel (BD Biosciences) diluted according to the manufacturer's instructions in ice cold DMEM/F-12 with 15mM HEPES medium (Stem Cell Technologies, Vancouver). Routine passaging was performed by incubating hiPSC colonies for 5 minutes in Accutase (Sigma) at 37C, collecting the suspension and adding 5mL DMEM/F-12 medium containing 10 micromolar Y-27632 (Tocris Biosciences, UK) solubilized in cell-grade DMSO (Sigma-Aldrich), centrifuging at 500 rpm for 3 minutes and resuspended in mTeSR Plus supplemented with 10 micromolar Y-27632 for counting.

Organoid culture

For differentiation experiments, hiPSC-GATA6 cells were seeded at 15,000 cells (unless noted) in mTeSR Plus supplemented with 10 micromolar Y-27632 and 1000 ng/mL doxycycline (Sigma-Aldrich) solubilized in cell-grade DMSO into a 96-well ultra-low attachment round-bottom plate (Corning, Corning, NY, USA) and centrifuged at 300 x *g* for 5 minutes at room temperature before incubation at 37°C supplemented with 5% CO₂. At 16 hours, the medium was changed to mTeSR Plus supplemented with 1000 ng/mL doxycycline and replaced daily

for 5 days. Subsequently, a non-pluripotency supporting medium, APEL2, (Stem Cell Technologies, Vancouver) was used to grow the cells and replaced daily from day 5 to day 10, every two days from day 10 to day 20, and every three days from day 20 to day 30. APEL2 contains human serum albumin. Therefore, when assaying for human albumin, organoids were switched to daily feedings with William's medium E prior to sampling for measurement.

Urea measurement, albumin and AFP Enzyme-linked Immunosorbent Assays (ELISA)

A colorimetric urea assay (Cell Biolabs, San Diego, CA, USA) was performed according to the manufacturer's instructions. The cell supernatant was assessed at multiple dilutions to optimize detection. Samples were assayed for human albumin via commercially available ELISA kits (Bethyl Labs, Montgomery, TX, USA) according to manufacturer's instruction. Sample dilutions were optimized to attain detection in the linear range of the standard curves for each individual assay.

Organoid Harvest for Downstream Dissociation into Single Cells for scRNAseq or Immunostaining

Plates containing organoids were centrifuged at 200 x *g* for 10 seconds. Media was disregarded and organoids were washed with 100 microliters of 1x PBS (Sigma-Aldrich) followed by 200 x *g* for 10 second centrifugation twice and supernatant discarded.

For dissociation of organoids into single cells for staining, these organoids were incubated in 50 microliters 2.5% trypsin (Corning) supplemented with 10 mM EDTA (Sigma-Aldrich) for 2 minutes. Well contents were transferred to 1.7 mL tubes and 500 microliters PBS was added to tubes and centrifuged at 300 x *g* for 4 minutes. Supernatant was aspirated and 50 microliters of Collagenase 4 (STEMCELL Technologies) was added prior to suspension being mechanically agitated by 15 strokes with a P-1000 and 15 strokes with a P-200. Suspension was incubated for 10 minutes prior to mechanical agitation by 30 strokes with a P-200. 750 microliters PBS was added prior to centrifugation at 300 x *g* for 4 minutes. Supernatant was aspirated and cells were resuspended in 50 microliters before being passed through a 40-

micron strainer into a 2.0 mL tube. Cells were washed with 200 microliter PBS and centrifuged at 300 x *g* for 4 minutes with supernatant discarded before counting.

Cell suspension Immunofluorescence

Single cells were fixed in 100uL 4% fixation Buffer (BioLegend, USA) for 5 minutes prior to repeating 200 microliter PBS and centrifugation as before. Cells within tubes were blocked and permeabilized in 100 microliters of 10% normal donkey serum (Abcam, USA) and 0.1% Triton X-100 in PBS (block/perm buffer) for 30 minutes at room temperature. Primary antibodies were diluted 1:500 in block/perm buffer and incubated for 30 minutes at room temperature prior to centrifugation and supernatant discarded. Cells were washed with 3 rounds PBS with incubation for 2 minutes and centrifugation with supernatant discarded. Secondary antibodies were diluted 1:500 in block/perm buffer and incubated for 30 minutes at room temperature prior to centrifugation and supernatant discarded. Cells were washed for 3 rounds as previously described before passed through a 40-micron strainer and flow cytometry using a BD LSRFortessa Custom (BD Biosciences).

Whole-organoid Immunofluorescence

Individual organoids were fixed within well for 20 minutes in 200 microliters 4% fixation buffer (BioLegend, USA) at room temperature with 5rpm gentle orbital shaking to prevent adhesion to plate. Wells were then washed three times with 200 microliters of 1x PBS followed by 20 minutes of incubation with 0.2% Triton X-100 in PBS. Subsequently, the wells were washed three times in 250 microliters PBS for 5 minutes prior to blocking with 250 microliters of 4% normal donkey serum (Abcam, USA) in PBS. Incubation with primary antibodies were performed for 1 hour at room temperature in 4% normal donkey serum in PBS followed by three washes in 250 microliters PBS for 5 minutes. Primary antibodies were anti-HNF4-alpha (ab41898 Abcam, USA), anti-desmin (ab32362 Abcam, USA), anti-CEBPA (af7094 R&D, USA), anti-CD31 (3528 and 77699 Cell Signaling Technologies, USA), and anti-CD34 (ab81289 Abcam, USA). Incubation of secondary antibodies (all appropriate anti-goat/rabbit/mouse

and AlexaFluor choices from Thermo Fisher Scientific, USA) were performed for 1 hour at room temperature in 4% normal donkey serum in PBS followed by three washes in 250 microliters PBS for 5 minutes. Organoids were transferred to 4% normal donkey serum blocked glass bottomed 96-well plates containing 200uL PBS. Confocal images were taken using a Leica TCS SP5 II 405UV confocal microscope (Leica Microsystems, Bannockburn, IL).

Bezafibrate Administration to Organoids

Bezafibrate (Sigma-Aldrich) was solubilized in 100% cell-grade DMSO (Sigma-Aldrich) to make a 100mM stock, followed by a 1:10 dilution into APEL2 media to form a 10mM working solution in 10% DMSO, followed by a 1:20 dilution into APEL2 media to form a 0.5mM solution in 0.5% DMSO and APEL2 for administration. Bezafibrate media solutions were made fresh daily and administered on day 28 and refreshed on day 29 prior to organoid harvest on Day 30. For applications other than 0.5mM in 0.5% DMSO, working solutions were made by changing stock solution formulation and 200-fold dilution to maintain 0.5% DMSO.

Cytotoxicity testing

Bezafibrate media solutions at indicated concentrations were applied to day 28 iPSC-Gata6 organoids and refreshed on day 29. Cellular toxicity and cellular viability were measured via commercially available fluorescent cytotoxicity (CellTox Green) and luminescent cell viability (CellTiter-Glo) kits (Promega Corporation, Madison, Wisconsin, USA).

Organoid Harvest for Metabolomics analysis

Plates containing organoids were centrifuged at 200 x *g* for 10 seconds. 100 microliters of supernatant per well was collected and the remainder discarded. Organoids were washed with 100 microliters of freshly prepared 0.9% NaCl (w/v) (Sigma-Aldrich) in autoclaved sterile water pre-heated to 37°C. Organoids were centrifuged at 200 x *g* for 10 seconds and supernatant discarded. This wash was repeated once more before being fully aspirated. Organoids were transferred to pre-weighed 1.7mL Safe-Lock tubes (Eppendorf) in 6-organoid

pools unless otherwise stated in the main text and weighed again. Open tubes were flash frozen in liquid nitrogen, placed on dry-ice for approximately 1 minute, and then closed before storage and dispatch at -80°C from MIT to BASF Metabolome solutions GmbH in Berlin.

Metabolite profiling

Mass spectrometry-based metabolite profiling was performed according to a standardized protocol described below.

Organoid samples were subjected to a freeze-drying process before extraction. The product temperature and the vapor pressure at the beginning of the freeze-drying process were -40°C and 0.120 mbar respectively changing to +30°C and 0.01 mbar during the total run-time of 42 h. Each sample was extracted as a whole with 240 µL of 80% isopropanol containing internal standards. Samples were processed, after addition of one 3 mm stainless steel ball to each sample, with a ball mill (Bead Ruptor Biolab, 3 cycles of 30 sec. each at 3.1 m/s). After centrifugation (13000 rpm, 10min at 20°C), 50 µL of each sample were transferred into an analysis vial, diluted with 200 µL of the extraction solution and mixed after closing the vials. 100 µL of each sample were transferred into a new vial for analysis.

2,5 µl of the extract were injected each for reversed-phase and hydrophilic interaction liquid chromatography (ZIC-HILIC, 2.1 x 10mm, 3.5 µm, Supelco) followed by MS/MS detection (AB Sciex QTrap 6500+) using the positive and negative ionization mode. For reverse-phase high performance liquid chromatography (RP-HPLC, Ascentis Express C18, 5cm x 2.1mm, 2,7µm Supelco), gradient elution was performed with mobile phase A, water/methanol/0.1 M ammonium formate (1:1:0.02, w/w), and B, methyl-tert-butylether/2-propanol/methanol/0.1M ammonium formate/formic acid (4:2:1:0.07:0.035, w/w) (linear gradients, 0 min 100% A, 0.5 min 75% A, 5.9 min 10% A, 600 µl/min). HILIC gradient elution was performed with mobile phase C, acetonitrile/water (99:1, v/v) with 0.2% (v) acetic acid, and D, 7 mM ammonium acetate with 0.2% (v) acetic acid (linear gradients, 0 min 100% C, 5 min 10% C, 600 µl/min).

When a metabolite failed in our internal quality control (linearity, variability, and pool contribution thresholds) for a particular group, data for the corresponding group and metabolite were excluded (For detailed information refer to Viant *et al*, 2019⁸²). This resulted in a few missing values in the dataset. In broad metabolite profiling, large numbers of metabolites are measured. They are characterized by their polarity (lipid vs polar), mass-charge-ratio (m/z ratio) and retention time in the chromatographic system used. While the combination of these parameters enables reproducible evaluation of metabolites, the exact chemical identity of a peak is not always known since the obtained mass typically leaves several options. To clearly confirm the identity of a metabolite, it was spiked in samples during method development. As many metabolites are not commercially available, fragmentation patterns and library matching were used to determine the most likely identity of those metabolites. The corresponding metabolites were then marked as “plausible”. There are still several metabolites remaining for which the available information was insufficient to provide a clear call on metabolite identity. In these cases, the metabolites were listed as “unknown” together with the phase they were found in as well as the analyte-identifier for differentiation of different unknowns.

All of the samples were analyzed at once in a randomized analytical sequence design to avoid artificial results with respect to analytical shifts. Data were normalized to the median of reference samples which were derived from a pool formed from aliquots of untreated samples to account for inter- and intra-instrumental variation if more than one analysis batch are compared.

For the measuring of bezafibrate intracellular concentrations, one calibration per analysis batch was included by spiking pooled extracts from organoids without bezafibrate treatment prior to analysis with bezafibrate amounts representing 0.96, 4.8, 19.2, 144 and 480 ng per sample from 6 organoids. Larger amounts have been extrapolated up to 3 μg per 6 organoids sample. The calculated bezafibrate concentrations were normalized to cell numbers using within sample metabolite median (see section below “Metabolome data analysis”).

Metabolomics data analysis

Pooled reference samples derived from aliquots of all separate dedicated control samples were measured in parallel throughout the entire analytical process. Data were normalized against the median in the pool reference samples to give pool-normalized ratios (performed for each sample per metabolite). This compensated for inter- and intra-instrumental variation. To correct for differences in cell numbers within and between different treatment groups, the data were also normalized to the within sample median, as described in detail by Ramirez *et al*, 2018²⁰. For the intracellular metabolomic analysis of the organoids used here, the median of each sample was calculated across all the 314 measured metabolites.

To generate metabolic profiles for the different treatments, the heteroscedastic t-test (Welch test) was applied to the log-transformed normalized (see above) metabolite data to compare treated groups with their respective controls. Results from these analyses were visualized in colored tables. The red-blue tables show the fold-change per metabolite and treatment group compared to the control. Here, the cell color and shading, as well as the font color, in the table cell indicates the direction and significance (p-value category) of change.

The entire study covered 2 separate experimental runs with a total of 30 biological samples. The first run had 10 controls and 6 bezafibrate samples, the second 10 controls and 4 bezafibrate samples (2 bezafibrate samples did not pass the quality control). The binomial distribution enrichment analysis was performed using Excel. For this purpose, the number of significant changes (*s*) at $p\text{-value} < 0.05$ were counted per treatment and ontology class. The binomial distribution test is used to indicate the probability of a specific number of successes (here the number of significant changes) occurring from a specific number *x* of independent evaluations (here *x* metabolites in the given ontology class). The resulting p-value for this enrichment is indicated (as category) by cell color in the tables (grey, light yellow or intense yellow).

The p-values, t-values and ratios of corresponding group medians versus controls were collected as the metabolic profiles.

The Principal Component Analysis (PCA) analysis was performed using RStudio Version 1.4.1103 (RStudio Team (2020). RStudio: Integrated Development for R. RStudio, PBC, Boston,

MA URL <http://www.rstudio.com/>). Input data for PCA were log₁₀-transformed. Analysis was conducted using the `ropls` package (Thevenot2015) with the default settings.

RNA Extraction and qRT-PCR

Frozen organoids were thawed in lysis buffer. RNA extractions were performed using commercially available Monarch RNA extraction and purification kits (New England Biolabs, Ipswich, MA, USA) according to manufacturer's instructions for whole tissue assays. cDNA was synthesized using ProtoScript II First Strand cDNA Kits (New England Biolabs). qRT-PCR was performed using PrimeTime qPCR Probes (Integrated DNA Technologies, Coralville, IA, USA) and PrimeTime Gene Expression Master Mix (Integrated DNA Technologies) with probes used in Supplemental Table 1. Relative gene expression was calculated via modified Pfaffl equation using arithmetic mean of 7-housekeeping genes (HPRT1, B2m, GUSB, ACTB, POLR2A, RPLP0, PPIA), an efficiency of 2.0, and reported as fold-change between treated samples and untreated controls.

scRNAseq

Liver organoids were made into single cell suspensions as described above. Suspensions were washed in PBS supplemented in 0.04% BSA twice before live cell counting performed. Cell suspensions were produced to 1000 cells / microliter and provided to the MIT BioMicroCenter for SeqWell-based single cell barcoding⁸³. cDNA library was prepared by MIT BioMicroCenter staff and sequenced using an Illumina NextSeq500. Read processing was performed as described in Gierahn *et al*, 2017. Reads were aligned using STAR⁸⁴ to a synthetic genome composed of reference genome GRCh38.84 plus a synthetic chromosome that included the GATA6 inducible system (Fig. 1A)³⁷. Standard scanpy-based workflows were used to filter cells based on mitochondrial RNA content, gene and read counts and to perform normalization, scaling, and clustering of the cells⁸⁵. A detailed Python workflow is available as part of the supplemental code.

References:

1. Hartung, T. Toxicology for the twenty-first century. *Nat.* 2009 4607252 **460**, 208–212 (2009).
2. Krewski, D. *et al.* Toxicity testing in the 21st century: a vision and a strategy. *J. Toxicol. Environ. Health. B. Crit. Rev.* **13**, 51–138 (2010).
3. Adeleye, Y. *et al.* Implementing Toxicity Testing in the 21st Century (TT21C): Making safety decisions using toxicity pathways, and progress in a prototype risk assessment. *Toxicology* **332**, 102–111 (2015).
4. Hartung, T. Perspectives on In Vitro to In Vivo Extrapolations. *Appl. Vitro. Toxicol.* **4**, 305–316 (2018).
5. Olson, H. *et al.* Concordance of the toxicity of pharmaceuticals in humans and in animals. *Regul. Toxicol. Pharmacol.* **32**, 56–67 (2000).
6. Baudy, A. R. *et al.* Liver microphysiological systems development guidelines for safety risk assessment in the pharmaceutical industry. *Lab Chip* **20**, 215–225 (2020).
7. Tralau, T. *et al.* Regulatory toxicology in the twenty-first century: challenges, perspectives and possible solutions. *Arch. Toxicol.* 2015 896 **89**, 823–850 (2015).
8. Mattes, W. *et al.* Detection of hepatotoxicity potential with metabolite profiling (metabolomics) of rat plasma. **230**, 467–478 (2014).
9. van Ravenzwaay, B. *et al.* The sensitivity of metabolomics versus classical regulatory toxicology from a NOAEL perspective. *Toxicol. Lett.* **227**, 20–28 (2014).
10. Kamp, H. *et al.* Application of in vivo metabolomics to preclinical/toxicological studies: case study on phenytoin-induced systemic toxicity. <http://dx.doi.org/10.4155/bio.12.214> **4**, 2291–2301 (2012).
11. Brockmeier, E. K. *et al.* The Role of Omics in the Application of Adverse Outcome Pathways for Chemical Risk Assessment. *Toxicol. Sci.* **158**, 252–262 (2017).
12. van Ravenzwaay, B. *et al.* The use of metabolomics for the discovery of new biomarkers of effect. *Toxicol. Lett.* **172**, 21–28 (2007).
13. García-Cañaveras, J. C., Castell, J. V., Donato, M. T. & Lahoz, A. A metabolomics cell-based approach for anticipating and investigating drug-induced liver injury. *Sci. Rep.* **6**, (2016).
14. Vinken, M. The adverse outcome pathway concept: a pragmatic tool in toxicology. *Toxicology* **312**, 158–165 (2013).
15. Onakpoya, I. J., Heneghan, C. J. & Aronson, J. K. Post-marketing withdrawal of 462 medicinal products because of adverse drug reactions: a systematic review of the world literature. *BMC Med.* **14**, (2016).
16. Waring, M. J. *et al.* An analysis of the attrition of drug candidates from four major pharmaceutical companies. *Nat. Rev. Drug Discov.* 2015 147 **14**, 475–486 (2015).
17. Guillouzo, A. *et al.* The human hepatoma HepaRG cells: a highly differentiated model for studies of liver metabolism and toxicity of xenobiotics. *Chem. Biol. Interact.* **168**, 66–73 (2007).
18. Gerets, H. H. J. *et al.* Characterization of primary human hepatocytes, HepG2 cells, and HepaRG cells at the mRNA level and CYP activity in response to inducers and their predictivity for the detection of human hepatotoxins. *Cell Biol. Toxicol.* **28**, 69 (2012).
19. Yong, H. Y. *et al.* Early detection of metabolic changes in drug-induced steatosis using metabolomics approaches. *RSC Adv.* **10**, 41047–41057 (2020).
20. Ramirez, T. *et al.* Prediction of liver toxicity and mode of action using metabolomics in

- in vitro in HepG2 cells. *Arch. Toxicol.* **92**, 893–906 (2018).
21. Guo, L. *et al.* Similarities and differences in the expression of drug-metabolizing enzymes between human hepatic cell lines and primary human hepatocytes. *Drug Metab. Dispos.* **39**, 528–38 (2011).
 22. Kammerer, S. & Küpper, J.-H. Human hepatocyte systems for in vitro toxicology analysis. *J. Cell. Biotechnol.* **3**, 85–93 (2018).
 23. Langhans, S. A. Three-Dimensional in Vitro Cell Culture Models in Drug Discovery and Drug Repositioning. *Front. Pharmacol.* **9**, 6 (2018).
 24. Birk, B. *et al.* Use of in vitro metabolomics in NRK cells to help predicting nephrotoxicity and differentiating the MoA of nephrotoxicants. *Toxicol. Lett.* **353**, 43–59 (2021).
 25. Kohonen, P. *et al.* A transcriptomics data-driven gene space accurately predicts liver cytopathology and drug-induced liver injury. *Nat. Commun.* **2017 81 8**, 1–15 (2017).
 26. Underhill, G. H. & Khetani, S. R. Bioengineered Liver Models for Drug Testing and Cell Differentiation Studies. *Cell. Mol. Gastroenterol. Hepatol.* **5**, 426 (2018).
 27. Clevers, H. Modeling Development and Disease with Organoids. *Cell* **165**, 1586–1597 (2016).
 28. King, S. M. *et al.* 3D Proximal Tubule Tissues Recapitulate Key Aspects of Renal Physiology to Enable Nephrotoxicity Testing. *Front. Physiol.* **8**, (2017).
 29. Plummer, S. *et al.* A Human iPSC-derived 3D platform using primary brain cancer cells to study drug development and personalized medicine. *Sci. Rep.* **9**, (2019).
 30. Richards, D. J. *et al.* Human cardiac organoids for the modelling of myocardial infarction and drug cardiotoxicity. *Nat. Biomed. Eng.* **4**, 446–462 (2020).
 31. Shinozawa, T. *et al.* High-Fidelity Drug-Induced Liver Injury Screen Using Human Pluripotent Stem Cell-Derived Organoids. *Gastroenterology* **160**, 831–846 (2021).
 32. de Souza, N. Organoids. *Nat. Methods* **15**, 23–23 (2018).
 33. Aydin, O. *et al.* Principles for the design of multicellular engineered living systems. *APL Bioeng.* **6**, 010903 (2022).
 34. Ho, C. & Morsut, L. Novel synthetic biology approaches for developmental systems. *Stem Cell Reports* **16**, 1051 (2021).
 35. Teague, B. P., Guye, P. & Weiss, R. Synthetic Morphogenesis. *Cold Spring Harb. Perspect. Biol.* **8**, (2016).
 36. Skylar-Scott, M. A. *et al.* Biomanufacturing of organ-specific tissues with high cellular density and embedded vascular channels. *Sci. Adv.* **5**, (2019).
 37. Guye, P. *et al.* Genetically engineering self-organization of human pluripotent stem cells into a liver bud-like tissue using Gata6. *Nat. Commun.* **2016 71 7**, 1–12 (2016).
 38. Velazquez, J. J. *et al.* Gene Regulatory Network Analysis and Engineering Directs Development and Vascularization of Multilineage Human Liver Organoids. *Cell Syst.* **12**, 41-55.e11 (2021).
 39. Issemann, I. & Green, S. Activation of a member of the steroid hormone receptor superfamily by peroxisome proliferators. *Nat.* **1990 3476294 347**, 645–650 (1990).
 40. Hays, T. *et al.* Role of peroxisome proliferator-activated receptor-alpha (PPARalpha) in bezafibrate-induced hepatocarcinogenesis and cholestasis. *Carcinogenesis* **26**, 219–227 (2005).
 41. Reddy, J. K., Azarnoff, D. L. & Hignite, C. E. Hypolipidaemic hepatic peroxisome proliferators form a novel class of chemical carcinogens. *Nat.* **1980 2835745 283**, 397–398 (1980).

42. Hoivik, D. J. *et al.* Fibrates induce hepatic peroxisome and mitochondrial proliferation without overt evidence of cellular proliferation and oxidative stress in cynomolgus monkeys. *Carcinogenesis* **25**, 1757–1769 (2004).
43. Takafumi, W. *et al.* Species differences in the effects of bezafibrate, a hypolipidemic agent, on hepatic peroxisome-associated enzymes. *Biochem. Pharmacol.* **38**, 367–371 (1989).
44. Hie, B. *et al.* Computational Methods for Single-Cell RNA Sequencing. *Annu. Rev. Biomed. Data Sci.* **27** (2020) doi:10.1146/annurev-biodatasci-012220.
45. Wolf, F. A., Angerer, P. & Theis, F. J. SCANPY: Large-scale single-cell gene expression data analysis. *Genome Biol.* **19**, 1–5 (2018).
46. McInnes, L., Healy, J. & Melville, J. UMAP: Uniform Manifold Approximation and Projection for Dimension Reduction. (2018) doi:10.48550/arxiv.1802.03426.
47. Traag, V. A., Waltman, L. & van Eck, N. J. From Louvain to Leiden: guaranteeing well-connected communities. *Sci. Reports* **9**, 1–12 (2019).
48. Guilliams, M. *et al.* Spatial proteogenomics reveals distinct and evolutionarily conserved hepatic macrophage niches. *Cell* **185**, 379-396.e38 (2022).
49. Ding, C. *et al.* A Cell-type-resolved Liver Proteome. *Mol. Cell. Proteomics* **15**, 3190 (2016).
50. Rudman, D. *et al.* Maximal rates of excretion and synthesis of urea in normal and cirrhotic subjects. *J. Clin. Invest.* **52**, 2241–2249 (1973).
51. Ballmer, P. E. *et al.* Measurement of albumin synthesis in humans: a new approach employing stable isotopes. *Am. J. Physiol.* **259**, (1990).
52. Monk, J. P. & Todd, P. A. Bezafibrate. A review of its pharmacodynamic and pharmacokinetic properties, and therapeutic use in hyperlipidaemia. *Drugs* **33**, 539–76 (1987).
53. Nakajima, T. *et al.* Bezafibrate at clinically relevant doses decreases serum/liver triglycerides via down-regulation of sterol regulatory element-binding protein-1c in mice: a novel peroxisome proliferator-activated receptor alpha-independent mechanism. *Mol. Pharmacol.* **75**, 782–792 (2009).
54. Goldenberg, I., Benderly, M. & Goldbourt, U. Update on the use of fibrates: focus on bezafibrate. *Vasc. Health Risk Manag.* **4**, 131–141 (2008).
55. Aoyama, T. *et al.* Altered constitutive expression of fatty acid-metabolizing enzymes in mice lacking the peroxisome proliferator-activated receptor alpha (PPARalpha). *J. Biol. Chem.* **273**, 5678–5684 (1998).
56. Song, S. *et al.* Peroxisome proliferator activated receptor alpha (PPARalpha) and PPAR gamma coactivator (PGC-1alpha) induce carnitine palmitoyltransferase IA (CPT-1A) via independent gene elements. *Mol. Cell. Endocrinol.* **325**, 54–63 (2010).
57. Bougarne, N. *et al.* Molecular Actions of PPARα in Lipid Metabolism and Inflammation. *Endocr. Rev.* **39**, 760–802 (2018).
58. *Guidance Document on Good In Vitro Method Practices (GIVIMP)*. (OECD, 2018). doi:10.1787/9789264304796-en.
59. Barrero, M. J., Camarero, N., Marrero, P. F. & Haro, D. Control of human carnitine palmitoyltransferase II gene transcription by peroxisome proliferator-activated receptor through a partially conserved peroxisome proliferator-responsive element. *Biochem. J.* **369**, 721 (2003).
60. Gutgesell, A. *et al.* Downregulation of peroxisome proliferator-activated receptor alpha and its coactivators in liver and skeletal muscle mediates the metabolic

- adaptations during lactation in mice. *J. Mol. Endocrinol.* **43**, 241–250 (2009).
61. Grabacka, M., Pierzchalska, M., Dean, M. & Reiss, K. Regulation of Ketone Body Metabolism and the Role of PPAR α . *Int. J. Mol. Sci.* **17**, (2016).
 62. Kersten, S. *et al.* Peroxisome proliferator-activated receptor alpha mediates the adaptive response to fasting. *J. Clin. Invest.* **103**, 1489–1498 (1999).
 63. Mehta, V. & Namboodiri, M. A. A. N-acetylaspartate as an acetyl source in the nervous system. *Brain Res. Mol. Brain Res.* **31**, 151–157 (1995).
 64. van Ravenzwaay, B. *et al.* The individual and combined metabolite profiles (metabolomics) of dibutylphthalate and di(2-ethylhexyl)phthalate following a 28-day dietary exposure in rats. *Toxicol. Lett.* **198**, 159–170 (2010).
 65. Wang, Y., Nakajima, T., Gonzalez, F. J. & Tanaka, N. PPARs as Metabolic Regulators in the Liver: Lessons from Liver-Specific PPAR-Null Mice. *Int. J. Mol. Sci.* **21**, (2020).
 66. Clarke, C.J. & Hannun, Y.A. Neutral sphingomyelinases and nSMase2: bridging the gaps. *Biochim Biophys Acta* **1758(12)**, 1893-901 (2006).
 67. Chinetti, G., Lestavel, S., Fruchart, J-C., Clavey, V., & Staels, B. Peroxisome proliferator-activated receptor alpha reduces cholesterol esterification in macrophages. *Circ. Res.* **92(2)**, 212-7 (2003).
 68. Baranowski, M., Zabielski, P., Blachnio, A., & Gorski, J. Effect of exercise duration on ceramide metabolism in the rat heart. *Acta Physiol (Oxf.)* **192(4)**, 519-29 (2008).
 69. van der Veen, J. N. *et al.* The critical role of phosphatidylcholine and phosphatidylethanolamine metabolism in health and disease. *Biochim. Biophys. Acta - Biomembr.* **1859**, 1558–1572 (2017).
 70. Lee, S. S. T. *et al.* Requirement of PPARalpha in maintaining phospholipid and triacylglycerol homeostasis during energy deprivation. *J. Lipid Res.* **45**, 2025–2037 (2004).
 71. Fernández-Alvarez, A. *et al.* Human SREBP1c expression in liver is directly regulated by peroxisome proliferator-activated receptor alpha (PPARalpha). *J. Biol. Chem.* **286**, 21466–21477 (2011).
 72. Li, F., Patterson, A. D., Krausz, K. W., Tanaka, N. & Gonzalez, F. J. Metabolomics reveals an essential role for peroxisome proliferator-activated receptor α in bile acid homeostasis. *J. Lipid Res.* **53**, 1625–1635 (2012).
 73. Post, S. M. *et al.* Fibrates Suppress Bile Acid Synthesis via Peroxisome Proliferator–Activated Receptor- α –Mediated Downregulation of Cholesterol 7 α -Hydroxylase and Sterol 27-Hydroxylase Expression. *Arterioscler. Thromb. Vasc. Biol.* **21**, 1840–1845 (2001).
 74. Trapani, L., Segatto, M. & Pallottini, V. Regulation and deregulation of cholesterol homeostasis: The liver as a metabolic ‘power station’. *World J. Hepatol.* **4**, 184–190 (2012).
 75. Motojima, K. & Seto, K. Fibrates and statins rapidly and synergistically induce pyruvate dehydrogenase kinase 4 mRNA in the liver and muscles of mice. *Biol. Pharm. Bull.* **26**, 954–958 (2003).
 76. Sugden, M. C. & Holness, M. J. Therapeutic potential of the mammalian pyruvate dehydrogenase kinases in the prevention of hyperglycaemia. *Curr. Drug Targets. Immune. Endocr. Metabol. Disord.* **2**, 151–165 (2002).
 77. Contreras, A. V. *et al.* PPAR α via HNF4 α regulates the expression of genes encoding hepatic amino acid catabolizing enzymes to maintain metabolic homeostasis. *Genes Nutr.* **10**, 1–16 (2015).

78. KERSTEN, S. *et al.* The peroxisome proliferator-activated receptor alpha regulates amino acid metabolism. *FASEB J.* **15**, 1971–1978 (2001).
79. Sheikh, K. *et al.* Beyond lipids, pharmacological PPARalpha activation has important effects on amino acid metabolism as studied in the rat. *Am. J. Physiol. Endocrinol. Metab.* **292**, (2007).
80. Makowski, L. *et al.* Metabolic profiling of PPARalpha^{-/-} mice reveals defects in carnitine and amino acid homeostasis that are partially reversed by oral carnitine supplementation. *FASEB J.* **23**, 586–604 (2009).
81. Nakajima, T. *et al.* Effect of bezafibrate on hepatic oxidative stress: comparison between conventional experimental doses and clinically-relevant doses in mice. *Redox Rep.* **15**, 123–130 (2010).
82. Viant, M. R. *et al.* Use cases, best practice and reporting standards for metabolomics in regulatory toxicology. *Nat. Commun.* **10**, 3041 (2019).
83. Gierahn, T. M. *et al.* Seq-Well: portable, low-cost RNA sequencing of single cells at high throughput. *Nat. Methods* **14**, 395–398 (2017).
84. Dobin, A. *et al.* STAR: ultrafast universal RNA-seq aligner. *Bioinformatics* **29**, 15 (2013).
85. Wolf, F. A., Angerer, P. & Theis, F. J. SCANPY: Large-scale single-cell gene expression data analysis. *Genome Biol.* **19**, 1–5 (2018).

Acknowledgements:

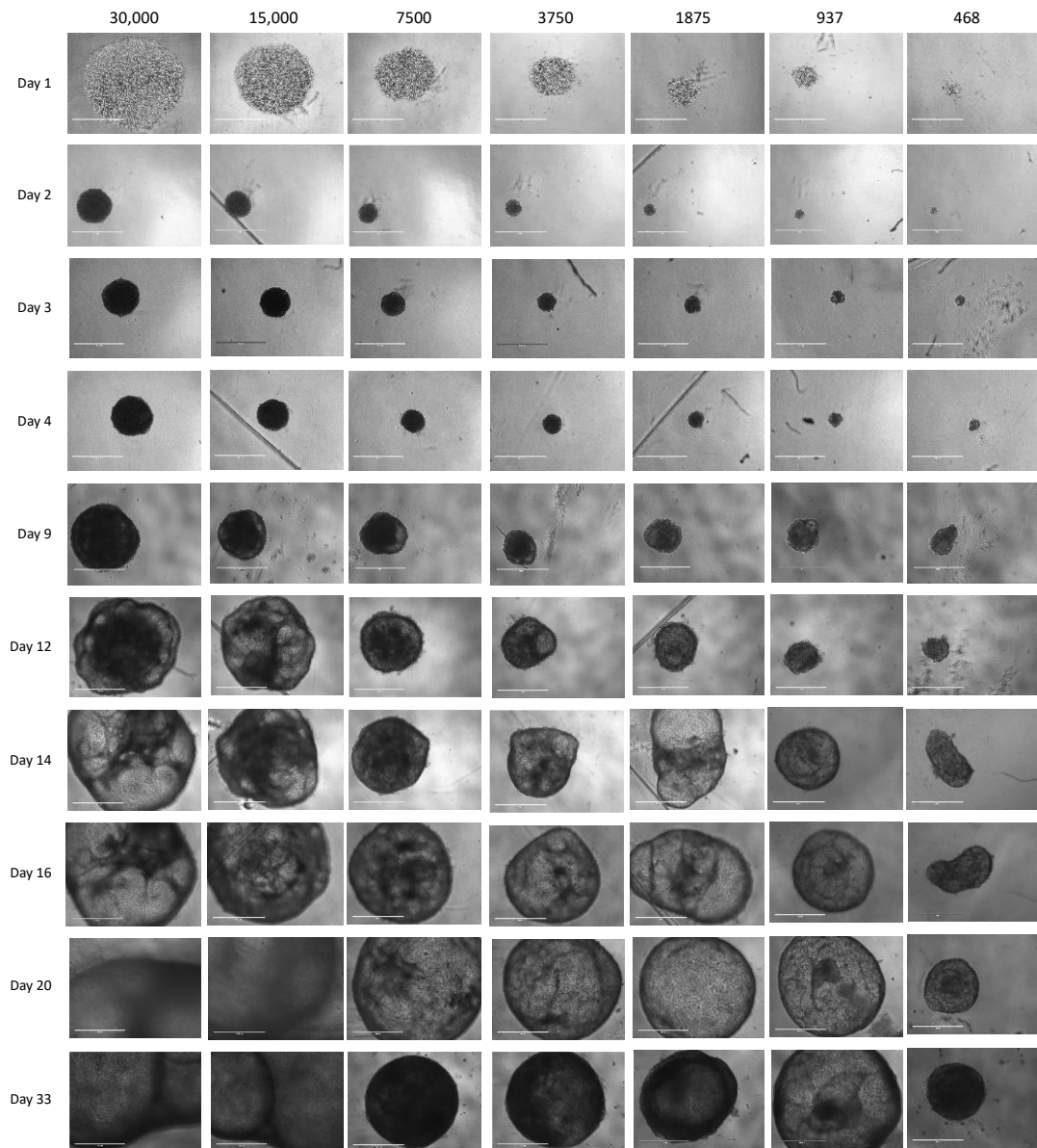
We thank Dr. Saskia Sperber (BASF SE) for initiating the project, and Dr. Varun Giri (BASF SE) for the bioinformatics support. We thank Dr. Andreas Baudy (Merck & Co) and Jose Lebron (Merck & Co) for productive experimental conversations. We thank the Koch/MIT Bio-Micro Center for assistance in single-cell RNA sequencing. **Funding:** The project was funded by BASF Corporate Research Funding (BASF-CP and BASF-KTC Alternative Toxicological Methods), the US National Institutes of Health R01 Grant for Programmed Differentiation (1R01EB025256), the Department of Defense / Advanced Manufacturing Research Institute (T0060). **Author Contributions:** BB, NMS, RK, BvR, RW proposed the project. BB, NMS, RK, BVR, RW funded the project. DM, EP, PF developed and analyzed 3D organoids. JVA designed, conducted and analyzed scRNAseq data. DM, EP, JVA, PF performed immunostaining. DM, EP, JVA, SR, PF designed urea and albumin assays for 3D organoids. EP, DM, SRH, BB, BVR, RW designed the toxicology experiments. DM performed toxicology studies, organoid growth, drug administration, harvest, and cryo-freezing. VH, MH performed and graded MS experiments. SRH, VH, MH, BB, BVR analyzed MS experiments. DM performed qPCR and analyzed transcriptomic experiments. DM, SRH generated all figures. DM, RW, SRH, BVR, BB wrote the manuscript. **Data and materials availability:** The scRNAseq dataset generated and analyzed during the current study is available in the NCBI Gene Expression Omnibus repository, Accession Number

GSE20959 (<https://www.ncbi.nlm.nih.gov/geo/query/acc.cgi?acc=GSE209597>).

The scRNAseq analysis code is available as a supplemental file on the journal website. All additional data requests should be directed to Ron Weiss (rweiss@mit.edu). **Competing Interests:** RW, DM, EP have disclosed a patent application on hiPSC-Gata6 organoids. BASF might use some of the presented technologies to register products in the future. The remaining authors do not have any competing interests.

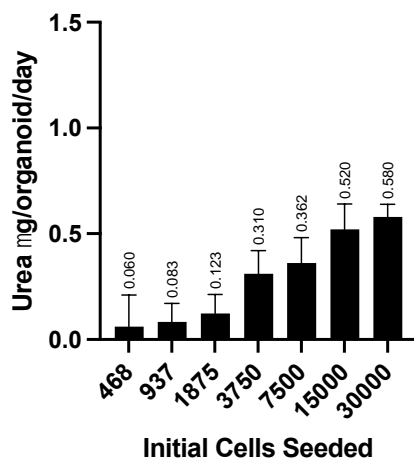
Supplementary information

Supplemental Figure 1. hiPSC-Gata6 liver organoids formation dependency on initial seeding density. Brightfield microscopy of hiPSC-Gata6 organoids seeded at indicated cells/well and grown in pluripotent media with DOX for 5 days prior to transfer to APEL2 media and grown to Day 33.

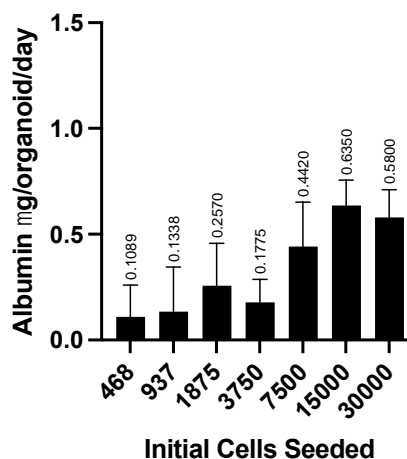


Supplemental Figure 2 Hepatocyte function of Day 25 and Day 26 organoids of varying initial seeding. Hepatocyte function measured within whole organoids by proxy of urea and albumin production. Urea production measured via BioAssay Systems QuantiChrom Urea Assay Kit. Albumin production measured via Bethyl Albumin ELISA Kit, n = 3 organoids and error bars represent standard deviation.

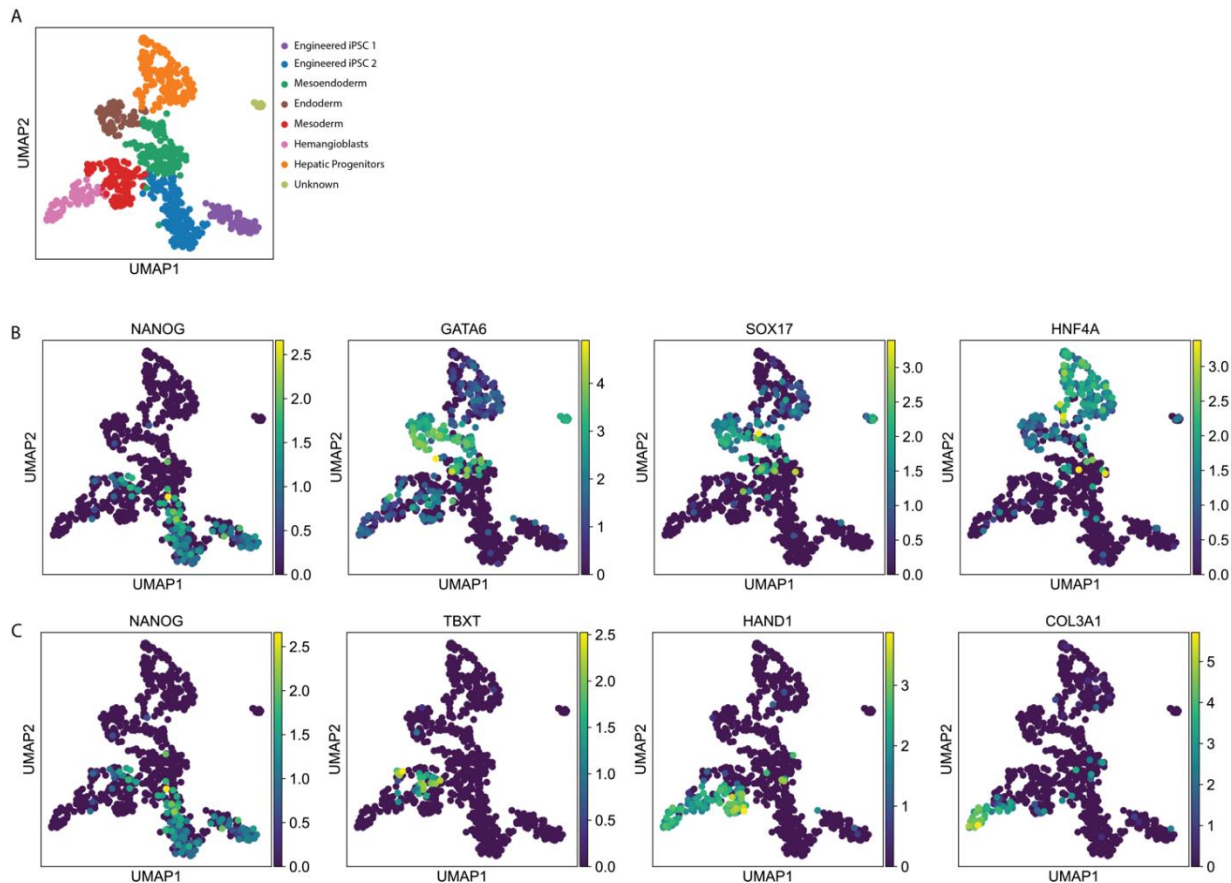
3D Organoid Urea Production, Day 25



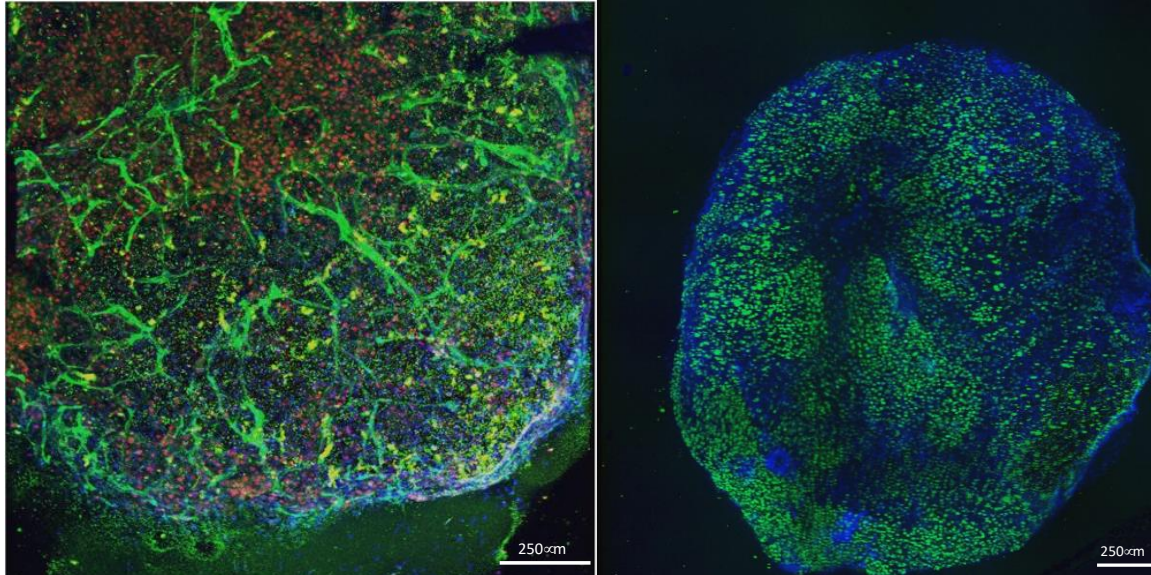
3D Organoid Albumin Production, Day 26



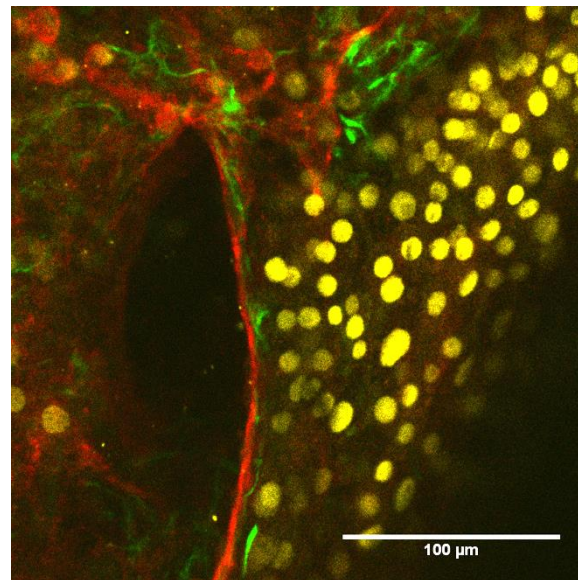
Supplemental Figure 3: scRNAseq clustering of iPSC-Gata6 organoids. a) Clustering of scRNAseq data from D0, D3, D5, and D9 dissociated organoids revealed distinct populations and two separate lineages. B) The lineage pathway towards fetal hepatocytes follows genes corresponding to iPSCs (NANOG) to primitive endoderm (GATA6, SOX17) to hepatic lineages including fetal hepatocytes (HNF4a). c) The lineage pathway towards other cell types follows genes corresponding to iPSCs (NANOG), mesoendoderm (TBXT), mesoderm (HAND1), to hemangioblasts (COL3A1).



Supplemental Figure 4: Immunostaining of 3D liver organoid structural elements. Immunostaining micrographs of hiPSC-Gata6 liver organoids. Left: endothelial cells stained for CD34 (green) and hepatic cells for CEBPa (red) with cell nuclei using Hoechst (blue) within a projection of multiple confocal slices. See Supplemental Movie 1. Right: hepatic lineage cells stained for FOXA2 (green) with cell nuclei using Hoechst (blue) within a projection of multiple confocal slices. See Supplemental Movie 2.

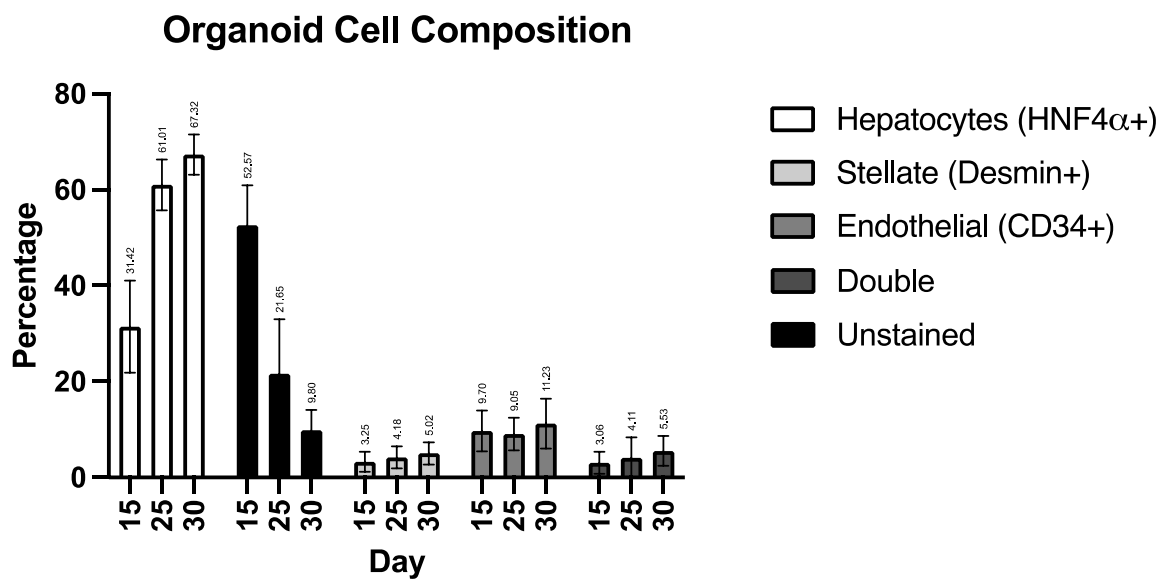


Supplemental Figure 5: Immunostaining of 3D liver organoid cell types. Immunostaining micrographs of hiPSC-Gata6 liver organoid at day 30. Endothelial cells stained for CD34 (red), hepatic cells for CEBPa (yellow), and putative Stellate cells for Desmin (green) within a single confocal slice.

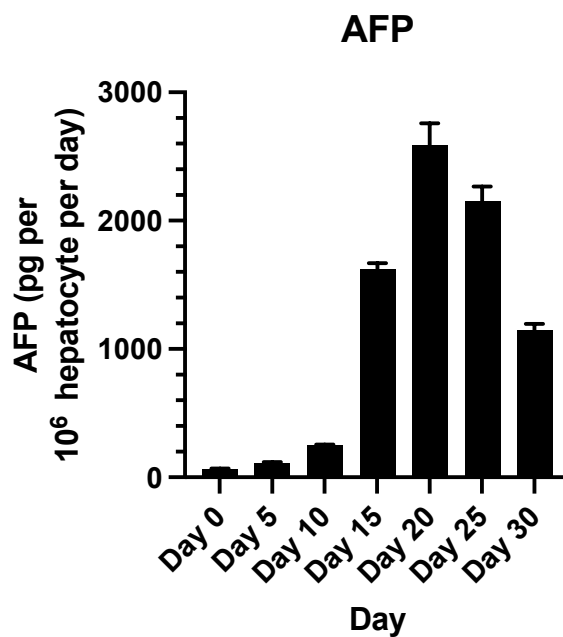


Supplemental Figure 6: Composition of organoids during development from Day 15 to Day 30. Immunostaining of dissociated organoids for cellular composition. N=3 biological replicates and error bars represent standard deviation. See

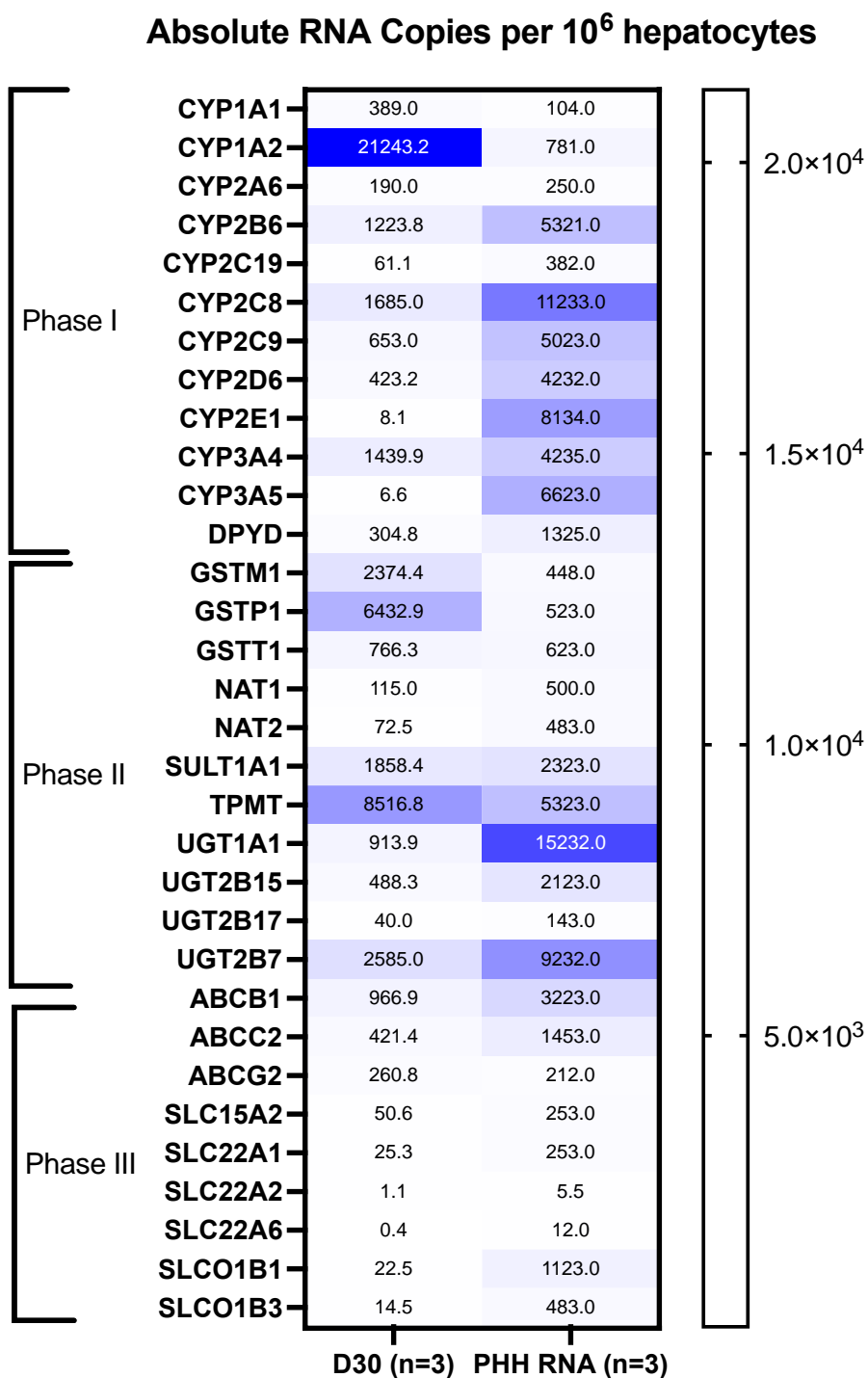
Figure 2A.



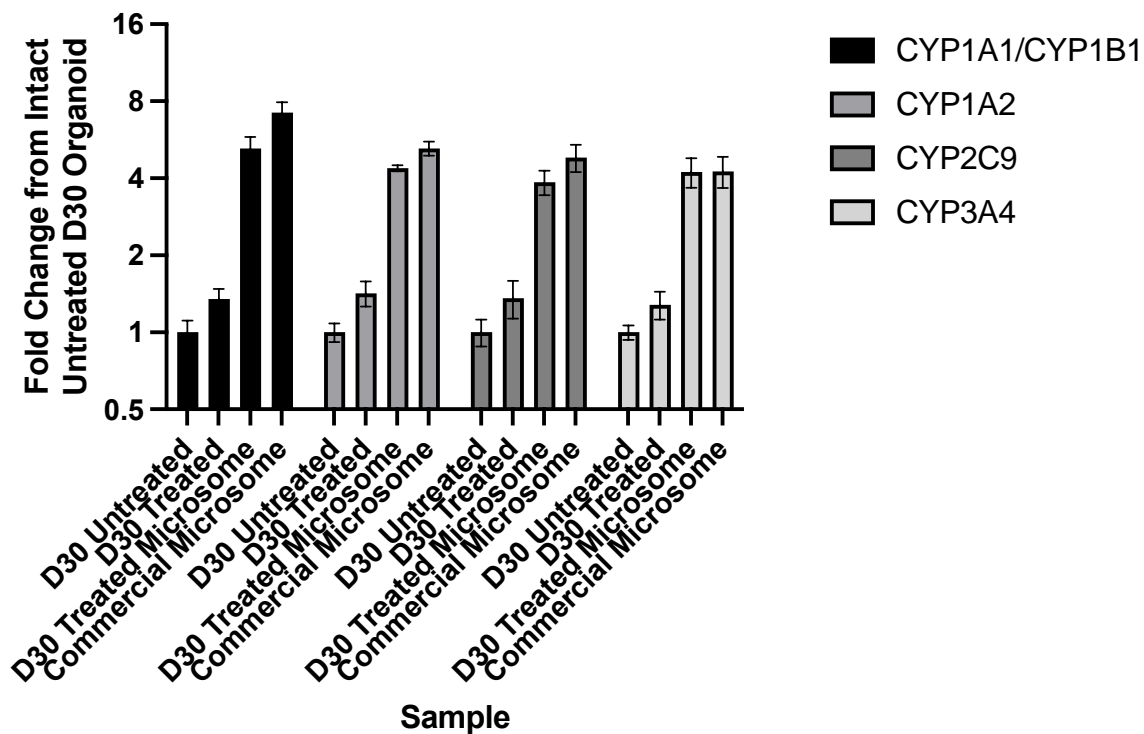
Supplemental Figure 7: Alpha-1-fetoprotein expression within developing 3D liver organoid. AFP production measured via Thermo Fisher Scientific AFP ELISA kit. N = 3 biological replicates and error bars represent standard deviation. Nominal AFP production in healthy adult human livers is <2000 pg secreted into blood serum.



Supplemental Figure 8: A selection of ADME gene expression within developing 3D liver organoid. Heat map of absolute gene expression measured for 32 core genes pertaining to ADME function during development of RNA from 3D liver organoid model (n = 3 biological replicates) compared to commercially available primary human hepatocyte RNA (ZenBio RNAmi-L10, n = 3 healthy donors with BMI between 25 and 30).



Supplemental Figure 9. Cytochrome P450 activity in 3D liver organoid and liver microsomes. Luminescent p450-Glo (Promega, USA) assays performed on whole organoid, prepared microsomes from whole organoids or using a commercial kit (ab206995, Abcam, USA), and commercial microsomes (Corning, USA). Reported values are normalized using subsequent CellTiter-Glo Luminescent Cell Viability Assay (Promega, USA) for organoids and using Pierce BCA Protein Assay Kit for microsomes. For CYP1A1 and CYP1A2 assays, organoids were incubated for 24 hours with omeprazole and for CYP2C9 and CYP3A4 assays, organoids were incubated for 24 hours with rifampicin. Mean of n = 6 biological replicates are reported as sample luminescence over untreated organoid luminescence. Microsomes are normalized to expected protein content of hepatocytes within D30 organoid.



Supplemental Table 1: qPCR Probes obtained from IDT.

NCBI Gene Symbol	IDT Assay ID Probes	Ref Seq #	Transcripts Hit	Exon Location
ABCA1	Hs.PT.58.2745242 9	NM_005502	NM_005502	3 - 4
ACAT1	Hs.PT.56a.232658 04	NM_000019	NM_000019	5 - 6
ACSL1	Hs.PT.58.2755666	NM_001995	NM_001995	7 - 10
ACTB	Hs.PT.39a.222148 47	NM_001101	NM_001101	1 - 2
ALDOA	Hs.PT.56a.392317 20.g	NM_0012431 77	NM_184043,NM_184041,NM_001243177,NM_001127617, NM_000034	4 - 5
APOA1	Hs.PT.56a.245501 8.g	NM_000039	NM_000039	2 - 3
APOA2	Hs.PT.56a.192402 98.g	NM_001643	NM_001643	2 - 3
B2M	Hs.PT.39a.222148 45	NM_004048	NM_004048	2 - 3
CPT1A	Hs.PT.58.2799026	NM_0010318 47	NM_001876,NM_001031847	16 - 17
CYP27A1	Hs.PT.58.2254512 5	NM_000784	NM_000784	1 - 2
CYP7A1	Hs.PT.58.2140822 1	NM_000780	NM_000780	3 - 4
GPD1	Hs.PT.58.4554819	NM_0012571 99	NM_005276,NM_001257199	7 - 8
GUSB	Hs.PT.58v.277375 38	NM_000181	NM_000181	10 - 11
HPRT1	Hs.PT.58v.456215 72	NM_000194	NM_000194	8 - 9
LPL	Hs.PT.58.4579291 3	NM_000237	NM_000237	5 - 6
NAT8L	Hs.PT.58.3906155 3	NM_178557	XM_003403774,NM_178557	2 - 3
PANK1	Hs.PT.58.2284965	NM_138316	NM_148978,NM_148977,NM_138316	3 - 4

<i>PCK2</i>	<i>Hs.PT.58.1943936</i> 9	<i>NM_004563</i>	<i>NM_004563,NM_001018073</i>	2 - 3
<i>PDK4</i>	<i>Hs.PT.58.2821279</i> 3	<i>NM_002612</i>	<i>NM_002612</i>	2 - 3
<i>PFKL</i>	<i>Hs.PT.58.2111400</i> 1	<i>NM_002626</i>	<i>NR_024108,NM_002626</i>	5 - 6
<i>POLR2</i> <i>A</i>	<i>Hs.PT.39a.196395</i> 31	<i>NM_000937</i>	<i>NM_000937</i>	1 - 2
<i>PPIA</i>	<i>Hs.PT.39a.222148</i> 51	<i>NM_021130</i>	<i>NM_021130</i>	4 - 5
<i>RPLP0</i>	<i>Hs.PT.39a.222148</i> 24	<i>NM_001002</i>	<i>NM_001002</i>	2 - 3
<i>SMPD1</i>	<i>Hs.PT.58.4500199</i>	<i>NM_000543</i>	<i>NM_001007593,NM_000543</i>	2 - 3
<i>SMPD2</i>	<i>Hs.PT.58.2042672</i> 2.g	<i>NM_003080</i>	<i>NM_003080</i>	1 - 3
<i>SPTSSA</i>	<i>Hs.PT.58.2836818</i> 3	<i>NM_138288</i>	<i>NM_138288</i>	1 - 2
<i>SPTSSB</i>	<i>Hs.PT.58.1412060</i>	<i>NM_0010401</i> <i>00</i>	<i>NM_001040100</i>	1 - 3
<i>UCP1</i>	<i>Hs.PT.58.3915700</i> 6	<i>NM_021833</i>	<i>NM_021833</i>	5 - 6

Supplemental Table 2. hiPSC-Gata6 organoids weights upon bezafibrate treatment. After bezafibrate treatment, treated and control organoids were weighted. The ratio of treated vs control organoids weights was calculated based on the median of the controls. The p-values were calculated by Welch-t-test. Two independent experimental batches were evaluated LC; low intracellular bezafibrate concentrations HC; high bezafibrate concentrations.

LC			
Control	Weight (mg)	Treated sample	Weight (mg)
1	22.00	1	29,00
3	21.00	2	29,00
4	23.00	3	29,00
5	28.00	4	26,00
6	30,00	5	26,00
7	20,00		
8	23,00		
9	33,00		
10	21,00		
Average	24,9	Average	27,8
SD	4,25	SD	1,47
Ratio treated vs control			1,22
p-value			0,10
HC			
Control	Weight (mg)	Treated sample	Weight (mg)
1	26,00	1	28,00
2	20,00	2	32,00
3	36,00	3	26,00
4	22,00		
5	33,00		
6	17,00		
7	29,00		
8	29,00		
9	22,00		
10	29,00		
Average	26,3	Average	28,67
SD	5,69	SD	2,49
Ratio treated vs control			1,07
p-value			0,23

Supplemental Table 3. Bezafibrate intracellular concentrations. Absolute Bezafibrate intracellular concentrations were measured per sample (6-pooled organoids) and normalized to cell numbers using within sample analyte median (SAM). Two independent experiments were carried out (Exp1 and Exp 2).

Sample	Bezafibrate (μg)	LC	
		SAM	Corrected Bezafibrate (μg)
1	2.84	1.28	2.21
2	2.47	1.10	2.24
3	2.15	0.99	2.18
4	2.17	1.10	1.97
5	2.02	0.84	2.40
Average			2.20 μg
SD			0.14 μg
Sample	Bezafibrate (μg)	HC	
		SAM	Corrected bezafibrate (μg)
1	2.51	0.225	11.12
5	2.44	0.172	14.20
3	2.39	0.179	13.33
Average			12.88 μg
SD			1.3 μg

Supplemental Table 4. Metabolite changes in TAGs, fatty acid oxidation and Acetyl-CoA pathways upon bezafibrate treatment. Statistically significantly increased and decreased values of metabolite changes after bezafibrate treatment. Changes are expressed as a relative value compared to controls by means of fold-change (Welch t test; $p < 0.05$). Numbers in red boxes are significantly increased and those in blue boxes significantly decreased metabolite value changes compared to the controls. The intensity of the color corresponds to the magnitude of the fold change.

Metabolite name	LC	HC
"Triacylglycerol (C30:0,C18:2)"	0,33	0,15
"Triacylglycerol (C32:0,C16:1)"	1,33	2,47
"Triacylglycerol (C34:0,C16:0)"	0,84	0,60
"Triacylglycerol (C34:0,C18:1)"	0,75	0,22
"Triacylglycerol (C34:1,C16:0)"	0,67	0,30
"Triacylglycerol (C34:1,C18:1)"	0,33	0,10
"Triacylglycerol (C34:1,C18:3)"	0,19	0,07
"Triacylglycerol (C34:2,C18:0)"	0,35	0,10
"Triacylglycerol (C34:2,C18:1)"	0,24	0,05
"Triacylglycerol (C36:1,C18:0)"	0,68	0,29
"Triacylglycerol (C36:1,C18:1)"	0,46	0,13
"Triacylglycerol (C36:1,C18:2)"	0,19	0,04
"Triacylglycerol (C36:2,C18:1)"	0,37	0,10
"Triacylglycerol (C36:3,C18:1)"	0,24	0,06
"Triacylglycerol (C36:3,C18:2)"	0,38	0,05
"Triacylglycerol (C36:3,C18:3)"	0,29	0,05
"Triacylglycerol (C36:4,C16:0)"	0,20	0,04
"Triacylglycerol (C36:4,C18:0)"	0,19	0,05
"Triacylglycerol (C36:4,C18:2)"	0,50	0,07
3-Hydroxybutyrate	1,89	1,40
Carnitine	1,33	2,05
O-Acetylcarnitine	1,27	1,95
Propionylcarnitine	5,17	18,44

N-Acetylaspartate	20,28	119,80
Pantothenic acid	16,39	28,57

Supplemental Table 5. Metabolite changes in ceramides and sphingomyelin upon bezafibrate treatment. Statistically significantly increased and decreased values of metabolite changes after bezafibrate treatment. Changes are expressed as a relative value compared to controls by means of fold-change (Welch t test; $p < 0.05$). Numbers in red boxes are significantly increased and those in blue boxes significantly decreased metabolite value changes compared to the controls. The intensity of the color corresponds to the magnitude of the fold change

Metabolite name	LC	HC
"Ceramide (d16:1,C24:0)"	0,26	0,25
"Ceramide (d17:1,C24:0)"	0,35	0,26
"Ceramide (d18:1,C16:0)"	0,31	0,17
"Ceramide (d18:1,C18:0)"	0,17	0,11
"Ceramide (d18:1,C20:0)"	0,15	0,08
"Ceramide (d18:1,C21:0)"	0,25	0,19
"Ceramide (d18:1,C22:0)"	0,14	0,10
"Ceramide (d18:1,C22:1)"	0,28	0,15
"Ceramide (d18:1,C23:0)"	0,17	0,09
"Ceramide (d18:1,C24:0)"	0,20	0,11
"Ceramide (d18:1,C24:1)"	0,10	0,07
"Ceramide (d18:1,C24:2)"	0,13	0,05
"Ceramide (d18:2,C16:0)"	0,54	0,25
"Ceramide (d18:2,C18:0)"	0,32	0,13
"Ceramide (d18:2,C22:0)"	0,13	0,11
"Ceramide (d18:2,C23:0)"	0,18	0,11
"Ceramide (d18:2,C24:0)"	0,16	0,19
"Ceramide (d18:2,C24:1)"	0,26	0,15
"Ceramide (d18:2,C24:2)"	0,24	0,11
Sphingomyelin (d32:1)	4,48	3,89
Sphingomyelin (d32:2)	7,10	7,07
Sphingomyelin (d33:1)	5,78	3,55
Sphingomyelin (d34:0)	3,50	2,14
Sphingomyelin (d34:1)	4,29	1,57
Sphingomyelin (d34:2)	13,00	7,20
Sphingomyelin (d35:1)	4,94	2,80
Sphingomyelin (d35:2)	9,42	7,05
Sphingomyelin (d36:1)	1,92	1,07
Sphingomyelin (d36:2)	7,40	3,67
Sphingomyelin (d36:3)	2,49	1,87
Sphingomyelin (d37:1)	7,50	3,55
Sphingomyelin (d38:1)	0,71	0,33
Sphingomyelin (d38:2)	1,68	1,09
Sphingomyelin (d39:1)	4,76	1,91
Sphingomyelin (d40:2)	2,43	1,68
Sphingomyelin (d41:1)	0,76	0,41
Sphingomyelin (d41:2)	3,42	1,30

Supplemental Table 6. Metabolite changes in Phospholipid metabolism upon bezafibrate treatment. Statistically significantly increased and decreased values of metabolite changes after bezafibrate treatment. Changes are expressed as a relative value compared to controls by means of fold-change (Welch t test; $p < 0.05$). Numbers in red boxes are significantly increased and those in blue boxes significantly decreased metabolite value changes compared to the controls. The intensity of the color corresponds to the magnitude of the fold change.

Metabolite name	LC	HC
Phosphatidylcholine (C32:0)	2,39	1,39
Phosphatidylcholine (C34:0)	3,18	1,76
Phosphatidylcholine (C34:1)	0,93	0,40
Phosphatidylcholine (C34:2)	0,20	0,09
Phosphatidylcholine (C34:3)	0,28	0,10
Phosphatidylcholine (C36:0)	1,99	1,38
Phosphatidylcholine (C36:1)	1,69	1,03
Phosphatidylcholine (C36:2)	0,39	0,26
Phosphatidylcholine (C36:3)	0,31	0,13
Phosphatidylcholine (C36:4)	0,21	0,10
Phosphatidylcholine (C36:5)	0,16	0,07
Phosphatidylcholine (C38:4)	0,59	0,38
Phosphatidylcholine (C38:5)	0,67	0,31
Phosphatidylcholine (C38:6)	0,21	0,13
Phosphatidylcholine (C40:6)	0,68	0,39
Phosphatidylcholine (C40:7)	0,49	0,20
Phosphatidylcholine (C40:8)	0,29	0,12
Lysophosphatidylcholine (C14:0)	2,60	4,99
Lysophosphatidylcholine (C16:0)	0,34	0,46
Lysophosphatidylcholine (C16:1)	2,06	4,32
Lysophosphatidylcholine (C17:0)	0,45	0,46
Lysophosphatidylcholine (C18:0)	0,31	0,36
Lysophosphatidylcholine (C18:1)	0,75	1,15
Lysophosphatidylcholine (C18:2)	0,14	0,25
Lysophosphatidylcholine (C18:3)	0,32	0,45
Lysophosphatidylcholine (C19:0)	1,48	2,19
Lysophosphatidylcholine (C20:0)	1,00	1,55
Lysophosphatidylcholine (C20:1)	2,22	2,15
Lysophosphatidylcholine (C20:3)	0,35	0,68
Lysophosphatidylcholine (C20:4)	0,16	0,36
Lysophosphatidylcholine (C20:5)	0,32	0,28
Lysophosphatidylcholine (C22:0)	3,11	4,56
Lysophosphatidylcholine (C22:4)	1,83	3,33
Lysophosphatidylcholine (C22:5)	1,10	1,44
Lysophosphatidylcholine (C22:6)	0,35	0,45
Lysophosphatidylcholine (C24:0)	2,70	6,86
Lysophosphatidylcholine (C24:1)	4,69	7,65

Supplemental Table 7. Metabolite changes in Phosphoethanolamine metabolism upon bezafibrate treatment. Statistically significantly increased and decreased values of metabolite changes after bezafibrate treatment. Changes are expressed as a relative value compared to controls by means of fold-change (Welch t test; $p < 0.05$). Numbers in red boxes are significantly increased and those in blue boxes significantly decreased metabolite value changes compared to the controls. The intensity of the color corresponds to the magnitude of the fold change.

Metabolite name	LC	HC
Phosphatidylethanolamine (C32:0)	1,37	0,61
Phosphatidylethanolamine (C34:0)	0,66	0,42
Phosphatidylethanolamine (C34:1)	0,83	0,37
Phosphatidylethanolamine (C34:2)	0,28	0,05
Phosphatidylethanolamine (C36:0)	0,27	0,19
Phosphatidylethanolamine (C36:1)	0,45	0,21
Phosphatidylethanolamine (C36:2)	0,17	0,06
Phosphatidylethanolamine (C36:3)	0,23	0,05
Phosphatidylethanolamine (C36:4)	0,23	0,03
Phosphatidylethanolamine (C38:3)	0,19	0,03
Phosphatidylethanolamine (C38:4)	0,16	0,05
Phosphatidylethanolamine (C38:5)	0,26	0,08
Phosphatidylethanolamine (C38:6)	0,12	0,02
Phosphatidylethanolamine (C40:6)	0,15	0,05
Phosphatidylethanolamine (C40:7)	0,22	0,05
Lysophosphatidylethanolamine (C16:0)	0,10	0,26
Lysophosphatidylethanolamine (C18:0)	0,07	0,14
Lysophosphatidylethanolamine (C18:1)	0,28	0,76
Lysophosphatidylethanolamine (C18:2)	0,32	0,38
Lysophosphatidylethanolamine (C20:4)	0,63	0,97
Lysophosphatidylethanolamine (C22:5)	1,82	2,06
Lysophosphatidylethanolamine (C22:6)	0,28	0,42

Supplemental Table 8. Metabolite changes in cholesterol metabolism upon bezafibrate treatment. Statistically significantly increased and decreased values of metabolite changes after bezafibrate treatment. Changes are expressed as a relative value compared to controls by means of fold-change (Welch t test; $p < 0.05$). Numbers in red boxes are significantly increased and those in blue boxes significantly decreased metabolite value changes compared to the controls. The intensity of the color corresponds to the magnitude of the fold change.

Metabolite name	LC	HC
"Cholesterol, free"	2,00	1,60
Cholesterylester (C16:0)	30,63	42,70
Cholesterylester (C16:1)	12,76	61,46
Cholesterylester (C18:0)	25,24	50,16
Cholesterylester (C18:1)	26,99	16,39
Cholesterylester (C18:2)	10,26	4,52
Cholesterylester (C18:3)	18,34	7,78
Cholesterylester (C20:1)	10,80	14,76
Cholesterylester (C20:4)	41,97	16,74
Cholesterylester (C20:5)	89,78	14,91

Cholesterylester (C22:4)	12,14	15,39
Cholesterylester (C22:5)	54,85	29,96
Taurine	2,50	13,96

Supplemental Table 9. Metabolite changes in carbohydrate metabolism upon bezafibrate treatment. Statistically significantly increased and decreased values of metabolite changes after bezafibrate treatment. Changes are expressed as a relative value compared to controls by means of fold-change (Welch t test; $p < 0.05$). Numbers in red boxes are significantly increased and those in blue boxes significantly decreased metabolite value changes compared to the controls. The intensity of the color corresponds to the magnitude of the fold change.

Metabolite name	LC	HC
Glucose	1,57	4,08
Sorbitol	6,24	13,11
"Fructose-1,6-diphosphate"	4,26	12,11
Glycerol-3-phosphate	0,39	0,76

Supplemental Table 10. Metabolite changes in amino acids upon bezafibrate treatment. Statistically significantly increased and decreased values of metabolite changes after bezafibrate treatment. Changes are expressed as a relative value compared to controls by means of fold-change (Welch t test; $p < 0.05$). Numbers in red boxes are significantly increased and those in blue boxes significantly decreased metabolite value changes compared to the controls. The intensity of the color corresponds to the magnitude of the fold change.

Metabolite name	LC	HC
Arginine	8,36	20,72
Asparagine	1,78	4,44
Glutamate	1,00	2,32
Glutamine	1,76	3,49
Isoleucine	2,46	5,34
Leucine	3,14	7,08
Methionine	3,10	6,10
Phenylalanine	4,48	7,37
Proline	7,46	11,40
Taurine	2,50	13,96
Threonine	6,22	13,04
Tryptophan	8,64	8,47
Tyrosine	5,98	9,84
Valine	4,14	6,96

Supplemental Table 11. Metabolite changes in antioxidants upon bezafibrate treatment. Statistically significantly increased and decreased values of metabolite changes after bezafibrate treatment. Changes are expressed as a relative value compared to controls by means of fold-change (Welch t test; $p < 0.05$). Numbers in red boxes are significantly increased and those in blue boxes significantly decreased metabolite value changes compared to the controls. The intensity of the color corresponds to the magnitude of the fold change.

Metabolite name	LC	HC
beta-Carotene	0,24	0,16
Coenzyme Q10	0,18	0,07
Coenzyme Q7	0,59	0,37
Coenzyme Q9	0,12	0,16
gamma-Tocopherol	0,43	0,55
Glutathione (GSH)	0,47	0,65

Supplemental Table 12. Full metabolic profile of bezafibrate-treated hiPSC-Gata6 organoids. Statistically significantly increased and decreased values of metabolite changes after bezafibrate treatment. Changes are expressed as a relative value compared to controls by means of fold-change (Welch t test; $p < 0.05$). Numbers in red boxes are significantly increased and those in blue boxes significantly decreased metabolites changes. The intensity of the color corresponds to the magnitude of the fold change.

Ontology name	Metabolite name	LC	HC
Acylglycerols	"Triacylglycerol (C30:0,C18:1)"	1,06	0,42
Acylglycerols	"Triacylglycerol (C30:0,C18:2)"	0,33	0,15
Acylglycerols	"Triacylglycerol (C32:0,C16:0)"	1,09	1,15
Acylglycerols	"Triacylglycerol (C32:0,C16:1)"	1,33	2,47
Acylglycerols	"Triacylglycerol (C32:1,C16:1)"	0,86	2,29
Acylglycerols	"Triacylglycerol (C34:0,C18:0)"	0,75	1,15
Acylglycerols	"Triacylglycerol (C34:0,C18:1)"	0,75	0,22
Acylglycerols	"Triacylglycerol (C34:1,C16:0)"	0,67	0,30
Acylglycerols	"Triacylglycerol (C34:1,C18:1)"	0,33	0,10
Acylglycerols	"Triacylglycerol (C34:1,C18:3)"	0,19	0,07
Acylglycerols	"Triacylglycerol (C34:2,C18:0)"	0,35	0,10
Acylglycerols	"Triacylglycerol (C34:2,C18:1)"	0,24	0,05
Acylglycerols	"Triacylglycerol (C36:0,C18:0)"	0,96	2,55
Acylglycerols	"Triacylglycerol (C36:1,C18:0)"	0,68	0,29
Acylglycerols	"Triacylglycerol (C36:1,C18:1)"	0,46	0,13
Acylglycerols	"Triacylglycerol (C36:1,C18:2)"	0,19	0,04
Acylglycerols	"Triacylglycerol (C36:2,C18:1)"	0,37	0,10
Acylglycerols	"Triacylglycerol (C36:3,C18:1)"	0,24	0,06
Acylglycerols	"Triacylglycerol (C36:3,C18:2)"	0,38	0,05
Acylglycerols	"Triacylglycerol (C36:3,C18:3)"	0,29	0,05
Acylglycerols	"Triacylglycerol (C36:4,C16:0)"	0,20	0,04
Acylglycerols	"Triacylglycerol (C36:4,C18:0)"	0,19	0,05

Acylglycerols	"Triacylglycerol (C36:4,C18:2)"	0,50	0,07
Amino acids	Arginine	8,36	20,72
Amino acids	Asparagine	1,78	4,44
Amino acids	Glutamate	1,00	2,32
Amino acids	Glutamine	1,76	3,49
Amino acids	Isoleucine	2,46	5,34
Amino acids	Leucine	3,14	7,08
Amino acids	Methionine	3,10	6,10
Amino acids	Phenylalanine	4,48	7,37
Amino acids	Proline	7,46	11,40
Amino acids	Taurine	2,50	13,96
Amino acids	Threonine	6,22	13,04
Amino acids	Tryptophan	8,64	8,47
Amino acids	Tyrosine	5,98	9,84
Amino acids	Valine	4,14	6,96
Amino acids related	1-Methylhistidine	0,64	6,73
Amino acids related	2-Methylserine	4,21	8,18
Amino acids related	Carnosine	19,75	165,42
Amino acids related	Creatine	1,29	5,04
Amino acids related	Ketoleucine	11,34	26,56
Amino acids related	Kynurenic acid	0,97	13,91
Amino acids related	Kynurenine	1,14	2,87
Amino acids related	N-Acetylaspartate	20,28	119,80
Amino acids related	N-Acetylhistidine	0,85	1,83
Amino acids related	N-Acetylleucine	0,93	9,61
Amino acids related	N-Acetylserine	7,03	157,02
Amino acids related	N-Phenylacetyl glycine	2,30	28,39
Amino acids related	Ophthalmic acid	0,31	0,40
Amino acids related	Pipecolic acid	1,56	8,17
Amino acids related	S-Adenosylhomocysteine	0,43	0,34
Carbohydrates and related	Glucose	1,57	4,08
Carbohydrates and related	N-Acetylglucosamine	2,49	25,88
Carbohydrates and related	Sorbitol	6,24	13,11
Cholesterol and related	"Cholesterol, free"	2,00	1,60
Cholesterol and related	Cholesterylester (C16:0)	30,63	42,70
Cholesterol and related	Cholesterylester (C16:1)	12,76	61,46
Cholesterol and related	Cholesterylester (C18:0)	25,24	50,16
Cholesterol and related	Cholesterylester (C18:1)	26,99	16,39
Cholesterol and related	Cholesterylester (C18:2)	10,26	4,52
Cholesterol and related	Cholesterylester (C18:3)	18,34	7,78
Cholesterol and related	Cholesterylester (C20:1)	10,80	14,76
Cholesterol and related	Cholesterylester (C20:4)	41,97	16,74
Cholesterol and related	Cholesterylester (C20:5)	89,78	14,91
Cholesterol and related	Cholesterylester (C22:4)	12,14	15,39
Cholesterol and related	Cholesterylester (C22:5)	54,85	29,96
Cholesterol and related	Cholic acid	1,14	1,71

Cholesterol and related	Isopentenyl pyrophosphate (IPP)	0,39	0,81
Energy metabolism and related	"Fructose-1,6-diphosphate"	4,26	12,11
Energy metabolism and related	3-Hydroxybutyrate	1,89	1,40
Energy metabolism and related	Carnitine	1,33	2,05
Energy metabolism and related	Choline	1,73	2,53
Energy metabolism and related	Glucose-6-phosphate	0,64	0,70
Energy metabolism and related	Glycerol-3-phosphate	0,39	0,76
Energy metabolism and related	Hexadecenoylcarnitine	0,84	4,04
Energy metabolism and related	O-Acetylcarnitine	1,27	1,95
Energy metabolism and related	Octadecenoylcarnitine	0,60	0,64
Energy metabolism and related	Octadecenoylcarnitine	0,78	0,35
Energy metabolism and related	Propionylcarnitine	5,17	18,44
Energy metabolism and related	Ribulose-5-phosphate	0,98	1,33
Energy metabolism and related	Tetradecenoylcarnitine	0,93	1,39
Glycerophospholipids	Choline plasmalogen (C36:4)	1,74	0,84
Glycerophospholipids	Choline plasmalogen (C36:5)	2,28	1,27
Glycerophospholipids	Phosphatidylcholine (C32:0)	2,39	1,39
Glycerophospholipids	Phosphatidylcholine (C34:0)	3,18	1,76
Glycerophospholipids	Phosphatidylcholine (C34:1)	0,93	0,40
Glycerophospholipids	Phosphatidylcholine (C34:2)	0,20	0,09
Glycerophospholipids	Phosphatidylcholine (C34:3)	0,28	0,10
Glycerophospholipids	Phosphatidylcholine (C36:0)	1,99	1,38
Glycerophospholipids	Phosphatidylcholine (C36:1)	1,69	1,03
Glycerophospholipids	Phosphatidylcholine (C36:2)	0,39	0,26
Glycerophospholipids	Phosphatidylcholine (C36:3)	0,31	0,13
Glycerophospholipids	Phosphatidylcholine (C36:4)	0,21	0,10
Glycerophospholipids	Phosphatidylcholine (C36:5)	0,16	0,07
Glycerophospholipids	Phosphatidylcholine (C38:4)	0,59	0,38
Glycerophospholipids	Phosphatidylcholine (C38:5)	0,67	0,31
Glycerophospholipids	Phosphatidylcholine (C38:6)	0,21	0,13
Glycerophospholipids	Phosphatidylcholine (C40:6)	0,68	0,39
Glycerophospholipids	Phosphatidylcholine (C40:7)	0,49	0,20
Glycerophospholipids	Phosphatidylcholine (C40:8)	0,29	0,12
Glycerophospholipids	Phosphatidylethanolamine (C32:0)	1,37	0,61
Glycerophospholipids	Phosphatidylethanolamine (C34:0)	0,66	0,42
Glycerophospholipids	Phosphatidylethanolamine (C34:1)	0,83	0,37
Glycerophospholipids	Phosphatidylethanolamine (C34:2)	0,28	0,05
Glycerophospholipids	Phosphatidylethanolamine (C36:0)	0,27	0,19
Glycerophospholipids	Phosphatidylethanolamine (C36:1)	0,45	0,21
Glycerophospholipids	Phosphatidylethanolamine (C36:2)	0,17	0,06
Glycerophospholipids	Phosphatidylethanolamine (C36:3)	0,23	0,05
Glycerophospholipids	Phosphatidylethanolamine (C36:4)	0,23	0,03
Glycerophospholipids	Phosphatidylethanolamine (C38:3)	0,19	0,03
Glycerophospholipids	Phosphatidylethanolamine (C38:4)	0,16	0,05
Glycerophospholipids	Phosphatidylethanolamine (C38:5)	0,26	0,08
Glycerophospholipids	Phosphatidylethanolamine (C38:6)	0,12	0,02

Glycerophospholipids	Phosphatidylethanolamine (C40:6)	0,15	0,05
Glycerophospholipids	Phosphatidylethanolamine (C40:7)	0,22	0,05
Lysoglycerophospholipids	Lysophosphatidylcholine (C14:0)	2,60	4,99
Lysoglycerophospholipids	Lysophosphatidylcholine (C15:0)	0,66	1,32
Lysoglycerophospholipids	Lysophosphatidylcholine (C16:0)	0,34	0,46
Lysoglycerophospholipids	Lysophosphatidylcholine (C16:1)	2,06	4,32
Lysoglycerophospholipids	Lysophosphatidylcholine (C17:0)	0,45	0,46
Lysoglycerophospholipids	Lysophosphatidylcholine (C18:0)	0,31	0,36
Lysoglycerophospholipids	Lysophosphatidylcholine (C18:1)	0,75	1,15
Lysoglycerophospholipids	Lysophosphatidylcholine (C18:2)	0,14	0,25
Lysoglycerophospholipids	Lysophosphatidylcholine (C18:3)	0,32	0,45
Lysoglycerophospholipids	Lysophosphatidylcholine (C19:0)	1,48	2,19
Lysoglycerophospholipids	Lysophosphatidylcholine (C20:0)	1,00	1,55
Lysoglycerophospholipids	Lysophosphatidylcholine (C20:1)	2,22	2,15
Lysoglycerophospholipids	Lysophosphatidylcholine (C20:2)	0,76	1,20
Lysoglycerophospholipids	Lysophosphatidylcholine (C20:3)	0,35	0,68
Lysoglycerophospholipids	Lysophosphatidylcholine (C20:4)	0,16	0,36
Lysoglycerophospholipids	Lysophosphatidylcholine (C20:5)	0,32	0,28
Lysoglycerophospholipids	Lysophosphatidylcholine (C22:0)	3,11	4,56
Lysoglycerophospholipids	Lysophosphatidylcholine (C22:4)	1,83	3,33
Lysoglycerophospholipids	Lysophosphatidylcholine (C22:5)	1,10	1,44
Lysoglycerophospholipids	Lysophosphatidylcholine (C22:6)	0,35	0,45
Lysoglycerophospholipids	Lysophosphatidylcholine (C24:0)	2,70	6,86
Lysoglycerophospholipids	Lysophosphatidylcholine (C24:1)	4,69	7,65
Lysoglycerophospholipids	Lysophosphatidylethanolamine (C16:0)	0,10	0,26
Lysoglycerophospholipids	Lysophosphatidylethanolamine (C18:0)	0,07	0,14
Lysoglycerophospholipids	Lysophosphatidylethanolamine (C18:1)	0,28	0,76
Lysoglycerophospholipids	Lysophosphatidylethanolamine (C18:2)	0,32	0,38
Lysoglycerophospholipids	Lysophosphatidylethanolamine (C20:4)	0,63	0,97
Lysoglycerophospholipids	Lysophosphatidylethanolamine (C22:5)	1,82	2,06
Lysoglycerophospholipids	Lysophosphatidylethanolamine (C22:6)	0,28	0,42
Miscellaneous	Biliverdin	10,22	5,07
Miscellaneous	Lycopene	0,56	0,06
Nucleobases and related	1-Methyladenosine	2,11	40,95
Nucleobases and related	5-Methylcytidine	4,34	2304,14
Nucleobases and related	7-Methylguanine	3,17	14,87
Nucleobases and related	Allantoin	10,92	112,12
Nucleobases and related	Thymine	2,99	27,11
Nucleobases and related	Uric acid	5,37	4,57
Nucleobases and related	Uridine	0,53	0,24
Signal substances and related	"N,N-Dimethylarginine (ADMA)"	3,79	29,27
Signal substances and related	5-Hydroxytryptophan	13,71	38,07
Signal substances and related	Acetylcholine	0,62	1,19
Signal substances and related	Metanephrine	1,19	5,23
Sphingolipids	"Ceramide (d16:1,C24:0)"	0,26	0,25
Sphingolipids	"Ceramide (d17:1,C24:0)"	0,35	0,26

Sphingolipids	"Ceramide (d18:1,C16:0)"	0,31	0,17
Sphingolipids	"Ceramide (d18:1,C18:0)"	0,17	0,11
Sphingolipids	"Ceramide (d18:1,C20:0)"	0,15	0,08
Sphingolipids	"Ceramide (d18:1,C21:0)"	0,25	0,19
Sphingolipids	"Ceramide (d18:1,C22:0)"	0,14	0,10
Sphingolipids	"Ceramide (d18:1,C22:1)"	0,28	0,15
Sphingolipids	"Ceramide (d18:1,C23:0)"	0,17	0,09
Sphingolipids	"Ceramide (d18:1,C24:0)"	0,20	0,11
Sphingolipids	"Ceramide (d18:1,C24:1)"	0,10	0,07
Sphingolipids	"Ceramide (d18:1,C24:2)"	0,13	0,05
Sphingolipids	"Ceramide (d18:2,C16:0)"	0,54	0,25
Sphingolipids	"Ceramide (d18:2,C18:0)"	0,32	0,13
Sphingolipids	"Ceramide (d18:2,C22:0)"	0,13	0,11
Sphingolipids	"Ceramide (d18:2,C23:0)"	0,18	0,11
Sphingolipids	"Ceramide (d18:2,C24:0)"	0,16	0,19
Sphingolipids	"Ceramide (d18:2,C24:1)"	0,26	0,15
Sphingolipids	"Ceramide (d18:2,C24:2)"	0,24	0,11
Sphingolipids	Sphingomyelin (d32:1)	4,48	3,89
Sphingolipids	Sphingomyelin (d32:2)	7,10	7,07
Sphingolipids	Sphingomyelin (d33:1)	5,78	3,55
Sphingolipids	Sphingomyelin (d34:0)	3,50	2,14
Sphingolipids	Sphingomyelin (d34:1)	4,29	1,57
Sphingolipids	Sphingomyelin (d34:2)	13,00	7,20
Sphingolipids	Sphingomyelin (d35:1)	4,94	2,80
Sphingolipids	Sphingomyelin (d35:2)	9,42	7,05
Sphingolipids	Sphingomyelin (d36:1)	1,92	1,07
Sphingolipids	Sphingomyelin (d36:2)	7,40	3,67
Sphingolipids	Sphingomyelin (d36:3)	2,49	1,87
Sphingolipids	Sphingomyelin (d37:1)	7,50	3,55
Sphingolipids	Sphingomyelin (d38:1)	0,71	0,33
Sphingolipids	Sphingomyelin (d38:2)	1,68	1,09
Sphingolipids	Sphingomyelin (d39:1)	4,76	1,91
Sphingolipids	Sphingomyelin (d40:1)	1,04	0,57
Sphingolipids	Sphingomyelin (d40:2)	2,43	1,68
Sphingolipids	Sphingomyelin (d41:1)	0,76	0,41
Sphingolipids	Sphingomyelin (d41:2)	3,42	1,30
Sphingolipids	Sphingomyelin (d42:1)	0,99	0,46
Sphingolipids	Sphingomyelin (d42:2)	1,60	0,84
Unknown	Unknown lipid (849590045)	2,37	1,06
Unknown	Unknown lipid (849590046)	0,63	0,30
Unknown	Unknown lipid (849590126)	0,62	0,22
Unknown	Unknown lipid (849590171)	11,16	5,71
Unknown	Unknown lipid (849590204)	0,22	0,06
Unknown	Unknown lipid (849590225)	0,30	0,07
Unknown	Unknown lipid (849590328)	2,11	2,05
Unknown	Unknown lipid (849590409)	1,09	0,80

Unknown	Unknown lipid (849590412)	0,76	0,74
Unknown	Unknown lipid (849590414)	0,66	3,02
Unknown	Unknown lipid (849590417)	1,02	0,40
Unknown	Unknown lipid (849590422)	0,56	0,13
Unknown	Unknown lipid (849590423)	0,48	1,27
Unknown	Unknown lipid (849590425)	0,67	0,31
Unknown	Unknown lipid (849590430)	0,51	0,54
Unknown	Unknown lipid (849590431)	0,55	0,17
Unknown	Unknown lipid (849590432)	0,45	0,20
Unknown	Unknown lipid (849590434)	0,23	0,09
Unknown	Unknown lipid (849590435)	0,12	0,12
Unknown	Unknown lipid (849590436)	0,26	0,30
Unknown	Unknown lipid (849590437)	0,36	0,25
Unknown	Unknown lipid (849590438)	0,17	0,10
Unknown	Unknown lipid (849590439)	0,12	0,13
Unknown	Unknown lipid (849590441)	0,57	2,44
Unknown	Unknown lipid (849590442)	0,25	0,15
Unknown	Unknown lipid (849590443)	0,30	0,27
Unknown	Unknown lipid (849590444)	0,41	0,28
Unknown	Unknown lipid (849590445)	0,18	0,08
Unknown	Unknown lipid (849590446)	0,20	0,09
Unknown	Unknown lipid (849590448)	0,24	0,16
Unknown	Unknown lipid (849590449)	0,13	0,10
Unknown	Unknown lipid (849590450)	0,20	0,10
Unknown	Unknown lipid (849590451)	0,21	0,24
Unknown	Unknown lipid (849590452)	0,12	0,15
Unknown	Unknown lipid (849590454)	4,18	1,38
Unknown	Unknown lipid (849590455)	11,55	8,55
Unknown	Unknown lipid (849590456)	1,04	0,60
Unknown	Unknown lipid (849590457)	1,12	0,82
Unknown	Unknown lipid (849590458)	4,92	3,43
Unknown	Unknown lipid (849590459)	5,48	3,57
Unknown	Unknown lipid (849590462)	23,36	17,78
Unknown	Unknown lipid (849590463)	0,94	0,39
Unknown	Unknown lipid (849590464)	2,01	1,48
Unknown	Unknown lipid (849590465)	0,24	0,10
Unknown	Unknown lipid (849590466)	1,92	1,20
Unknown	Unknown lipid (849590467)	0,19	0,06
Unknown	Unknown lipid (849590468)	0,60	0,33
Unknown	Unknown lipid (849590469)	0,34	0,11
Unknown	Unknown lipid (849590470)	3,20	1,51
Unknown	Unknown lipid (849590472)	3,23	2,16
Unknown	Unknown lipid (849590473)	0,74	0,36
Unknown	Unknown lipid (849590474)	1,01	1,02
Unknown	Unknown lipid (849590475)	1,28	1,14
Unknown	Unknown lipid (849590476)	2,66	4,25

Unknown	Unknown lipid (849590478)	2,18	1,83
Unknown	Unknown lipid (849590479)	1,88	2,08
Unknown	Unknown lipid (849590480)	4,44	3,13
Unknown	Unknown lipid (849590481)	5,36	3,81
Unknown	Unknown lipid (849590482)	0,98	0,30
Unknown	Unknown lipid (849590483)	0,46	0,11
Unknown	Unknown lipid (849590484)	1,38	0,71
Unknown	Unknown lipid (849590485)	0,64	0,22
Unknown	Unknown lipid (849590486)	1,04	0,66
Unknown	Unknown lipid (849590487)	2,70	1,29
Unknown	Unknown lipid (849590488)	2,98	0,94
Unknown	Unknown lipid (849590489)	2,97	2,05
Unknown	Unknown lipid (849590490)	1,39	0,56
Unknown	Unknown lipid (849590491)	0,14	0,08
Unknown	Unknown lipid (849590499)	0,20	0,09
Unknown	Unknown lipid (849590500)	1,01	1,82
Unknown	Unknown lipid (849590502)	1,60	0,68
Unknown	Unknown lipid (859590013)	4,07	6,30
Unknown	Unknown lipid (859590071)	0,27	0,27
Unknown	Unknown polar (869590388)	1,36	7,54
Unknown	Unknown polar (869590390)	3,60	8,92
Unknown	Unknown polar (869590395)	1,09	3,32
Unknown	Unknown polar (869590398)	1,05	6,18
Unknown	Unknown polar (869590400)	4,78	8,99
Unknown	Unknown polar (869590402)	0,63	2,07
Unknown	Unknown polar (869590406)	5,91	7,56
Unknown	Unknown polar (869590417)	4,43	17,60
Unknown	Unknown polar (869590419)	6,93	288,21
Unknown	Unknown polar (869590424)	5,05	9,05
Unknown	Unknown polar (869590431)	84,37	222,75
Unknown	Unknown polar (869590432)	7,39	11,25
Unknown	Unknown polar (869590442)	1,36	4,32
Unknown	Unknown polar (869590444)	2,56	27,36
Unknown	Unknown polar (869590452)	0,71	0,85
Unknown	Unknown polar (869590453)	0,89	0,30
Unknown	Unknown polar (869590456)	5,04	10,43
Unknown	Unknown polar (869590459)	1,06	1,11
Unknown	Unknown polar (879590072)	2,46	7,18
Unknown	Unknown polar (879590074)	14,27	171,27
Unknown	Unknown polar (879590076)	1,01	0,79
Unknown	Unknown polar (879590407)	1,37	1,64
Unknown	Unknown polar (879590422)	0,88	3,95
Unknown	Unknown polar (879590425)	0,80	0,54
Vitamins, cofactors and related	"5,6,7,8-Tetrahydrobiopterin"	5,16	18,33
Vitamins, cofactors and related	"Nicotinamide adenine dinucleotide phosphate, reduced (NADPH)"	2,09	2,37

Vitamins, cofactors and related	"Nicotinamide adenine dinucleotide, reduced (NADH)"	0,25	0,04
Vitamins, cofactors and related	alpha-Tocopherol	0,35	0,13
Vitamins, cofactors and related	beta-Carotene	0,24	0,16
Vitamins, cofactors and related	Coenzyme Q10	0,18	0,07
Vitamins, cofactors and related	Coenzyme Q7	0,59	0,37
Vitamins, cofactors and related	Coenzyme Q9	0,12	0,16
Vitamins, cofactors and related	Folic acid	8,23	11,33
Vitamins, cofactors and related	gamma-Tocopherol	0,43	0,55
Vitamins, cofactors and related	Glutathione (GSH)	0,47	0,65
Vitamins, cofactors and related	Glutathione disulfide (GSSG)	1,12	0,86
Vitamins, cofactors and related	Nicotinamide	7,59	12,45
Vitamins, cofactors and related	Nicotinamide adenine dinucleotide phosphate (NADP)	1,15	1,76
Vitamins, cofactors and related	Pantothenic acid	16,39	28,57
Vitamins, cofactors and related	Pyridoxal	3,42	5,95
Vitamins, cofactors and related	Pyridoxamine	1,42	1,82
Vitamins, cofactors and related	Thiamine	9,54	15,09

Chapter 5: final discussion, outlook and conclusions

Toxicology has its origins in the millenary practice of exploring the use of poisons. Over the time, industrialization brought about the mass manufacturing and commercialization of numerous chemicals which resulted in the further development of the toxicology field into the study of the adverse effects of chemicals and physical agents on living organisms (Klaassen and Amdur 2013). Nowadays, toxicology has been commissioned with the major task of providing relevant data for the protection of the human population and environment by evaluating potential risks posed by any commercialized substance (Greim and Snyder 2018). Consequently, toxicological studies are not only a mandatory but also a decisive step in chemical and drug developmental pipelines (OECD 1997).

The low throughput, high costs, limited predictivity and ethical concerns related to traditional animal-based toxicity studies evidenced a need for a fundamental change in toxicology. In 2007, a vision and roadmap for toxicity testing in the 21st century was proposed by the US National institute of science (National Research Council 2007). This vision called for the modernization of the field of toxicology through the implementation of recent technological advances and the development of human-centered *in vitro* methods, *in silico* models and high throughput systems that allow to expand the understanding of cellular and molecular mechanisms that lead to adverse effects. The progress since then is remarkable; numerous alternative methods, currently addressed as “*New Approach methodologies*” (NAMS), comprising *in vitro* cell based, *in silico* computational models and *Omic*s technologies, have been developed, validated, and incorporated in toxicity assessment (Hartung 2019; Krewski et al. 2020b; Leist et al. 2012; Prior et al. 2019). However, the increasing number and complexity of compounds (e.g., formulations, nanomaterials, polymers) and their formulations together with the increasing implementation of more demanding regulations, indicate the current need to develop innovative, reliable, cost effective and high throughput methods that can be incorporated not only in hazard identification and characterization,

which has been and continues to be the main use of NAMs, but also to advance its use in regulatory safety assessment (Ball et al. 2022). A strategy for integrating NAMs-generated data into safety decision-making, known as next generation risk assessment (NGRA), has been proposed (EPA 2014). NGRA is defined as an exposure-led, hypothesis driven risk assessment approach that integrates *in silico* and *in vitro* approaches with the aim of preventing potential harms. This strategy is meant to be conducted in a tiered and iterative approach, starting from a thorough evaluation of all the available data, followed by the implementation of relevant methodologies and testing strategies (Dent et al. 2021). Specific examples showing the successful application of NAMs to meet regulatory requirements have been recently presented (Stucki et al. 2022).

Multiparametric Omics technologies offer the advantage over conventional *in vitro* testing of the simultaneous measurement of multiple endpoints, delivering a comprehensive picture of an organism response upon a substance exposure (Mortimer et al. 2022; Nguyen et al. 2022). In particular, metabolomics represents the last step of the Omics cascade, measuring downstream molecular events closer to the organism phenotype (Fiehn 2002). The use of this technique has been successfully explored for toxicity assessment showing immense potential in diverse applications such as hazard (or adverse outcome) identification (Kamp et al. 2012; Kleinstreuer et al. 2011; Mattes et al. 2014; Van Ravenzwaay et al. 2015), chemical grouping to inform biologically based read-across of toxicity (Jacques et al. 2021; Van Ravenzwaay et al. 2016) and identifying metabolic points-of-departure (Crizer et al. 2021a; Malinowska et al. 2023). However, there are still challenges that hamper the expansion of metabolomics beyond a research tool to a feasible and implementable technology for toxicology assessment in industrial settings.

The aim of this dissertation was to tackle three of the major challenges for the implementation of metabolomics in order to advance its widespread application in toxicology. The first challenge addressed in this work was the restrictive high cost and low throughput of *in vitro* metabolomics. In chapter 2, the development and proof of concept of a technical feasible and economically effective targeted LC-MS/MS *in vitro* metabolomics platform for the characterization of hepatotoxicity was presented. In this work, the reduction of biomass quantity was a critical step to increase the throughput and consequently different key parameters of an *in vitro* test such as cell seeding density, passage number, cytotoxicity

testing, sample preparation, metabolite extraction, analytical method, and data processing were optimized and standardized to perform with low biomass samples in 96-well plate format using the liver hepatocarcinoma HepG2 cell line. The system was tested with 7 substances exhibiting previously known MoAs. The results showed dose responses of the metabolic effects, differentiation between liver toxicity MoAs and the identification of markers indicative of general liver toxicity as well as specific metabolite patterns for each MoA.

Noteworthy, this approach was one of the first high throughput *in vitro* metabolomics methods to be developed for the identification of potential toxicities and MoA, opening the possibility of using this technique in the chemical and pharmaceutical industry to screen large numbers of compounds in a cost effective and high throughput manner. Identifying MoA during early stages of compound development represents important economical, public health and animal welfare implications (Meigs et al. 2018). Timely terminating the development of a compound with a non-favorable toxicological profile represents immense time and resources savings (“fail early fail cheap”) and could prevent unwanted health effects (Krystal et al. 2019). In addition, understanding the MoA as a base to perform compound prioritization, direct more targeted studies and to assess human relevance (Ball et al. 2022; Olesti et al. 2021). The use of MoA classification for read-across approaches provides an important opportunity to the reduction of animal testing and accelerate the data generation of already commercialized compounds that lack toxicological information (Hartung 2009). These factors are critical for reaching the goal of the EU's chemicals strategy for sustainability towards a toxic-free environment (chemical strategy towards sustainability COM/2022).

The system presented in chapter 2 is readily implementable and is currently in use by BASF SE in the context of the European (EU-TOX RISK) and German (SysBioTopMoving, BMBF) funded projects.

The proof of concept for this assay was performed with seven substances, representative of three different liver toxicity MoAs. Even though consistent patterns of metabolite changes per MoA were identified, they were built based on only three compounds per MoA and in the case of liver enzyme inhibition, only one compound was used (ketoconazole). Therefore, these patterns need to be further validated and refined by testing more substances

representatives of each of the tested MoA. The next step would be to expand the number of tested compounds and diversify the MoAs in order to create and validate different patterns. Generated metabolomics patterns can be stored in a database which would allow to compare toxicological profiles for MoA classification and prediction. Thus, following the metabolome testing of a new compound, statistical techniques such as a PCA or a hierarchical clustering analysis can be used to compare the metabolome profile with that of a reference compound in order to identify the probable MoA. This type of database would also offer the possibility of biological-based read across analysis (Van Ravenzwaay et al. 2016). For the last 15 years, such an *in vivo* plasma-based metabolomics database for toxicological MoAs identification and prediction has been developed by BASF SE (MetaMapTox®)(Van Ravenzwaay et al. 2015). Building a large database with the presented 96-well plate *in vitro* system would be much faster and would represent significantly lower costs. This system can be automated by the use of robots, which would grant the parallel and rapid testing of numerous compounds, resulting in a large dataset with increased power of prediction.

This study was carried out by a targeted metabolomics method, which allows to measure a pre-defined set of metabolites with high confidence and accuracy and therefore less features are identified in comparison with untargeted metabolomics methods, in which thousands of features, covering a broad range of metabolites are detected. Untargeted metabolomics allows to obtain an extensive overview of the test compound's effect on the organism serving as a hypothesis-generating tool. Yet, analyte annotation is a tedious and challenging process which hampers the detailed mechanistic interpretation of the effects (Olesti et al. 2021). In this dissertation, through a targeted approach, 220 to 260 metabolites were identified with high confidence by their analytical parameters: polarity (lipid vs polar), MRM transition (m/z ratios), and retention time. Measuring analytes with previously known identity offered readily mechanistically interpretable data that served to understand the effect of the compound in the system and thus was key for establishing confidence in the use of metabolomics technologies in toxicology. However, the combination of both strategies represents a powerful approach that can be used for both, the identification and extensive characterization of mechanisms of toxicity. An initial untargeted analysis can be performed to gain a global overview that can be expanded by a following targeted approach directed to

obtain more detailed and quantitative information of more specific pathways of interests (Garcia-Calvo et al. 2020).

One of the critical factors that allowed to achieve lowering the costs of this assay was the selection of LC-MS/MS as the unique chromatography-mass spectrometry technique. Previous developments were based on the combination of both GC-MS and LC-MS techniques in order to achieve a broad metabolite coverage of different compound classes (Ramirez et al. 2018b). Recent advances in next generation LC-MS technologies, have broaden its coverage allowing to detect a wide range of molecule classes (Danne-Rasche et al. 2018; Dubuis et al. 2018; Malinowska et al. 2022b; Walvekar et al. 2018). By performing exclusively LC-MS chromatography (HILIC for polar metabolites and RP optimized for lipid species), the sample extraction was facilitated, only one sample aliquot was needed, which reduces the necessary amount of initial biomass, and eliminated the need for compound derivatization characteristic of GC approaches (Littlewood 2013). These factors enabled the assembly of a high throughput, relatively simple to perform, and cost-effective system. However, lipid metabolites accounted for 75% of the total measured features, indicating that the detection of polar metabolites was limited. Polar metabolites such as those in central carbon metabolism, play an important role in normal growth and development and are fundamental components of metabolic pathways essential for survival (Noor et al. 2010). Thus, changes in polar metabolites could be important indicatives of adverse outcomes. Therefore, even though a good MoA separation by means of PCA was achieved, the future inclusion of different metabolites that currently lack representation would expand the mechanistic understanding offered by the system.

In 2021, funded by the European Chemicals Agency, a large systematic review of multiple toxicological resources was conducted, generating a list of 722 metabolite biomarkers that have toxicological relevance (called MTox700+)(Sostare et al. 2022). It was suggested that the metabolomics community should attempt to measure as many of the MTox700+ metabolites as possible, to identify them confidently, and report their relative quantitative changes in response to chemical exposure, as this will increase the metabolic knowledge associated with the panel and increase its ability to predict downstream biological effects (Sostare et al. 2022). The MTox700+ list can serve as a future guide to expand the metabolite coverage in the 96-well plate *in vitro* metabolomics system presented in this dissertation. More specifically, the

method could potentially be improved by optimizing the HILIC protocol as shown by (Gerdemann et al. 2022), by adding pre-column derivatization steps (Walvekar et al. 2018) or by implementing an additional method for energy metabolism metabolites (Balcke et al. 2011). However, it is important to mention that additional sample preparations and the need of different aliquots would increase the experimental time and cost.

The limited measurement of polar metabolites and the lack of unique identifiers for different lipid species in public databases (e.g., KEGG database) (Kanehisa 2002), hampered the application of a representative pathway analysis pointing out the substantial underrepresentation of lipid species in public repositories.

Importantly, there are two factors that can cause differences in metabolite levels in *in vitro* metabolomics assays; the first factor is related to variations in the cell numbers in each sample and the second one originates from an actual treatment-related metabolic effect. Therefore, in order to account for differences in cell numbers obtained during harvesting, the normalization procedure is a critical step in cell-based assays (Cuykx et al. 2018b). This is specially challenging for miniaturized metabolomics studies where sample perturbations and biomass losses must be avoided. In the presented LC-MS *in vitro* metabolomics assay, a statistical normalization to the median of all covered metabolites values for each sample was applied. The Sample Analyte Median (SAM) normalization strategy presents the advantage of not requiring additional experiments. Additionally, the median can be determined in the measured sample rather than a sister culture as is typically done in *in vitro* metabolomics studies, where protein quantification is measured in a parallel plate (Cuykx et al. 2018b). However, the SAM normalization assumes that around 50% of the total measured metabolites are unchanged and therefore, the median of all analytes would only be influenced by differences in the cell numbers. This strategy performs well at subtoxic ranges where the effect on the metabolome is relatively mild, however, at higher concentrations (e.g., EC₅₀ and EC₈₅) where more than 50% of the metabolites are expected to change in some degree, this strategy might not be able to fully compensate for the cell number differences. In these concentrations, due to the very high signal density caused by the strong substance effect on the metabolome, the SAM normalization process assumes a higher cell number, resulting in a higher correction factor that attenuates the effect outcome. In these cases,

normalization to the cell confluence, monitored by real-time imaging analysis can be implemented in order to fully correct for differences arising from cell numbers.

Even though it poses some limitations, the SAM normalization procedure offers practical advantages and was found suitable for reducing the variability due to differences in the cell number even in the high tested concentrations (chapter 2). In order to test the suitability of the SAM normalization for the developed *in vitro* metabolomics platform, the effect of applying a biomass-normalization procedure was tested in an experiment performed with different cell seeding densities (Chapter 2, Suppl. Fig. 2). After applying SAM correction, the variability explained in the PC1, corresponding to differences in cell numbers, was reduced to almost half (from 83.5% in the unnormalized PCA to 48% after normalization). In addition, after normalization the major contributor for the variability in the PC1 was the group corresponding to 5,000 seeded cells. As shown in the manuscript Fig 1b, these cells showed a drastically reduced cell growth and therefore this group is expected to be physiologically different than the cells from higher cell seeding densities. These results suggest that after normalization, biological differences originating from the cell-growth are the drivers for separation in the PCA and are not compensated by solely the cell-number normalization. However, the PCA loadings of the unnormalized data are skewed, evidencing a systematic effect in the PCA, most likely due the differences on the cell numbers. After SAM normalization, the loading plots show a spread of the data points, suggesting that the normalization procedure was able to eliminate the systematic quantitative effect and the quality of the data was improved. Therefore, acknowledging the limitations of the procedure, the SAM normalization offered practical advantages and showed to correct (to some extent) the differences caused by cell numbers and importantly it was useful for reducing the variability of the data due to differences in cell number even in the high tested concentration. Current strategies, including the improvement of the SAM normalization and the inclusion of cell confluence data for the normalization procedure are being evaluated by the BASF's metabolome research group.

One of the main limitations of this assay is the use of an immortalized cell line such as HepG2. This human cell line has been widely used for toxicity studies since it is easy to handle, readily available and highly reproducible. Importantly, it retains differentiated hepatic functions such as the synthesis and secretion of plasma proteins, cholesterol and TG metabolism, lipoprotein

metabolism and transport, bile acid synthesis, glycogen synthesis insulin signaling and important pathways such as the ones related to cell cycle regulation and apoptosis are also present (Guo et al. 2011; Jennen et al. 2010). However, the HepG2 cell line expresses low levels of phase I and phase II metabolism enzymes (Gerets et al. 2012; Hart et al. 2010). Thus, compounds requiring metabolic activation to exert its MoA like acetaminophen (CYP2E1)(Lee et al. 1996) or nitro benzodiazepines (CYP3A4) (Mizuno et al. 2009) may not be accurately detected by this assay, due to the low expression of these enzymes in HepG2 cells (Ramirez et al. 2018b). This limitation can be overcome by genetically modifying HepG2 cells for expressing cytochrome P450 enzymes. In addition, the HepG2 presents lower expression of different nuclear receptors (Tolosa et al. 2016). Therefore, compounds like phenobarbital, which acts via activation of CAR and PXR receptors, might not display the complete toxicological profile compared to the *in vivo* situation. Different strategies to manipulate the gene expression of multiple CYPs enzymes and transporter in HepG2 cells have been described and could be applied to the presented platform to expand its applicability domain (Kwon et al. 2014; Negoro et al. 2022; Xuan et al. 2016). Acknowledging their metabolic limitations, the HepG2 cell lines still represents a valid alternative for initial compound high throughput screening and, as it was shown with this work, is a suitable model for early stages of hepatotoxicity characterization. In the future, preserving the same experimental workflow, HepG2 cells can be replaced by metabolically competent cells such as HepaRG cells or hiPSCs.

Liver toxicity is a leading systemic toxicity of drugs and chemicals demanding more human-relevant, high throughput, cost effective *in vitro* solutions (Onakpoya et al. 2016). Therefore, this dissertation focused on the development of assays for hepatotoxicity testing. However, the workflow described here can be implemented with different cell types, including hiPSCs to screen for different organ toxicities.

Metabolomics *in vitro* has been implemented as a research tool for toxicological assessment and hazard characterization, however, the application of metabolomics data in regulatory toxicology for risk assessment has been limited to date. Related to the high number of low volume chemicals that still need to be tested under REACH, there are indications that regulatory frameworks may open up to consider NAMs such as omics techniques data in risk assessment (Ball et al. 2022; Westmoreland et al. 2022). Due to low throughput and cost limitations, metabolomics *in vitro* assays are usually done only in few concentrations,

hindering the calculation of meaningful dose response metrics and consequently limiting the applicability of *in vitro* systems in risk assessment (Olesti et al. 2021). By escalating the throughput, the developed 96-well-plate LC-MS/MS-based *in vitro* metabolomics system allowed to test five different concentrations, covering key points of the dose response curve from very mild effects to overt toxicity, opening the possibility to derive important metrics, such as point of departure, essential for extrapolating *in vitro* results for human risk assessment.

The second aim of this dissertation was to expand the use of *in vitro* metabolomics beyond simply hazard identification, to its implementation for deriving dose- and time response metrics that could be used for PoD estimations for human risk assessment. Therefore, in chapter 3, the developed LC-MS/MS-based *in vitro* metabolomics assay was employed to study metabolic dose- and time-response dynamics of the antibiotic nitrofurantoin. In this study, a mechanistic-anchored approach to derive and interpret dose and time response metrics from metabolomics data was proposed.

It has been shown that the activation of cellular stress response exhibits unique temporal- and concentration-dependent patterns for different hepatotoxic model compounds (Wijaya et al. 2021). In chapter 3, the effect of each tested of the five tested nitrofurantoin concentration was evaluated at four different time points. The mechanistic information offered by the assay allowed to track the differential activation of cellular pathways as potential indicators of early adaptive and hepatotoxic responses. This is particularly important since one of the major challenges of implementing NAM's in risk assessment has been and still is, the differentiation of adaptive changes from adverse effects (Olesti et al. 2021). The intrinsic sensitivity of Omics techniques to capture even subtle changes, has posed a major challenge to define adversity. At what point do biological changes become so severe to produce an adverse outcome? Answering this often involves the investigation of multiple endpoints at multiple time-points to understand the progression of different key events along an AOP (Buesen et al. 2017). Therefore, the high throughput nature of the developed *in vitro* metabolomics assay, leveraged here to explore the concentration response and the temporal dimension opens the possibility, as shown in chapter 3, of using of this type of data for understanding the transition from adaptive to adverse effects and for a more quantitative applications of metabolomics in risk assessment. Noteworthy, further analyses are required

to clearly define adversity in terms of Omics techniques. Recently, ECETOC has published a paper on their workshop about Omics threshold on non-adversity with particular emphasis on the determination of PoD (Gant et al. 2023).

For molecular POD determination, there is no current consensus on best practices. Global metabolite changes as estimated by principal component analysis (PCA) exhibit exposure concentration dependency as shown in chapter 2 and 3. Therefore, after confirming the mechanistic relevance of the data, an alternative way to derive metabolomics-based PoD by PCA using the whole set of measured metabolite profiles was proposed. The use of metabolomics for deriving PoD has recently started to be explored mainly with untargeted metabolomics data through the use of benchmark dosing applied to single metabolic features (Crizer et al. 2021b; Malinowska et al. 2023). The PCA-based approach proposed in this dissertation, presents several advantages over the previously proposed methodologies in the literature. First, instead of single features, it allows to obtain values from the entire dataset. In addition, targeted metabolomics approaches allow to derive PoDs that can be mechanistically anchored to established key events and adverse outcome pathways can be identified. Finally, this information can help in the distinction between non adverse (adaptive) responses and adverse effects. The variation in the PC1 was mainly driven by the different tested concentrations, particularly the highest applied concentration, which was in the cytotoxic range and as such is likely to represent an element of adversity. Therefore, investigating a set of metabolites that could be predictive for adversity grant further investigations. In addition, the dimensions of the PCA are potentially driven by differential effects (e.g. MoA related, toxicity, adversity), thus analysis directed to decipher the nature of the effects in the main principal components such as PC1, PC2 and PC3 can help to further understand the transition between adaptive and toxic responses.

In the PoD derivation approach proposed in chapter 3, a 95% confidence interval of the control samples variability was selected for defining the PoD. A 90% confidence interval has been frequently employed in the literature for the definition of a benchmark concentration. A benchmark response of 10% is the approach currently being used in standard toxicology dose–response analyses (Johnson et al. 2014). Since Omics technologies are highly sensitive, in this work, a 95% threshold was selected to provide a conservative PoD. Future studies that perform a systematic comparison of different cut-off values (e.g., 90%, 95%) with a bigger set

of test substances are needed to clearly define the most suitable approach for PoD derivation using metabolomics data.

Deriving PoDs from *in vitro* dose response data is the first step to obtain reference values for human risk assessment. Therefore, in order to evaluate the relevance of the data obtained here, the calculated PoD value need to be further transformed by means of *in vitro* to *in vivo* extrapolation (IVIVE) models (Wilk-Zasadna et al. 2015). For this, substance specific data on the pharmacokinetics parameters absorption, distribution, metabolism, and excretion (ADME), such as hepatic clearance and protein binding, derived from experiments or prediction models are needed. In addition, kinetic data and physicochemical properties of the test substance need to be integrated as input parameters for the so-called reverse-dosimetry by Physiologically Based Toxicokinetic (PBTK) Modelling where the ADME characteristics of the target organism are included to finally predict tissue and plasma concentrations for the toxicological endpoint of interest (Louisse et al. 2017). Then, integrating the PBTK derived tissue or plasma concentration and the *in vitro* derived dose response analysis, the corresponding *in vivo* dose-response curves that are required for risk assessment can be calculated (Algharably et al. 2022). This analysis would be the next necessary step in order to evaluate the predictivity and accuracy of the method to describe reference values expressed in mg/kg bw. In addition, the study presented in chapter 3 was carried out with nitrofurantoin as a single model compound, in order to validate the proposed strategy, more substances need to be tested and evaluated.

Due to the high sensitivity of the method, using initial biological responses for risk assessment is a conservative approach which will not underestimate the characterization of hazard and can be used in a tiered approach. This tiered approach can start with the generation of concentration response metrics from Omics data in order to explore the perturbed pathways and potency of the compound. Based on the obtained information, more targeted *in vitro* methods can be further performed (Fang et al. 2020).

Importantly, the work presented in chapter 3 proposes a new workflow for PoD derivation that offers the possibility of integrating the global metabolic changes while obtaining mechanistic information that can be linked to AOPs and offer some insights into potential adversity. These factors serve to build trust in implementing metabolomics data in risk

assessment. In addition, data generated by sampling dynamic metabolomics across large sample cohorts with this assay, could significantly improve the data basis (e.g., on substance dynamics and kinetics) for computational models intended to be used for toxicological predictions. Moreover, evaluating different time points not only provides mechanistic temporal insights but is also valuable for the selection of relevant *in vitro* sampling time points for risk assessment.

Finally, the development of *in vitro* models that can better recapitulate human physiology and sensitivity to hepatotoxicants in combination with -omics technologies offer a powerful system to expand the investigation of organ toxicity. Therefore, in order to increase the applicability of the *in vitro* metabolomics data for more advanced studies (e.g., last stages of compound development), the third aim of this dissertation was to increase the human relevance of *in vitro* assays by implementing a system that more closely recapitulate the liver physiology and cell composition. In chapter 4, the application and evaluation of *in vitro* metabolomics in a hiPSCs-derived 3D liver organoid system was presented. The liver organoid was characterized by single cell RNA sequencing (scRNAseq), and immunostaining showing that approximately 80% of all cells identified were reflective of the three most common cell types found in human livers: hepatocytes, Stellate cells and endothelial cells. Furthermore, the hepatocytes were capable of producing urea and albumin at physiological equivalent levels when normalized for hepatocyte composition (Ballmer et al. 1990; Rudman et al. 1973).

The liver organoids were as well characterized with respect to alpha-1-fetoprotein expression (AFP), bulk RNA qPCR, and cytochrome P450 activity to estimate hepatocyte maturation. The AFP expression was comparable to the expression levels found in human development and microsomes generated from intact liver organoids showed a cytochrome P450 enzymatic turnovers comparable to commercially sourced microsomes. However, it is well known that hepatocytes derived from stem cells are generally fetal in their phenotype (Suter-Dick et al. 2015). Further studies to explore differences in ADME-related gene expression and compound bioavailability in the liver organoids in comparison to primary hepatocytes or human microsomes are still needed to estimate the full physiological similarity to mature human livers. As future step, different cytokines, growth factors and targeted mRNA expression can be used to enhance the complete maturation of the hiPSCs in the organoids (work in progress by the MIT scientists).

Following the characterization of the 3D hiPSCs-derived organoids, their suitability for toxicometabolomics studies was tested using bezafibrate as a model compound. Bezafibrate is a PPAR α agonist that has served as an internal quality control for the metabolomics studies at BASF SE. This compound exerts a pronounced metabolome effect and presents a well characterized MoA which exhibit species differences in humans and rodents (Reddy et al. 1980; Takafumi et al. 1989). Intracellular metabolites were extracted for semiquantitative targeted metabolite profiling via LC-MS/MS. Metabolomics and qPCR analysis on target genes showed clear metabolite and transcriptional changes consistent with the *in vivo* described bezafibrate MoA (Issemann and Green 1990).

Intracellular concentration-response changes were observed in lipid metabolism, beta oxidation of fatty acids, cholesterol metabolism, energy metabolism, amino acids and antioxidants. Here, we combined metabolite measurement with targeted gene expression analysis to better characterize the affected pathways and gain a comprehensive understanding of the effect of bezafibrate on the treated organoids. Analysis via qPCR of pathways that were considered responsible for the change in metabolic profile enabled more comprehensive understanding of bezafibrate treatment within the 3D organoid. Therefore, multi-Omics approaches can provide useful insights into the flow of biological information at multiple levels and thus can assist in unraveling the mechanisms underlying the toxicological effect (Subramanian et al. 2020).

In order to test the experimental and organoids reproducibility, the metabolomics experiments were carried out in two different batches comprising a total of 192 tested organoids. In addition to the intracellular metabolome, to confirm and quantify substance uptake by the organoids, the intracellular concentrations of bezafibrate were determined as well via mass-spectrometry. Although the same nominal concentration was applied, there was approximately a 6-fold difference in the intracellular bezafibrate concentrations between the two batches. Importantly, the observed biological responses directly correlated to the magnitude of the metabolites fold changes. Although these differences in intra-organoid bezafibrate concentrations were far from desirable, these results show the importance of measuring the intracellular concentrations of the test compounds in *in vitro* assays as a good practice. Obtaining estimations of whether the test compound reached the cells and in which quantity, is key for the correct interpretation of the results. Integrating metabolomics

technologies in *in vitro* studies offers the advantage of incorporating intracellular compound concentrations measurements without the need for additional experiments. Recent reports have highlighted the importance of extrapolating from the *in vitro* measured intracellular concentration and not from the nominal concentration to the tissue/organ concentration to come up with an appropriate QIVIVE for the relevant adverse effects (Algharably et al. 2022). These observations evidence the advantage of metabolomics experiments for extrapolating *in vitro* concentrations to *in vivo* values useful for risk assessment.

The exact reason of the observed differences in intracellular compound concentrations were not clear and require further examination. However, it evidences a batch-to-batch variation pointing towards a current limitation in the reproducibility of the organoids. Therefore, for the industrial use of these organoids efforts are required towards their standardization in order to ensure reproducible results.

One of the major disadvantages of 3D cultures is the limited perfusion. When vascularization is lacking, oxygen, nutrients and the compound to be tested have a limited flow into the interior of the organoid generating an anoxic environment that results in differences with an *in vivo* organ. In the presented 3D hiPSCs-derived organoids, the formation of vascular-like structures was observed. Future studies should be directed in order to fully characterize and further enhance the organoid vascularization.

Overall, the results provided in chapter 4 evidence that the tested 3D liver organoid system, in combination with transcriptomics and metabolomics, is capable of detecting human relevant changes associated with the mode of action of bezafibrate. For industrial screening purposes the system is not yet completely developed and further work on characterization, standardization, thorough validation and further *in vitro* to *in vivo* comparison is required before the system can be readily established. However, feasibility evaluations with microphysiological systems such as the one presented here, are highly valuable to identify areas of potential improvement, helping to move forward the establishment of this systems beyond basic research to applied industrial settings. The further development of this type of organoids, opens the possibility of implementing a physiologically relevant tool to understand mechanisms of action and evaluate hepatotoxicity. Combining these systems with

metabolomics and transcriptomics analysis, represents a valuable tool for the advanced toxicological studies within chemical and pharmaceutical development pipelines.

In summary, this dissertation has addressed three of the major challenges for the implementation of *in vitro* metabolomics in toxicology. In chapter 2, a highly standardized, high throughput *in vitro* metabolomics platform was developed and tested. Then, chapter 3 covered the application of the developed assay for substance dynamics over concentration and time and an alternative to calculate PoD for risk assessment was proposed. Finally, in chapter 4, a hiPSCs-derived liver organoid was developed and tested for its suitability in toxicometabolomics studies.

By advancing the applications of metabolomics in toxicology, this work has significantly contributed to the aim of toxicology of the 21st century for a human-relevant non-animal toxicological testing, supporting the toxicology endeavor of protecting human health and the environment. Consequently, the results developed in this dissertation ultimately contribute to the collective goal of granting that future generations, not only of humans, but also of all leaving species can benefit from a toxic free environment.

Acknowledgments

"...There are magical people. I promise you; I've seen them. They are hidden in all corners of the planet. Disguised as normal. concealing his special way of being. They seem to behave like others. That's why sometimes it's so hard to find them. But when you discover them there is no turning back. You can't get rid of his memory. Don't tell anyone, but they say their magic is so strong that if it touches you once, it touches you forever."

-Author unknown

First, I want to express my ever-growing gratitude to life. Thanks to a series of fortunate events that led me to a place 9,042 km from home, I have been honored with the task of through this work, contributing with my grain of sand towards the protection of not only our human fellows, but all the species that, together with us, cohabit our beautiful planet Earth.

From the more than 200 pages that compose this thesis, the following were perhaps the most difficult paragraphs to write, simply because the gratitude I feel towards the people that had been with me, challenging, supporting, empowering, believing, uplifting, motivating, and loving me throughout this journey, goes beyond any written language construction. To all the people I'm about to name: you have been truly a gift and a blessing.

First, I would like to start with my "Doktorvater" Prof. Dr. Bennard van Ravenzwaay, who believed in me from the beginning and gave me on the first place the opportunity to be here and to carry out this project. An excellent scientist, leader, businessman, pilot and chef. A life enthusiast and the exception to the rule that says that someone can't be good at everything. Ben, I have learned tremendously from you, from your scientific knowledge and from your contagious joy, positivity and humor. Thank you for seeing my potential, challenging me and guiding me relentlessly through every step of this journey. My deepest gratitude, admiration, respect and affection.

I would also like to express my gratitude and admiration to my main BASF supervisor, Dr. Barbara Birk, who from the day I arrived in Germany and started my PhD in her lab, in the middle of the lockdown and in times of uncertainty and fear, cared about me and made me

feel that I was not alone. Barbara, thank you from the bottom of my heart for being there always, for the countless hours you dedicated to guide and advise me, always in such a patient and gently way. I greatly admire the grace with which you carry out your role as leader, bringing up the best in people, making them feel valuable and heard. It was a pleasure and an honor working with and learning from you daily.

I am deeply grateful to my university supervisor Prof. Dr. Elke Richling, from the Rheinland-Pfälzische Technische Universität Kaiserslautern-Landau, who generously gave me the opportunity to work with her and has been always present, kindly guiding and supporting me through my project. Prof. Richling, thank you very much for always extending your hand whenever I needed it, for your insightful suggestions and for taking up the role of my supervision. I greatly appreciate it.

To Dr. Franziska Zickgraf who since she joined BASF as a Metabolome team leader and to the last page of this thesis, was present, helping me kindly and closely with anything I needed. Franziska, thank you for your constant support, scientific advice and interesting discussions. You are an example for young female leaders.

I would like to recognize the immense help I received from the members of the LABALT team. Andreas, Hans-Albrecht, Nadine, Carina and Shana, I will be always grateful for your support, for kindly teaching me cell culture methods, for your patient guide, skillful support with the experiments in the lab, and for the friendly and welcoming atmosphere you create in the team. You are a big part of this work.

Importantly, I would also like to thank Dr. Varun Giri, Dr. Volker Haake and Dr. Philipp Ternes, highly experience and skilled data analysts experts from the BASF's metabolome team, who supported and helped me tirelessly, spending hours of their time teaching me and explaining me all sort of things from statistics and mathematics to coding and data analysis. Thank you from the bottom of my heart, I wouldn't be able to be here without your support.

To all the members of the BASF metabolome team, a group of expert scientists from whom I had the honor of working with and learning from the past three and a half years. Thank you for your constant input and enriching discussions.

Acknowledgments

I am also thankful to Dr. Dorothee Funk-Weyer, the Vice President Experimental Toxicology and Ecology department at BASF, for her professional and personal advice and for her helpful input and comments in my publications and thesis.

My love gratitude and admiration also go to all the amazing people that are or were part of the Student Container. Specially to my dear friends Dunja, Aish, Andy, Alina, Pia, Luisa, Anastasia and Kosta. You brightened and lightened my days. I am so proud and grateful for the opportunity of sharing side by side, rowing in the same boat, this journey with such unique, funny, talented and smart people. I cherish your friendship and have witnessed your development and growth over the last years. I will be there, as you did with me, to celebrate each of your steps as my own: I want to see you shine.

To my Wednesday night chicas, whose friendship came during the locked down as an unexpected gift from life and showed me that the world is full of beautiful, talented, strong and loving women willing to support and encourage each other. Svenja, Miri, Lisa, Michi, Jenni, Irene, Meli, Katrin, Elif and Hannah, thank you for your refreshing friendship, for cheering me up during the difficult and stressful times, for making my weeks lighter, for being a safe place to learn and practice German, for leaving me feeling more alive after I am with you. Herzlichen dank.

To the Böhmer's, my new German family, who have warmly welcomed me and have given me the family atmosphere of love and emotional support that has been key to navigate my PhD time. Michael, Isa, Sophie and Chris, I am so blessed to become part of such a beautiful family.

I am forever grateful to my love and best friend, my life partner and future husband, who since the moment we met has tenaciously walked with me through every single step of this journey, giving me his hand, his shoulder and all of himself. Who during the last years has seen my best and my worse and has accompanied me like nobody else through my ups and downs. Who has been my rock and my lighthouse. Ulrik, you are the living, breathing proof of the infinite generosity of life.

Finally, and undoubtedly most important, my infinite gratitude and love is to my #1 fans, my parents, Migdonia and Luis Alfonso. Who believe in me like nobody else in the world, who have always supported and loved me unconditionally, who put my education as their absolute

Acknowledgments

priority, even before their own needs. Who from the distance, have witnessed and cherished every chapter of this work. Mami y papi, making you proud is my greatest reward. This is for you. Los amo.

References

- Abdullah R, Alhusainy W, Woutersen J, Rietjens IM, Punt A (2016) Predicting points of departure for risk assessment based on in vitro cytotoxicity data and physiologically based kinetic (PBK) modeling: the case of kidney toxicity induced by aristolochic acid I. *Food and chemical toxicology* 92:104-116
- Alexander-Dann B, Pruteanu LL, Oerton E, et al. (2018) Developments in toxicogenomics: understanding and predicting compound-induced toxicity from gene expression data. *Molecular omics* 14(4):218-236
- Algharably EA, Di Consiglio E, Testai E, Pistollato F, Mielke H, Gundert-Remy U (2022) In Vitro–In Vivo Extrapolation by Physiologically Based Kinetic Modeling: Experience With Three Case Studies and Lessons Learned. *Frontiers in Toxicology* 4:885843
- Almazroo OA, Miah MK, Venkataramanan R (2017) Drug metabolism in the liver. *Clinics in liver disease* 21(1):1-20
- Alseekh S, Aharoni A, Brotman Y, et al. (2021) Mass spectrometry-based metabolomics: a guide for annotation, quantification and best reporting practices. *Nature methods* 18(7):747-756
- Andersen ME, Krewski D (2009) Toxicity testing in the 21st century: bringing the vision to life. *Toxicological sciences* 107(2):324-330
- Andresen C, Boch T, Gegner HM, et al. (2022) Comparison of extraction methods for intracellular metabolomics of human tissues. *Frontiers in Molecular Biosciences* 9:826
- Ankley GT, Bennett RS, Erickson RJ, et al. (2010) Adverse outcome pathways: a conceptual framework to support ecotoxicology research and risk assessment. *Environmental Toxicology and Chemistry: An International Journal* 29(3):730-741
- Babai S, Auclert L, Le-Louët H (2021) Safety data and withdrawal of hepatotoxic drugs. *Therapies* 76(6):715-723
- Balcke GU, Kolle SN, Kamp H, et al. (2011) Linking energy metabolism to dysfunctions in mitochondrial respiration--a metabolomics in vitro approach. *Toxicol Lett* 203(3):200-9 doi:10.1016/j.toxlet.2011.03.013
- Ball N, Bars R, Botham PA, et al. (2022) A framework for chemical safety assessment incorporating new approach methodologies within REACH. *Archives of Toxicology* 96(3):743-766
- Ballmer P, McNurlan M, Milne E, et al. (1990) Measurement of albumin synthesis in humans: a new approach employing stable isotopes. *American Journal of Physiology-Endocrinology And Metabolism* 259(6):E797-E803
- Balzer W, Eleftheriadis A (1991) A reconstruction of the hippocratic humoral theory of health. *Journal for General Philosophy of Science* 22:207-227
- Basketter DA, York M, McFadden JP, Robinson MK (2004) Determination of skin irritation potential in the human 4-h patch test. *Contact Dermatitis* 51(1):1-4

References

- Beger RD, Sun J, Schnackenberg LK (2010) Metabolomics approaches for discovering biomarkers of drug-induced hepatotoxicity and nephrotoxicity. *Toxicol Appl Pharmacol* 243(2):154-66 doi:10.1016/j.taap.2009.11.019
- Bell SM, Chang X, Wambaugh JF, et al. (2018) In vitro to in vivo extrapolation for high throughput prioritization and decision making. *Toxicology in vitro* 47:213-227
- Bercu JP, Morinello EJ, Sehner C, Shipp BK, Weideman PA (2016) Point of departure (PoD) selection for the derivation of acceptable daily exposures (ADEs) for active pharmaceutical ingredients (APIs). *Regulatory Toxicology and Pharmacology* 79:S48-S56
- Beyoglu D, Idle JR (2013) The metabolomic window into hepatobiliary disease. *J Hepatol* 59(4):842-58 doi:10.1016/j.jhep.2013.05.030
- Bilzer M, Roggel F, Gerbes AL (2006) Role of Kupffer cells in host defense and liver disease. *Liver International* 26(10):1175-1186
- Bird IM (1989) High performance liquid chromatography: principles and clinical applications. *BMJ: British Medical Journal* 299(6702):783
- Birk B, Haake V, Sperber S, et al. (2021) Use of in vitro metabolomics in NRK cells to help predicting nephrotoxicity and differentiating the MoA of nephrotoxicants. *Toxicology Letters* 353:43-59
- Bischoff K, Mukai M, Ramaiah SK (2018) Liver toxicity *Veterinary toxicology*. Elsevier, p 239-257
- Bouhifd M, Hartung T, Hogberg HT, Kleensang A, Zhao L (2013) Review: toxicometabolomics. *J Appl Toxicol* 33(12):1365-83 doi:10.1002/jat.2874
- Bourdon-Lacombe JA, Moffat ID, Deveau M, et al. (2015) Technical guide for applications of gene expression profiling in human health risk assessment of environmental chemicals. *Regulatory Toxicology and Pharmacology* 72(2):292-309
- Bouwens L, De Bleser P, Vanderkerken K, Geerts B, Wisse E (1992) Liver cell heterogeneity: functions of non-parenchymal cells. *Enzyme* 46:155-155
- Brockmeier EK, Hodges G, Hutchinson TH, et al. (2017) The role of omics in the application of adverse outcome pathways for chemical risk assessment. *Toxicological Sciences* 158(2):252-262
- Buesen R, Chorley BN, da Silva Lima B, et al. (2017) Applying omics technologies in chemicals risk assessment: Report of an ECETOC workshop. *Regulatory Toxicology and Pharmacology* 91:S3-S13
- Carberry CK, Ferguson SS, Beltran AS, Fry RC, Rager JE (2022) Using liver models generated from human-induced pluripotent stem cells (iPSCs) for evaluating chemical-induced modifications and disease across liver developmental stages. *Toxicology in Vitro*:105412
- Castell JV, Jover R, Martinez-Jimnez CP, Gomez-Lechn MJ (2006) Hepatocyte cell lines: their use, scope and limitations in drug metabolism studies. *Expert opinion on drug metabolism & toxicology* 2(2):183-212
- Chang X, Tan Y-M, Allen DG, et al. (2022) IVIVE: facilitating the use of in vitro toxicity data in risk assessment and decision making. *Toxics* 10(5):232
- Chen G, Fan M, Liu Y, et al. (2019) Advances in MS based strategies for probing ligand-target interactions: Focus on soft ionization mass spectrometric techniques. *Frontiers in Chemistry* 7:703

References

- Council NR (2007) Applications of toxicogenomic technologies to predictive toxicology and risk assessment.
- Crawford SE, Hartung T, Hollert H, et al. (2017) Green toxicology: a strategy for sustainable chemical and material development. *Environmental Sciences Europe* 29(1):1-16
- Crizer DM, Ramaiahgari SC, Ferguson SS, et al. (2021a) Benchmark concentrations for untargeted metabolomics versus transcriptomics for liver injury compounds in in vitro liver models. *Toxicological Sciences* 181(2):175-186
- Crizer DM, Ramaiahgari SC, Ferguson SS, et al. (2021b) Benchmark Concentrations for Untargeted Metabolomics Versus Transcriptomics for Liver Injury Compounds in In Vitro Liver Models. *Toxicol Sci* 181(2):175-186 doi:10.1093/toxsci/kfab036
- Cuykx M, Claes L, Rodrigues RM, Vanhaecke T, Covaci A (2018a) Metabolomics profiling of steatosis progression in HepaRG® cells using sodium valproate. *Toxicology letters* 286:22-30
- Cuykx M, Rodrigues RM, Laukens K, Vanhaecke T, Covaci A (2018b) In vitro assessment of hepatotoxicity by metabolomics: a review. *Archives of Toxicology* 92(10):3007-3029
- Dalgaard L (2015) Comparison of minipig, dog, monkey and human drug metabolism and disposition. *Journal of pharmacological and toxicological methods* 74:80-92
- Danne-Rasche N, Coman C, Ahrends R (2018) Nano-LC/NSI MS refines lipidomics by enhancing lipid coverage, measurement sensitivity, and linear dynamic range. *Analytical chemistry* 90(13):8093-8101
- Davis AP, Wieggers TC, Johnson RJ, Sciaky D, Wieggers J, Mattingly CJ (2023) Comparative Toxicogenomics database (CTD): update 2023. *Nucleic acids research* 51(D1):D1257-D1262
- Davis JA, Gift JS, Zhao QJ (2011) Introduction to benchmark dose methods and US EPA's benchmark dose software (BMDS) version 2.1. 1. *Toxicology and applied pharmacology* 254(2):181-191
- De Graaf IA, Olinga P, De Jager MH, et al. (2010) Preparation and incubation of precision-cut liver and intestinal slices for application in drug metabolism and toxicity studies. *Nature protocols* 5(9):1540-1551
- De Hoffmann E, Stroobant V (2007) *Mass spectrometry: principles and applications*. John Wiley & Sons
- Dent M, Vaillancourt E, Thomas R, et al. (2021) Paving the way for application of next generation risk assessment to safety decision-making for cosmetic ingredients. *Regulatory Toxicology and Pharmacology* 125:105026
- Dettmer K, Nürnberger N, Kaspar H, Gruber MA, Almstetter MF, Oefner PJ (2011) Metabolite extraction from adherently growing mammalian cells for metabolomics studies: optimization of harvesting and extraction protocols. *Analytical and bioanalytical chemistry* 399:1127-1139
- Di Minno A, Gelzo M, Stornaiuolo M, Ruoppolo M, Castaldo G (2021) The evolving landscape of untargeted metabolomics. *Nutrition, Metabolism and Cardiovascular Diseases* 31(6):1645-1652
- Dix DJ, Houck KA, Martin MT, Richard AM, Setzer RW, Kavlock RJ (2007) The ToxCast program for prioritizing toxicity testing of environmental chemicals. *Toxicological sciences* 95(1):5-12
- Doll S, Burlingame AL (2015) Mass spectrometry-based detection and assignment of protein posttranslational modifications. *ACS chemical biology* 10(1):63-71

References

- Dooley JS, Lok AS, Garcia-Tsao G, Pinzani M (2018) *Sherlock's diseases of the liver and biliary system*. John Wiley & Sons
- Dubuis S, Ortmayr K, Zampieri M (2018) A framework for large-scale metabolome drug profiling links coenzyme A metabolism to the toxicity of anti-cancer drug dichloroacetate. *Communications biology* 1(1):1-11
- Dunn WB, Hankemeier T (2013) *Mass spectrometry and metabolomics: past, present and future*. vol 9. Springer, p 1-3
- Edwards SW, Tan Y-M, Villeneuve DL, Meek M, McQueen CA (2016) Adverse outcome pathways—organizing toxicological information to improve decision making. *Journal of Pharmacology and Experimental Therapeutics* 356(1):170-181
- EFSA, More SJ, Bampidis V, et al. (2022) Guidance on the use of the benchmark dose approach in risk assessment. *EFSA Journal* 20(10):e07584
- Eisler R (2000) *Handbook of chemical risk assessment: health hazards to humans, plants, and animals*, three volume set.
- EPA U (2014) *Next Generation Risk Assessment: Incorporation of Recent Advances in Molecular, Computational, and Systems Biology (Final Report)*. EPA/600/R-14/004. US EPA, Office of Research and Development, National Center for ...
- Fang W, Peng Y, Yan L, Xia P, Zhang X (2020) A tiered approach for screening and assessment of environmental mixtures by omics and in vitro assays. *Environmental Science & Technology* 54(12):7430-7439
- Farmahin R, Williams A, Kuo B, et al. (2017) Recommended approaches in the application of toxicogenomics to derive points of departure for chemical risk assessment. *Archives of toxicology* 91:2045-2065
- Fiehn O (2002) Metabolomics—the link between genotypes and phenotypes. *Functional genomics*:155-171
- Filipsson AF, Sand S, Nilsson J, Victorin K (2003) The benchmark dose method—review of available models, and recommendations for application in health risk assessment. *Critical reviews in toxicology* 33(5):505-542
- Food, Administration D (2009) *Drug-induced liver injury: premarketing clinical evaluation. Guidance for industry*
- Fritsche E, Haarmann-Stemmann T, Kapr J, et al. (2021) Stem cells for next level toxicity testing in the 21st century. *Small* 17(15):2006252
- Fujita T, Amuro Y, Hada T, Higashino K (1999) Plasma levels of pipercolic acid, both L- and D-enantiomers, in patients with chronic liver diseases, especially hepatic encephalopathy. *Clinica chimica acta* 287(1-2):99-109
- Gant T, Auerbach S, Von Bergen M, et al. (2023) *Applying genomics in regulatory toxicology: a report of the ECETOC workshop on omics threshold on non-adversity*. *Archives of Toxicology* doi:10.1007/s00204-023-03522-3
- Garcia-Calvo E, Machuca A, Nerín C, Rosales-Conrado N, Anunciação DS, Luque-Garcia JL (2020) Integration of untargeted and targeted mass spectrometry-based metabolomics provides novel insights into the potential toxicity associated to surfynol. *Food and Chemical Toxicology* 146:111849

References

- García-Cañaveras JC, Castell JV, Donato MT, Lahoz A (2016) A metabolomics cell-based approach for anticipating and investigating drug-induced liver injury. *Scientific reports* 6(1):1-12
- García-Cañaveras JC, Jimenez N, Gomez-Lechon MJ, Castell JV, Donato MT, Lahoz A (2015) LC-MS untargeted metabolomic analysis of drug-induced hepatotoxicity in HepG2 cells. *Electrophoresis* 36(18):2294-2302 doi:10.1002/elps.201500095
- Gerdemann A, Behrens M, Esselen M, Humpf H-U (2022) Metabolic profiling as a powerful tool for the analysis of cellular alterations caused by 20 mycotoxins in HepG2 cells. *Archives of toxicology* 96(11):2983-2998
- Gerets H, Tilmant K, Gerin B, et al. (2012) Characterization of primary human hepatocytes, HepG2 cells, and HepaRG cells at the mRNA level and CYP activity in response to inducers and their predictivity for the detection of human hepatotoxins. *Cell biology and toxicology* 28:69-87
- Goldberg S (2015) Mechanical/physical methods of cell distribution and tissue homogenization. *Proteomic Profiling: Methods and Protocols*:1-20
- Gomez-Lechon M, Donato M, Castell J, Jover R (2004) Human hepatocytes in primary culture: the choice to investigate drug metabolism in man. *Current drug metabolism* 5(5):443-462
- Gottmann E, Kramer S, Pfahringer B, Helma C (2001) Data quality in predictive toxicology: reproducibility of rodent carcinogenicity experiments. *Environmental health perspectives* 109(5):509-514
- Greim H, Snyder R (2018) *Toxicology and risk assessment: a comprehensive introduction*. John Wiley & Sons
- Griffiths WJ, Koal T, Wang Y, Kohl M, Enot DP, Digner HP (2010) Targeted metabolomics for biomarker discovery. *Angewandte Chemie International Edition* 49(32):5426-5445
- Gu X, Manautou JE (2012) Molecular mechanisms underlying chemical liver injury. *Expert reviews in molecular medicine* 14:e4
- Guijas C, Montenegro-Burke JR, Warth B, Spilker ME, Siuzdak G (2018) Metabolomics activity screening for identifying metabolites that modulate phenotype. *Nature biotechnology* 36(4):316-320
- Guo L, Dial S, Shi L, et al. (2011) Similarities and differences in the expression of drug-metabolizing enzymes between human hepatic cell lines and primary human hepatocytes. *Drug metabolism and disposition* 39(3):528-538
- Gwinn WM, Auerbach SS, Parham F, et al. (2020) Evaluation of 5-day in vivo rat liver and kidney with high-throughput transcriptomics for estimating benchmark doses of apical outcomes. *Toxicological Sciences* 176(2):343-354
- Hart SN, Li Y, Nakamoto K, Subileau E-a, Steen D, Zhong X-b (2010) A comparison of whole genome gene expression profiles of HepaRG cells and HepG2 cells to primary human hepatocytes and human liver tissues. *Drug metabolism and disposition* 38(6):988-994
- Hartung T (2008) Food for thought... on animal tests. *ALTEX-Alternatives to animal experimentation* 25(1):3-16
- Hartung T (2009) Toxicology for the twenty-first century. *Nature* 460(7252):208-212
- Hartung T (2018) Perspectives on in vitro to in vivo extrapolations. *Applied in vitro Toxicology* 4(4):305-316

References

- Hartung T (2019) Research and testing without animals: Where are we now and where are we heading? *Animal Experimentation: Working Towards a Paradigm Change*. Brill, p 673-687
- Hetz C, Papa FR (2018) The unfolded protein response and cell fate control. *Molecular cell* 69(2):169-181
- Huang J-W, Kuo C-H, Kuo H-C, Shih J-Y, Tsai T-W, Chang L-C (2021) Cell metabolomics analyses revealed a role of altered fatty acid oxidation in neurotoxicity pattern difference between nab-paclitaxel and solvent-based paclitaxel. *PloS one* 16(3):e0248942
- Idle JR, Gonzalez FJ (2007) Metabolomics. *Cell metabolism* 6(5):348-351
- Issemann I, Green S (1990) Activation of a member of the steroid hormone receptor superfamily by peroxisome proliferators. *Nature* 347:645-650
- Jacques C, Jamin EL, Jouanin I, et al. (2021) Safety assessment of cosmetics by read across applied to metabolomics data of in vitro skin and liver models. *Archives of Toxicology* 95(10):3303-3322
- Jennen DG, Magkoufopoulou C, Ketelslegers HB, van Herwijnen MH, Kleinjans JC, van Delft JH (2010) Comparison of HepG2 and HepaRG by whole-genome gene expression analysis for the purpose of chemical hazard identification. *Toxicological sciences* 115(1):66-79
- Jeon BK, Jang Y, Lee EM, Moon JH, Lee HJ, Lee DY (2021) A systematic approach to metabolic characterization of thyroid-disrupting chemicals and their in vitro biotransformants based on prediction-assisted metabolomic analysis. *Journal of Chromatography A* 1649:462222
- Johnson G, Soeteman-Hernández L, Gollapudi B, et al. (2014) Derivation of point of departure (PoD) estimates in genetic toxicology studies and their potential applications in risk assessment. *Environmental and molecular mutagenesis* 55(8):609-623
- Kamp H, Fabian E, Groeters S, et al. (2012) Application of in vivo metabolomics to preclinical/toxicological studies: case study on phenytoin-induced systemic toxicity. *Bioanalysis* 4(18):2291-2301
- Kanehisa M The KEGG database. In: 'In Silico' Simulation of Biological Processes: Novartis Foundation Symposium 247, 2002. vol 247. Wiley Online Library, p 91-103
- Karczewski KJ, Snyder MP (2018) Integrative omics for health and disease. *Nature Reviews Genetics* 19(5):299-310
- Kawano Y, Cohen DE (2013) Mechanisms of hepatic triglyceride accumulation in non-alcoholic fatty liver disease. *Journal of gastroenterology* 48:434-441
- Keller DA, Juberg DR, Catlin N, et al. (2012) Identification and characterization of adverse effects in 21st century toxicology. *Toxicological Sciences* 126(2):291-297
- Kiernan F (1833) XXIX. The anatomy and physiology of the liver. *Philosophical transactions of the Royal Society of London*(123):711-770
- King SM, Higgins JW, Nino CR, et al. (2017) 3D proximal tubule tissues recapitulate key aspects of renal physiology to enable nephrotoxicity testing. *Frontiers in physiology* 8:123
- Klaassen CD, Amdur MO (2013) *Casarett and Doull's toxicology: the basic science of poisons*, vol 1236. McGraw-Hill New York
- Kleinstreuer N, Smith A, West P, et al. (2011) Identifying developmental toxicity pathways for a subset of ToxCast chemicals using human embryonic stem cells and metabolomics. *Toxicology and applied pharmacology* 257(1):111-121

References

- Krewski D, Andersen ME, Tyshenko MG, et al. (2020a) Toxicity testing in the 21st century: progress in the past decade and future perspectives. *Archives of toxicology* 94(1):1-58
- Krewski D, Andersen ME, Tyshenko MG, et al. (2020b) Toxicity testing in the 21st century: progress in the past decade and future perspectives. *Archives of toxicology* 94:1-58
- Krystal AD, Pizzagalli DA, Mathew SJ, et al. (2019) The first implementation of the NIMH FAST-FAIL approach to psychiatric drug development. *Nature Reviews Drug Discovery* 18(1):82-84
- Kurz J, Parnham MJ, Geisslinger G, Schiffmann S (2019) Ceramides as novel disease biomarkers. *Trends in molecular medicine* 25(1):20-32
- Kwon SJ, Lee DW, Shah DA, et al. (2014) High-throughput and combinatorial gene expression on a chip for metabolism-induced toxicology screening. *Nat Commun* 5:3739
doi:10.1038/ncomms4739
- Lamers WH, Hilberts A, Furt E, et al. (1989) Hepatic enzymic zonation: a reevaluation of the concept of the liver acinus. *Hepatology* 10(1):72-76
- Lee SS, Buters JT, Pineau T, Fernandez-Salguero P, Gonzalez FJ (1996) Role of CYP2E1 in the Hepatotoxicity of Acetaminophen (*). *Journal of Biological Chemistry* 271(20):12063-12067
- Leist M, Hasiwa N, Daneshian M, Hartung T (2012) Validation and quality control of replacement alternatives—current status and future challenges. *Toxicology Research* 1(1):8-22
- León Z, García-Cañaveras JC, Donato MT, Lahoz A (2013) Mammalian cell metabolomics: experimental design and sample preparation. *Electrophoresis* 34(19):2762-2775
- Lin JH (1995) Species similarities and differences in pharmacokinetics. *Drug Metabolism and Disposition* 23(10):1008-1021
- Littlewood AB (2013) *Gas chromatography: principles, techniques, and applications*. Elsevier
- Liu S, Fu S, Wang G, et al. (2021) Glycerol-3-phosphate biosynthesis regenerates cytosolic NAD⁺ to alleviate mitochondrial disease. *Cell metabolism* 33(10):1974-1987. e9
- Lough WJ, Wainer IW (1995) *High performance liquid chromatography: fundamental principles and practice*. cRc press
- Louisse J, Beekmann K, Rietjens IM (2017) Use of physiologically based kinetic modeling-based reverse dosimetry to predict in vivo toxicity from in vitro data. *Chemical Research in Toxicology* 30(1):114-125
- Lundanes E, Reubsaet L, Greibrokk T (2013) *Chromatography: basic principles, sample preparations and related methods*. John Wiley & Sons
- Madeira C, Costa PM (2021) Proteomics in systems toxicology. *Advances in Protein Chemistry and Structural Biology* 127:55-91
- Malinowska JM, Palosaari T, Sund J, et al. (2022a) Integrating in vitro metabolomics with a 96-well high-throughput screening platform. *Metabolomics* 18(1):11 doi:10.1007/s11306-021-01867-3
- Malinowska JM, Palosaari T, Sund J, et al. (2022b) Automated Sample Preparation and Data Collection Workflow for High-Throughput In Vitro Metabolomics. *Metabolites* 12(1)
doi:10.3390/metabo12010052
- Malinowska JM, Palosaari T, Sund J, et al. (2023) Derivation of metabolic point of departure using high-throughput in vitro metabolomics: investigating the importance of sampling time points on benchmark concentration values in the HepaRG cell line. *Archives of toxicology*:1-15

References

- Marion M-J, Hantz O, Durantel D (2010) The HepaRG cell line: biological properties and relevance as a tool for cell biology, drug metabolism, and virology studies. *Hepatocytes: methods and protocols*:261-272
- Martínez-Sena T, Moro E, Moreno-Torres M, Quintás G, Hengstler J, Castell JV (2023) Metabolomics-based strategy to assess drug hepatotoxicity and uncover the mechanisms of hepatotoxicity involved. *Archives of Toxicology*:1-16
- Marx-Stoelting P, Rivière G, Luijten M, et al. (2023) A walk in the PARC: developing and implementing 21st century chemical risk assessment in Europe. *Archives of Toxicology*:1-16
- Mattes W, Davis K, Fabian E, et al. (2014) Detection of hepatotoxicity potential with metabolite profiling (metabolomics) of rat plasma. *Toxicol Lett* 230(3):467-78
doi:10.1016/j.toxlet.2014.07.021
- Meigs L, Smirnova L, Rovida C, Leist M, Hartung T (2018) Animal testing and its alternatives—The most important omics is economics. *ALTEX-Alternatives to animal experimentation* 35(3):275-305
- Micheel CM, Nass SJ, Omenn GS (2012) Omics-based clinical discovery: Science, technology, and applications Evolution of Translational Omics: Lessons Learned and the Path Forward. National Academies Press (US)
- Milman BL (2015) General principles of identification by mass spectrometry. *TrAC Trends in Analytical Chemistry* 69:24-33
- Mirahmad M, Sabourian R, Mahdavi M, Larijani B, Safavi M (2022) In vitro cell-based models of drug-induced hepatotoxicity screening: progress and limitation. *Drug Metabolism Reviews* 54(2):161-193
- Mitra V, Metcalf J (2009) Metabolic functions of the liver. *Anaesthesia & Intensive Care Medicine* 10(7):334-335
- Mizuno K, Katoh M, Okumura H, et al. (2009) Metabolic activation of benzodiazepines by CYP3A4. *Drug Metabolism and Disposition* 37(2):345-351
- More SJ, Bampidis V, Benford D, et al. (2022) Guidance on the use of the benchmark dose approach in risk assessment. *EFSA Journal* 20(10):e07584
- Mortensen HM, Senn J, Levey T, Langley P, Williams AJ (2021) The 2021 update of the EPA's adverse outcome pathway database. *Scientific Data* 8(1):169
- Mortimer M, Fang W, Zhou X, Vodovnik M, Guo L-H (2022) Omics Approaches in Toxicological Studies Advances in Toxicology and Risk Assessment of Nanomaterials and Emerging Contaminants. Springer, p 61-94
- Murakami S, Ono A, Kawasaki A, Takenaga T, Ito T (2018) Taurine attenuates the development of hepatic steatosis through the inhibition of oxidative stress in a model of nonalcoholic fatty liver disease in vivo and in vitro. *Amino Acids* 50(9):1279-1288
- Nagana Gowda G, Raftery D (2019) Overview of NMR spectroscopy-based metabolomics: opportunities and challenges. *NMR-Based Metabolomics: Methods and Protocols*:3-14
- National Research Council (2007) Toxicity testing in the 21st century: a vision and a strategy. National Academies Press
- Negoro R, Tasaka M, Deguchi S, Takayama K, Fujita T (2022) Generation of HepG2 Cells with High Expression of Multiple Drug-Metabolizing Enzymes for Drug Discovery Research Using a PITCh System. *Cells* 11(10):1677

References

- Nguyen N, Jennen D, Kleinjans J (2022) Omics technologies to understand drug toxicity mechanisms. *Drug Discovery Today*:103348
- Ning J, Chen L, Strikwold M, Lousse J, Wesseling S, Rietjens IM (2019) Use of an in vitro–in silico testing strategy to predict inter-species and inter-ethnic human differences in liver toxicity of the pyrrolizidine alkaloids lasiocarpine and riddelliine. *Archives of toxicology* 93:801-818
- Noor E, Eden E, Milo R, Alon U (2010) Central carbon metabolism as a minimal biochemical walk between precursors for biomass and energy. *Molecular cell* 39(5):809-820
- OECD (1997) OECD Guidelines for the Testing of Chemicals/Section 4: Health Effects.
- OECD (2016a) Guidance Document on the Reporting of Defined Approaches to be Used Within Integrated Approaches to Testing and Assessment. OECD Publishing
- OECD (2016b) Users' Handbook supplement to the Guidance Document for developing and assessing Adverse Outcome Pathways. Environment
- Olesti E, Gonzalez-Ruiz V, Wilks MF, Boccard J, Rudaz S (2021) Approaches in metabolomics for regulatory toxicology applications. *Analyst* 146(6):1820-1834 doi:10.1039/d0an02212h
- Olson H, Betton G, Robinson D, et al. (2000) Concordance of the toxicity of pharmaceuticals in humans and in animals. *Regul Toxicol Pharmacol* 32(1):56-67 doi:10.1006/rtp.2000.1399
- Onakpoya IJ, Heneghan CJ, Aronson JK (2016) Post-marketing withdrawal of 462 medicinal products because of adverse drug reactions: a systematic review of the world literature. *BMC medicine* 14(1):1-11
- Paini A, Leonard JA, Joossens E, et al. (2019) Next generation physiologically based kinetic (NG-PBK) models in support of regulatory decision making. *Computational Toxicology* 9:61-72
- Pallocca G, Moné MJ, Kamp H, Luijten M, Van de Water B, Leist M (2022) Next-generation risk assessment of chemicals—Rolling out a human-centric testing strategy to drive 3R implementation: The RISK-HUNT3R project perspective. *ALTEX-Alternatives to animal experimentation* 39(3):419-426
- Palma E, Doornebal EJ, Chokshi S (2019) Precision-cut liver slices: a versatile tool to advance liver research. *Hepatology international* 13:51-57
- Pelecha M, Villanueva-Badenas E, Timor-Lopez E, Donato MT, Tolosa L (2021) Cell Models and Omics Techniques for the Study of Nonalcoholic Fatty Liver Disease: Focusing on Stem Cell-Derived Cell Models. *Antioxidants (Basel)* 11(1) doi:10.3390/antiox11010086
- Pitt JJ (2009) Principles and applications of liquid chromatography-mass spectrometry in clinical biochemistry. *The Clinical Biochemist Reviews* 30(1):19
- Plummer S, Wallace S, Ball G, et al. (2019) A Human iPSC-derived 3D platform using primary brain cancer cells to study drug development and personalized medicine. *Scientific reports* 9(1):1-11
- Poisson J, Lemoine S, Boulanger C, et al. (2017) Liver sinusoidal endothelial cells: Physiology and role in liver diseases. *Journal of hepatology* 66(1):212-227
- Prior H, Casey W, Kimber I, Whelan M, Sewell F (2019) Reflections on the progress towards non-animal methods for acute toxicity testing of chemicals. *Regulatory Toxicology and Pharmacology* 102:30-33
- Program NT (2018) NTP research report on national toxicology program approach to genomic dose-response modeling.

References

- Qiao T, Wang X (2019) A new light of proteomics in cell biology and toxicology. vol 35. Springer, p 289-291
- Ramirez-Hincapie S, Birk B, Ternes P, et al. (2023) A high-throughput metabolomics in vitro platform for the characterization of hepatotoxicity. *Cell Biology and Toxicology*:1-19
doi:10.1007/s10565-023-09809-6
- Ramirez T, Daneshian M, Kamp H, et al. (2013) Metabolomics in toxicology and preclinical research. *Altex* 30(2):209
- Ramirez T, Strigun A, Verlohner A, et al. (2018a) Prediction of liver toxicity and mode of action using metabolomics in vitro in HepG2 cells. *Archives of toxicology* 92(2):893-906
- Ramirez T, Strigun A, Verlohner A, et al. (2018b) Prediction of liver toxicity and mode of action using metabolomics in vitro in HepG2 cells. *Arch Toxicol* 92(2):893-906 doi:10.1007/s00204-017-2079-6
- Ravenzwaay BV, Kamp H, Montoya-Parra GA, et al. (2015) The development of a database for metabolomics-looking back on ten years of experience. *International Journal of Biotechnology* 14(1):47-68
- Reddy J, Azarnoff D, Hignite C (1980) Hypolipidaemic hepatic peroxisome proliferators form a novel class of chemical carcinogens. *Nature* 283:397-398
- Ribbenstedt A, Ziarrusta H, Benskin JP (2018) Development, characterization and comparisons of targeted and non-targeted metabolomics methods. *PLoS One* 13(11):e0207082
- Richards DJ, Li Y, Kerr CM, et al. (2020) Human cardiac organoids for the modelling of myocardial infarction and drug cardiotoxicity. *Nature biomedical engineering* 4(4):446-462
- Riekeberg E, Powers R (2017) New frontiers in metabolomics: from measurement to insight. *F1000Research* 6
- Ritz C, Streibig JC (2005) Bioassay analysis using R. *Journal of statistical software* 12:1-22
- Rossini GP, Thomas H (2012) Towards tailored assays for cell-based approaches to toxicity testing. *ALTERNATIVES TO ANIMAL EXPERIMENTATION* 29:359-372
- Rovida C, Daneshian M, Hartung T (2015) Integrated testing strategies (ITS) for safety assessment. *Alternatives to animal experimentation: ALTEX* 32(1):25-40
- Ruddigkeit L, Van Deursen R, Blum LC, Reymond J-L (2012) Enumeration of 166 billion organic small molecules in the chemical universe database GDB-17. *Journal of chemical information and modeling* 52(11):2864-2875
- Rudman D, DiFulco TJ, Galambos JT, Smith RB, Salam AA, Warren WD (1973) Maximal rates of excretion and synthesis of urea in normal and cirrhotic subjects. *The Journal of clinical investigation* 52(9):2241-2249
- Ruoß M, Vosough M, Königsrainer A, et al. (2020) Towards improved hepatocyte cultures: Progress and limitations. *Food and Chemical Toxicology* 138:111188
- Russell WMS, Burch RL (1959) *The principles of humane experimental technique*. Methuen
- Saito J, Okamura A, Takeuchi K, Hanioka K, Okada A, Ohata T (2016) High content analysis assay for prediction of human hepatotoxicity in HepaRG and HepG2 cells. *Toxicology In Vitro* 33:63-70

References

- Santiago-Díaz P, Rivero A, Rico M, González González A, González-Dávila M, Santana-Casiano M (2023) Copper toxicity leads to accumulation of free amino acids and polyphenols in *Phaeodactylum tricornutum* diatoms. *Environmental Science and Pollution Research*:1-10
- Schadt S, Simon S, Kustermann S, et al. (2015) Minimizing DILI risk in drug discovery—a screening tool for drug candidates. *Toxicology in vitro* 30(1):429-437
- Schrimpe-Rutledge AC, Codreanu SG, Sherrod SD, McLean JA (2016) Untargeted metabolomics strategies—challenges and emerging directions. *Journal of the American Society for Mass Spectrometry* 27(12):1897-1905
- Senoo H (2004) Structure and function of hepatic stellate cells. *Medical Electron Microscopy* 37:3-15
- Serrano J (2014) LiverTox: An online information resource and a site for case report submission on drug-induced liver injury. *Clinical Liver Disease* 4(1):22
- Shi M, Bouwmeester H, Rietjens IM, Strikwold M (2020) Integrating in vitro data and physiologically based kinetic modeling-facilitated reverse dosimetry to predict human cardiotoxicity of methadone. *Archives of toxicology* 94:2809-2827
- Shin HK, Kang Y-M, No KT (2017) Predicting ADME properties of chemicals. *Handbook of computational chemistry* 59:2265-2301
- Shinozawa T, Kimura M, Cai Y, et al. (2021) High-fidelity drug-induced liver injury screen using human pluripotent stem cell-derived organoids. *Gastroenterology* 160(3):831-846. e10
- Smith L, Villaret-Cazadamont J, Claus SP, et al. (2020) Important considerations for sample collection in metabolomics studies with a special focus on applications to liver functions. *Metabolites* 10(3):104
- Sostare E, Lawson TN, Saunders LR, et al. (2022) Knowledge-driven approaches to create the MTox700+ metabolite panel for predicting toxicity. *Toxicological Sciences* 186(2):208-220
- Spielberg S, Gordon G (1981) Nitrofurantoin cytotoxicity. In vitro assessment of risk based on glutathione metabolism. *The Journal of Clinical Investigation* 67(1):37-41
- Stucki AO, Barton-Maclaren TS, Bhuller Y, et al. (2022) Use of new approach methodologies (NAMs) to meet regulatory requirements for the assessment of industrial chemicals and pesticides for effects on human health. *Frontiers in Toxicology*:98
- Subramanian I, Verma S, Kumar S, Jere A, Anamika K (2020) Multi-omics data integration, interpretation, and its application. *Bioinformatics and biology insights* 14:1177932219899051
- Suter-Dick L, Alves PM, Blaauboer BJ, et al. (2015) Stem cell-derived systems in toxicology assessment. *Stem cells and development* 24(11):1284-1296
- Tabibian JH, Masyuk AI, Masyuk TV, O'Hara SP, LaRusso NF (2013) Physiology of cholangiocytes. *Comprehensive Physiology* 3(1)
- Takafumi W, Shuichi H, Junji Y, et al. (1989) Species differences in the effects of bezafibrate, a hypolipidemic agent, on hepatic peroxisome-associated enzymes. *Biochemical pharmacology* 38(2):367-371
- Thomas RS, Allen BC, Nong A, et al. (2007) A method to integrate benchmark dose estimates with genomic data to assess the functional effects of chemical exposure. *Toxicological sciences* 98(1):240-248
- Thomas SN, French D, Jannetto PJ, Rappold BA, Clarke WA (2022) Liquid chromatography–tandem mass spectrometry for clinical diagnostics. *Nature Reviews Methods Primers* 2(1):96

References

- Underhill GH, Khetani SR (2018) Bioengineered liver models for drug testing and cell differentiation studies. *Cellular and molecular gastroenterology and hepatology* 5(3):426-439. e1
- van Dijk J, Leopold A, Flerlage H, et al. (2021) The EU Green Deal's ambition for a toxic-free environment: Filling the gap for science-based policymaking. *Integrated environmental assessment and management* 17(6):1105-1113
- Van Ravenzwaay B, Cunha GC-P, Leibold E, et al. (2007) The use of metabolomics for the discovery of new biomarkers of effect. *Toxicology letters* 172(1-2):21-28
- Van Ravenzwaay B, Kamp H, Montoya-Parra GA, et al. (2015) The development of a database for metabolomics-Looking back on ten years of experience. *International Journal of Biotechnology* 14(1):47-68
- Van Ravenzwaay B, Montoya G, Fabian E, et al. (2014) The sensitivity of metabolomics versus classical regulatory toxicology from a NOAEL perspective. *Toxicology Letters* 227(1):20-28
- Van Ravenzwaay B, Sperber S, Lemke O, et al. (2016) Metabolomics as read-across tool: A case study with phenoxy herbicides. *Regulatory Toxicology and Pharmacology* 81:288-304
- Venter JC, Adams MD, Myers EW, et al. (2001) The sequence of the human genome. *science* 291(5507):1304-1351
- Viant MR, Ebbels TM, Beger RD, et al. (2019a) Use cases, best practice and reporting standards for metabolomics in regulatory toxicology. *Nature communications* 10(1):3041
- Viant MR, Ebbels TMD, Beger RD, et al. (2019b) Use cases, best practice and reporting standards for metabolomics in regulatory toxicology. *Nat Commun* 10(1):3041 doi:10.1038/s41467-019-10900-y
- Villeneuve DL, Coady K, Escher BI, et al. (2019) High-throughput screening and environmental risk assessment: State of the science and emerging applications. *Environmental toxicology and chemistry* 38(1):12-26
- Vinken M (2013) The adverse outcome pathway concept: a pragmatic tool in toxicology. *Toxicology* 312:158-165
- Vinken M (2019) Omics-based input and output in the development and use of adverse outcome pathways. *Current Opinion in Toxicology* 18:8-12
- Walker PA, Ryder S, Lavado A, Dilworth C, Riley RJ (2020) The evolution of strategies to minimise the risk of human drug-induced liver injury (DILI) in drug discovery and development. *Archives of toxicology* 94(8):2559-2585
- Walvekar A, Rashida Z, Maddali H, Laxman S (2018) A versatile LC-MS/MS approach for comprehensive, quantitative analysis of central metabolic pathways. *Wellcome Open Res* 3:122 doi:10.12688/wellcomeopenres.14832.1
- Wang Y, Gray JP, Mishin V, Heck DE, Laskin DL, Laskin JD (2008) Role of cytochrome P450 reductase in nitrofurantoin-induced redox cycling and cytotoxicity. *Free Radical Biology and Medicine* 44(6):1169-1179
- Wang Z, Walker GW, Muir DC, Nagatani-Yoshida K (2020) Toward a global understanding of chemical pollution: a first comprehensive analysis of national and regional chemical inventories. *Environmental science & technology* 54(5):2575-2584
- Waring MJ, Arrowsmith J, Leach AR, et al. (2015) An analysis of the attrition of drug candidates from four major pharmaceutical companies. *Nature reviews Drug discovery* 14(7):475-486

References

- Westmoreland C, Bender HJ, Doe JE, et al. (2022) Use of New Approach Methodologies (NAMs) in regulatory decisions for chemical safety: Report from an EPAA Deep Dive Workshop. *Regulatory Toxicology and Pharmacology* 135:105261
- Wijaya LS, Rau C, Braun TS, et al. (2022) Stimulation of de novo glutathione synthesis by nitrofurantoin for enhanced resilience of hepatocytes. *Cell biology and toxicology*:1-18
- Wijaya LS, Trairatphisan P, Gabor A, et al. (2021) Integration of temporal single cell cellular stress response activity with logic-ODE modeling reveals activation of ATF4-CHOP axis as a critical predictor of drug-induced liver injury. *Biochemical Pharmacology* 190:114591
- Wilk-Zasadna I, Bernasconi C, Pelkonen O, Coecke S (2015) Biotransformation in vitro: An essential consideration in the quantitative in vitro-to-in vivo extrapolation (QIVIVE) of toxicity data. *Toxicology* 332:8-19
- Wishart DS (2011) Advances in metabolite identification. *Bioanalysis* 3(15):1769-1782
- Xuan J, Chen S, Ning B, Tolleson WH, Guo L (2016) Development of HepG2-derived cells expressing cytochrome P450s for assessing metabolism-associated drug-induced liver toxicity. *Chemico-biological interactions* 255:63-73
- Yong HY, Larrouy-Maumus G, Zloh M, et al. (2020) Early detection of metabolic changes in drug-induced steatosis using metabolomics approaches. *RSC Adv* 10(67):41047-41057
doi:10.1039/d0ra06577c
- Zhang L, Pu K, Liu X, et al. (2021) The Application of Induced Pluripotent Stem Cells Against Liver Diseases: An Update and a Review. *Frontiers in Medicine*:986

Appendix

List of abbreviations

AA	Amino acid
ABCA1	ATP-binding cassette transporter
ACAT1	acetyl-CoA acetyltransferase
ACSL1	Acyl-CoA Synthetase Long Chain Family Member 1
ACTB	Actin Beta
ADI	acceptable daily intake
ADMA	N, N-Dimethylarginine

Appendix

ADME	absorption, distribution, metabolism, and excretion
AFP	alpha-1-fetoprotein
ALDO	aldolase
AOP	adverse outcome pathway
APOA1	Apolipoprotein A1
APOA2	Apolipoprotein A2
ATP	Adenosine triphosphate
<i>BCA</i>	Bicinchoninic acid assay
BMBF	Bundesministerium für Bildung und Forschung
BMC	Benchmark concentrations
BMD	Benchmark dose
<i>BMI</i>	Body mass index
BSA	Bovines Serumalbumin
CAR	chimeric antigen receptor
CD31	cluster of differentiation 31
CD34	cluster of differentiation 34
<i>CEBP</i>	CCAAT-enhancer-binding proteins
CEBPA	CCAAT/enhancer-binding protein alpha
CHOP	DNA damage-inducible transcript 3
CO ₂	Carbon dioxide
COL3A1	Type III Collagen alpha-1 chain
CPT1	Carnitine palmitoyltransferase I
CPT1A	Carnitine palmitoyltransferase I A
CYP	Cytochromes P450
DAPI	4',6-Diamidino-2-phenylindole
DILI	Drug-Induced Liver Injury

Appendix

DMEM	Dulbecco's Modified Eagle Medium
DMSO	Dimethyl sulfoxide
DNA	Deoxyribonucleic acid
DNEL	Derived no-effect level
DOX	Doxycycline
EC	Effective concentration
EDTA	Ethylenediaminetetraacetic acid
ELISA	Enzyme-linked Immunosorbent Assay
FAD	Flavin adenine dinucleotide
FBS	Fetal bovine serum
<i>FOXA2</i>	Forkhead box protein A2
GATA6	Transcription factor GATA-6
GC	Gas chromatography
GIVIMP	Good <i>in vitro</i> method practices
GPD1	Glycerol-3-Phosphate Dehydrogenase
GSH	Glutathione
GSSG	Glutathione disulfide
GUSB	β -Glucuronidase
HMGR	3-hydroxy-3-methylglutaryl-coenzyme
HNF4	Hepatocyte Nuclear Factor 4
HPLC	High-performance liquid chromatography
HPRT1	Hypoxanthine-guanine phosphoribosyltransferase
HT	High throughput
HTS	High throughput screening
<i>IDT</i>	Integrated DNA Technologies
IVIVE	In Vitro–In Vivo Extrapolation

Appendix

KE	Key events
KEGG	Kyoto Encyclopedia of Genes and Genomes
KER	Key event relationships
LC	Liquid chromatography
LOAEL	Lowest Observed Adverse Effect Level
LPL	Lipoprotein lipase
MALDI	Matrix Assisted Laser Desorption/Ionization
MIE	Molecular initiating event
MIV	Metabolomics in vitro
MPS	Microphysiological systems
MRF	Metabolomics Reporting Framework
MRM	Multiple Reaction Monitoring
MS	Mass spectrometry
NAA	N-Acetyl-Aspartate
NAD	Nicotinamide adenine dinucleotide oxidized
NADH	Nicotinamide adenine dinucleotide reduced
NADP	Nicotinamide adenine dinucleotide phosphate oxidized
NADPH	Nicotinamide adenine dinucleotide phosphate reduced
NAM	New Approach methodologies
NANOG	Homeobox protein NANOG
NAT8L	N-Acetyltransferase 8 Like
NGRA	Next generation risk assessment
NMR	Nuclear magnetic resonance
NOAEL	No-Observed-Adverse-Effect Level
NORA	Northeast Research Alliance
NPLC	Normal phase liquid chromatography

Appendix

NRC	National Research Council
OECD	The Organisation for Economic Co-operation and Development
PANK1	Pantothenate Kinase 1
PBS	Phosphate-buffered saline
PBTK	Physiologically Based Toxicokinetic Modell
PCA	Principal Component Analysis
PCK2	Phosphoenolpyruvate Carboxykinase 2
PCR	Polymerase chain reaction
PDK4	Pyruvate dehydrogenase lipoamide kinase isozyme 4,
PE	Phosphatidylethanolamine
PFK	Phosphofructokinase
PFKL	6-phosphofructokinase, liver type
PHH	Primary human hepatocytes
POD	Point of departure
POLR2A	DNA-directed RNA polymerase II subunit
PPAR	Peroxisome proliferator-activated receptors
PPIA	Peptidylprolyl isomerase A
PXR	Pregnane X receptor
QC	Quality control
QIVIVE	Quantitative in Vitro to in Vivo Extrapolation
REACH	The Regulation on the registration, evaluation, authorisation and restriction of chemicals
RNA	Ribonucleic acid
ROS	Reactive oxygen species
RP	Reverse phase
RPLC	Reverse phase liquid chromatography

Appendix

RSD	Relative standard deviation
SAM	Sample Analyte median
SD	Standard deviation
SM	Sphingomyelinase
SMPD1	Sphingomyelinase 1
SMPD2	Sphingomyelinase 2
SOX17	SRY-Box Transcription Factor 17
SPTSSA	Palmitoyltransferase subunit A
SPTSSB	Palmitoyltransferase subunit B
SREBP	Sterol regulatory element-binding proteins
SREBP1	Sterol regulatory element-binding protein 1
TAG	Triacylglycerols
TBXT	T-Box Transcription Factor T
TDI	Tolerable daily intake
TG	Triglyceride
TOF	Time of flight
UCP1	Thermogenin
UMAP	Uniform Manifold Approximation and Projection
UPR	Unfolded protein response

Curriculum Vitae

Education

03/2020 – 05/2023

Doctoral candidate

BASF SE, Ludwigshafen am Rhein & Rheinland-Pfälzische Technische Universität Kaiserslautern-Landau

Supervision by Prof. Dr. Elke Richling, Prof.Dr. Bennard van Ravenzwaay & Dr. Barbara Birk

Topic: "Advancing the Implementation of *In Vitro* Metabolomics in Toxicology"

08/2017 – 01/2018

Master-Thesis intern

BASF SE, Ludwigshafen am Rhein

Supervision by Prof.Dr. Bennard van Ravenzwaay & Dr. Christina Behr

Topic: "Influence of Lincosamides Antibiotics on the Gut Microbiome. An Inter-omics Approach"

Final mark: 100%, awarded honors. Scientific publication.

06/2013 – 11/2018

Diploma in Biology with emphasis in Molecular Biology

Universidad EAFIT. Medellin Colombia

Final mark 96%

Graduated with highest honours. Awarded best academic performance honor.

01/2018 – 05/2018

Academic exchange, Concordia University

Concordia University. Montreal, Canada

Mark 88%

01/2016 – 05/2016

Academic exchange, Concordia University

Concordia University. Montreal, Canada

Mark: 92%

01/1999 – 12/2012

Elementary, Middle, and High School

Colegio Jesus María. Medellin, Colombia

Academic excellence award from the 8th grade to the last year of High school

Work experience

03/2019 – 12/2012

Research assistant, Molecular Biology lab

Universidad EAFIT. Medellin, Colombia

07/2018 –11/2018

Biochemistry teaching assistant

Universidad EAFIT. Medellin, Colombia

07/2016 –11/2016

Genetics and Molecular Biology teaching Assistant

Universidad EAFIT. Medellin, Colombia

01/2015 –11/2015

Microbiology research assistant

Universidad EAFIT. Medellin, Colombia

Selected courses

06/2022 – 07/2022

Science Communication in the post COVID-19

University of Geneva summer school

Geneva, Switzerland

04/2022	The future of Science communication 2.0 Brussels, Belgium
04/2022	Basic principles of Toxicology Advanced training for "Fachtoxikologe/in GT"
03/2021	BB3R Spring School on alternative test methods to animal experimentation. Freie Universität Berlin (online)
Selected achievements	
12/2018	Best academic performance of the 2018 graduating class Medellin, Colombia
12/2018	Honors awarded "Influence Of lincosamides Antibiotics on the Gut Microbiome: An Inter-omics Approach" Medellin, Colombia
06/2018	The Emerging Leaders in the Americas Program Scholarship Providing outstanding students from Latin America and the Caribbean with exchange opportunities for study or research in Canada
Jan 2015 — Nov 2017	Research grants Medellin, Colombia In silico determination of the relevance of mutual exclusivity and cooccurrence patterns in cancer driver genes (2017); Isolation and characterization of lactic acid bacteria that exhibit antagonistic activity against pathogenic microorganisms (2015).

Scientific presentations

01/2022

European Society of Toxicology In Vitro 2022

Congress

Poster presentations. (1) Liver metabolomics in vitro– a miniaturized screening approach to predict the mode of action of liver toxicants in HepG2 cells. (2) Implementing an in vitro metabolomics screening method to study liver toxicants in HepG2 cells. A case study with Nitrofurantoin.

01/2021-2022-2023

Liver Toxicity module, Universität Koblenz

Landau

Landau, Germany

Guest lecturer. Ecotoxicology Master's Degree

03/2022

German Pharm-Tox Summit 2022

Oral presentation

Miniaturization of in vitro liver metabolomics– a screening approach to predict the mode of action of liver toxicants in HepG2 cells.

03/2022

Society of Toxicology (SOT) 2022 congress

Poster presentation

Liver metabolomics *in vitro*– a screening approach to predict the mode of action of liver toxicants in HepG2 cells.

09/2021

EUROTOX 2021

Poster presentation

Miniaturization of *in vitro* liver metabolomics– a screening approach to predict the Mode of Action of liver toxicants in HepG2 cells.

08/2021

The World Congress on Alternatives and

Animal Use in the Life Sciences 2021

Poster presentation

Miniaturizing liver metabolomics *in vitro* – a new screening approach to generate metabolic fingerprint in HepG2 cells.

03/2021

German Pharm-Tox Summit 2021

Poster presentations (1) Programmable iPSCs-derived 3DLiver Organoids as a Novel *in vitro* Model for Toxicology Studies by Metabolomic Phenotyping. (2) Influence of pregnancy and non-fasting conditions on the plasma metabolome in a rat prenatal toxicity control study.

Publications

Ramirez-Hincapie S, Birk B, Ternes P, Giri V, Haake V, I Herold M, Zickgraf FM, Verlohner A, Huener H, Kamp H, Driemert P, Landsiedel R, Richling E, Funk-Weyer D, van Ravenzwaay B (2023) A high-throughput metabolomics *in vitro* platform for the characterization of hepatotoxicity. *Cell Biology and Toxicology*:1-19. <https://doi.org/10.1007/s10565-023-09809-6>.

Ramirez-Hincapie S, Birk B, Ternes P, Giri V, Zickgraf FM, Haake V, I Herold M, Kamp H, Driemert P, Landsiedel R, Richling E, Funk-Weyer D, van Ravenzwaay B. Application of High Throughput *In vitro* Metabolomics for Hepatotoxicity Mode of Action characterization and Mechanistic-anchored Point of Departure Derivation: A Case Study with Nitrofurantoin. Submitted to *Archives of Toxicology* on May 30, 2023. Submission ID: ATOX-D-23-00403.

Ramirez-Hincapie S*, Mishra D*, Birk B, Haake V, Herold M, Pery E, Vargas-Asencio J, Razavi S, Fortuna P, Summers N, Konradi R, van Ravenzwaay B, Weiss R. Mechanistic Toxicometabolomic Studies of a Model PPAR α Agonist on Human Pluripotent Stem Cell-derived Liver Organoids. First round of revisions submitted to *Nature Scientific Reports*. Submission ID: [SREP-22-01564A](#).

Ramirez-Hincapie S, Giri V, Keller J, et al. (2021) Influence of pregnancy and non-fasting conditions on the plasma metabolome in a rat prenatal toxicity study. *Archives of Toxicology* 95:2941-2959.

Behr, C., **Ramírez-Hincapié, S.**, Cameron, H. J., Strauss, V., Walk, T., Herold, M., ... & van Ravenzwaay, B. (2018). Impact of lincosamides antibiotics on the composition of the rat gut microbiota and the metabolite profile of plasma and feces. *Toxicology letters*, 296, 139151.

Robledo-Cardona, **RamírezHincapié**, S., & Alvarez, J. C. (2018). Implementation of a Non-Invasive Bioprospecting Protocol for Isolation of Lactobacillus from Feces of Hens Under Foraging Conditions. *Ingeniería y Ciencia*,14(28), 93-111.